Functions of *MICRORNA172* and *APETALA2-LIKE* genes during floral transition at the shoot apical meristem

Inaugural-Dissertation

zur

Erlangung des Doktorgrades
der Mathematisch-Naturwissenschaftlichen
der Universität zu Köln

vorgelegt von

Enric Bertran Garcia de Olalla

aus Tarragona, Spanien

Köln, 2023

Functions of *MICRORNA172* and *APETALA2-LIKE* genes during floral transition at the shoot apical meristem

Inaugural-Dissertation

zur

Erlangung des Doktorgrades
der Mathematisch-Naturwissenschaftlichen Fakultät
der Universität zu Köln

vorgelegt von

Enric Bertran Garcia de Olalla

aus Tarragona, Spanien

Köln, Juni 2023

Die vorliegende Arbeit wurde am Max-Planck-Institut für Pflanzenzüchtungsforschung in Köln in der Abteilung für Entwicklungsbiologie der Pflanzen (Direktor: Prof. Dr. George Coupland), Arbeitsgruppe Prof. Dr. George Coupland durchgeführt.

The work described in this thesis was conducted at the Max Planck Institute for Plant Breeding Research in the Department of Plant Developmental Biology (Director: Prof. Dr. George Coupland) under the supervision of Prof. Dr. George Coupland.

MAX-PLANCK-INSTITUT
FÜR PFLANZENZÜCHTUNGSFORSCHUNG

Berichterstatter (Gutachter):	**Prof. Dr. George Coupland**
	Prof. Dr. Stanislav Kopriva
Prüfungsvorsitzender:	**Prof. Dr. Bart Thomma**
Tag der mündlichen Prüfung:	**28. September 2023**

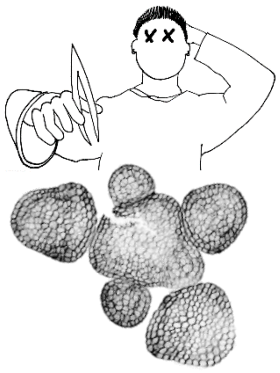

“Voy a reírme cuando tenga ochenta y mire p’atrás.”

ROSALÍA (2022). SAKURA – MOTOMAMI

Abstract

The integration of environmental and internal signals controls floral transition at the shoot apical meristem (SAM), which contains one of the stem-cell niches that generate aerial organs. During floral transition, the identity of the SAM changes from a vegetative meristem that initiates leaf primordia at its periphery, to an inflorescence meristem that produces floral primordia. Five *MICRORNA172* (*MIR172*) genes encode microRNA172 (miR172), which is a small RNA molecule that accumulates at the SAM during floral transition and promotes flowering by repressing the expression of the *APETALA2-LIKE* (*AP2-LIKE*) genes. *MIR172A, MIR172B* and *MIR172D* are expressed at the SAM during floral transition, and their onset of expression is earlier under inductive long days compared to short days. Notably, miR172 is also a positive regulator of inflorescence meristem size, largely by down-regulating the expression of the positive SAM area regulator *AP2.*

Considering the earlier expression of *MIR172* genes at the SAM under inductive long days, the genetic relationships between the main components of the photoperiodic pathway and *MIR172* and *AP2-LIKE* genes were characterised. In the second chapter of this dissertation, it is shown that although the regulation of flowering time by *MIR172* and *AP2-LIKE* genes is influenced by inductive photoperiods, these genes also regulate flowering time in a photoperiod-independent manner.

In light of the negative role of miR172 and the positive role of *APETALA2* (*AP2*) in the regulation of inflorescence meristem size, the involvement of *MIR172* and *AP2* genes in the enlargement of the SAM during floral transition was explored. The results in the third chapter of this dissertation show that *AP2* is a positive regulator of shoot meristem size during floral transition and is essential for changes in SAM size. A genetic relation between *AP2* and *SUPPRESSOR OF OVEREXPRESSION OF CONSTANS 1*, which encodes a MADS domain transcription factor, was proposed as a mechanism that couples changes in SAM morphology and floral transition.

The involvement of *MIR172* genes in the regulation of flowering time was analysed by comparing the transcriptome profile of dissected plant apices from Col-0 vs. *mir172* mutants. The constant mRNA levels of *TARGET OF EAT 2,* an *AP2-LIKE* gene, are a candidate main alteration that underlies the late-flowering of *mir172* mutants. The transcription factor TOE2 was then characterised and a genetic relation between *TOE2*, *AP2* and *SQUAMOSA PROMOTER-BINDING PROTEIN-LIKE 4* is proposed.

This work provides a framework for understanding the positive role of miR172 in the regulation of flowering time by repressing *AP2-LIKE* genes and constitutes evidence for the involvement of flowering-time regulators in the changes of SAM morphology during floral transition.

Table of contents

1 Introduction

Animals and plants possess populations of cells that retain the capacity for self-renewal via cell division, and act as a reservoir of cells that differentiate into specialised cell types. These cells are the so-called stem cells, which have captured the attention of biomedical researchers due to their potential applications in regenerative medicine (reviewed in Mahla, 2016). The ability of plants to maintain stem cells throughout their life cycle is beneficial in terms of crop production and biofuels, among others, and a spectacular example of their longevity is the stem cells of the tree *Sequoia sempervirens*, which can be active for over 2,000 years (reviewed in Scheres, 2007). Stem cells are present at particular locations in the plant that constitute specialised microenvironments known as stem-cell niches. In plants, three main stem-cell niches have been characterised, which are located at the points of plant growth (reviewed in Greb & Lohmann, 2016). These include the root apical meristem (RAM) and the shoot apical meristem (SAM), which are responsible for the longitudinal growth of plants and are located at the root and the stem tip, respectively. In addition, the stem cells within the cambium give rise to radial growth. There are additional stem-cell niches, such as the axillary meristems, that are generated at the boundaries of the SAM, which will then be located at the apices of the branches that arise from the main stem.

The structure of the RAM remains constant throughout the plant life; however, the structure of the SAM changes, especially upon floral transition when it increases in size in many plant species (reviewed in Kwiatkowska, 2004, 2008). Another unique feature of the SAM is that lateral organs are initiated continuously at its periphery. Following germination, the SAM initially forms leaves, but upon floral transition, a change in meristem structure is accompanied by a change in identity, and the SAM gives rise to flowers, thus enabling reproductive growth. Flowering in angiosperms is regulated by environmental and developmental signals that ensure that the transition to reproductive growth is synchronised with changes in the environment (reviewed in Andrés & Coupland, 2012 and Yanovsky & Kay, 2003). Thus, the changes in organisation and identity of the SAM constitute an example of how changes in

environment impact on plant development. Notably, the change in meristem identity has been described for the SAM, but not for other stem-cell niches that continuously form aerial organs, such as axillary meristems.

This dissertation characterises the contribution of the small RNA molecule microRNA172 (miR172) within the gene regulatory network that controls the timing of flowering in *Arabidopsis thaliana* (hereafter Arabidopsis). In addition, it studies in detail one target of miR172, the transcription factor APETALA2 (AP2), which promotes SAM growth and negatively regulates floral transition. Therefore, this chapter provides an overview of the genetic pathways that regulate flowering time in Arabidopsis, with specific focus on the regulation of flowering by daylength. Additionally, the function of miR172 is described, together with its six target genes whose encoded proteins comprise the AP2-LIKE transcription factor family. Finally, the organisation of the SAM and the morphological changes it undergoes during floral transition are summarised.

1.1 Floral transition is a key developmental step

1.1.1 Plants exhibit different life histories

The regulation of flowering time in angiosperms is important to ensure optimum reproductive success in appropriate environments. Thus, flowering is synchronised with environmental cues, particularly those associated with the changing seasons (reviewed in Yanovsky & Kay, 2003). The flowering process involves two major stages. Floral induction is the change the identity of the SAM to an inflorescence meristem that forms floral primordia. Floral evocation is the outgrowth of the primordia to form mature fertile flowers that give rise to seeds. Moreover, plants exhibit diverse life histories: annual plants such as maize, tomato or Arabidopsis undergo the transition to flowering once in their life cycle, whereas perennial species such as long-lived trees and some relatives of Arabidopsis in the *Brassicaceae* family, such as *Arabidopsis lyrata* and *Arabis alpina*, flower several times and live for several or many years. The characterisation of the gene regulatory networks that regulate flowering in the model species Arabidopsis enables comparative studies to understand how flowering is regulated in

other species, and to examine how differences in life history are established. In this dissertation, the focus is on the gene regulatory networks that regulate floral transition in Arabidopsis, because these are the most thoroughly understood and studied experimentally in subsequent chapters.

1.1.2 Long days induce flowering in Arabidopsis

Flowering in Arabidopsis is promoted by exposure to long summer days via the so-called photoperiodic pathway. The identification of mutants that flowered later than wild type under long days (LDs) but at a similar time to wild type under short days (SDs) led to the identification of the main regulators of flowering time under inductive photoperiods (Koornneef et al., 1991; Rédei, 1962). One of these master regulators of flowering time is the transcription factor CONSTANS (CO*;* Putterill et al., 1995). *CO* mRNA is present in both LDs and SDs and its expression profile follows a circadian rhythm, in which its abundance increases between 10–12 h after dawn (Suárez-López et al., 2001). Notably, *CO* mRNA only accumulates during the dark in SDs, but under LDs its expression exhibits a peak at the end of the day, when there is still light and this induces stabilization of CO protein. One mechanism by which *CO* transcription is linked to the circadian clock is its positive regulation by *GIGANTEA* (*GI*)*,* whose transcription exhibits circadian oscillations (Fowler et al., 1999). Notably, *gi* mutants exhibit oscillations in *CO* transcription but with a much decreased amplitude (Suárez-López et al., 2001). This positive regulation of *CO* transcription is mediated by the interaction between GI and another component of the circadian clock, namely FLAVIN-BINDING, KELCH REPEAT, F-BOX 1 (FKF1; Sawa et al., 2007). The GI–FKF1 complex forms during late afternoon under LDs (in contrast to in SDs, where only a small amount of the complex is formed), and associates with the promoter of *CO*, where GI associates with CYCLING DOF FACTOR 1 (CDF1), a repressor of *CO* transcription that is then degraded by FKF1. In addition to the positive regulation of *CO* transcription under LDs, the photoreceptors PHYTOCHROME A (PhyA), CRYPTOCHROME 1 (CRY1) and CRY2 promote CO protein stability at the end of the light period under LDs, whereas PhyB leads to destabilisation of CO in the morning (Valverde

et al., 2004). In summary, LDs constitute an inductive photoperiod by enabling a peak of CO protein accumulation to be generated in the late afternoon.

CO induces flowering by activating the transcription of the floral integrator genes *FLOWERING LOCUS T* (*FT*) and *SUPPRESSOR OF OVEREXPRESSION OF CONSTANS* (*SOC1*). The introduction of *35S::FT* into the *co* mutant background rescues the late-flowering phenotype of *co* (Kardailsky et al., 1999), but the introduction of the *ft* mutation into *35S::CO* plants leads to later flowering than *35S::CO* (Onouchi et al., 2000), which demonstrates that *CO* functions upstream of *FT.* Moreover, the *FT* mRNA level peaks at a similar time to that of CO under LDs (Suárez-López et al., 2001; reviewed in Turck et al., 2008). The increase in *FT* expression observed using CO-inducible systems further confirmed that CO activates *FT* expression (Kobayashi et al., 1999). The activation of *SOC1* by CO was initially proposed to occur due to the observed upregulation of *SOC1* following the induction of CO expression (Samach et al., 2000). However, this was based on induction of *CO* expression under the control of the 35S promoter and in a comparative microarray analysis between SD-grown plants that were exposed to 16 h light vs. a control group grown in an 8 h photoperiod, *FT* and not *SOC1* was identified as the main target of CO in leaves (Wigge et al., 2005). By contrast, *35S::CO soc1-2* plants flowered earlier than *soc1-2* plants (Yoo et al., 2005). A homologue of *FT*, *TWIN SISTER OF FT* (*TSF1*), was identified as a positive regulator of floral transition and is also regulated by CO (Yamaguchi et al., 2005). Notably, *FT* and *TSF* have also been reported to positively regulate *SOC1*.

SOC1 is expressed in leaves and the SAM (Lee et al., 2000; Samach et al., 2000). However, *FT* mRNA has not been detected at the shoot apex (Schmid et al., 2003). The term “florigen” was proposed by Chailakhyan (1936) to refer to a mobile signal that in response to appropriate day lengths moves from leaves to the shoot apex and induces floral transition (reviewed in Zeevaart, 2006). Both *FT* and *TSF* encode phosphatidylethanolamine-binding proteins (PEBPs) and are now considered florigens. Grafting experiments demonstrated that FT tagged with GFP and expressed under the promoter of *SUCROSE-PROTON SYMPORTER 2* (*SUC2*), a phloem companion-cell-specific promoter (*SUC2::FT:GFP*), could be translocated

over graft junctions and over long distances to reach the shoot apex or roots (Corbesier et al., 2007). Moreover, the introduction of *SUC2::FT:GFP* into *ft* mutants rescued the late-flowering phenotype of *ft*. Rescue of the late-flowering phenotype was also observed when either *SUC2::FT* or *SUC2::TSF* was introduced into *ft tsf* double mutants (Jang et al., 2009). Because FT can be translocated to the shoot apex when it is expressed in phloem companion cells (Mathieu et al., 2007), this suggests that the FT protein functions at the shoot apex. It is important to consider that the introduction of *SUC2::CO* into *ft tsf* double mutants does not rescue the late-flowering phenotype of *ft tsf* mutants, which indicates that CO regulates flowering time via *FT* and *TSF*. At the SAM, FT and TSF interact with the basic leucine zipper (bZIP) domain transcription factor FD (Abe et al., 2005, 2019; Jang et al., 2009; Wigge et al., 2005), which leads to the activation of expression of the floral integrator gene *SOC1* and to floral transition.

1.1.3 Several pathways regulate flowering time in Arabidopsis

Other pathways regulate flowering in addition to the photoperiodic pathway (Figure 1-1; reviewed in Fornara et al., 2010) and these allow flowering to occur in the absence of inductive LDs. For example, an increase in temperature, which is characteristic of summer, promotes flowering in Arabidopsis even in SDs. The MADS-box gene *SHORT VEGETATIVE PHASE* (*SVP*) was reported to respond to ambient temperature, due to the inability of *svp* mutants to induce flowering in response to temperature changes (Jeong et al., 2007). Moreover, the stability of SVP protein was shown to be compromised at high temperatures (Lee et al., 2013). The MADS-domain transcription factor FLOWERING LOCUS C (FLC) physically interacts with SVP in the leaves and leads to the repression of *FT* and *TSF* expression. This complex also forms at the shoot apex, where it directly represses the transcription of *SOC1* (Li et al., 2008). Notably, *FLC* expression is negatively regulated via the vernalisation pathway, which is triggered upon prolonged exposure to low temperatures (reviewed in Andrés & Coupland, 2012). However, natural variation in the components of this pathway has occurred, and accessions have been described that contain mutations in these genes (Shindo et al., 2005;

Werner et al., 2005). The maintenance of *FLC* repression after vernalization and return to normal temperatures is mediated via histone modifications at the chromatin of the *FLC* locus, induced by components, such as VERNALIZATION INSENSITIVE 3 and POLYCOMB REPRESSIVE COMPLEX 2 (Heo & Sung, 2011). In the absence of vernalization, the so-called autonomous pathway represses the expression of *FLC* (reviewed in Simpson, 2004).

SOC1 also directly induces the expression of genes of the *SQUAMOSA PROMOTER BINDING PROTEIN-LIKE* (*SPL*) family (Jung et al., 2012). Out of the 16 *SPL* genes in Arabidopsis, 10 are targeted by microRNA156 (miR156; Xu et al., 2016). The downregulation of miR156 is a hallmark of plant ageing; thus, miR156 and SPL transcription factors are considered to be the core components of the so-called ageing pathway. Mutations in *MIR156* genes cause extreme early flowering (J. Gao et al., 2022). The SPL proteins bind to and activate promoters of flowering genes, including *SOC1, FRUITFULL* (*FUL*)*, LEAFY* (*LFY*) and *APETALA1* (*AP1*) (Jung et al., 2012; Wang et al., 2009; Yamaguchi et al., 2009). The expression of *SOC1* is positively regulated by gibberellins (GAs), which are positive regulators of flowering as evidenced by the flowering-time defect of *ga1* mutants, and GAs are essential for flowering under SDs (Blázquez & Weigel, 1999; Wilson et al., 1992). Importantly, the SOC1-interacting protein SPL15 is a major regulator of flowering time under SDs and activates *FUL* and *MIR172B* transcription (Hyun et al., 2016). These studies demonstrate that SOC1 functions as a floral integrator irrespective of the photoperiod.

Thus, different environmental parameters and internal factors constitute signals that regulate flowering in Arabidopsis and converge in the regulation of the so-called floral integrator genes (reviewed in Fornara et al., 2010). A first layer of regulation can be defined in leaves, which converges on the transcription of *FT.* However, the different pathways that regulate flowering ultimately converge at the SAM where flower development will occur and one of the first steps is the activation of *SOC1* transcription. Whereas the induction of flowering under LDs relies on the expression of *FT* in the leaf vasculature, under non-inductive SDs *FT* is not expressed there, thus leading to later flowering, because floral induction must rely on other signals that act more slowly to induce the developmental change at the SAM.

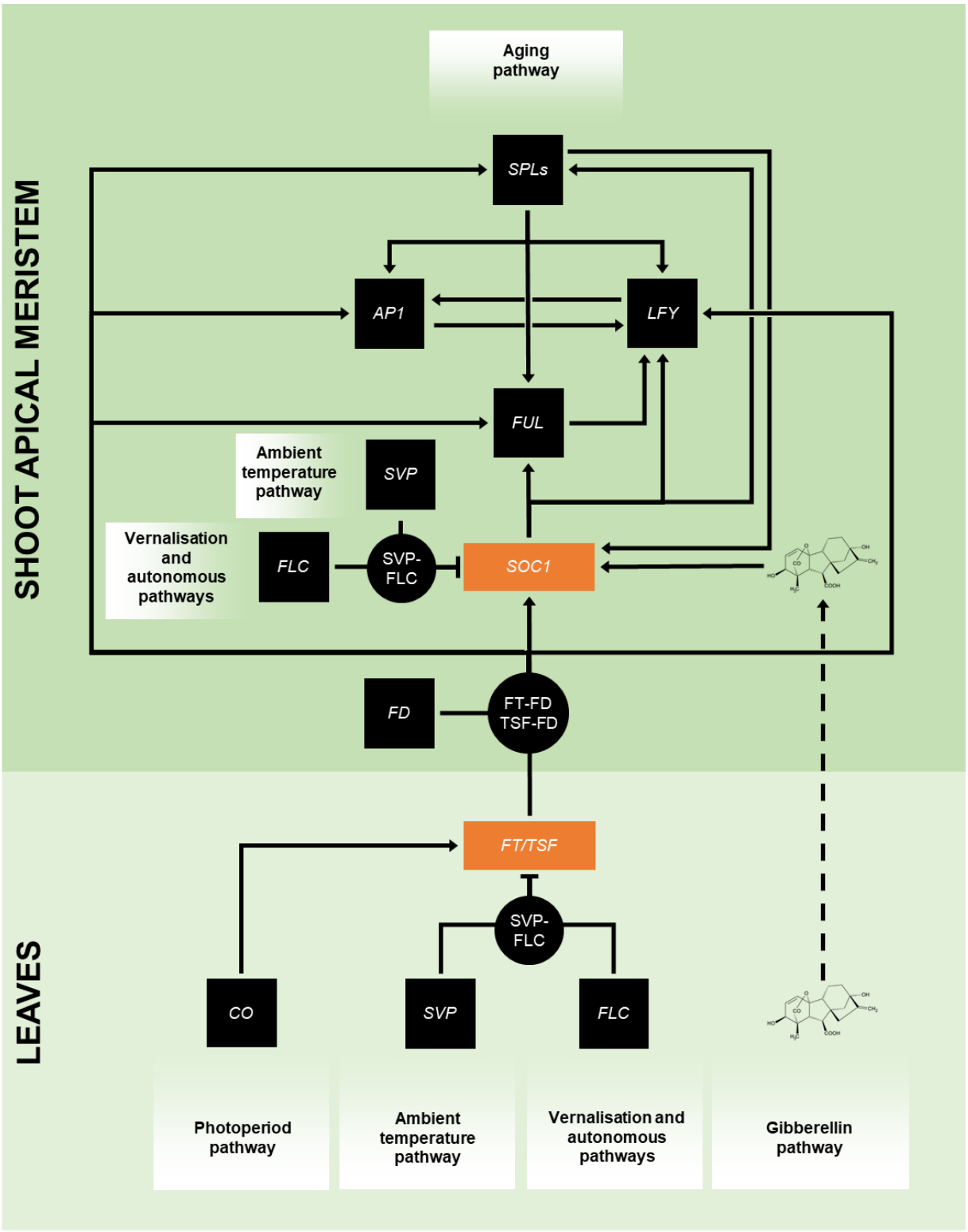

Figure 1-1. Genetic interactions among the main regulators of the flowering pathways in Arabidopsis.

Genes are represented as black boxes. Floral integrator genes are represented as orange boxes. Positive relationships between genes are shown by arrows, whereas negative relationships are indicated with blunt-ended lines. When these genetic relationships are dependent on the formation of a protein complex, this complex is represented within a circle on the line depicting the relationship. Note that FT and TSF proteins can move from the leaves to the SAM, where they form complexes with FD. Gibberellins are synthesised in different tissues and are transported to the SAM. Loss-of-function mutants for *soc1* are able to flower: note that other flowering-promoting genes such as *FUL, AP1* and *LFY*, are also positively regulated by FT-FD/TSF-FD. The roles of APETALA2-LIKE proteins are shown separately in Figure 1-2. Figure adapted from Fornara et al. (2010).

1.2 miR172 is a positive regulator of flowering time

1.2.1 Small RNAs represent a widespread mechanism to regulate gene expression

Small RNAs are short molecules of 20–30 nucleotides (nt) that are involved in regulatory processes at the DNA or RNA level in eukaryotes. Small RNAs were firstly described in the nematode *Caenorhabditis elegans*, in which *lin-4*, a regulator that represses the *lin-14* gene during larval development, was found to encode a 61-nt and a 22-nt transcript with complementarity to the 3' untranslated region (UTR) of *lin-14* mRNA (Lee et al., 1993). Subsequently, *let-7* was identified as a second regulator of later stages of larval development and it encodes a 21-nt RNA, thus highlighting the relevance of small RNAs in the regulation of developmental transitions during the larval stages of *C. elegans* (Reinhart et al., 2000). The identification of *let-7* RNA in several animal species demonstrated the conservation of small RNAs in other species, and provided evidence for small RNAs being a widespread mechanism for the regulation of gene expression (Pasquinelli et al., 2000).

Small RNAs are classified into three major classes according to their biogenesis: microRNAs (miRNAs), small interefering RNAs (siRNAs) and Piwi-interacting RNAs (piRNAs). The piRNAs are specific to animal cells. One initial common step in the processing of miRNA and siRNA precursors is the action of the Dicer endonuclease (reviewed in Lam et al., 2015). siRNAs are produced from double-stranded RNA that has been either transcribed (e.g. from a transposon) or artificially introduced (e.g. via viral infection or via transformation of a transgene), which are processed via the ribonuclease Dicer. On the other hand, miRNAs are encoded by specific loci in the genome (reviewed in Kamthan et al., 2015). More specifically, the transcription of *MICRORNA* (*MIR*) genes by RNA Polymerase II leads to the formation of a hairpin structure termed pri-miRNA, which is then cleaved by Drosha to form pre-miRNA, which is the precursor that is then processed by Dicer, yielding miRNA molecules. siRNA and miRNA can be loaded into the RNA-induced silencing complex (RISC). Argonaute, one of the components of the RISC complex, leads to the removal of the so-called passenger strand (or sense strand), so

that only the guide strand (or antisense strand), which is complementary to the target mRNA, will remain in the complex. Finally, gene silencing is induced by the RISC complex by complementarity between the guide strand and the mRNA of the target gene. The complete complementarity between the guide strand of siRNA with the target mRNA leads to mRNA cleavage and subsequent degradation. Incomplete complementarity between the miRNA guide strand can lead to different mechanisms of gene repression that include translational repression, mRNA degradation and mRNA cleavage. Notably, the incomplete complementarity between the guide strand of miRNAs and the target mRNA means that miRNAs have several targets, contrary to siRNAs, which have a single target.

Argonaute proteins are divided into the Argonaute (AGO) and Piwi families. AGO proteins are ubiquitously expressed and as already described, are a component of the RISC complex that mediates the function of miRNAs and siRNAs. By contrast, Piwi proteins are expressed mainly in germline cells of animals and form the RISC complex together with piRNAs (reviewed in Iwasaki et al., 2015). The piRNAs of animals are slightly longer (24–31 nt) than siRNAs and miRNAs and are processed from so-called piRNA clusters, which are intergenic regions that are transcribed into single-stranded precursors.

1.2.2 miRNAs are involved in the regulation of plant development

The previous section described the general features of small RNA pathways in plants and animals. Some features are specific to plants: for example, the Drosha and Dicer endonuclease activities described in animals (see previous section) are carried out by a single DICER-LIKE (DCL) enzyme in plants. In Arabidopsis, small RNAs are generated by four DCL enzymes (reviewed in Vaucheret, 2008). Although Piwi proteins have not been described in plants, the Arabidopsis genome contains 10 AGO proteins, 5 of which are functionally relevant for the generation of small RNAs. Moreover, among these 5 AGO proteins, AGO1 and AGO10 are associated with miRNA activity (reviewed in Vaucheret, 2008). In addition, AGO7 associates with miR390 to produce *trans*-acting siRNA (Montgomery et al., 2008). The

pleiotropic effects of mutants for the biosynthesis of miRNAs indicate the multiple functions of miRNAs in plants (reviewed in Ramachandran & Chen, 2008).

1.2.3 miR172 regulates floral transition by repressing the expression of *AP2-LIKE* genes

In Arabidopsis, miR172 is encoded by five *MICRORNA172* (*MIR172*) genes, whose transcripts were firstly identified via isolation and sequencing of miRNAs in a comparative analysis between wild type and a double knock-out mutant for *CARPEL FACTORY* (or *DCL1*) and *HUA ENHANCER 1* (*HEN1*), which is a methyltransferease that methylates the ribose residue of the last 3' nucleotide of miRNAs and siRNAs (Park et al., 2002; Yu et al., 2005). Expression of *MIR172* genes has been reported in several tissues, including leaves, stems, flowers and inflorescences, and this has been confirmed via characterisation of the spatial expression patterns of *MIR172* transcriptional reporters for each of the five *MIR172* genes (Lian et al., 2021; Ó'Maoiléidigh et al., 2021). The expression of *MIR172* genes in leaves was suggested to increase *FT* mRNA levels (Jung et al., 2011; Lian et al., 2021; Ó'Maoiléidigh et al., 2021; B. Zhang et al., 2015), and therefore miR172 has been proposed to be a positive regulator of *FT* expression and floral transition. However, *MIR172A*, *MIR172B* and *MIR172D* are also expressed during floral transition at the SAM, concomitant with miR172 accumulation (Lian et al., 2021; Ó'Maoiléidigh et al., 2021; Wollmann et al., 2010); therefore, miR172 appears to function as a positive regulator of floral transition both in leaves and in the SAM (Figure 1-2A–C).

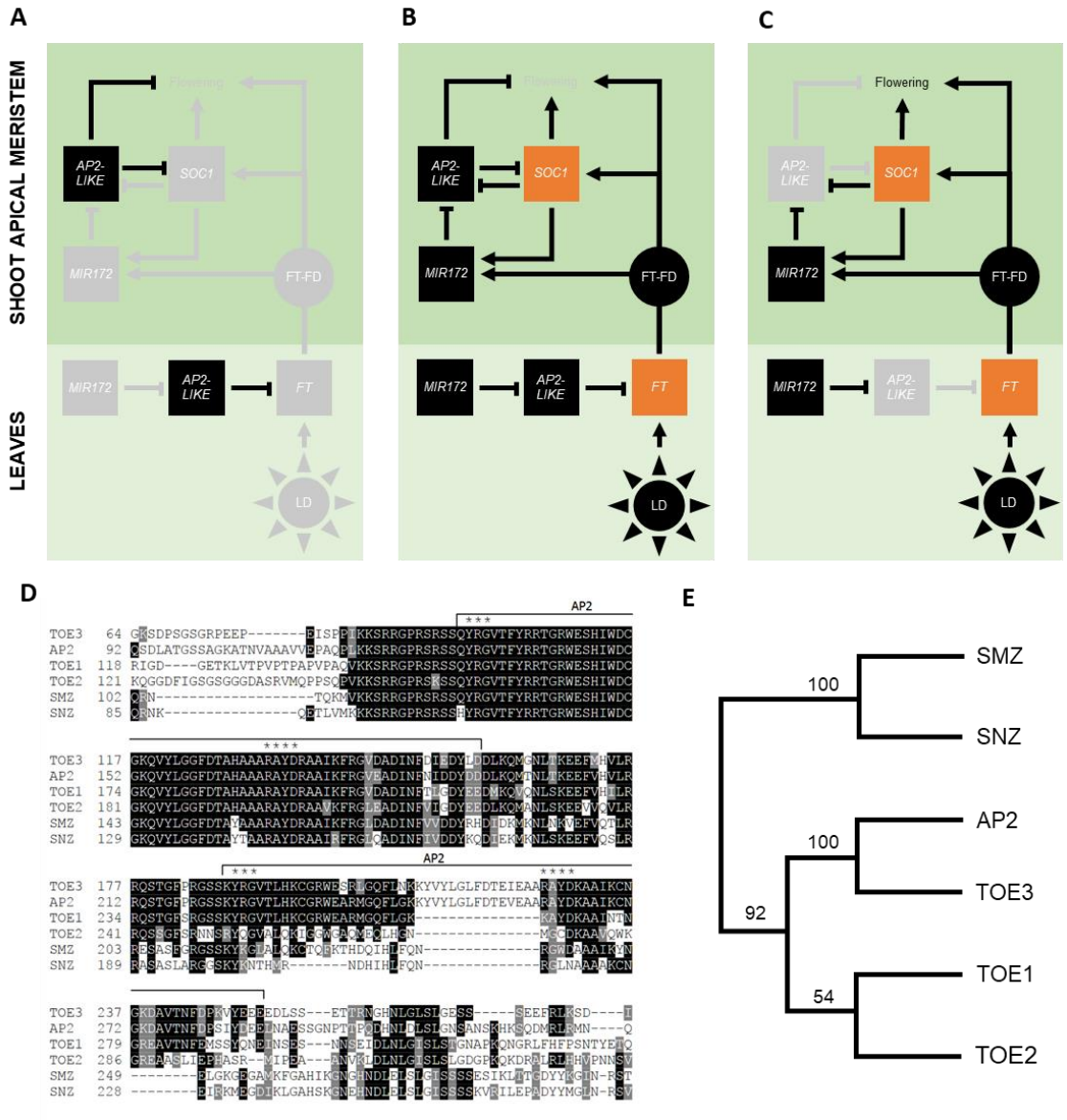

Figure 1-2. AP2-LIKE transcription factors are a family of flowering repressors.

(A–C) The proposed involvement of *MIR172* and *AP2-LIKE* genes in the gene regulatory network controlling flowering during (A) vegetative growth, (B) floral transition and (C) reproductive growth. There are 6 *AP2-LIKE* genes and their individual roles are unclear. There are also 5 *MIR172* genes. Genes are represented as black boxes. Floral integrator genes are represented as orange boxes. Positive relationships between genes are shown by arrows, whereas negative relationships are indicated with blunt-ended lines. When these genetic relationships are dependent on the formation of a protein complex, this complex is represented within a circle on the line depicting the relationship. Note that FT protein can move from the leaves to the SAM, where it forms a complex with FD. Genes that are not expressed or absent during a certain stage are coloured in grey. (D) Protein sequence alignment of AP2-LIKE proteins. TOE3 and AP2 contain two AP2 domains that are indicated above the sequences. The asterisks indicate conserved motifs such as YRG and RAYD. Numbers indicate position of the residue after the first methionine. Figure obtained from Jung et al. (2014) (E) Cladogram of the AP2-LIKE transcription factors. This cladogram was generated after pair-wise alignment of sequences obtained from NCBI: APETALA2 (AP2, NP_001190938.1), TARGET OF EAT1 (TOE1, NP_565674.1), TOE2 (NP_001331666.1), TOE3 (NP_201519.1), SCHLAFMÜTZE (SMZ, NP_191059.2) and SCHNARCHZAPFEN (SNZ, NP_850313.2). Local bootstrap probabilities are shown in each branch.

miR172 negatively regulates the expression of the *AP2-LIKE* gene family of flowering-time repressors (Aukerman & Sakai, 2003; Chen, 2004; Mathieu et al., 2009; Schwab et al., 2005). The six *AP2-LIKE* genes [*AP2*, *TARGET OF EAT 1* (*TOE1*), *TOE2*, *TOE3*, *SCHLAFMÜTZE*

(*SMZ*) and *SCHNARCHZAPFEN* (*SNZ*)] encode a family of transcription factors (known as AP2-LIKE, or also referred as euAP2-LIKE) that contain two conserved AP2 DNA-binding domains (Figure 1-2D–E; Weigel, 1995). The founding member of the *AP2-LIKE* family, *AP2*, was initially characterised due to its regulation of floral development, and its loss of function leads to the appearance of stigmoid or carpelloid leaves in the first floral whorl, and the presence of staminoid petals (Bowman et al., 1989; Jofuku et al., 1994). However, subsequent reports showed that *ap2* mutants are pleiotropic and have additional phenotypes including early flowering, larger seeds, disturbed fruit development and smaller meristems (Ohto et al., 2005; Ripoll et al., 2011; Würschum et al., 2006). The *ap2* mutants flowered early in terms of both reduced leaf number and early bolting (Ó'Maoiléidigh et al., 2021; Ohto et al., 2005; Yant et al., 2010). *SMZ* was identified via an activation-tagging screen for late-flowering plants, and subsequently led to the characterisation of its homologue *SNZ* (Mathieu et al., 2009; Schmid et al., 2003). An activation-tagging strategy was also used to identify the late-flowering *early activation tagged dominant* (*eat-D*) mutant, which was shown to overexpress *MIR172B* and to exhibit the altered floral development and early flowering that are characteristic for *ap2* mutants (Aukerman & Sakai, 2003). This finding motivated the characterisation of the three further members of the *AP2-LIKE* family, whose sequence shared complementarity with the miRNA isoform encoded by *MIR172B,* and these genes were named *TOE1, TOE2* and *TOE3*. The function of *TOE1* as a repressor of flowering was demonstrated by the early flowering of the *toe1-2* mutant under LDs and the late flowering of the *toe1-D* line (Aukerman & Sakai, 2003). Moreover, the *toe2* mutant is early flowering, especially when combined with *toe1* (Aukerman & Sakai, 2003; Jung et al., 2007). The constitutive expression of *TOE2, SMZ, SNZ* or *AP2* from heterologous promoters leads to late flowering (Chen, 2004; Jung et al., 2007); however, this was not the case for *TOE3*-overexpressing lines, which flowered at a comparable time to wild type, as did *toe3* mutants (Jung et al., 2014). A late-flowering phenotype was only reported when a miR172-resistant version of TOE3 (rTOE3) was overexpressed from the *35S* promoter. In light of the defective development of flowers of rTOE3-overexpressing plants, *TOE3* has been implicated to regulate other developmental functions, such as floral development (Jung

et al., 2014; Schwab et al., 2005). Notably, the effects of *AP2-LIKE*-overexpressing lines on flowering time were enhanced when miR172-resistant versions of these genes were expressed from heterologous, constitutively active promoters (Chen, 2004; Jung et al., 2014; Mathieu et al., 2009; Schwab et al., 2005). The early flowering of higher-order mutants such as *toe1 toe2*, *smz snz*, *smz snz toe1 toe2* and the sextuple mutant for all six *AP2-LIKE* genes demonstrates that members of the *AP2-LIKE* gene family redundantly regulate flowering time (Figure 1-2A–C; Aukerman & Sakai, 2003; Mathieu et al., 2009).

AP2 is expressed in young floral primordia and later in specific regions of developing flowers (Wollmann et al., 2010; Würschum et al., 2006). The mRNA of all *AP2-LIKE* genes has been reported to be present in leaves to different extents (Mathieu et al., 2009; Schwab et al., 2005). Moreover, AP2 protein accumulates at the SAM during the vegetative stage, and the abundance of the protein becomes greatly reduced after floral transition (Ó'Maoiléidigh et al., 2021; Sang et al., 2022). In plant apices, AP2 has been shown to bind the regulatory region of flowering-time genes, including *SOC1*, *AP1* and *MIR172B* (Yant et al., 2010). Moreover, AP2 represses transcription of other flowering genes, such as *FUL.* Information about the genomic regions bound by SMZ is available, and SMZ shares common gene targets with AP2 (Mathieu et al., 2009). Furthermore, SMZ and TOE1 bind the regulatory region of *FT* (Mathieu et al., 2009; B. Zhang et al., 2015) and TOE1 and TOE2 regulate *FT* expression by directly interacting with CO (Du et al., 2020). This link between *AP2-LIKE* genes and *FT* expression is consistent with the aforementioned function of miR172 in regulating *FT* expression in leaves. In summary, the *AP2-LIKE* genes are negative regulators of flowering time because they directly repress the expression of positive regulators of flowering time (Figure 1-2A–C).

Clustered regularly interspaced short palindromic repeats [CRISPR/CRISPR-associated protein 9 (Cas9)] technology has allowed mutation of each of the five *MIR172* genes to assess their contribution to the regulation of flowering time (Lian et al., 2021; Ó'Maoiléidigh et al., 2021). Flowering-time analyses have demonstrated that *MIR172A*, *MIR172B* and *MIR172D* are the main regulators of flowering time among the *MIR172* genes. This is because similarly to plants that overexpress a *MIM172* mimicry construct, *mir172* mutants are late flowering

(Todesco et al., 2010). Notably, the *mir172a-2 b-3 d-3* mutant flowered as late as the quintuple *mir172a-2 b-3 c-1 d-3 e-1* mutant. To analyse the function of *AP2* in the regulation of flowering time downstream of miR172, the quadruple *mir172a-2 b-3 d-3 ap2-12* mutant was generated and its flowering time was measured. The *mir172a-2 b-3 d-3 ap2-12* mutant flowered earlier than *mir172a-2 b-3 d-3*, which provides evidence that miR172 regulates flowering time partly by negatively regulating *AP2* gene expression. Due to the high sequence similarity between the miR172 isoforms and their binding sites in the mRNA of the *AP2-LIKE* genes, mRNA cleavage is expected to be the major mechanism by which miR172 regulates its targets and this was demonstrated via *in vitro* assays (Schwab et al., 2005). Nevertheless, Chen, (2004) provided evidence for translational inhibition as a major mechanism of *AP2* repression by miR172. Similarly, the mRNA levels of *AP2, TOE1* and *TOE2* were similar in *eat-D*, whereas their protein levels were greatly reduced (Aukerman & Sakai, 2003). Currently, the relative relevance of transcript cleavage or translational inhibition in the repression of *AP2-LIKE* gene expression by miR172 remains unclear.

1.2.4 The repression of *AP2-LIKE* by miR172 is widely conserved in the plant kingdom

The identification of miR172 and its corresponding targets in other species indicates the ancient origin of this small RNA (reviewed in Zhu & Helliwell, 2011). A microarray designed to assess changes in miRNA accumulation in Arabidopsis was used to detect the presence of different miRNAs in other species (Axtell & Bartel, 2005). In addition to being present in Arabidopsis, miR172 was detected in the core eudicot *Nicotiana benthamiana,* the monocot *Oryza sativa*, the magnoliid *Liriodendron tulipifera*, the gymnosperm *Pinus resinosa* and in the fern *Ceratopteris thalictroides*, but it was not detected in the lycopod *Selaginella uncinata*, the moss *Polytrichum juniperinum*, nor in wheat (*Triticum aestivum*). Considering the sensitivity of the assay to nucleotide substitutions as well as the limitations in the sampling of material from the different species, the authors concluded that the list of species in which miR172 was conserved might be an underestimation of the actual extent of its conservation. In fact, miR172

has been predicted to be present in wheat (Yao et al., 2007). Axtell & Bartel, (2005) also validated the ability of miR172 to cleave its targets in gymnosperms and ferns via 5' RACE, using gene-specific oligonucleotides. These data constitute evidence for the antiquity and conservation of miR172.

The miR172 genes and their corresponding *AP2-LIKE* targets have been characterised and validated in rice (*Oryza sativa)* and poplar (*Populus trichocarpa;* reviewed in Jones-Rhoades et al., 2006). Moreover, the function of miR172 in maize, rice and barley has been related to the regulation of phase transition and the determination of floral organ identity. *Glossy15* (*gl15*) is an *AP2-LIKE* gene in maize that is involved in the juvenile-to-adult transition, due to the precocious development of adult phenotypes in epidermal cells of *gl15-m1* mutants (Moose & Sisco, 1994) in which the *gl15* gene is disrupted because of the insertion of a *defective Suppressor-Mutator* (*dSpm*) element. The appearance of revertant sectors in this mutant indicated that *gl15* acts in a cell-autonomous manner (Moose & Sisco, 1996). Later reports identified an inverse correlation between maize miR172 accumulation and *gl15* expression, and the cleavage site in *gl15* was defined by 5' RACE mapping (Lauter et al., 2005). Furthermore, the maize *tasselseed4* (*ts4*) mutant exhibits increased branching in the distal portion of the inflorescence, as well as feminization of the tassel, because after the initial bisexual nature of spikelet development, pistils usually do not abort and male organs do not develop (Chuck et al., 2007). The *ts4* gene was cloned via chromosome walking and was annotated as *zma-MIR172e.* The additive phenotypic effect of the *ts4* and *gl15* mutations suggested that *gl15* is unlikely to be a target of *ts4.* However, mutation of the *AP2-LIKE* gene *indeterminate spikelet 1* (*ids1*) suppressed to a large extent the developmental defects of *ts4* tassels. Moreover, the *Ts6* mutation, which caused random phyllotaxy at the floral meristem that resembled that of *ts4* mutants, was found to be to a miR172-resistant version of *ids1*. One of the potential targets of maize miR172 identified in Chuck et al. (2007) was characterised due to its high sequence similarity to *ids1*, and was named *sister of ids1* (*sid1;* Chuck et al., 2008). The single *sid* mutant did not exhibit a mutant phenotype; however, in combination with *ids1*, the number of tassel branches was reduced, which led to reduced seed set (Chuck et al.,

2008). Notably, the *ZmRap2.7* gene, which is closely related to *TOE1*, has been related to flowering time in maize, because its overexpression leads to late flowering (Salvi et al., 2007).

In rice, cleavage of *AP2-LIKE* genes by miR172 was reported to occur in a tissue-specific manner (Zhu et al., 2009). The overexpression of rice mir172b leads to several effects that include a delay in the transition from spikelet meristem to floral meristem, as well as developmental defects in floral organ determination. Importantly, the phenotype of a rice mutant for the *AP2-LIKE* gene *SUPERNUMERARY BRACT* is similar to that of plants overexpressing mir172b (Lee et al., 2007). In barley, the *Cleistogamy 1* (*Cly1*) locus, which regulates flower opening during the period of pollen release, was found to encode an AP2-LIKE transcription factor (later named *HvAP2*; Nair et al., 2010). The causal difference between cleistogamy (non-open flower) and non-cleistogamy (open flower) was found to reside in the miR172-binding-site, which determined the resistance or sensitivity of *Cly1* to miR172 regulation. The studies described in this section provide evidence for the conservation of the repression of *AP2-LIKE* genes by miR172, and for the involvement of the *AP2-LIKE* gene family in the regulation of reproductive development in many different species.

1.3 The SAM undergoes doming during floral transition

1.3.1 The SAM contains a stem-cell niche

The aerial growth of plants is dependent on the stem cells at the SAM, which is the site of integration of signals that regulate the transition to reproductive development. This involves a change of identity of the SAM from a vegetative meristem that continuously forms leaves to an inflorescence meristem that continuously initiates flowers. The SAM is organised into several functional domains (Figure 1-3A–B; reviewed in Fuchs & Lohmann, 2020). The two most apical layers, which are referred to as L1 and L2, constitute two clonal layers of cells that divide anticlinally (i.e. perpendicular to the outer surface). The cell layer that subtends the L1 and L2 is called L3 and contains cells that can divide periclinally (i.e. parallel to the outer surface) as well as anticlinally. The SAM can alternatively be divided into two zones along the central–radial axis: the central zone (CZ) and the peripheral zone (PZ), and the rib meristem lies

beneath the CZ. The CZ contains a pool of stem cells that continuously divide and displace cells laterally into the peripheral zone (PZ) or basally into the rib meristem. The fate of cells in plants relies on local signals rather than lineage cues. Cells in the PZ differentiate into lateral organ primordia in response to specification signals and those in the rib meristem differentiate into the vasculature.

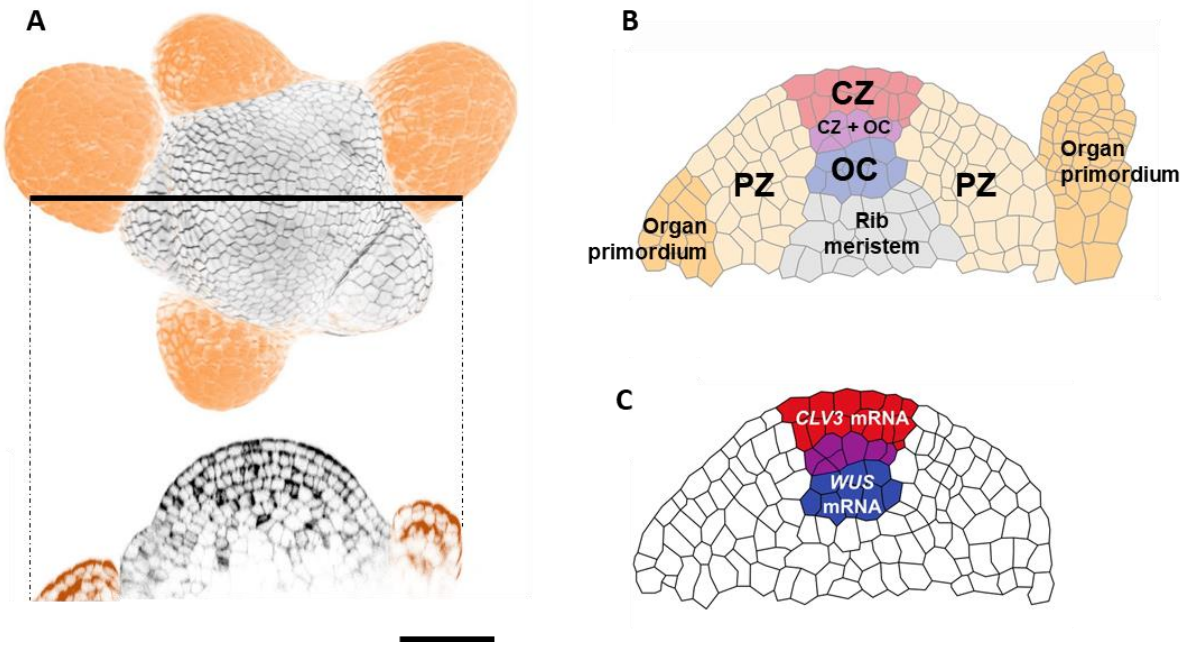

Figure 1-3. The zonation of the shoot apical meristem of Arabidopsis.

(A) Top and lateral view of an inflorescence shoot apical meristem (SAM). The continuous black line of the top view indicates the plane in which the lateral view was generated. Developing flowers are coloured in orange. The meristem together with the youngest developing primordia is coloured in black and white. (B) SAM zonation. Acronyms: central zone (CZ), organising centre (OC) and peripheral zone (PZ). Notice an overlap between the CZ and the OC. (C) Expression domains of *CLAVATA 3* (*CLV3*) and *WUSCHEL* (*WUS*). Figures B–C have been adapted from Fuchs & Lohmann, (2020).

The zonation of the SAM has been characterised via histological analyses and the expression of marker genes (reviewed in Kwiatkowska, 2004 & 2008). The maintenance of indeterminacy of the cells within the meristem is enabled by *SHOOTMERISTEMLESS* (*STM*), and consistent with this function, seedlings of *stm* knock-out mutants lack a SAM (Barton & Poethig, 1993; reviewed in Hake, 1996). The expression of *STM* is detectable in embryos at the 32–64 cell stage, and persists in the SAM and axillary meristems (Long et al., 1996). Importantly, *STM* expression is absent at the position of incipient leaf primordia. Cells in the CZ are characterised by the expression of *CLAVATA3* (*CLV3;* Figure 1-3C*;* Fletcher, 1999). Despite being a stem-cell marker, *CLV3* is not essential for stem-cell maintenance, because *clv3* mutants exhibit

enlarged meristems (Clark et al., 1995). The *CLV3* gene encodes a small peptide that binds the ectodomain of CLV1 (Ogawa et al., 2008), which is a receptor kinase that is expressed in the contiguous regions to the CZ in the basal direction (Clark et al., 1997). Similar to *clv3, clv1* mutants exhibit enlarged meristems (Clark et al., 1993; Leyser & Furner, 1992). The domain of *CLV1* expression comprises the organising centre (OC) and overlaps with the expression of one of the main regulators of stem-cell maintenance, namely *WUSCHEL* (*WUS;* Figure 1-3C; Mayer et al., 1998; Schoof et al., 2000). The *wus* mutant was identified from an EMS screen for mutants defective in shoot development, because it fails to maintain a SAM (Laux et al., 1996). Notably, the WUS protein can move from OC cells into CZ cells, where it activates *CLV3* expression (Schoof et al., 2000). Moreover, CLV3 can also move out of the CZ and bind to CLV1, which leads to the repression of *WUS*, thus establishing a feedback loop that is central for stem-cell maintenance at the SAM (reviewed in Uchida & Torii, 2019).

1.3.2 Morphological changes at the SAM are hallmarks of floral transition

During floral transition, the SAM increases in size and acquires its characteristic dome-like shape (reviewed in Kwiatkowska, 2004 & 2008). This process has been described for several flowering species (Bernier, 1988; Lyndon & Battey, 1985), including Arabidopsis (Hempel & Feldman, 1994; Miksche & Brown, 1965; Vaughan, 1951). The increase in the area of the SAM is due to progressive increases in cell number and cell area, and the SAM area reaches a maximum value before the end of floral transition (Kinoshita et al., 2020). Moreover, this maximum area is the result of a disproportionate increase in height in relation to width, which is known as doming. Inductive photoperiods have been reported to positively regulate doming by promoting cell division (Jacqmard et al., 2003), which is consistent with the absence of doming in *ft-10 tsf-1* mutants, at least at the early stages of floral transition (Kinoshita et al., 2020). The involvement of the cell cycle in floral transition has been addressed in Klepikova et al. (2015). Although a change in SAM area is one of the morphological changes that occurs during floral transition, these have also been described by measuring changes in meristem height and width (Jacqmard et al., 2003; Schlegel et al., 2021), or by approximating the shape

of the meristem to a parabola (Gruel et al., 2016; Laufs et al., 1998; Romberger & Gregory, 1977). Moreover, changes in SAM shape have been related to the change in identity and timing of initiation (i.e. plastochron) of lateral organs and to the stem-cell maintenance regulatory network (reviewed in Kwiatkowska, 2004). Despite the characterisation of changes in meristem morphology during floral transition, the regulation of doming and its function remain unclear. Larger meristems show altered phyllotactic patterns because they have increased space for accommodating organs on their periphery during development , and the inhibition field created by a developing organ that prevents the formation of new organs nearby does not scale with meristem size (Landrein et al., 2015; Mirabet et al., 2012). Therefore, increased meristem size has been related to faster organ production, and this might be important during inflorescence development. Similarly, floral primordia may require more space to grow and mature than leaf primordia. The significance of SAM doming for primordia and organ production requires further characterisation.

1.3.3 *AP2* is a positive regulator of meristem size

MIR172 has been proposed to be a negative regulator of inflorescence meristem size because *mir172d* mutants exhibit larger SAMs (Lian et al., 2021). This is consistent with the enlarged meristems of *mir172a-2 b-3 d-3* mutants (Sang et al., 2022). As described above, miR172 downregulates the expression of the *AP2-LIKE* genes. Among the *AP2-LIKE* genes, *AP2* has been described to be a positive regulator of meristem size, in light of the reduced SAM area of *ap2* mutants in the embryo and the inflorescence (Würschum et al., 2006). Moreover, plants carrying a miR172-resistant version of AP2 (rAP2) exhibited larger inflorescence meristems than wild type (Sang et al., 2022). Importantly, the area of the inflorescence meristem of *mir172a-2 b-3 d-3 ap2-12* quadruple mutants was comparable to that of *ap2-12*, which suggests that the function of miR172 in the regulation of meristem area is dependent on AP2. The function of AP2 in regulating meristem size has been related to *AUXIN RESPONSE TRANSCRIPTION FACTOR 3* (*ARF3*) and *WUS* (Sang et al., 2022). However, the similar levels of *WUS* and *CLV3* expression in *ap2-12* and *rAP2* inflorescence meristems as assessed

by *in situ* hybridization suggests that AP2 does not regulate *WUS* function at the level of gene expression (Sang et al., 2022). Moreover, although AP2 protein accumulates in vegetative meristems, the level of AP2 protein in inflorescence meristems is greatly reduced.

1.4 Aims of the dissertation

The overall aim of this dissertation was to use *mir172* mutants and *MIR172* transcriptional reporters to understand better the mechanisms of regulation of floral transition by miR172, particularly at the SAM.

Chapter 2 describes extensive flowering-time analyses of the *ap2-like* mutants, as well as a dissection of the relationship between *MIR172* genes and the photoperiodic pathway. In addition, the regulation of *MIR172* genes by the photoperiodic pathway was assessed by characterising their temporal and spatial patterns of expression in the *ft-10 tsf-1* mutant background.

Chapter 3 describes segmentation analyses and the quantification of meristem morphology, to test the function of *AP2* in the regulation of SAM area and doming during floral transition. Global transcriptome profiling via RNA-Sequencing (RNA-Seq) was used to characterise the genes that are differentially regulated upon *ap2* mutation, which leads to the absence of doming. Confocal imaging of translational reporters was used to characterize the reciprocal repression between *AP2* and *SOC1* at the spatial and temporal levels, and to link this regulation to the coupling of doming and floral transition. Furthermore, I aimed to confirm the functional implications of the regulation of *AP2* expression via miR172 during floral transition.

Chapter 4 describes an RNA-Seq experiment to compare the transcriptomes of dissected plant apices from Col-0 and *mir172a-2 b-3 d-3* plants. This identified candidate genes that might underlie the late flowering of *mir172a-2 b-3 d-3* mutants under SDs. The *TOE2* gene was selected as a candidate, and to characterise its function, the flowering-time of *toe2* was measured and a TOE2-mScarlet-2HA translational reporter line was generated and analysed.

Further experiments aimed to confirm the functional implications of *TOE2* in the regulation of flowering time via *SPL4* and *FT/TSF.*

2 Genetic dissection of the tissue-specific functions of microRNA172 and its *APETALA2-LIKE* targets in controlling floral transition of Arabidopsis

2.1 Introduction

miR172 is a positive regulator of flowering time because it targets transcripts of AP2-LIKE transcription factors, at least some of which are negative regulators of floral transition (Aukerman & Sakai, 2003; Chen, 2004; Jung et al., 2014; Ohto et al., 2005; Schmid et al., 2003). The generation of *mir172* loss-of-function mutants and *MIR172* reporter lines has allowed the identification of which *MIR172* genes are important for the regulation of floral transition (i.e. *MIR172A, MIR172B* and *MIR172D*), as well as determining the expression of these genes in leaves and the SAM, which are relevant tissues for floral transition in inductive photoperiodic conditions (Lian et al., 2021; Ó'Maoiléidigh et al., 2021).

This chapter presents a comparison of the flowering times of mutants in each of the six *AP2-LIKE* genes, to identify which of them are the most important regulators of floral transition. Moreover, flowering-time measurements were used to confirm genetic interactions between components of the photoperiodic pathway and the miR172/AP2-LIKE pathway. For example, analysis of the flowering time of higher-order mutants that contained loss-of-function mutations in components of the florigen activation complex in addition to loss-of-function mutations of either *AP2-LIKE* or *MIR172* genes.

Inductive photoperiods lead to the earlier onset of expression of *MIR172* genes at the SAM (Lian et al., 2021; Ó'Maoiléidigh et al., 2021). To confirm whether the photoperiodic pathway positively regulates *MIR172* expression at the SAM, the *MIR172* reporters that were constructed within the group were introduced into the *ft-10 tsf-1* mutant background to assess any potential differences in their spatial and temporal patterns of expression.

2.2 Results

2.2.1 *AP2, TOE1* and *TOE2* are the most important repressors of flowering time among the *AP2-LIKE* genes

The AP2-LIKE proteins comprise a family of transcription factors that have been proposed to function redundantly as floral repressors (Aukerman & Sakai, 2003; Chen, 2004; Jung et al., 2014; Ohto et al., 2005; Schmid et al., 2003). Nevertheless, the flowering time of loss-of-function mutants of individual *AP2-LIKE* genes has rarely been compared. To define which of the *AP2-LIKE* genes are the most important floral repressors, the flowering time of loss-of-function mutants for each of the six *AP2-LIKE* genes was measured under LDs. The earliest-flowering mutant among the *ap2-like* mutants was *toe1-2,* which on average produced 3.8 fewer rosette leaves and bolted 3.7 days earlier than Col-0 (Figure 2-1A–D). Moreover, *toe1-2* was the only mutant for which the first flower opened earlier than that of Col-0 under these conditions. Previous studies reported no significant reduction in leaf number for some *ap2-like* mutants compared with wild type (Aukerman & Sakai, 2003; Mathieu et al., 2009). Consistent with these reports, not all of the analysed mutants in this study exhibited a reduction in rosette leaf number under LD conditions, and only *ap2-12* exhibited a reduction in cauline leaf number (Figure 2-1C). Similar to the finding of Mathieu et al., (2009), the *smz-2* mutant in this study flowered at a similar time as Col-0. The mutant status of the single *toe3-1* mutant was validated (Supplemental Figure 2-1) and the reduced expression of *TOE3* indicates that *toe3-1* is a partial loss-of-function allele. Similar to other *toe3* alleles (Jung et al., 2014), *toe3-1* mutants flowered at a comparable time to Col-0. However, *toe3-1* mutants on average produced 1.7 rosette leaves more than Col-0 (Figure 2-1B). Notably, although the *snz-1* mutant was reported to flower at a similar time as Col-0 (Mathieu et al., 2009), s*nz-1* flowered later than Col-0 in this analysis. The absence of a late-flowering phenotype in previous analyses of *toe3* mutants led to the suggestion that *TOE3* might function in other developmental processes, such as floral development (Jung et al., 2014). Collectively, these results indicate that under LDs *AP2-LIKE*

genes act as floral repressors to different extents, with *TOE1* being the strongest flowering-time repressor among the *AP2-LIKE* family.

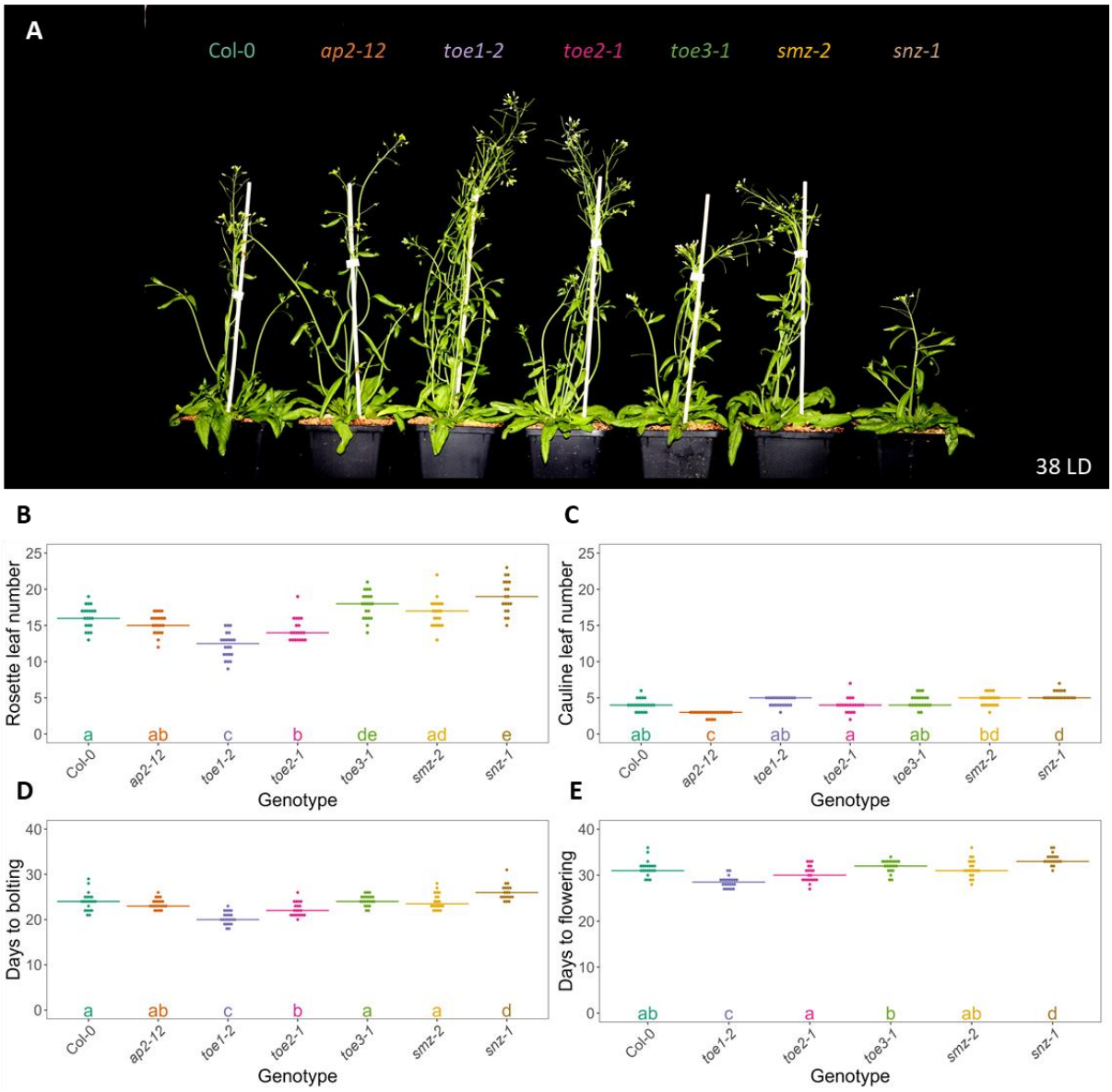

Figure 2-1. The *ap2-12, toe1-2* and *toe2-1* mutants are early flowering under LDs.

(A) Photograph of representative plants of the six *ap2-like* mutants grown for 38 days under long-day (LD) conditions. (B–C) Flowering time of the *ap2-like* mutants according to the parameters: (B) rosette leaf number, (C) cauline leaf number, (D) days to bolting and (E) days to the opening of the first flower. Days to flowering were not scored in *ap2-12* mutants due altered floral development. The horizontal bars represent the median value for each genotype. Significant differences were determined via one-way ANOVA, followed by Tukey post-hoc comparisons ($p < 0,05$). Data sets that share a common letter do not differ significantly. $N = 19–22$.

Some *ap2-like* mutants flower earlier than wild type under SDs (Aukerman & Sakai, 2003; Ó'Maoiléidigh et al., 2021). Moreover, the flowering time of *ap2* mutants in this study was more affected under SDs than LDs (Figure 2-1 and Figure 2-2), which suggests that this gene has a more critical role in the regulation of flowering time under non-inductive photoperiods. The

variation in the measured parameters in this flowering-time experiment was greater than that for other experiments performed under SD conditions (Table 2-1), which influenced the significance of subtle differences in flowering time. Among all the *ap2-like* mutants grown under SDs, only *ap2-12* had a significantly different flowering-time phenotype from Col-0: *ap2-12* produced on average 13.3 fewer rosette leaves and bolted 11.9 days earlier than Col-0 (Figure 2-2A, C). Similar to in LDs, *ap2-12* was the only *ap2-like* mutant in SDs that had fewer cauline leaves than Col-0 (Figure 2-2B). These results indicate that *AP2* is the strongest flowering-time repressor among the *AP2-LIKE* family under SDs.

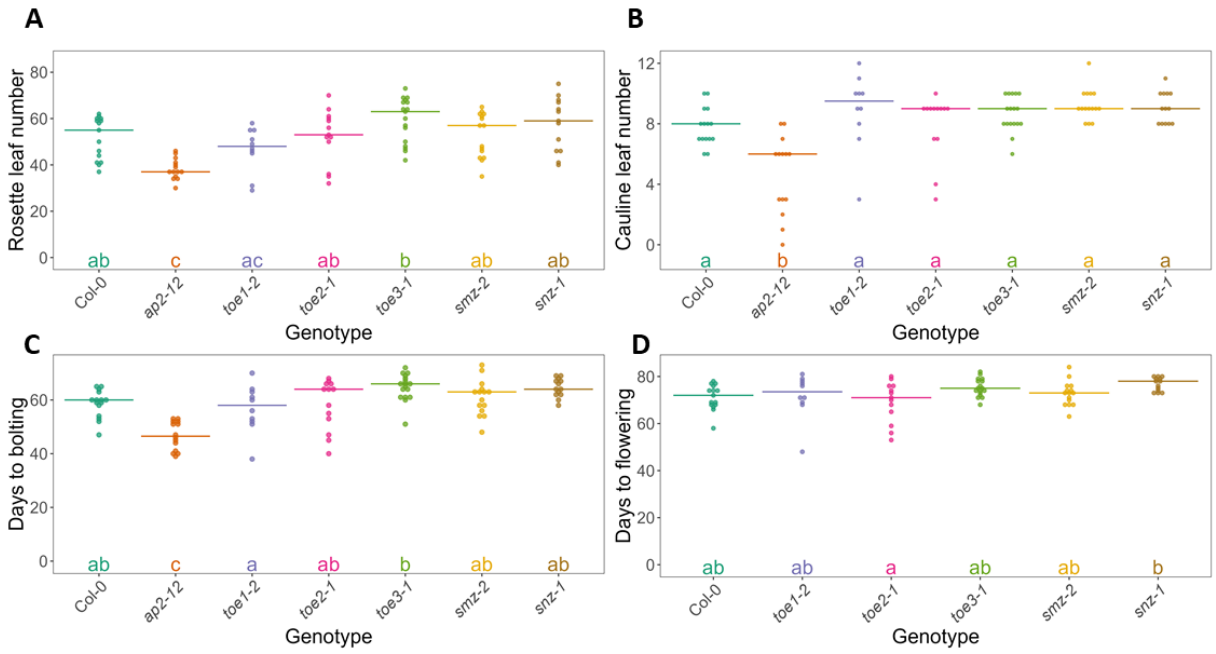

Figure 2-2. *ap2-12* is early flowering under SDs.

Flowering time of the *ap2-like* mutants according to the parameters: (A) rosette leaf number, (B) cauline leaf number, (C) days to bolting and (D) days to the opening of the first flower. Days to flowering were not scored in *ap2-12* mutants due altered floral development. The horizontal bars represent the median value for each genotype. Significant differences were determined via one-way ANOVA, followed by Tukey post-hoc comparisons ($p < 0,05$). Data sets that share a common letter do not differ significantly. $N = 10–17$.

2.2.2 The effect of AP2 on flowering time is partially dependent on the photoperiodic pathway

Some AP2-LIKE transcription factors directly bind *FT* regulatory regions and repress *FT* transcription (Mathieu et al., 2009; B. Zhang et al., 2015), which suggests that AP2-LIKE transcription factors are repressors of the photoperiodic pathway. To test whether deregulation of the photoperiodic pathway contributes to early flowering of *ap2* mutants, the flowering time

of the *ft-10 tsf-1 ap2-12* triple mutant was analysed under LD. The flowering time of the triple mutant was intermediate between that of the early-flowering *ap2-12* mutant and late-flowering *ft-10 tsf-1* mutant on the basis of rosette leaf number, cauline leaf number and days to bolting (Figure 2-3A and C). This suggests that the early flowering of *ap2* mutants is partly dependent on the photoperiodic pathway. Notably, the greater rosette leaf number, cauline leaf number and days to bolting of *ft-10 tsf-1 ap2-12* mutants in comparison to Col-0 indicate that *ft-10 tsf-1 ap2-12* is later flowering and that the photoperiodic pathway is required for the early-flowering phenotype of *ap2-12*. This again demonstrates that AP2 negatively regulates flowering time at least partially within the photoperiodic pathway.

The ectopic expression of *FT TSF* in loss-of-function mutants of *AP2-LIKE* genes (specifically, in *toe1-1 toe2-1* double mutants) leads to early flowering in SDs (B. Zhang et al., 2015); however, this has not been analysed in detail genetically. To test for genetic interactions between mutants in photoperiodic pathway components and *ap2-like* mutants in the regulation of flowering under SDs, the flowering time of *ft-10 tsf-1 ap2-12* triple mutant plants was analysed under SDs. Consistent with the results under LDs, the flowering time of *ft-10 tsf-1 ap2-12* under SDs was intermediate between that of *ap2-12* and *ft-10 tsf-1* mutants (Figure 2-3B and D). However, *ap2-12* and *ft-10 tsf-1 ap2-12* produced fewer rosette leaves and bolted earlier than Col-0, indicating that *ft-10 tsf-1 ap2-12* is early flowering under SDs. Although the early flowering of *ap2-12* mutants might be partly due to ectopic activation of the components of the photoperiodic pathway, this represents only one of the mechanisms by which *AP2* regulates flowering time under SDs. Moreover, by contrast to LDs, this mechanism is not required to lead to early flowering of *ap2-12* mutants in comparison to Col-0 in SDs. Taken together, AP2 negatively regulates flowering time under LDs and SDs, and under both conditions it reduces the activity of photoperiodic pathway genes.

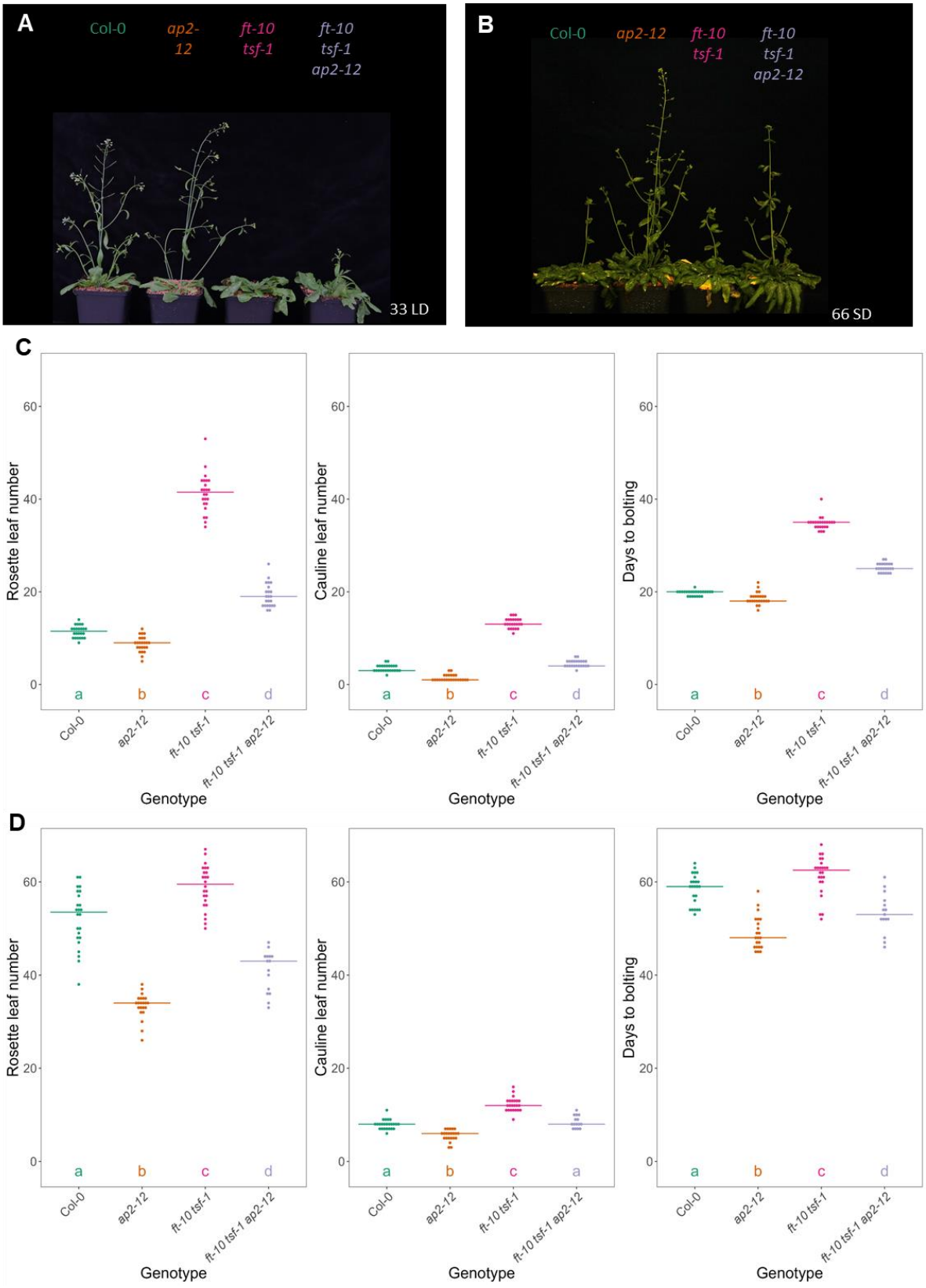

Figure 2-3. The regulation of flowering time by AP2 is partially dependent on the photoperiodic pathway.

(A–B) Representative plants used in the (A) long-day (LD) and (B) short-day (SD) flowering-time analyses. The age of the plants is indicated in the lower right corner. (C–D) Rosette leaf number, cauline leaf number and days to bolting under (C) LDs and (D) SDs. The horizontal bars correspond to the median value for each genotype. Significant differences were determined via one-way ANOVA, followed by Tukey post-hoc comparisons ($p < 0,05$). Data sets that share a common letter do not differ significantly. N = 15–24.

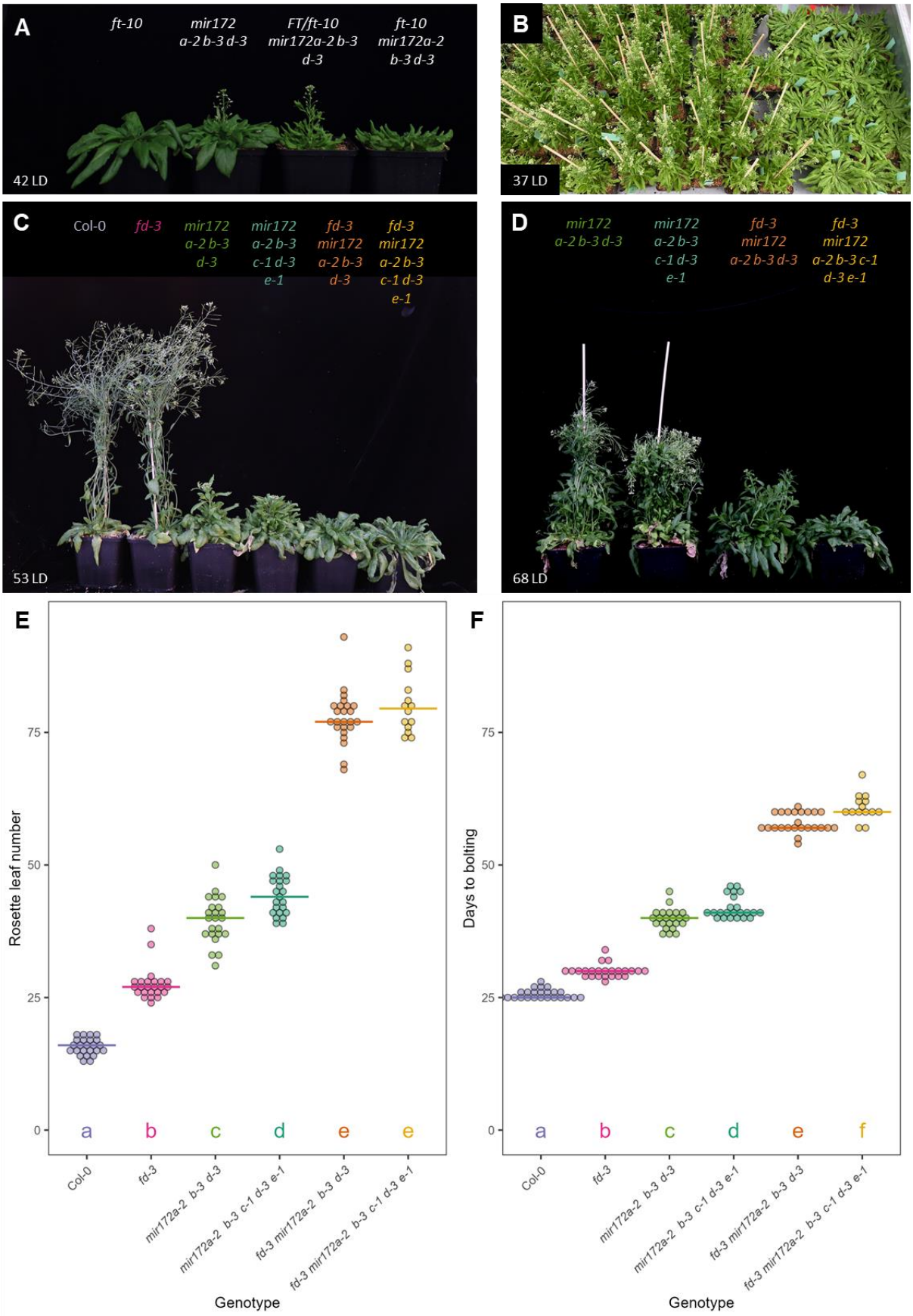

Figure 2-4. miR172 regulates flowering time independently of the photoperiodic pathway.

(See description in the next page)

Flowering-time analysis of higher-order *mir172* mutants combined with mutants in components of the photoperiodic pathway. Images A and B represent independent experiments. (A) Comparison of the flowering time of the parental lines (*ft-10* and *mir172a-2 b-3 d-3*) with that of *ft-10 mir172a-2 b-3 d*-3. The age of the plants is indicated at the lower left corner of the images. *ft-10 mir172a-2 b-3 d-3* plants had not bolted at the time the picture was taken. (B) Flowering time of segregating progeny of the *FT/ft-10 mir172a-2 b-3 d-3* line. The plants with sticks are homozygous or heterozygous for the wild-type allele of *FT*. (C–F) Flowering-time analysis of *fd-3 mir172a-2 b-3 d-3* and *mir172a-2 b-3 c-1 d-3 e-1* higher-order mutants. (C–D) Representative photographs of different genotypes. The age of the plants is indicated at the lower left corner of each picture. (E–F) Flowering time measured by (E) rosette leaf number or (F) days to bolting. The horizontal bars correspond to the median of each genotype. Significant differences were determined via one-way ANOVA, followed by Tukey post-hoc comparisons ($p < 0,05$). A common letter between two data sets indicate no significant differences. $N = 14–24$.

2.2.3 miR172 also regulates flowering time independently of the photoperiodic flowering pathway

miR172 is a major negative regulator of the expression of *AP2-LIKE* genes (Aukerman & Sakai, 2003; Chen, 2004; Schwab et al., 2005). Because *AP2* function is influenced by the photoperiodic pathway, I tested whether the photoperiodic pathway is also required for the regulation of flowering time by miR172. For this, the aim was to analyse the flowering time of *ft-10 tsf-1 mir172a-2 b-3 d-3* and *ft-10 tsf-1 mir172a-2 b-3 c-1 d-3 e-1* mutants, as well as that of *fd-3 mir172a-2 b-3 d-3* and *fd-3 mir172a-2 b-3 c-1 d-3 e-1* mutants. The generation of the *ft-10 tsf-1 mir172a-2 b-3 d-3* mutant is ongoing, but preliminary data showed that *ft-10 mir172a-2 b-3 d-3* flowered later than *ft-10* and *mir172a-2 b-3 d-3* (Figure 2-4A and B). This synergistic effect on the flowering time of higher-order mutants is consistent with that observed on the flowering time of *fd-3 mir172a-2 b-3 d-3* and *fd-3 mir172a-b-3 c-1 d-3 e-1* mutants, which both flowered later in terms of rosette leaf number and days to bolting in comparison with *fd-3, mir172a-2 b-3 d-3* and *mir172a-b-3 c-1 d-3 e-1* plants (Figure 2-4C–F). Consistent with the partly photoperiod-dependent action of *AP2*, miR172 probably also acts partly independently of the photoperiod pathway. This is consistent with the regulation of flowering time by miR172 under non-inductive SDs, as shown by the late flowering of *mir172a-2 b-3 d-3* triple mutants and *mir172a-2 b-3 c-1 d-3 e-1* quintuple mutants (Lian et al., 2021; Ó'Maoiléidigh et al., 2021). Taken together, the results show that miR172 impacts flowering time partly dependent on the photoperiodic pathway, but also independently of photoperiod.

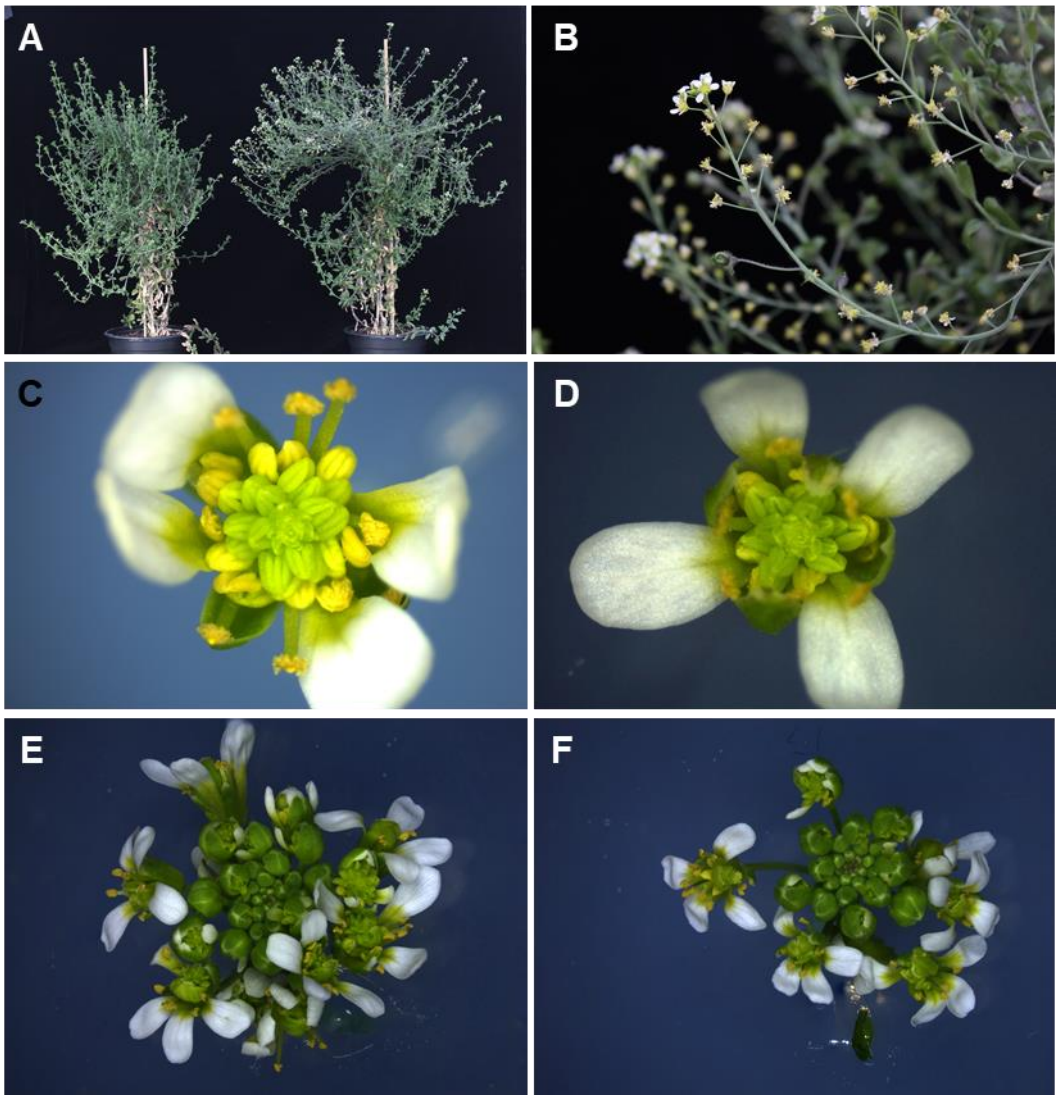

Figure 2-5. Synergistic interaction between inactivation of the photoperiodic pathway and miR172 mutations.

(A–C) The phenotype of 100-LD-old *ft-10 MIR172A/mir172a-2 b-3 d-3* plants. (A) Mature plants in Ø 15 cm pots. (B) Detail of the axillary shoots. (C) A close-up of a representative flower. (D) A representative flower of a *fd-3 mir172a-2 b-3 d-3* quadruple mutant plant. (E–F) Secondary inflorescences from (E) *fd-3 mir172a-2 b-3 d-3* and (F) *fd-3 mir172a-2 b-3 c-1 d-3 e-1* mutants.

In addition to showing a late-flowering phenotype, the higher-order mutants that containing *mir172* mutations as well as loss-of-function of the main regulators of the photoperiodic pathway showed defects in floral development (Figure 2-5). These floral phenotypes included floral indeterminacy, with the presence of additional whorls of stamens and carpels, as well as a mass of undifferentiated cells at the centre of the flower. Many of these alterations in floral development were also reported in plants that overexpress miR172-resistant versions of *AP2-LIKE* genes (Chen, 2004; Jung et al., 2014; Schwab et al., 2005). This suggests that miR172 and FT/FD (as well as TSF/FD) redundantly repress the expression of *AP2-LIKE* genes.

Moreover, *ft-10 tsf-1 ap2-12* mutants flower earlier than *ft-10 tsf-1* (Figure 2-3), which suggests that the late-flowering phenotype of this double mutant could be partly explained by increased AP2 activity. Taken together, these data constitute preliminary evidence that both miR172 and the photoperiodic pathway redundantly repress *AP2-LIKE* genes, which ultimately impacts on flowering time and floral development.

2.2.4 FT and TSF positively regulate *MIR172* expression

The analysis of plants carrying *ft-10 tsf-1* and *mir172* mutations suggested that FT/TSF lead to the downregulation of *AP2-LIKE* gene expression, which can occur in both a miR172-dependent and miR172-independent manner. To understand how *MIR172* genes are regulated by FT/TSF, *MIR172* transcriptional reporter constructs were introduced into the *ft-10 tsf-1* mutant background. Because some *MIR172* genes are expressed at the SAM during floral transition, the effect of the *ft-10 tsf-1* mutations on *MIR172* gene expression was evaluated at the SAM via confocal microscopy (Lian et al., 2021; Ó'Maoiléidigh et al., 2021). The onset of expression of *MIR172A* at the SAM in *ft-10 tsf-1* occurred at 10 LD, similar to in the wild-type background (Figure 2-6A), which indicates that FT/TSF are not required for the induction of *MIR172A* expression. At subsequent time points, the domain of *MIR172A* expression expanded laterally and even more basally in the Col-0 background, reaching the developing stem by 17 and 19 LD; however, in the *ft-10 tsf-1* background, *MIR172A* expression was limited to the organising centre and the rib meristem (Supplemental Figure 2-2A). Similar to the expression pattern of *MIR172A* in wild type, expression of *MIR172D* expanded to the periphery of the SAM as well to the most basal regions, including the developing stem (Figure 2-6B; Supplemental Figure 2-2B). In the *ft-10 tsf-1* background, there was a reduction in the expansion of the *MIR172D* pattern of expression and, moreover, the onset of *MIR172D* expression was delayed to 17 LD from 14 LD in Col-0. These results demonstrate that: (1) FT/TSF positively regulate *MIR172* expression (at least that of *MIR172D*) and (2) FT/TSF enhance the expansion of the spatial domain of expression of *MIR172* genes.

The accumulation of miR172 occurs in different plant tissues, reflecting the patterns of expression of *MIR172* genes (Lian et al., 2021; Ó'Maoiléidigh et al., 2021). Because *FT/TSF* transcription is induced in the leaf vasculature by LDs (An et al., 2004; Yamaguchi et al., 2005), the spatial patterns of expression of *MIR172* genes were analysed after floral transition in leaves, as well as in inflorescences and roots via ß-glucuronidase (GUS) staining of plants carrying *MIR172* reporter genes (Ó'Maoiléidigh et al., 2021). As well as being the most broadly expressed *MIR172* gene during floral transition, *MIR172B* was also the most broadly member of the family in leaves (Figure 2-6D). In contrast, *MIR172A* and *MIR172D* expression was more limited and largely confined to the vasculature (Figure 2-6C and E). The three *MIR172A, MIR172B* and *MIR172D* genes were expressed in wild-type roots. The introduction of the *ft-10 tsf-1* mutations did not cause major alterations in the spatial patterns of expression observed in wild type, with the exception of *MIR172D.* In *ft-10 tsf-1* plants, *MIR172D* expression was not observed in roots. These results indicate that whereas FT/TSF are not required for the onset of *MIR172* expression, they positively regulate the expansion of the patterns of expression of *MIR172* genes. Notably, I provide evidence that FT/TSF are required for the early induction of *MIR172D* expression in roots.

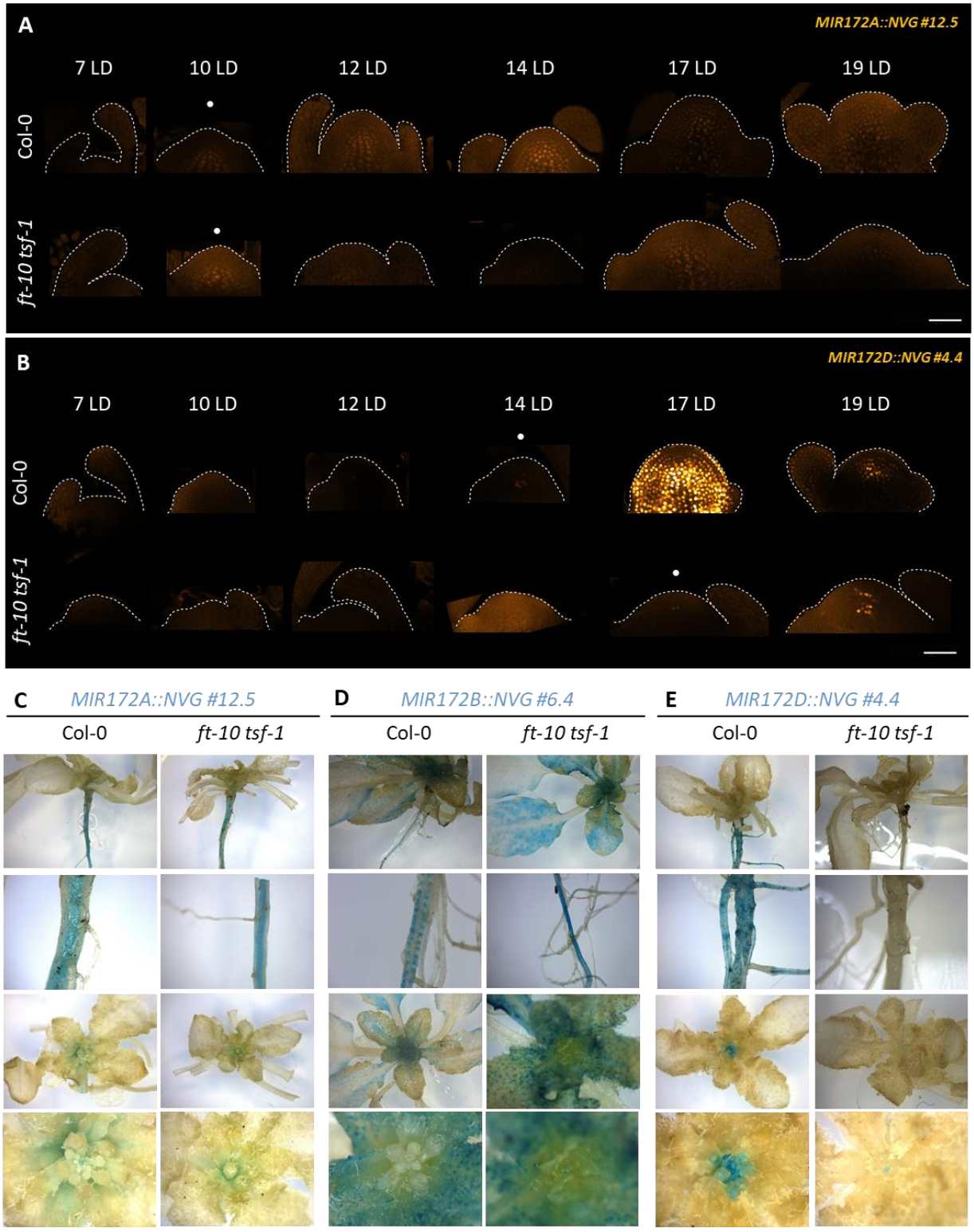

Figure 2-6. The photoperiodic pathway positively regulates *MIR172* expression at the SAM.

(A–B) Pattern of expression of (A) *MIR172A::NVG (NLS, VENUS, GUS) #12.5* and (B) *MIR172D::NVG #4.4* at the shoot apical meristem during floral transition under continuous LD in Col-0 and *ft-10 tsf-1* mutant background. The background of each line is indicated in at the left of each panel. The age of the plant is indicated at the top of each acquisition. A white dot indicates the first time point at which expression of the reporter was detectable at the SAM. The shape of the meristem and lateral organs is indicated with a dotted white line. Scale bar = 50 µm. (C–E) GUS staining of 22-day-old plants grown in LDs containing the (C) *MIR172A::NVG #12.5,* (D) *MIR172A::NVG #6.4* and (E) *MIR172D::NVG #4.4* reporters in the Col-0 and *ft-10 tsf-1* backgrounds. The genotype of each plant is indicated at the top of each column. Each column of images corresponds to the same plant.

2.3 Discussion

2.3.1 The AP2-LIKE transcription factors are repressors of flowering-time

Previous studies measured the flowering time of some single *ap2-like* mutants and showed that they flowered earlier than wild-type plants (Aukerman & Sakai, 2003; Jung et al., 2007; Mathieu et al., 2009; Ó'Maoiléidigh et al., 2021; Ohto et al., 2005; Yant et al., 2010; Zhai et al., 2015; B. Zhang et al., 2015). However, these analyses rarely included all *ap2-like* single mutants, preventing a comparative analysis among the different mutants. In this chapter, the flowering time of loss-of-function mutants for the six *AP2-LIKE* genes was measured. The *ap2* mutant has been reported to flower earlier than wild type on the basis of the number of rosette leaves or total leaves (Ohto et al., 2005). Consistent with this, *ap2-12* mutants were reported to flower with an average 3.5 fewer rosette leaves (Yant et al., 2010) or 1.6 fewer rosette leaves (Ó'Maoiléidigh et al., 2021) than Col-0 under LD, which is consistent with the results in Figure 2-1B and Figure 2-3C. A reduction in cauline leaf number and bolting time was also reported for *ap2-12* in Ó'Maoiléidigh et al. (2021). The *toe1-1* mutant was reported to be early flowering in terms of slightly earlier bolting and fewer rosette leaves than wild type (B. Zhang et al., 2015). Moreover, *toe1-2* mutants were reported to produce approximately 2 rosette leaves fewer (Aukerman & Sakai, 2003; Jung et al., 2007) or 4.3 leaves fewer than wild type (Mathieu et al., 2009), and to bolt earlier than wild type (Zhai et al., 2015). In the growth conditions in this study, *toe1-2* had the strongest effects of all the *ap2-like* mutants on both rosette leaf number and bolting time under LDs, and also led to a reduction in the days to the first open flower (Figure 2-1). The *toe2-1* mutant showed a smaller reduction in rosette leaf number in comparison with wild type than *toe1-2*. This relatively mild phenotype of *toe2-1* is similar to that reported in Zhai et al., (2015) and was not statistically significant in other analyses (Aukerman & Sakai, 2003). However, in the conditions in this study, *toe2-1* mutants bolted at a time point intermediate between that of Col-0 and *toe1-2*, as was reported in Zhai et al. (2015). Because *toe1 toe2* double mutants flower earlier than both *toe1* and *toe2* single mutants (Aukerman & Sakai, 2003; Jung et al., 2007; Mathieu et al., 2009; Zhai et al., 2015; B. Zhang et al., 2015)

and due to the high sequence similarity between the AP2 domains of *TOE1* and *TOE2*, it is likely that *TOE1* and *TOE2* redundantly regulate flowering time. The *SMZ* and *SNZ* genes were firstly isolated as flowering-time repressors via an activation-tagged screen for late-flowering plants (Schmid et al., 2003). Neither the single *smz-2* and *snz-1* mutants nor the double *smz-2 snz-1* mutants exhibited an early-flowering phenotype in terms of leaf number (Mathieu et al., 2009); in fact, the *smz-2 snz-1* mutations only accelerated flowering when introduced into the *toe1-2 toe2-1* double mutant background. Although in this study no early-flowering phenotype was observed for *smz-2*, *snz-1* mutants were slightly late flowering under LDs, because they produced more leaves, bolted later and opened their first flower later than Col-0. Previous analyses under LDs did not report an early-flowering phenotype for *toe3-2* mutants (Jung et al., 2014). The combination of the *toe3-1* mutation and *ap2-12* into a quadruple mutant background for the other four *AP2-LIKE* genes accelerated flowering; however, no data were available concerning the flowering time of the single *toe3-1* mutant (Yant et al., 2010). In this study, the *toe3-1* allele was demonstrated to be a partial null allele and produced slightly more rosette leaves than wild type. The reproducibility of the observed flowering-time phenotypes of *snz-1* and *toe3-1* mutants should be tested. Moreover, the flowering time of the *toe3-2* mutant could also be tested. If the loss of function of *SNZ* or *TOE3* is confirmed to cause the production of more leaves than wild type, this would indicate that they are not floral repressors but may have a weak effect in promoting flowering.

The early-flowering phenotype of *ap2-12* mutants was more extreme under SDs than under LDs (Table 2-1), which is consistent with previous reports (Ó'Maoiléidigh et al., 2021; Yant et al., 2010). This suggests that the function of *AP2-LIKE* genes in regulating flowering time is more important under SDs than LDs. Nevertheless, flowering-time data for all *ap2-like* mutants under SD were not available. No flowering-time data were previously published for single mutants of *TOE2, TOE3, SMZ* or *SNZ* under SDs. The *toe1-1* mutant was reported to show a reduction in rosette leaf number and bolting time under SDs (B. Zhang et al., 2015), and a mean reduction of 23.4 rosette leaves for *toe1-2* compared with Col-0 was reported in Jung et al. (2007). Although the results in this study showed a mean reduction of 4.9 rosette leaves for

toe1-2 mutants in comparison with wild type, this reduction was less than that for *ap2-12* and was not nearly as severe as that previously reported (Jung et al., 2007). As already mentioned, the variability in flowering time between individuals of the same genotype in this experiment was greater than that in other flowering-time experiments. Therefore, it would be relevant to include the *ap2-like* mutants in future experiments under SD to test the reproducibility of the flowering-time data under SD conditions. The wild-type flowering-time phenotypes of some *ap2-like* mutants does not exclude an involvement in the regulation of flowering time by *AP2-LIKE* genes. An example of this would be the analysis of higher-order mutants, such as the *toe1 toe2* double mutant, in which the presence of the *toe2* mutation accelerates further the reported early flowering of *toe1* mutants, and was observed in both LDs and SDs (Aukerman & Sakai, 2003; Jung et al., 2007; Mathieu et al., 2009; Zhai et al., 2015; B. Zhang et al., 2015).

Among all the *ap2-like* mutants, only *ap2-12* exhibited a reduction in cauline leaf number in LDs and SDs, and this is consistent with previous results (Ó'Maoiléidigh et al., 2021). Notably, as previously described, *snz-1* produced slightly more cauline leaves than wild-type under LDs. Previous studies reported no differences among the number of cauline leaves of *smz-2, snz-1, toe1-2* and *toe2-1* under LDs (Mathieu et al., 2009). Notably, the number of cauline leaves of the quadruple mutant *smz-2 snz-1 toe1-2 toe2-1* was similar to that of Col-0 (Mathieu et al., 2009). Also, the gain-of-function *toe1-2D* line shows an increase in the number of rosette leaves, but the cauline leaf number is unaffected (Jung et al., 2007). The unique relationship between *AP2* and the determination of cauline leaf number is further addressed in Chapter 3.

2.3.2 miR172 and *AP2* functions are influenced by the photoperiod

As discussed previously, *ap2* mutants flower earlier under LDs and SDs. This was previously interpreted as demonstrating that the role of AP2 in repressing flowering is daylength-independent (Yant et al., 2010). Nevertheless, mutations in the photoperiod pathway were shown to delay flowering of *ap2* mutants, for example the leaf number of *ft-10 ap2-12* was intermediate between that of *ft-10* and *ap2-12*, and *soc1-2 ap2-12* leaf number was intermediate between that of *soc1-2* and *ap2-12* (Yant et al., 2010). Moreover, AP2 negatively

regulated several genes that are upregulated in inductive photoperiods, such as *SOC1* or *FUL*. Therefore, *AP2* can have photoperiod-independent effects on flowering time, but its genetic interaction with the photoperiodic pathway and its effect on the expression of components of the photoperiodic pathway suggests that it can also function within the photoperiodic pathway. Furthermore, *TOE1* and *TOE2* can directly bind the regulatory regions of *FT* and repress its expression (Mathieu et al., 2009; B. Zhang et al., 2015). These observations suggest that there is a relationship between *AP2-LIKE* genes and the photoperiodic pathway.

In this study, the genetic relationship between *ap2-12* and *ft-10 tsf-1* mutants in LDs and SDs was analysed. The intermediate leaf number of *ft-10 tsf-1 ap2-12* triple mutants compared to *ap2-12* and *ft-10 tsf-1* under LDs was similar to that reported for *ft-10 ap2-12* double mutants (Yant et al., 2010). The results here have been interpreted by considering that *FT/TSF* are potentially repressed by AP2, consistent with the direct repression of *FT* expression by other AP2-LIKE proteins. From the results, it was concluded that the function of *FT/TSF* is required for *ap2-12* mutants to flower earlier than Col-0 under LDs, but not under SDs. However, because the flowering time of the *ft-10 tsf-1 ap2-12* triple mutant was not comparable to that of *ft-10 tsf-1* or *ap2-12*, this experiment suggests a genetic relationship in which *FT/TSF* negatively regulate *AP2*. In other words, the increased leaf number and bolting time of *ft-10 tsf-1* mutants might be partly explained by an increase in the expression of *AP2* under LDs and SDs, because *AP2* is a repressor of flowering-time under both photoperiodic conditions. To further clarify these relationships between *FT/TSF* and *AP2* requires the quantification of *AP2* expression in the *ft-10 tsf-1* mutant and *FT/TSF* expression in *ap2-12*. It would also be relevant to do this in LDs and SDs, because *FT* is ectopically expressed in *toe1 toe2* double mutants under SDs (B. Zhang et al., 2015).

The characterisation of *ft-10 tsf-1 mir172a-2 b-3 d-3* and *fd-3 mir172a-2 b-3 d-3* mutants might provide evidence for the repression of *AP2-LIKE* genes both by miR172 and the photoperiodic pathway. The combination of mutations for the main components of the photoperiodic pathway with *mir172* mutants had a synergistic effect, leading to later-flowering phenotypes. Moreover, these higher-order mutants exhibited aberrations in floral development that resembled those

of plants that overexpress miR172-resistant versions of *AP2-LIKE* genes (Chen, 2004; Jung et al., 2014; Schwab et al., 2005). Therefore, these results represent evidence for the repression of *AP2-LIKE* genes by miR172, which occurs at the post-transcriptional level, and the photoperiodic pathway, which could occur at the transcriptional level.

FT/TSF might repress *AP2-LIKE* genes by enhancing the expression of factors, such as SOC1 and FUL, that lead to the repression of transcription of *AP2-LIKE* genes and to factors that positively regulate *MIR172* genes. To test the effect of FT/TSF on *MIR172* expression, the expression pattern of reporters for *MIR172* at the SAM in Col-0 and *ft-10 tsf-1* mutant backgrounds were characterised during floral transition by confocal microscopy. Expression of the *MIR172* reporters was detected at the SAM of Col-0 and *ft-10 tsf-1* plants, which suggests that *FT/TSF* are not essential for the expression of *MIR172* genes at the SAM during LDs, and is consistent with the observed expression of these genes at the SAM during SDs (Ó'Maoiléidigh et al., 2021). However, according to the time course performed here, *FT/TSF* induce the expression of *MIR172D* and positively regulate the expansion of the domain of *MIR172A* expression. The expression of *MIR172D* in *ft-10 tsf-1* mutants should also be analysed at additional time points, to understand whether *ft-10 tsf-1* compromise the expansion of the pattern of expression of *MIR172D.*

2.3.3 Understanding the systemic signalling of *FT/TSF*–miR172–*AP2-LIKE*

The *MIR172* and *AP2-LIKE* genes are expressed in several tissues in addition to the SAM (Jung et al., 2007; Lian et al., 2021; Ó'Maoiléidigh et al., 2021). The most broadly expressed *MIR172* gene in leaves in this study was *MIR172B,* which was consistent with previous results (Ó'Maoiléidigh et al., 2021). Importantly, the expression of *FT* in *mir172* mutants, was considerably reduced (Lian et al., 2021; Ó'Maoiléidigh et al., 2021), which suggests that miR172 function in leaves is relevant to repress the expression of *AP2-LIKE* genes, which then negatively regulate *FT.* Since, FT/TSF also activate *MIR172* expression at the SAM, this suggests that miR172 acts both upstream and downstream of FT/TSF. In this chapter, other plant tissues were analysed via GUS staining to analyse the potential positive regulation of

MIR172 expression by *FT/TSF,* similar to that observed at the SAM. In most tissues, *FT/TSF* were not required for *MIR172* expression. However, in roots, no *MIR172D* expression was detected in *ft-10 tsf-1* mutants. These results should be validated using plants grown on agar plates, to avoid potential artefacts due to the manipulation of roots from plants grown on soil. Moreover, it would be relevant to determine whether these differences in *MIR172D* expression result from the translocation of FT/TSF to the roots, a second messenger activated by FT/TSF in leaves and translocated to roots or to the expression of *FT/TSF* in roots. Ultimately, it would be relevant to characterise the roots of *mir172* mutants to understand whether miR172 has a function in root development. An example of involvement of *MIR172* in root development was shown in Díaz-Manzano et al. (2018), were *MIR172* genes were upregulated in the galls formed upon *Meloidogyne javanica* infection.

On the basis of previous reports and the results in this chapter, there is evidence for genetic relationships among *FT/TSF, MIR172* and *AP2-LIKE* genes (Figure 2-7). Future studies should aim to understand the relative importance of these relationships in different plant tissues, as well as to determine which *MIR172* and *AP2-LIKE* genes are involved.

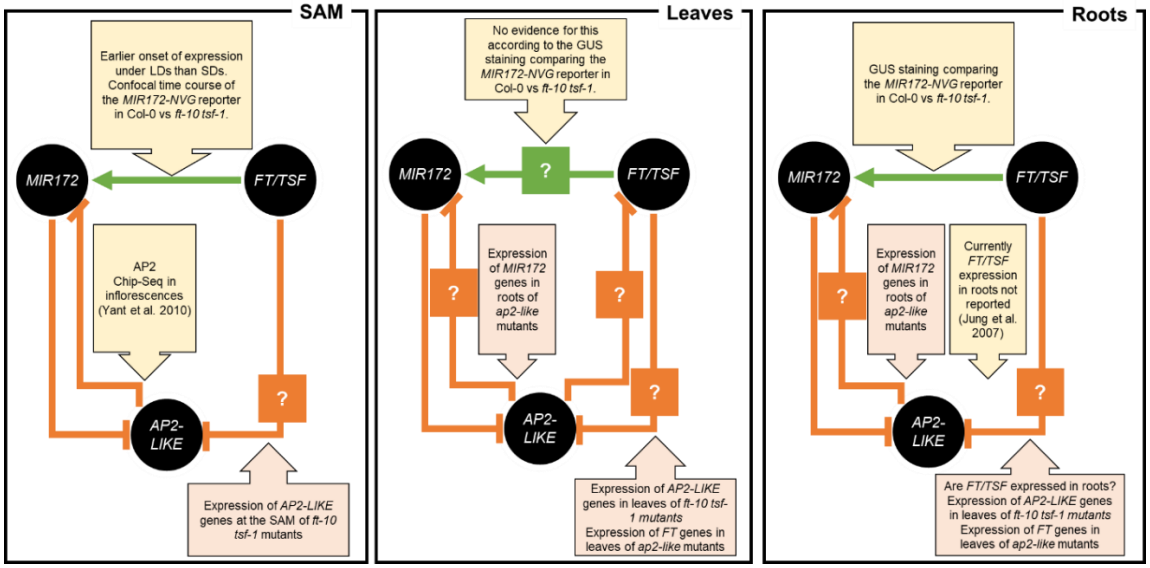

Figure 2-7. Relationship between *FT/TSF, MIR172* and *AP2-LIKE* genes.

The genetic relationships among *FT/TSF, MIR172* and *AP2-LIKE* genes are represented as positive regulations (green) or negative regulations (orange). A box with a question mark shows that a relationship requires further confirmation. The observations on which these relationships are based are placed in yellow boxes. Experimental strategies to confirm the depicted relationships are shown in orange boxes.

Table 2-1. Data for the flowering time experiments described this chapter.

s.d. = standard deviation; n.a. = not applicable, i.e., the measurements were not performed.

Experiment	Genoytpe	*N*	Rosette leaf number		Cauline leaf number		Days to bolting		Days to first open flower	
			Mean	s.d.	Mean	s.d.	Mean	s.d.	Mean	s.d.
Figure 2-1 LD	Col-0	21	16.1	1.59	4.1	0.81	24.0	2.05	31.5	1.72
	ap2-12	21	15.2	1.37	2.8	0.40	23.5	1.12	n.a.	n.a.
	toe1-2	22	12.3	1.75	4.5	0.59	20.3	1.36	28.5	1,.19
	toe2-1	20	14.4	1,.57	4.0	1.03	22.3	1.53	30.2	1.74
	toe3-1	21	17.8	1.83	4.5	0.87	24.2	1.18	32.0	1.36
	smz-2	20	16.8	1.94	4.8	0.85	24.0	1.79	31.5	1.93
	snz-1	19	19.0	2.29	5.4	0.59	26.1	1.75	33.5	1.26
Figure 2-2 SD	Col-0	15	51.5	9.12	7.8	1.26	58.6	5.14	71.1	5.41
	ap2-12	14	38.2	4.48	4.6	2.59	46.7	5.30	n.a.	n.a.
	toe1-2	10	46.6	9.73	8.9	2.51	56.8	8.93	71.8	9.48
	toe2-1	13	52.3	11.60	7.9	2.14	58.2	9.42	69.2	8.69
	toe3-1	17	59.4	9.64	8.7	1.17	64.8	5.01	75.3	3.80
	smz-2	15	52.7	9.65	9.3	1.03	60.9	6.57	72.7	5.19
	snz-1	13	57.5	11.60	9.1	1.04	64.5	3.48	76.8	2.86
Figure 2-3 LD	Col-0	24	11.4	1.28	3.5	0.72	19.8	0.53	n.a.	n.a.
	ap2-12	24	8.75	1.67	1.4	0.65	18.6	1.28	n.a.	n.a.
	ft-10 tsf-1	24	41.3	4.13	13.2	1.07	34.8	1.38	n.a.	n.a.
	ft-10 tsf-1 ap2-12	23	19.2	2.55	4.5	0.73	25.2	0.95	n.a.	n.a.
Figure 2-3 SD	Col-0	24	52.2	6.09	7.9	1.02	58.4	3.27	n.a.	n.a.
	ap2-12	22	33.4	2.70	5.6	1.18	49.0	3.58	n.a.	n.a.
	ft-10 tsf-1	23	59.1	4.68	12.2	1.51	61.7	3.85	n.a.	n.a.
	ft-10 tsf-1 ap2-12	15	40.8	4.51	8.47	1.30	53.3	4.25	n.a.	n.a.
Figure 2-4 LD	Col-0	24	15.8	1.54	n.a.	n.a.	25.7	0.87	n.a.	n.a.
	fd-3	24	27.5	3.05	n.a.	n.a.	30,0	1.23	n.a.	n.a.
	mir172a-2 b-3 d-3	23	39.6	4.37	n.a.	n.a.	39,8	1,88	n.a.	n.a.
	mir172a-2 b-3 c-1 d-3 e-1	23	44.3	3.72	n.a.	n.a.	41,9	2,09	n.a.	n.a.
	fd-3 mir172a-2 b-3 d-3	24	77.8	4.85	n.a.	n.a.	58,0	1,84	n.a.	n.a.
	fd-3 mir172a-2 b-3 c-1 d-3 e-1	14	80.1	5.38	n.a.	n.a.	60,9	2,54	n.a.	n.a.

2.4 Supplemental figures

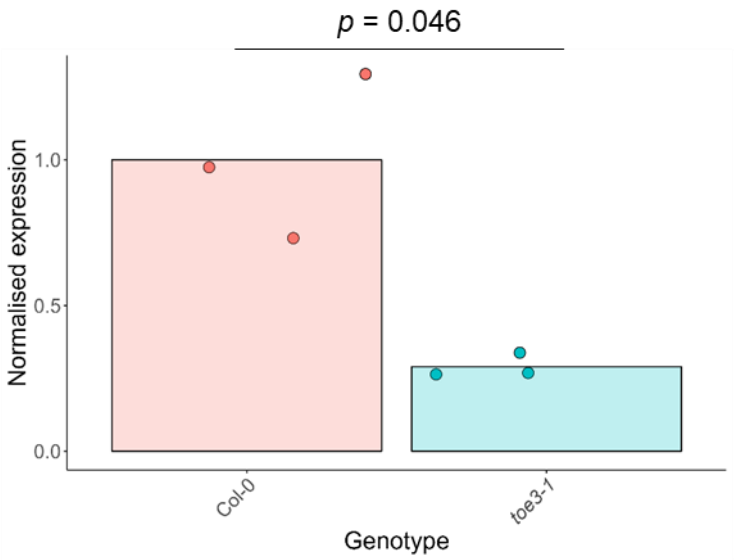

Supplemental Figure 2-1. Quantification of *TOE3* expression in wild type and *toe3-1* allele.

Quantification of *TOE3* expression by RT-PCR normalized to the expression of *PEROXIN4* in main inflorescences harvested after growth for 28 long days. The columns represent the mean values of three biological replicates, whose individual values are also shown. Means were compared with the Student's *t* test (*p*-value = 0.046).

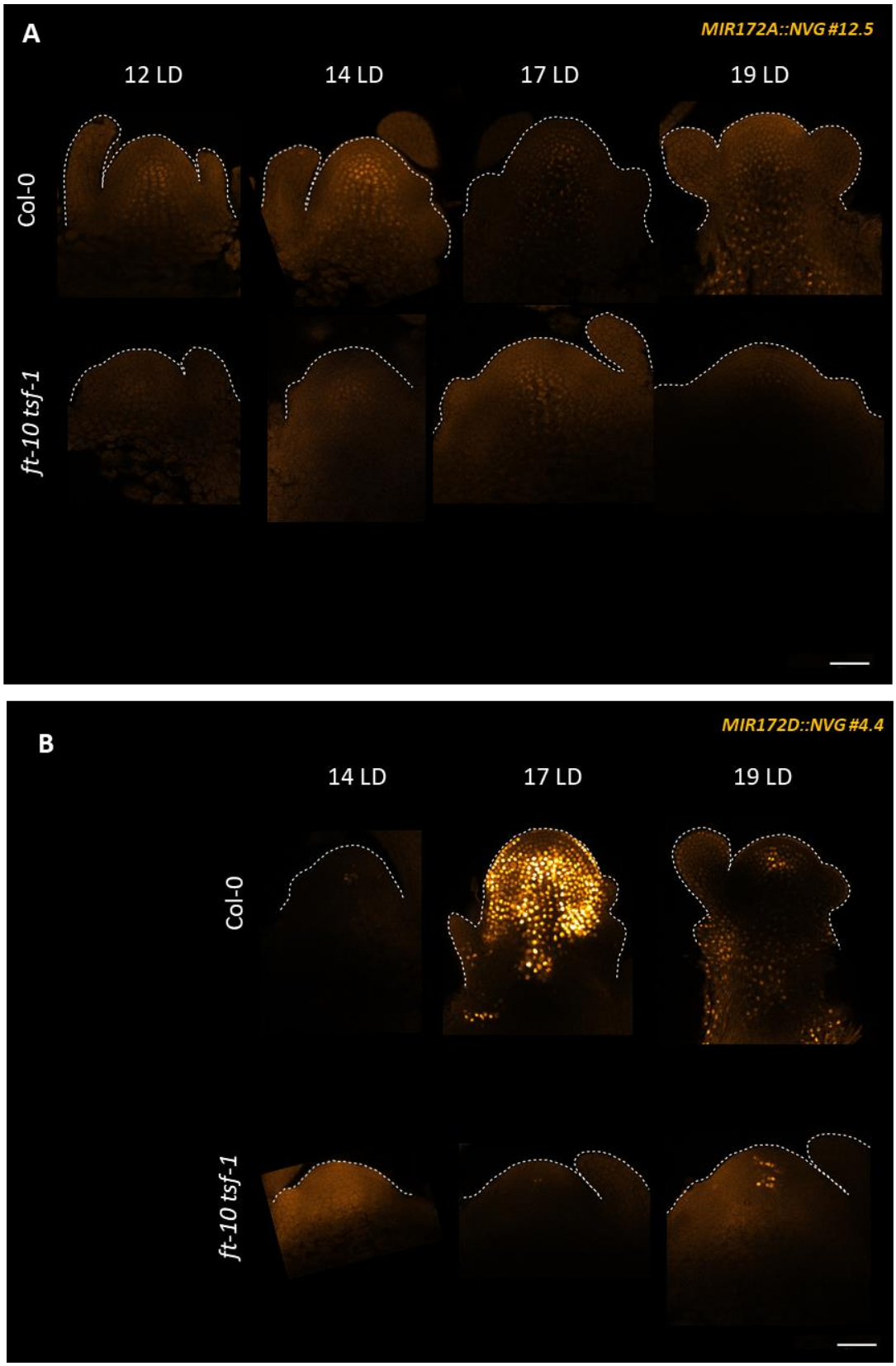

Supplemental Figure 2-2. Selected confocal acquisitions from Figure 2-6 with visible basal regions.

Pattern of expression of (A) *MIR172A::NVG (NLS, VENUS, GUS) #12.5* and (B) *MIR172D::NVG #4.4* at the SAM of Col-0 and *ft-10 tsf-1* plants during floral transition under long days. The age of the plant is indicated at the top of each acquisition. The shape of the meristem and its lateral organs is indicated with a dotted white line. The look-up table scale of the 14 LD *ft-10 tsf-1 image* in panel A has been reduced to make the expression of *MIR172A* at the basal region of the SAM clearer. Scale bar = 50 µm.

3 Mutual repression of *APETALA 2* and *SUPPRESSOR OF OVEREXPRESSION OF CONSTANS 1* couples changes in shoot apical meristem morphology with floral transition in Arabidopsis

3.1 Introduction

The SAM contains a population of stem cells that give rise to all above-ground tissues. Cells are continuously displaced away from the stem cell niche within the SAM towards the meristem periphery where they differentiate and form lateral organs, but the population of stem cells is maintained throughout the life of the plant, which allows continuous organ production (Fuchs & Lohmann, 2020; Uchida & Torii, 2019). The structure and function of the SAM change with plant age and in response to environmental signals. Notably, during the transition to flowering, the SAM changes in size and shape, and initiates flowers instead of leaves (Kinoshita et al., 2020; Tal et al., 2017). The increase in SAM size during floral transition persists in the inflorescence meristem, and likely contributes to the number of flowers formed in the inflorescence (Bommert et al., 2013; Kinoshita et al., 2020; Sang et al., 2022; C. Xu et al., 2015). However, how the changes in SAM shape and identity are synchronized remains unclear.

Exposure of Arabidopsis plants to LDs causes the SAM to transition rapidly from the vegetative to the reproductive state, which involves a radical reprogramming of the SAM transcriptome (Schmid et al., 2003; Torti et al., 2012). As part of this process, genes encoding transcription factors that repress flowering are downregulated, whereas those that encode floral promoters are upregulated. *SOC1*, which encodes a MADS-domain transcription factor, is one of the earliest induced genes, and floral transition is delayed in *soc1* mutants (Borner et al., 2000; H.

Lee et al., 2000; Samach et al., 2000). During floral transition, the shape of the SAM changes. In particular, the height of the SAM increases relative to the width, creating a tall domed shaped meristem. This change in shape, referred to as doming, produces a larger SAM, which reaches a maximum size before the formation of floral primordia, and the mature inflorescence meristem remains larger than the vegetative SAM. Mutations in *SOC1* also delay SAM doming (Kinoshita et al., 2020).

Several mechanisms that influence SAM size have been elucidated (Bartrina et al., 2011; Chickarmane et al., 2012; S. E. Clark et al., 1995; Kosentka et al., 2019; Leibfried et al., 2005; Mandel et al., 2016; Mayer et al., 1998; Schlegel et al., 2021; Würschum et al., 2006; L. Zhang et al., 2021), although which of these regulate SAM doming during floral transition is unclear. The AP2 transcription factor, which confers sepal and petal identity in floral primordia (Bowman et al., 1993; Jofuku et al., 1994), is expressed in the SAM and *ap2* mutants are early flowering and have smaller meristems at the embryonic and inflorescence stages (Sang et al., 2022; Würschum et al., 2006; Yant et al., 2010). By contrast, gain-of-function *AP2* transgenes that are resistant to miR172 increase inflorescence meristem size and cause late flowering (Sang et al., 2022; Würschum et al., 2006). A feedback loop between the WUS homeodomain transcription factor, which is expressed in the organizing centre below the stem cell niche, and the CLV3 peptide, which is expressed in the stem cell niche, maintains the size of the SAM (Brand et al., 2000; S. E. Clark et al., 1995; Fletcher, 1999; Rojo et al., 2002; Schoof et al., 2000). AP2 promotes *WUS* transcription, although it remains unclear how direct this effect is because AP2 increases SAM size when expressed in either the OC or the stem-cell niche (Sang et al., 2022; Yant et al., 2010).

Here, the AP2 and SOC1 transcription factors are shown to mutually repress each other's expression in the SAM of Arabidopsis and this regulatory motif is found to ensure that AP2 induces SAM doming specifically during the early stages of floral transition.

3.2 Results

3.2.1 AP2 positively regulates meristem area during floral transition

AP2 accumulates at the vegetative SAM (Ó'Maoiléidigh et al., 2021; Sang et al., 2022; Wollmann et al., 2010); therefore, whether the meristem size of *ap2* mutants differed from that of Col-0 plants prior to the floral transition was tested. No significant differences in meristem area between *ap2-12* mutants and Col-0 were found after growth for 2 weeks under non-inductive SDs (2 wSD; Figure 3-1). However, AP2 protein was present broadly at the SAM during the early stages of floral transition, before ceasing to be expressed in the inflorescence meristem (Figure 3-2A; Ó'Maoiléidigh et al., 2021). To test whether AP2 contributes to the determination of meristem size during floral transition, plants were transferred after 2 wSD to inductive LD conditions and SAM size was measured at regular intervals for 11 LDs. The size of the Col-0 SAM increased 5.7-fold during the LD treatment (i.e. +11 LD vs 2 wSD) and reached a maximum (mean = 16.5 • 10^3 μm^2) upon doming (+7 LD; Figure 3-1A). The area of the *ap2-12* mutant SAM increased to a much lesser extent than that of Col-0 during exposure to LDs, so that the mean SAM area of *ap2-12* mutants was almost half that of Col-0 at the time of doming. These results indicate that AP2 does not detectably affect meristem size during vegetative development, but is required for the rapid increase in SAM size observed in Col-0 during floral transition after exposure to LDs.

To test whether increasing AP2 levels above those of Col-0 further increases SAM size during floral transition, apices from plants carrying a miR172-resistant version of *AP2* tagged with VENUS (*rAP2-V*), which exhibit enlarged inflorescence meristems (Sang et al., 2022), were analysed. The meristem area of *rAP2-V* plants and Col-0 was comparable at 2 wSD, and the meristem area of *rAP2-V* plants increased at a comparable rate to that of Col-0 during doming (Figure 3-1A). However, *rAP2-V* meristems did not reduce in size after doming (+9 LD and +11), as observed for Col-0 (Kinoshita et al., 2020), but remained at an approximately constant size. Therefore, *rAP2-V* meristems were on average 1.6 times larger than those of Col-0 at +11 LD. Contrary to the absence of AP2 accumulation after floral transition at the SAM, rAP2-

V also accumulated in the inflorescence meristem (Sang et al., 2022), indicating a positive regulation of meristem area by persistent expression of AP2 after floral transition (Figure 3-2A). These results provide evidence for a transient positive role of AP2 in increasing the area of the Col-0 SAM during floral transition.

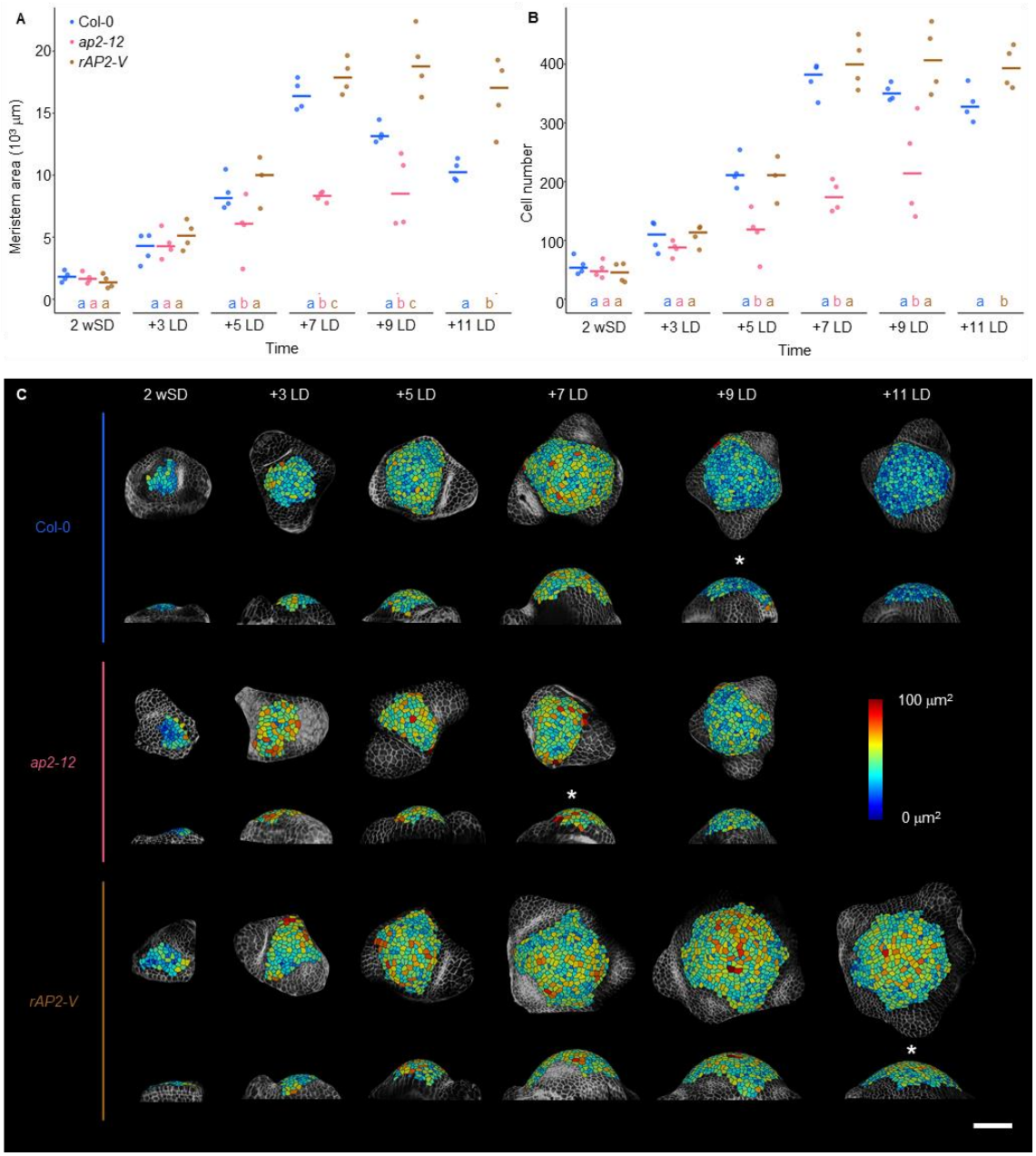

Figure 3-1. AP2 positively regulates SAM size during floral transition.

Segmentation analyses of Col-0, *ap2-12* and *rAP2-VENUS* shot apical meristems (SAMs) from 2-week-old plants grown under short-day (SD) conditions (2 wSD) and then transferred to continuous long days (LDs). (A–B) Quantification of (A) meristem area and (B) cell number. The horizontal bars represent the median value for each genotype. Significant intra-time point differences among genotypes were determined via one-way ANOVA, followed by Tukey post-hoc comparisons ($p < 0.05$). Data sets that share a common letter do not differ significantly. (C) Top and lateral views of the heatmap quantification of cell area in the meristem region. White asterisks indicate the first time point at which floral primordia were detected in the analysis of the corresponding genotype. Scale bar = 50 µm. $N = 4$ (except *rAP2-VENUS* at +5 LD, $N = 3$).

3.2.2 AP2 positively regulates cell proliferation

The enlargement of the SAM during floral transition is associated with increases in cell number and cell area in the epidermis (Kinoshita et al., 2020); therefore, these parameters were measured in *ap2-12* and *rAP2-V* plants during floral transition. In Col-0, cell number and cell area reached a maximum during SAM doming (+7 LD), with a mean of approximately 374 cells and 44 μm^2, respectively (Figure 3-1B, Supplemental Figure 3-1). Fewer cells were present in the SAM epidermis of *ap2-12* mutants, such that the epidermis of *ap2-12* meristems contained roughly half (47%) of the number of cells of the Col-0 meristem epidermis at +7 LD. Considering that the smaller mature inflorescence SAMs of *ap2-12* mutants also exhibit fewer cells than Col-0 (Sang et al., 2022), these results suggest that the reduction in meristem area in *ap2* mutants during floral transition is a consequence of decreased cell number.

The epidermis of Col-0 and *rAP2-V* SAMs had similar cell numbers during floral transition, consistent with the comparable SAM area of these two genotypes, at least until +7 LD (Figure 3-1A–B). However, epidermal cell number and area were greater in *rAP2-V* compared with Col-0 from +9 LD and +11 LD and the difference in median cell area between Col-0 and *rAP2-V* reached 10 μm^2 at +11 LD (Supplemental Figure 3-1). Therefore, extended expression of *rAP2-V* leads to increased cell expansion and cell number after extended exposure to LDs, when AP2 expression decreases in wild-type plants. The primary effect in *rAP2-V* may be an increase in cell division rates, which can also lead to an increase in mean cell size (Jones et al., 2017). Considering both *ap2-12* and *rAP2-V* plants, the primary role of AP2 in controlling SAM size is probably to promote cell proliferation during floral transition.

3.2.3 AP2 is essential for doming

The SAM of *ap2-12* was smaller and differed in morphology compared with the SAM of Col-0, especially at the point of doming of Col-0 (Figure 3-1). To quantify the difference in shape of *ap2-12* and Col-0 SAMs, their height and width were measured (Supplemental Figure 3-2A). The observed morphology of the SAMs could be reconstructed as a parabola (Gruel et al., 2016; Laufs et al., 1998) from the measurements (Supplemental Figure 3-2C–D). The

observed changes in meristem morphology in these reconstructions were comparable to those found by drawing a parabola directly onto the confocal microscope image acquisitions, confirming that the fitted parabolas were accurate (Supplemental Figure 3-3). In agreement with the increase in SAM area during floral transition (Figure 3-1A), both the height and width of the Col-0 SAM increased during the time course (Figure 3-2B–C). However, whereas meristem width roughly doubled (1.7-fold mean increase) from 2 wSD to +7 LD, meristem height showed an almost 4-fold mean increase (3.9; Supplemental Figure 3-2B). In agreement with the similar areas of Col-0 and *ap2-12* mutant meristems until +5 LD, the height and width of the meristems of *ap2* mutants were comparable to those of Col-0 at this stage (Figure 3-2B–C). However, at the doming stage of Col-0 (+7 LD), the width and height of *ap2-12* SAMs were 17.4% and 47.8% lower, respectively, than those of Col-0. By contrast, the height of *rAP2-V* and Col-0 meristems was comparable at all the analysed time points, but *rAP2-V* SAMs were wider than those of Col-0 at the two time points at which *rAP2-V* meristems were increased in area (i.e. +9 LD and + 11 LD; Figure 3-1A, Figure 3-2C). These variations in height and width determine different SAM morphologies during floral transition (Figure 3-2D), and demonstrate that AP2 is required for doming of the Col-0 meristem during floral transition.

3.2.4 AP2 regulates both doming and floral transition

In addition to its involvement in flower development (Chen, 2004; Bowman et al., 1993; Jofuku et al., 1994), *AP2* is a negative regulator of flowering time (Yant et al., 2010). The early flowering of *ap2-12* mutants and the late flowering of *rAP2-V* plants were detected in the microscopic analyses by scoring the time point at which floral primordia were first observed (Figure 3-1C, Figure 3-2D). This occurred in Col-0 at +9LD, 2 LD after the doming stage. Furthermore, cauline leaves of Col-0 were first detected by their characteristic morphology (Supplemental Figure 3-2E–G) at the doming stage. The SAM of *rAP2-V* plants reached its peak doming stage at a similar time to Col-0 (+7 LD), and remained at the same size until +9 LD, suggesting an extended doming stage that is consistent with the longer duration of rAP2-V expression than that of AP2 (Figure 3-2A). However, floral primordia in *rAP2-V* were only

detected at +11 LD, 4LD after it entered the doming stage (+7 LD). The majority of *ap2-12* mutants (>50%) already exhibited floral primordia at +7 LD, which was not accompanied by the changes in meristem size observed in Col-0 plants. These observations demonstrate a temporal sequence of events in Col-0 in which meristem size increases and then decreases prior to floral development, and that these events are uncoupled in *ap2-12* mutants.

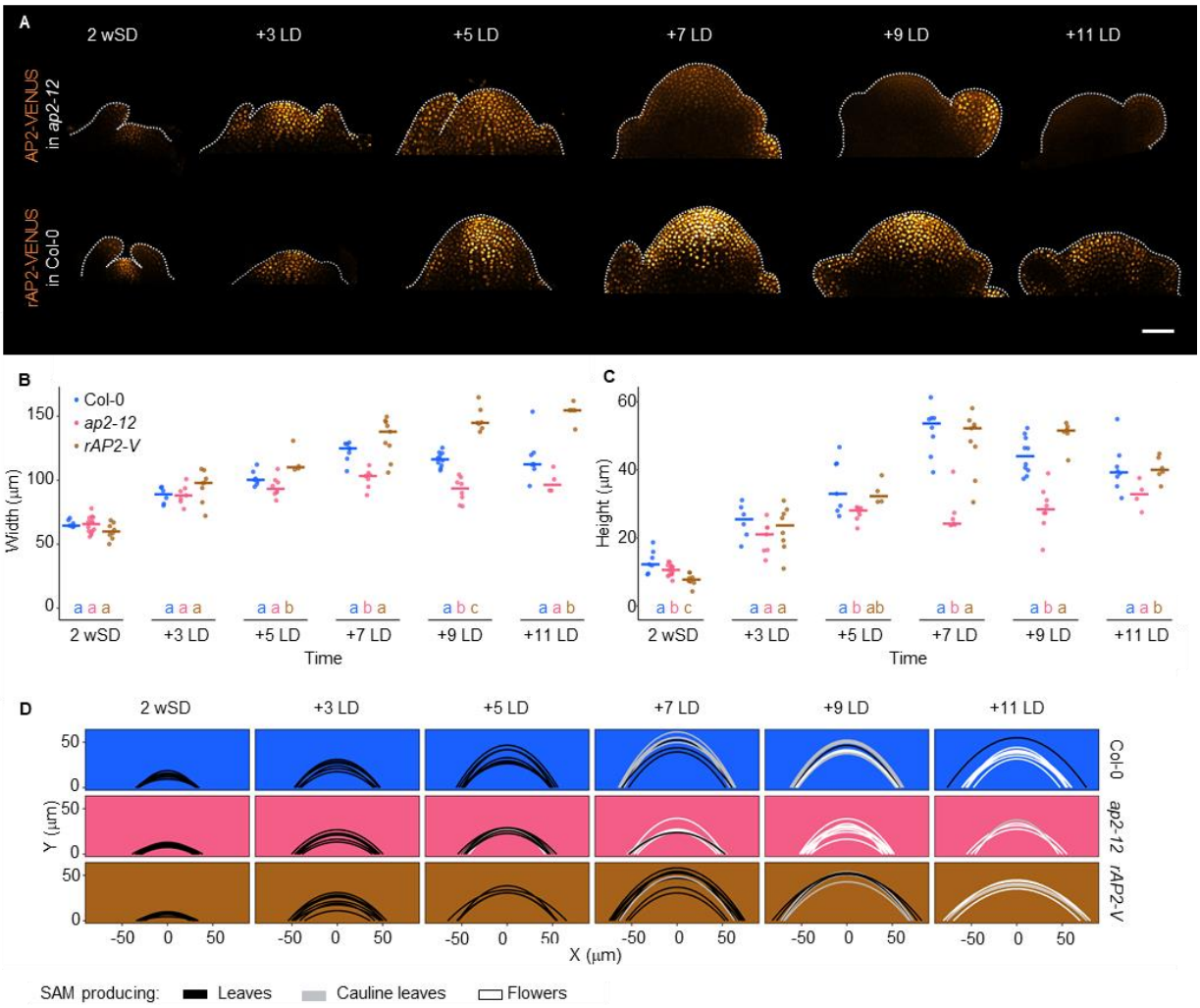

Figure 3-2. AP2 is essential for doming.

(A) Pattern of protein accumulation of *AP2::AP2:VENUS* in *ap2-12* and *AP2::rAP2:VENUS* in Col-0 at the shoot apical meristem (SAM) of 2-week-old plants grown under short day (SD) conditions (2 wSD) and then transferred to continuous long days (LDs). The shape of the acquired meristem and its lateral organs at the meristem periphery is indicated with a dotted white line. Scale bar = 50 µm. (B–C) Measurement of (B) width and (C) height of the SAM in 2wSD-grown plants that were then transferred to LDs. The horizontal bars represent the median value for each genotype. Significant intra-time point differences among genotypes were determined via one-way ANOVA, followed by Tukey post-hoc comparisons ($p < 0.05$). Data sets that share a common letter do not differ significantly. (D) SAM morphology adjusted to parabolas generated by the measurements in B–C. The parabolas are coloured according to the identity of primordia that were formed at the SAM periphery. N = 4–15.

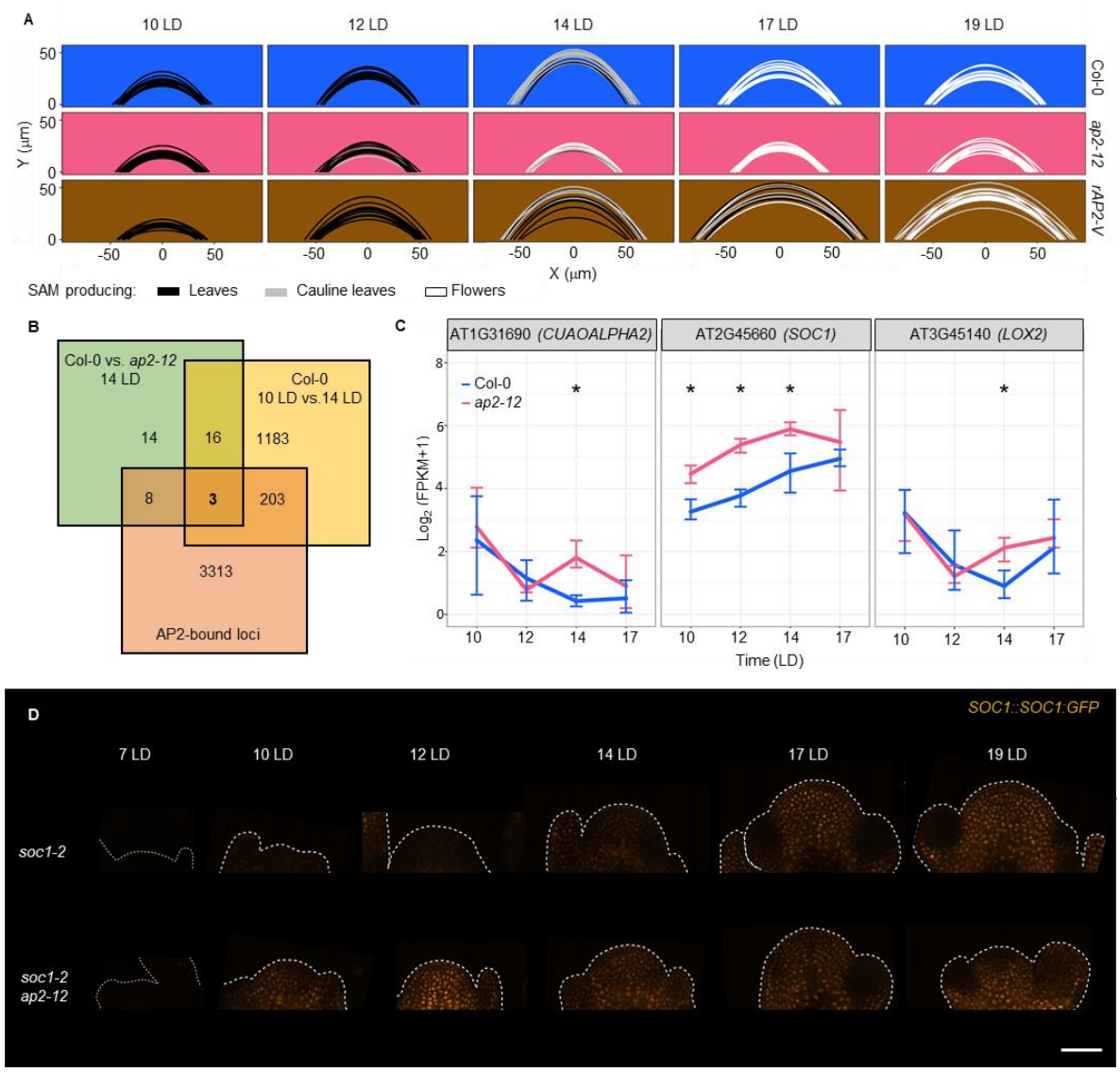

Figure 3-3. AP2 negatively regulates *SOC1* expression at the shoot apical meristem during floral transition.

(A) Shoot apical meristem (SAM) morphology of Col-0, *ap2-12* and *rAP2-VENUS* transgenic plants. The parabolas are coloured according to the identity of primordia that were formed at the SAM periphery. *N* = 10–21. (B–C) Global transcriptome profiling via RNA-Seq of dissected meristem-enriched apices of Col-0 and *ap2-12* plants. (B) Venn diagram showing the overlap between the list of differentially expressed genes (DEGs) at 14 long days (LD) between Col-0 and *ap2-12*, the list of DEGs in Col-0 between 10 LD and 14 LD, and the AP2-bound loci (Yant et al., 2010). (C) Expression profiles of the genes that are present in the three lists compared in B under LDs. The gene symbol is represented on top of each plot. The colour code corresponds to the genotype and is indicated at the top of the panel. Error bars represent the range between the maximum and minimum value among the three used replicates. Statistical differences between Col-0 and the rest of genotypes are is indicated with an asterisk (adjusted *p*-value < 0.05). Gene symbols: *COPPER AMINE OXIDASE ALPHA 2* (*CUAOALPHA2*), *SUPPRESSOR OF OVEREXPRESSION OF CONSTANS 1* (*SOC1*) and *LYPOXYGENASE 2* (*LOX2*). (D) Pattern of protein accumulation of *SOC1::SOC1:GFP* at the SAM in *soc1-2* and *soc1-2 ap2-12* plants under continuous LDs. The shape of the acquired meristem and its lateral organs is indicated with a dotted white line. Scale bar = 50 μm.

The experiments described above involved transferring plants from SDs to LDs, and therefore, to ensure that this regime did not influence the analysis of the role of AP2 in SAM doming, the SAMs of *ap2-12*, Col-0 and *rAP2-V* were analysed under continuous LDs. Col-0 formed a domed SAM at 14 LD (Supplemental Figure 3-4A–B) and the *ap2-12* mutant exhibited a

smaller meristem from 14 LD onwards (Supplemental Figure 3-4B), whereas *rAP2-V* showed an enlarged meristem from 12LD. The smaller meristem size of *ap2-12* mutants was associated again with a reduction in cell number (Supplemental Figure 3-4C). The maximum values of height and width from Col-0 were also detected at 14 LD, confirming that this time point corresponded to the doming stage (Figure 3-3A, Supplemental Figure 3-5). At this time, *ap2-12* SAMs exhibited a mean reduction in height and width of 50% and 25%, respectively, compared with Col-0 SAMs, and therefore *ap2-12* did not form a domed meristem. Moreover, whereas the height of *rAP2-V* and Col-0 meristems was comparable at 14 LD, *rAP2-V* meristems were wider and reached a maximum width at 17 LD, which was 1.4-fold greater than Col-0 meristems. Therefore, doming of the Col-0 meristem occurs during floral transition induced by exposure to continuous LDs or by transfer from SDs to LDs, meristems of *ap2* mutants do not dome under both conditions, and the SAM of *rAP2-V* plants is wider than that of Col-0 at the time of doming.

3.2.5 AP2 negatively regulates SOC1 during floral transition

To understand how AP2 contributes to SAM doming, a global expression analysis was performed by RNA sequencing (RNA-Seq) using apices of Col-0 and *ap2-12* mutants sampled at the same time points used for the phenotypic analysis under continuous LDs (10 LD, 12 LD, 14 LD and 17 LD). This approach yielded 103 genes that were differentially expressed (DEGs) in *ap2-12* compared with Col-0 at one or more time point (Supplemental Table 3-1). To identify candidate genes for regulators of meristem doming, DEGs between domed and non-domed meristems were selected by comparing the RNA-Seq data between genotypes and among time points. Specifically, the transcriptome of the non-domed meristem of the *ap2-12* mutant at 14 LDs was compared with that of the domed meristem of Col-0 at the same time point, and these DEGs were cross-referenced with the DEGs identified by comparing gene expression of the domed meristem of Col-0 at 14 LDs with that of the non-domed meristem of Col-0 at 10 LD. The resulting list of DEGs common to both comparisons (Supplemental Table 3-2) was then compared with the list of direct target genes of AP2 identified by ChIP-Seq analysis (Yant

et al., 2010). This approach identified only three candidate genes (Figure 3-3B), including *SOC1*. *SOC1* is a positive regulator of flowering time downstream of the main effector of the photoperiodic flowering pathway, *FT* (Samach et al., 2000). Moreover, SOC1 accumulates at the SAM during floral transition and persists in the inflorescence meristem (Immink et al., 2012). *SOC1* is also one of the earliest responsive genes to the loss-of-function of *AP2,* and was expressed more highly already at 10 LDs in *ap2* mutants compared with Col-0 (Figure 3-3C).

To understand the implications of *SOC1* upregulation in *ap2* mutants, clusters of co-expressed genes were identified among the DEGs at doming in the comparison between Col-0 and *ap2*. Co-expression modules were identified separately in Col-0 and *ap2* mutants. Three main co-expression modules were identified in Col-0 (Supplemental Figure 3-6A). The co-expression module organisation identified in Col-0 was comparable in *ap2-12* mutants (Supplemental Figure 3-6B–C), except that co-expression module 2 of Col-0, which contains *SOC1*, was split into two related but separate modules in *ap2* (modules 3 and 4). The genes included in the co-expression module of *SOC1* in *ap2-12* (module 4) fell into the semantic space of the GO-term “meristem maintenance” (Supplemental Figure 3-6D–E; Supplemental Figure 3-7). This association of SOC1 with meristematic genes suggests that its upregulation in *ap2-12* is related to changes in the regulation of meristem maintenance.

To compare the temporal and spatial pattern of SOC1 protein accumulation at the SAM in *ap2-12* and wild-type plants, the *SOC1::SOC1:GFP* reporter was introduced into *soc1-2* and *soc1-2 ap2-12* mutant backgrounds and analysed by confocal microscopy (Figure 3-3D). During the early stages of floral transition in the wild-type background (*soc1-2 SOC1::SOC1:GFP* at 10 LD) SOC1-GFP was detected at the base of the SAM, and its spatial pattern of accumulation broadened progressively until by the end of floral transition at 14 LD it was detected throughout the SAM. Moreover, SOC1-GFP was absent in young floral primordia (shown at 19 LD), but was present in the basal region of the primordia. By contrast, in the *soc1-2 ap2-12 SOC1::SOC1:GFP* background, SOC1-GFP was detected throughout the SAM already at 10 LD, and this accumulation persisted until the end of the analysis. Taken together, these results

indicate that AP2 negatively regulates *SOC1* expression at the SAM before and during floral transition.

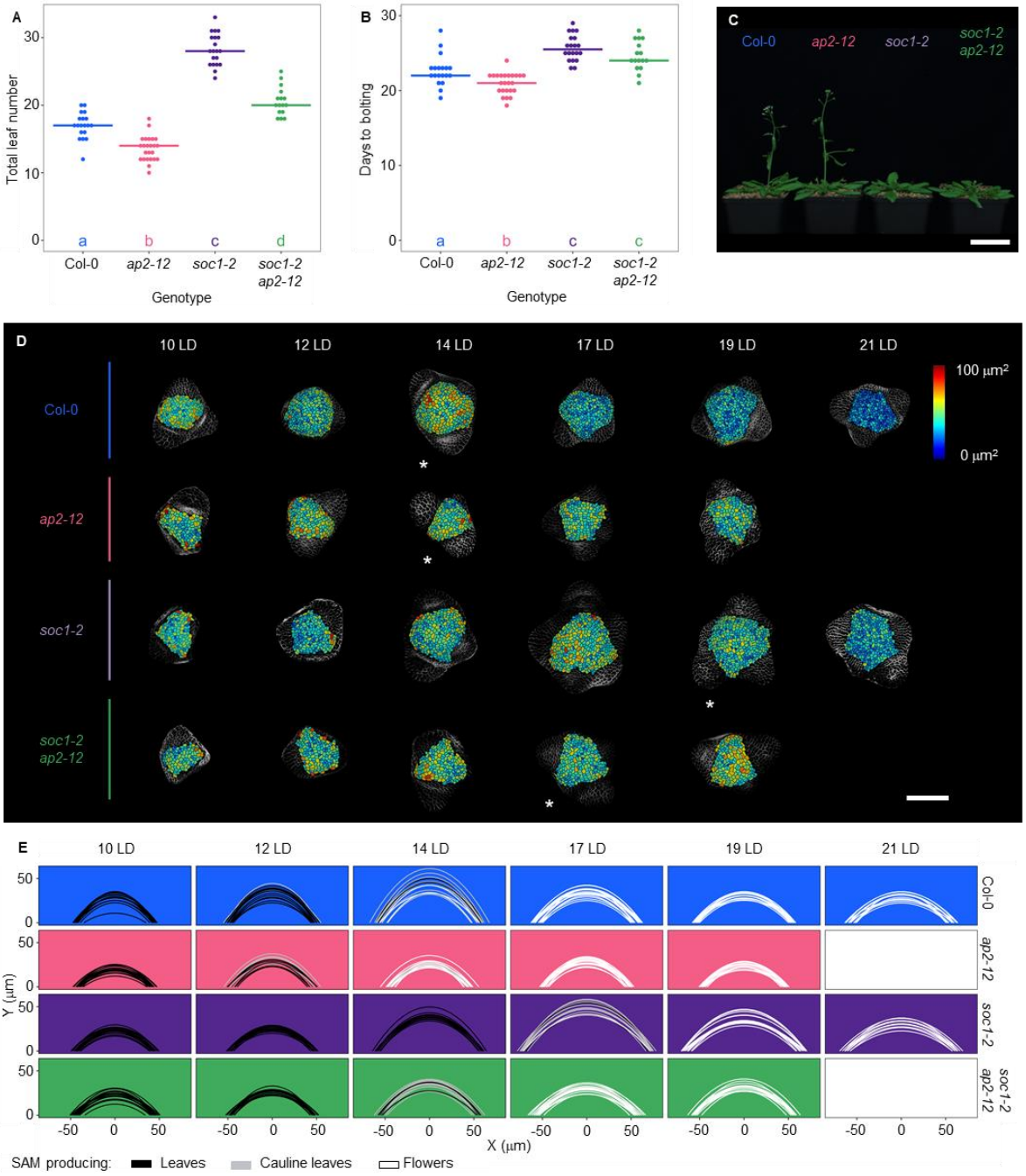

Figure 3-4. *SOC1* positively regulates flowering time downstream of *AP2*.

(A–C) Flowering-time analysis of Col-0, *ap2-12*, *soc1-2* and *soc1-2 ap2-12* under long days (LDs). (A–B) Flowering time according to (a) total leaf number and (b) days to bolting. The horizontal bars represent the median value for each genotype. Significant differences between genotypes were determined via one-way ANOVA, followed by Tukey post-hoc comparisons ($p < 0.05$). Data sets that share a common letter do not differ significantly. $N = 16–24$. (C) Photograph of representative plants of the genotypes grown for 27 days under LD conditions. Scale bar = 5 cm. (D) Top view of the heatmap quantification of cell area in the meristem region via segmentation in shoot apical meristems (SAMs) of Col-0, *ap2-12*, *soc1-2* and *soc1-2 ap2-12.* White asterisks indicate the first time point at which floral primordia were detected in the analysis of the corresponding genotype. Scale bar = 50 µm. $N = 4$. (E) SAM morphology of Col-0, *ap2-12*, *soc1-2* and *soc1-2 ap2-12* under continuous LDs. The parabolas are coloured according to the identity of the primordia that were formed at the SAM periphery. $N = 11–18$.

3.2.6 The interaction between SOC1 and AP2 couples doming to the floral transition

SOC1 is one of the earliest upregulated genes at the SAM upon exposure to inductive photoperiods (Borner et al., 2000; Lee et al., 2000; Samach et al., 2000; Figure 3-3C). Previously, *soc1-2 ap2-12* double mutants were found to produce more leaves than *ap2-12* but fewer than *soc1-2* (Yant et al., 2010). The interaction between *soc1-2* and *ap2-12* was characterised further by comparing the number of rosette and cauline leaves formed, as well as the days to bolting, for *soc1-2*, *ap2-12* and *soc1-2 ap2-12.* The *soc1-2 ap2-12* double mutants formed an intermediate number of rosette and cauline leaves between *soc1-2 and ap2-12* (Figure 3-4A–C, Supplemental Figure 3-8). The *soc1-2 ap2-12* double mutant also bolted later than Col-0 and similarly to *soc1-2* (Figure 3-4), with more rosette leaves than Col-0. The *soc1-2 ap2-12* double mutant is therefore later flowering than Col-0, and *SOC1* promotes flowering downstream of *AP2,* but because *soc1-2* is not entirely epistatic to *ap2-12*, other genes also contribute to the early flowering of *ap2-12.*

The increase in SAM area that occurs during floral transition is delayed in *soc1* mutants (Kinoshita et al., 2020). To test whether *soc1* meristems exhibit delayed doming, the changes in meristem morphology of *soc1-2* mutants were quantified under continuous LD. Maximum meristem area was reached at 17 LD, which was three days later than for Col-0, and the SAM was larger than that of Col-0 at 14 LD (Figure 3-4D, Supplemental Figure 3-9A). Moreover, doming of *soc1-2* meristems also occurred at 17 LD when the maximum meristem height and width were reached, and the meristem was wider than the Col-0 meristem at 14 LD (Figure 3-4E, Supplemental Figure 3-10). Therefore, *SOC1* accelerates doming of Col-0 and contributes to the timing of the change in SAM morphology.

Whether the delayed doming and wider meristem of *soc1-2* mutants is mediated by AP2 was addressed by analysing SAM morphology of the double mutant *soc1-2 ap2-12*. Throughout floral transition under continuous LD, the meristem area of *soc1-2 ap2-12* was comparable to that of *ap2-12* (Supplemental Figure 3-9A). Moreover, despite a slight increase in meristem

width and height in *soc1-2 ap2-12* mutants compared with *ap2-12* from 14 LD onwards, the *soc1-2 ap2-12* double mutant showed a mean reduction in meristem height of 9.77 µm in comparison with Col-0 at 14 LD and a mean reduction in height of 18.28 µm in comparison with *soc1-2* at 17 LD, which suggests that doming was greatly reduced in the double mutant and that the delayed doming of *soc1-2* mutants depends on AP2 activity.

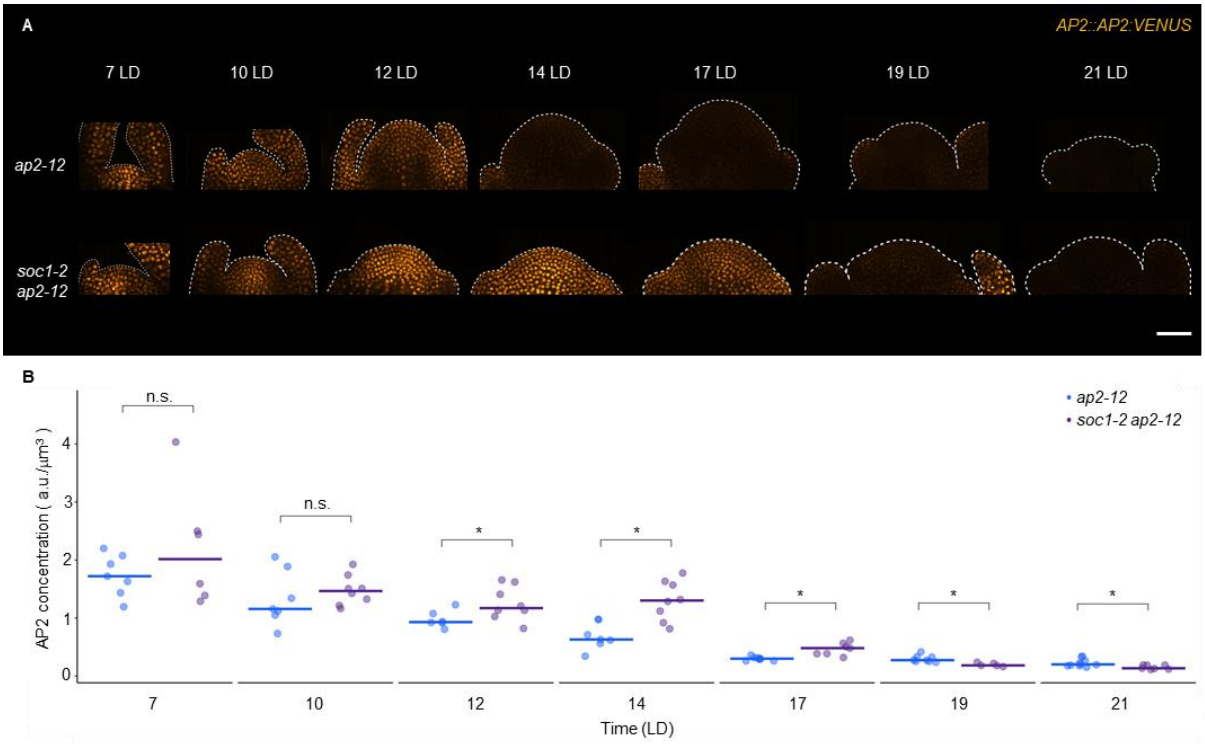

Figure 3-5. SOC1 negatively regulates *AP2* expression at the SAM during floral transition.

(A) Pattern of protein accumulation of *AP2::AP2:VENUS* at the shoot apical meristem (SAM) in *ap2-12* and *soc1-2 ap2-12* plants under continuous LDs. The shape of the meristem and its lateral organs at the periphery is indicated with a dotted white line. Scale bar = 50 µm. (B) Quantification of AP2 concentration at the SAM by fluorescence intensity measurement of AP2:VENUS in *ap2-12* and *soc1-2 ap2-12* mutant backgrounds during continuous LDs. Intra-time point comparisons between genotypes were performed via one-way ANOVA, followed by Tukey post-hoc comparisons ($p < 0.05$). Statistical significance is indicated with an asterisk, whereas the absence of significance is indicated by "n.s." $N = 6–8$.

SOC1 is a direct repressor of *AP2* (Immink et al., 2012; Tao et al., 2012). Therefore, to test whether the delayed doming of *soc1-2* is associated with a prolonged expression of AP2 in the SAM, the spatial pattern of *AP2::AP2:VENUS* was compared in the *ap2-12* and *soc1-2 ap2-12* mutant backgrounds in LD-grown plants. In the *ap2-12* mutant prior to floral transition, AP2-VENUS accumulated throughout the whole SAM and developing leaves (Figure 3-5). This accumulation persisted until the doming stage (14 LD), during which the fluorescence of AP2-VENUS decreased and was only detectable in developing primordia. After floral transition,

AP2-VENUS protein accumulation decreased greatly, as observed previously after transfer from SDs to LDs (Figure 3-2A). This trend was also observed in the *soc1-2 ap2-12* mutant background, but AP2-VENUS persisted in the SAM until 17 LD in the *soc1-2 ap2-12* mutant background, approximately 5 days longer than in *ap2-12*. Therefore, AP2 protein at the SAM persists for longer in the *soc1-2* mutant, and because doming is delayed in *soc1* mutants, the induction of meristem doming by AP2 takes longer than in Col-0.

AP2-VENUS fluorescence at the SAM was quantified in the *ap2-12* and *soc1-2 ap2-12* backgrounds. During the vegetative stage (i.e. 7 LD), no differences in AP2-VENUS fluorescence were detected between *ap2-12* and *soc1-2 ap2-12* backgrounds (Figure 3-5B), consistent with the absence of SOC1 protein accumulation at the SAM during the vegetative stage (Figure 3-3). From 12 LD until 17 LD, AP2-VENUS fluorescence increased in the *soc1-2 ap2-12* mutant background in comparison with *ap2-12*, consistent with persistent accumulation of AP2-VENUS in *soc1-2 ap2-12*. After floral transition, AP2-VENUS fluorescence decreased greatly in both *ap2-12* and *soc1-2 ap2-12* mutant backgrounds. Therefore, *SOC1* negatively regulates *AP2* expression at the SAM during floral transition, and AP2 promotes SAM doming during floral transition prior to its repression by SOC1.

3.2.7 AP2 affects the plastochron in a quantitative manner

Previously published data suggest that the number of functional copies of the *AP2* gene correlates with the number of leaves (Sang et al., 2022). The *soc1-2 ap2-12* double mutant was isolated from the F3 progeny of an F2 plant that was homozygous for the *soc1-2* mutation and heterozygous for *ap2-12.* Among this F3 population, individuals that were heterozygous for the *ap2-12* mutation exhibited an intermediate number of rosette and cauline leaves between plants that were wild type for *AP2* and those that were homozygous for the *ap2-12* mutation (Supplemental Figure 3-11A–B). However, in line with the similar bolting time of the *soc1-2 ap2-12* double mutants and *soc1-2,* all the progeny of the *soc1-2/soc1-2 AP2/ap2-12* line bolted at a similar time (Supplemental Figure 3-11C). This result is consistent with an acceleration of aerial organ production (i.e. shorter plastochron) by AP2, which has been

observed for plants with increased AP2 expression (i.e. *mir172* mutants and *rAP2* plants; Ó'Maoiléidigh et al., 2021; Sang et al., 2022). Collectively, these observations suggest that the number of functional alleles of *AP2* correlates positively with leaf number.

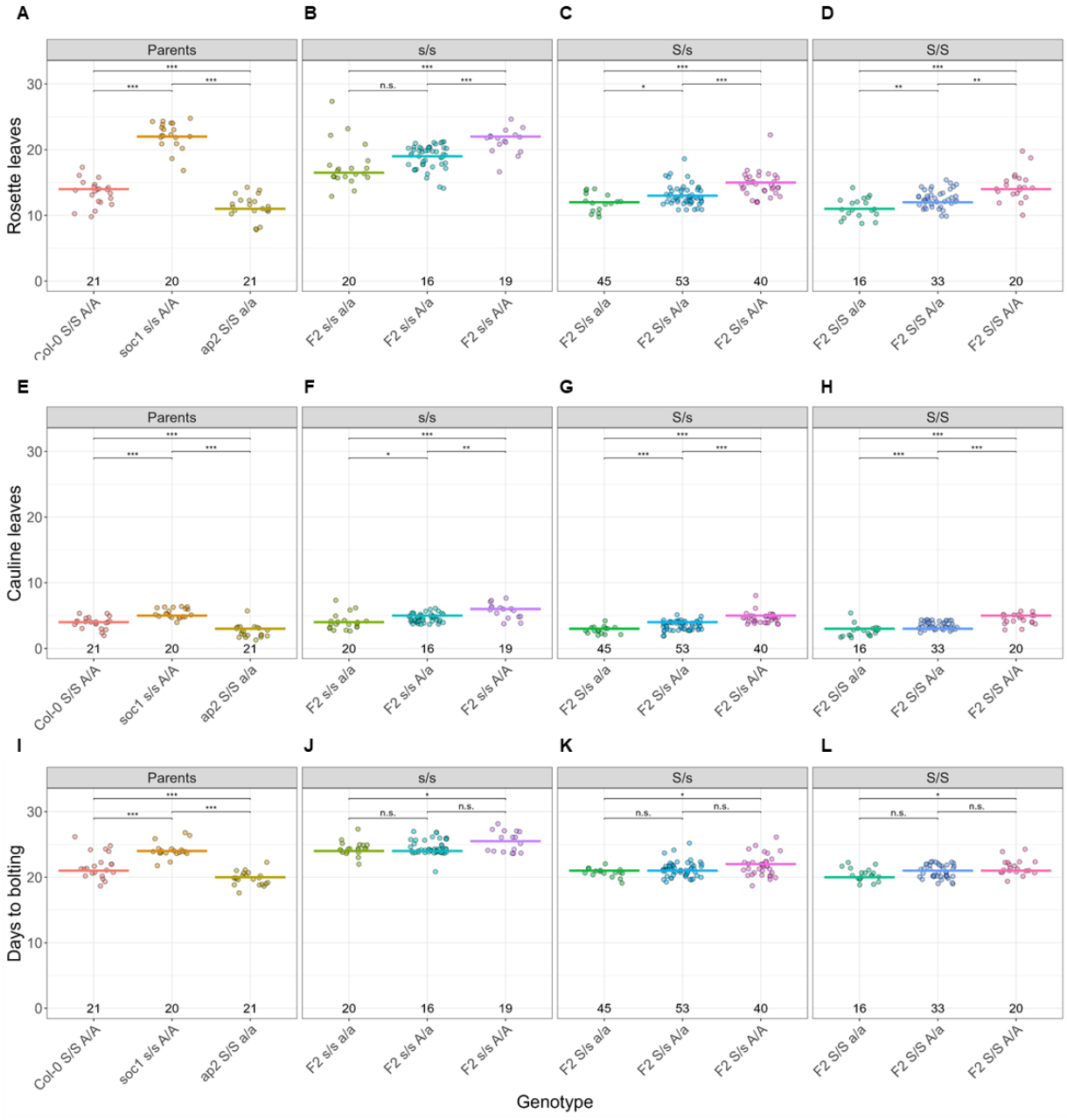

Figure 3-6. The F2 population from the *soc1-2* × *ap2-12* cross exhibits a distorted distribution of leaf number.

Flowering-time measurements of the F2 population from the *soc1-2* × *ap2-12* cross under LD in terms of (A–D) rosette leaf number, (E–H) cauline leaf number and (I–L) days to bolting. The wild-type (WT) and parental lines are plotted in panels A, E and I. The plants are grouped according to their genotype. The horizontal bars represent the median value for each genotype. Immediately above the x axis, the number of samples for each genotype is indicated. The genotype for *SOC1* is represented as S (WT) or s (*soc1-2),* and the genotype for *AP2* is represented as A (WT) or a (*ap2-12)*. Statistical significance between two groups was determined via Student's *t*-test. Lack of significance ($p > 0.05$) is indicated as n.s. $p < 0.05$ is indicated as *, $p < 0.01$ is indicated as ** and $p < 0.001$ is indicated as ***. $N = 16–53$.

Because only segregating material in the *soc1-2* mutant background was analysed in Supplemental Figure 3-11, the flowering time of the F2 population from the *soc1-2* × *ap2-12* cross was measured in a greenhouse experiment, to test whether the relationship between the number of functional *AP2* alleles and leaf number was influenced by the genotype for *SOC1.* The early flowering of *ap2-12* and the late flowering of *soc1-2* were observed in terms of rosette and cauline leaf number, as well as days to bolting (Figure 3-6A,E,I and Table 3-1). Consistent with Figure 3-4A–C, the number of leaves of the *soc1-2/soc1-2 ap2-12/ap2-12* plants was intermediate between that of the parental *soc1-2* and *ap2-12* mutants*.* Regardless of the genotype for *SOC1, ap2-12/ap2-12* plants produced fewer leaves than *ap2-12/AP2,* and *ap2-12/AP2* had fewer leaves than *AP2/AP2* plants. Whereas *ap2-12/ap2-12* bolted slightly earlier than *AP2/AP2,* the differences in bolting-time were smaller than those in leaf number, and no correlation between the presence of *AP2* wild-type alleles and bolting-time was observed. These smaller differences in bolting time rather than in leaf number influenced by the genotype for *AP2* are consistent with a *SOC1*-independent regulation of the rate of organ production by *AP2* (Supplemental Figure 3-12)*,* but a *SOC1*-dependent major effect of *AP2* in the regulation of bolting-time. Notably, in this analysis, regardless of the *AP2* genotype, the flowering times of *SOC1/soc1-2* plants were comparable to those of *SOC1/SOC1*, confirming that the flowering-time phenotype determined by the *soc1-2* mutation follows a recessive mode of inheritance (Supplemental Figure 3-13). Taken together, these observations indicate that the number of wild-type copies of the *AP2* gene affects leaf number, probably by reducing the plastochron.

3.2.8 miR172 and SOC1 affect flowering time and meristem identity by negatively regulating AP2

miR712 (Ó'Maoiléidigh et al., 2021; Sang et al., 2022) and SOC1 (Figure 3-5) are negative regulators of *AP2* at the SAM during floral transition. To understand whether miR172 and *SOC1* are mutually dependent in the negative regulation of *AP2*, the flowering time of *rAP2-V soc1-2* plants was measured (Figure 3-7). The combination of *rAP2-V* and *soc1-2* had a clear

synergistic effect, leading to plants that produced on average 85.9 rosette and 51.4 cauline leaves. Thus, *rAP2-V soc1-2* produced on average 70.9 more rosette and 47.9 more cauline leaves than Col-0, and bolted 18.5 days later than Col-0. The less extreme synergistic effect of *rAP2-V* and *soc1-2* on bolting-time compared to leaf number suggested an acceleration of organ production by rAP2-V. Because *rAP2-V soc1-2* stopped forming leaves before bolting (Supplemental Figure 3-14A), the rate of leaf production was estimated by dividing the total leaf number by the bolting time (Supplemental Figure 3-14D). Consistent with a faster leaf production rate i.e. a shorter plastochron, the calculated rate of leaf production of *rAP2-V soc1-2* was the highest (i.e. 2.9 leaves/day), whereas the other genotypes were below 1 leaf/day. These results indicate that miR172 and *SOC1* regulate flowering time by converging on the negative regulation of *AP2* in a non-mutually dependent manner.

All the *rAP2-V soc1-2* SAMs lost inflorescence meristem identity after producing a few flowers, and then initiated a terminal flower (Figure 3-7I). Inflorescence meristem identity appeared to be lost at the early bolting stage, because at this stage the SAM appeared very large, misshapen and was surrounded by closely spaced developing stamens (Supplemental Figure 3-14A–C). The structure of the terminal structure of *rAP2-V soc1-2* was complex. The flowers that were produced immediately before the loss of the inflorescence identity exhibited subtending bracts (Supplemental Figure 3-14E). Subsequently, several whorls of stamens were initiated and in the centre of the terminal flower, sepalloid organs were produced that sometimes formed ovules. Moreover, elongated filaments were interspersed among the sepalloid organs. Although further characterisation of these *rAP2-V soc1-2* flowers is required, the presence of increased whorls of stamens is characteristic of flowers of plants that overexpress *AP2* or other *AP2-LIKE* genes (Chen, 2004; Jung et al., 2014; Schwab et al., 2005). Furthermore, the generation of a terminal flower was reported for plants that overexpressed AP2 (*rAP2-V*) under the regulation of the *FD* promoter (Sang et al., 2022). These results suggest that higher levels of overexpression of AP2 caused both by miR172-resistance and increased transcription in the *soc1* mutant compromises the indeterminacy of

the SAM. This conclusion supports the idea that miR172 and *SOC1* redundantly maintain the inflorescence meristem identity of the SAM by negatively regulating *AP2.*

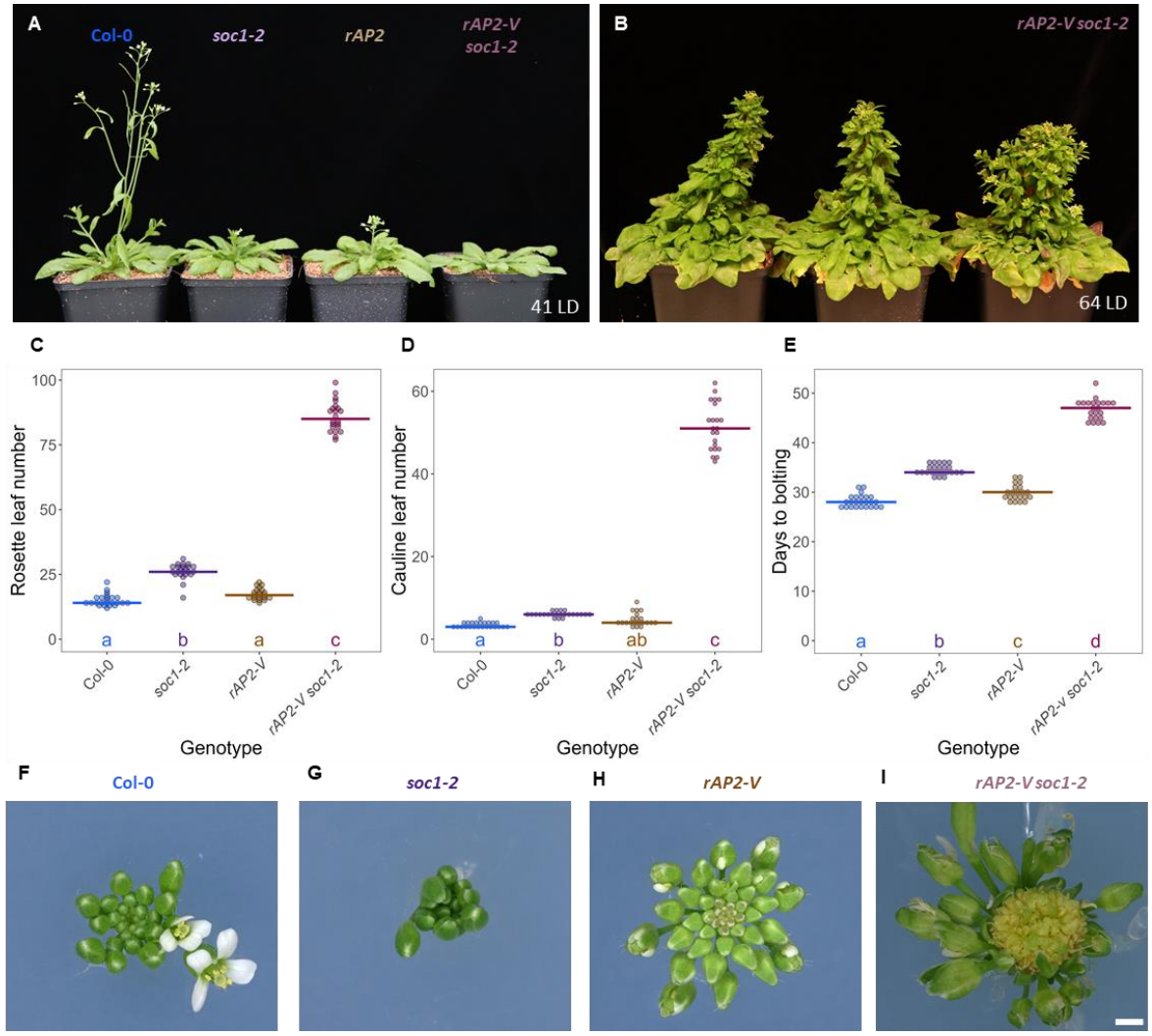

Figure 3-7. The combination of *rAP2* and *soc1* affects meristem maintenance.

(A–E) Flowering time of *rAP2-V soc1-2.* (A) Photograph of representative 41-day-old plants grown in long days (LDs). (B) Photograph showing the altered plant architecture of *rAP2-V soc1-2* plants at 64 LD. (C–E) Flowering-time measurements in terms of (C) rosette leaf number, (D) cauline leaf number and (E) days to bolting. The horizontal bars represent the median value for each genotype. Significant differences were determined via one-way ANOVA, followed by Tukey post-hoc comparisons (p < 0,05). Data sets that share a common letter do not differ significantly. N = 21–24. (F–I) Inflorescences at 10–12-cm-bolting stage of (F) Col-0, (G) *soc1-2*, (H) *rAP2-V* and (I) *rAP2-V soc1-2*. Scale bar = 1 mm.

3.2.9 Meristem doming occurs under continuous SDs with altered height and width compared with doming in inductive photoperiods

Cell proliferation at the SAM of Arabidopsis is induced by LDs (Jacqmard et al., 2003) and *ft-10 tsf-1* double mutants do not exhibit doming during the early stages of floral transition under LDs (Kinoshita et al., 2020); however, it is unknown whether meristem doming does occur

during floral transition under non-inductive SDs. To analyse SAM doming under SD conditions, segmentation analyses were performed on the epidermis of SAMs from plants grown under continuous SDs. Meristems were dissected every week on the basis of preliminary data gathered twice weekly by Alice Vayssières (data not shown). Similar to under LDs, floral transition under continuous SDs involved an increase in meristem size, and a mean maximum meristem area of $17.32 \cdot 10^3$ μm^2 was reached at 6 wSD (Figure 3-8A-B). The maximum meristem area at 6wSD reflected a maximum cell number and cell area of 450 cells and 38.49 μm^2, respectively (Supplemental Figure 3-15). Notably, the SAM area at 6 wSD was comparable to that at the doming stage following the shift from SDs to LDs or under continuous LDs (Figure 3-8F). These data suggest that an increase in SAM area is a hallmark of floral transition, regardless of the photoperiod.

To understand whether the increase in meristem area was accompanied by SAM doming, the height and the width of the Col-0 SAM were measured. Consistent with the changes under LDs, both width and height increased under continuous SD: there was a mean 2.4-fold increase in width and a mean 4.2-fold increase in meristem height from 2 wSD until 6 wSD (Figure 3-8C–D). Although there was a disproportionate increase in height in comparison to width in the SAMs of Col-0 in SDs, domed SAMs under SDs were wider but were reduced in height compared with the domed SAMs under inductive photoperiods (Figure 3-8G–H). These observations suggest that doming is a hallmark of floral transition in both LDs and SDs.

3.2.10 The differences in meristem area determined by AP2 are influenced by photoperiod

ap2 mutants exhibit smaller inflorescence meristems (Würschum et al., 2006). Because larger inflorescence meristems were produced by *ap2* plants that were grown under SDs and then transferred to LDs, compared with plants that grew continuously under LDs (Landrein et al., 2015), it is possible that the positive regulation of SAM area by *AP2* is influenced by photoperiod. To analyse this, SAM area was measured at the 1-cm-bolting stage. The area of Col-0 meristems at this stage was approximately 34% lower under SDs than LDs (Figure 3-9B).

This was the result of a mean reduction of 34% in cell number, because no differences in cell area were observed (Figure 3-9C–D). Importantly, Col-0 SAM area and cell number at 1 cm bolting under SDs was comparable to that of *ap2-12* mutants. Notably, the increased cell area in the meristem of *ap2-12* compared with Col-0 in LDs was not present under SDs. This suggests that the regulation of meristem area by *AP2* is dependent on the photoperiod.

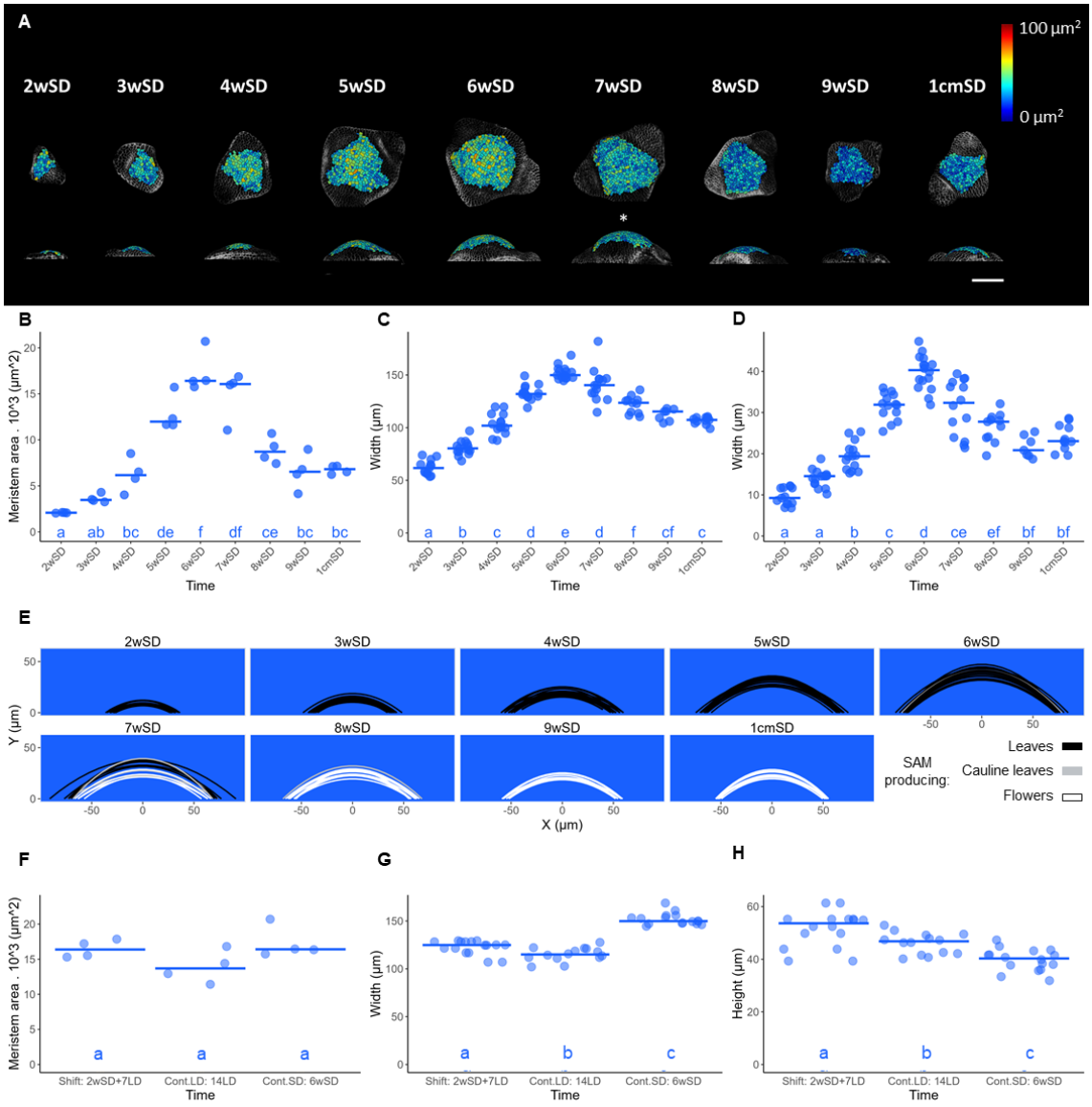

Figure 3-8. Doming occurs under short-day conditions.

(A–B) Segmentation analysis (N = 4) of shoot apical meristems (SAMs) of Col-0 during continuous short days (SDs). (A) Heatmap quantification of cell area in the meristem region. The colour code of the heatmap is shown in the upper right corner. 1cmSD corresponds to the 1-cm-bolting stage. Scale bar = 50 µm. (B) Plot depicting SAM area. (C–E) Quantitative morphology analysis by measuring (C) width and (D) height of the SAM. N = 7–16. (E) Representation of the parabolas adjusted to the morphology of the SAM. The parabolas are coloured according to the organs that were being initiated at the boundaries of the meristem. (F–H) Comparative analysis between time courses of (F) SAM area, (G) meristem width and (H) meristem height. N = 14–16. In the plots B–D and F–H, the horizontal bars represent the median value for each time point. Significant differences were determined via one-way ANOVA, followed by Tukey post-hoc comparisons (p < 0,05). Data sets that share a common letter do not differ significantly.

rAP2-V plants were grown in parallel with the previously analysed Col-0 and *ap2-12* mutants. Almost all the *rAP2-V* plants exhibited alterations in flower development, marked by increased stamen production and the maintenance of undifferentiated tissue in the central part of the flower, which are consistent with the floral aberrations upon *AP2-LIKE* gene overexpression (Chen, 2004; Jung et al., 2014; Schwab et al., 2005; Figure 3-9E). Moreover, 2 out of the 24 plants exhibited a fasciated SAM (Figure 3-9F). Under SDs, AP2 accumulates in the SAM during the vegetative stage and early during floral transition, but its accumulation is greatly reduced after floral transition, whereas rAP2-V persists after floral transition at the SAM (PhD dissertation from Annabel van Driel). These patterns are similar to those observed in LDs. These observations indicate that *AP2* positively regulates meristem area, but its role in SDs is not as important as that in continuous LDs. This conclusion is consistent with previous results of this chapter, which showed that the photoperiodic pathway (which included *SOC1*) enhanced *AP2* function in regulating meristem size.

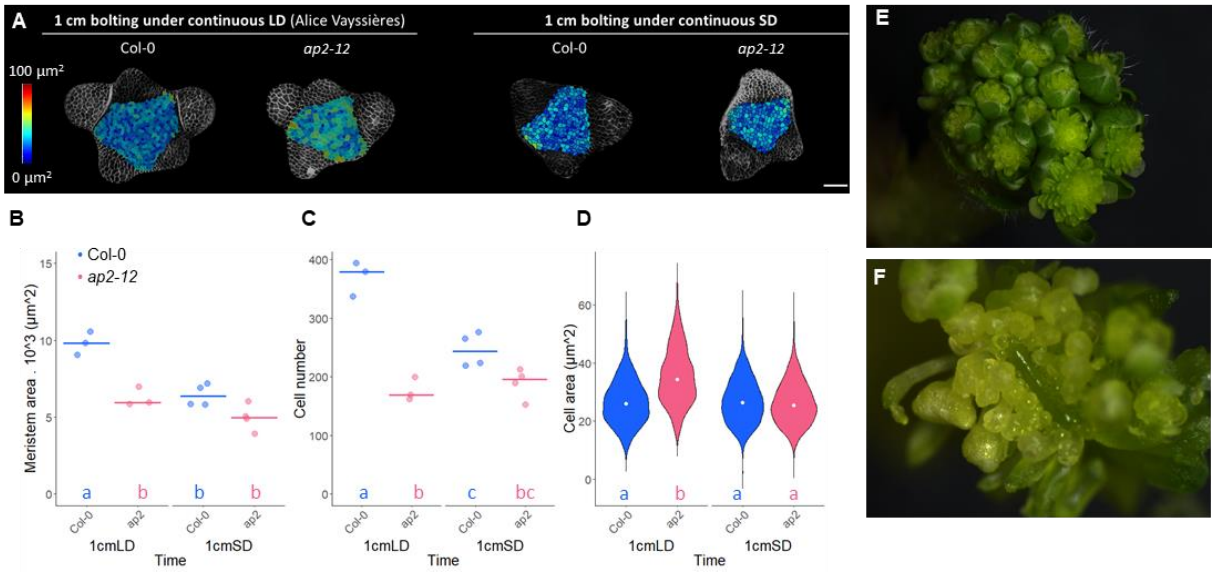

Figure 3-9. The positive regulation of meristem area by AP2 is dependent on inductive photoperiods.

(A–D) Segmentation analysis (*N* = 3–4) of the inflorescence meristem at the 1-cm bolting stage. (A) Heatmap quantification of cell are in the meristem region. The colour code of the heatmap is shown on the left side. Scale bar = 50 µm. (B–D) Plots depicting (B) shoot apical meristem (SAM) area, (C) cell number and (D) area of the cells forming the SAM. Horizontal bars (B–C) and white dots (D) represent the median value for each genotype. Significant differences were determined via one-way ANOVA, followed by Tukey post-hoc comparisons ($p < 0,05$). Data sets that share a common letter do not differ significantly. (E–F) Photographs from the (E) inflorescence and (F) SAM of a *rAP2-VENUS* plant grown under SD at 1 cm bolting. Both images are of the same plant.

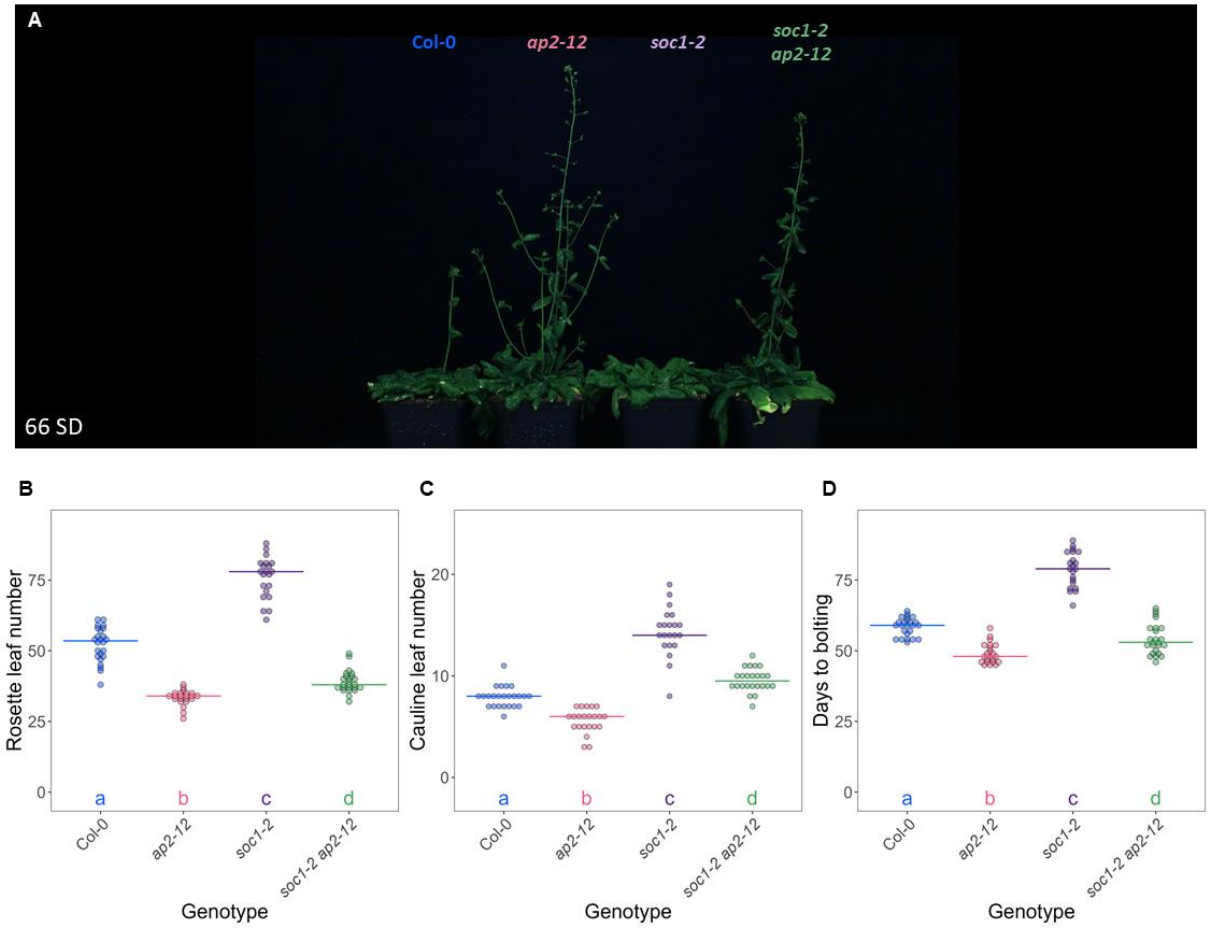

Figure 3-10. The function of *SOC1* is more important for the early flowering of *ap2-12* mutants under LDs than SDs.

Flowering time of the *soc1-2 ap2-12* double mutants under SDs. (A) Representative picture of 66-day-old plants grown under SDs (B–D) Flowering-time measurements in terms of (B) rosette leaf number, (C) cauline leaf number and (D) days to bolting. The horizontal bars represent the median value for each genotype. Significant differences were determined via one-way ANOVA, followed by Tukey post-hoc comparisons ($p < 0,05$). Data sets that share a common letter do not differ significantly. $N = 21–24$.

3.2.11 The genetic interaction between SOC1 and AP2 is influenced by photoperiod

A genetic interaction between *SOC1* and *AP2* in the regulation of flowering time was established under inductive photoperiods (Figure 3-4A–C; Yant et al., 2010). Because the regulation of inflorescence meristem size by *AP2* is more apparent under LDs than SDs (Figure 3-9), the genetic relationship between *SOC1* and *AP2* was studied under continuous SDs by measuring the flowering time of *soc1-2 ap2-12* in non-inductive photoperiod conditions. The *soc1-2 ap2-12* mutants produced an intermediate number of leaves compared with *ap2-12* and *soc1-2* mutants (Figure 3-10A–C). Notably, whereas *soc1-2 ap2-12* produced more rosette leaves than Col-0 under LDs (Supplemental Figure 3-8A), *soc1-2 ap2-12* mutants produced

on average 13.1 fewer rosette leaves than Col-0 under SDs (Figure 3-10B). Moreover, *soc1-2 ap2-12* produced on average 1.7 cauline leaves more than Col-0 under SDs. Contrary to under LDs, the bolting-time of *soc1-2 ap2-12* mutants was intermediate between that of *soc1-2* and *ap2-12* mutants (Figure 3-10D). Moreover, *soc1-2 ap2-12* bolted 4.3 days earlier than Col-0. Despite this early-bolting phenotype, *soc1-2 ap2-12* mutants bolted on average 5 days later than *ap2-12* mutants. These data indicate that *SOC1* promotes flowering time under SDs downstream of *AP2*, and in particular increases cauline leaf number. However, the function of *SOC1* downstream of *AP2* in the determination of rosette leaf number or bolting-time in SDs is not as apparent as under LDs, and suggests that in SDs the *SOC1*-independent mechanisms by which *AP2* regulates flowering time become more important.

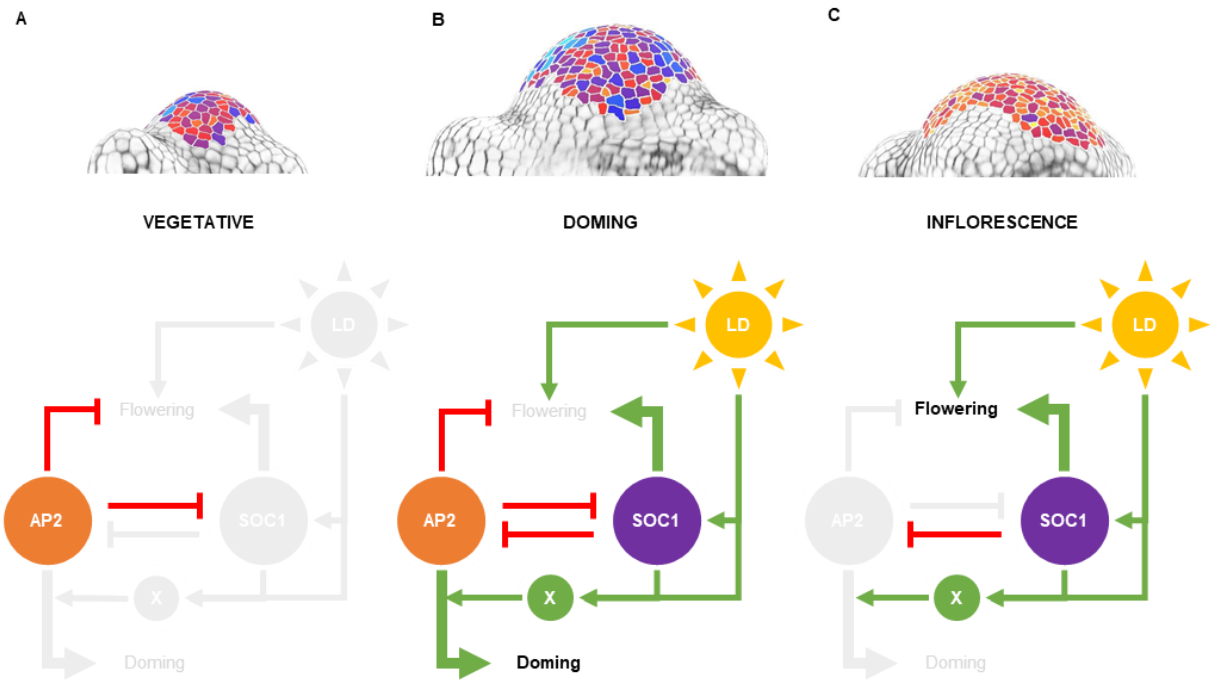

Figure 3-11. The mutual repression of *AP2* and *SOC1* couples changes in shoot apical meristem morphology with floral transition.

Schematic representation of the regulation of meristem morphology and flowering at the shoot apical meristem (SAM) by AP2 and SOC1 during the vegetative, doming, and inflorescence stages. At the vegetative stage, AP2 is present at the SAM, where it represses flowering, in part via *SOC1* repression. Long days constitute an inductive signal that triggers *SOC1* expression at the SAM. Whereas *SOC1* is a negative regulator of *AP2* expression, the data here suggest that an unknown mechanism (here labelled as X) leads to acceleration of doming by affecting AP2 function. The repression of *AP2* expression, in part by SOC1, leads to the formation of the inflorescence meristem, as well as the end of the doming stage.

3.3 Discussion

3.3.1 SAM morphology is controlled by flowering-time regulators

Doming of the SAM is a hallmark of the floral transition, but it is unknown how this change in meristem shape is co-regulated with the change in SAM identity that initiates floral development. In this chapter, it is shown that direct mutual repression of the expression of genes encoding the AP2 and SOC1 transcription factors plays a central role in integrating these processes. AP2 is a positive regulator of SAM size (Sang et al., 2022; Würschum et al., 2006) and during the vegetative phase it delays floral transition (Yant et al., 2010), largely by repressing *SOC1* transcription, especially under LDs. At this stage, AP2 does not detectably influence SAM meristem size (Figure 3-11A). However, exposure of plants to environments such as LDs eventually overcomes the repression of *SOC1* by AP2, and the resulting increase in the level of SOC1 initiates the repression of *AP2* transcription (Figure 3-11B). At about this stage, AP2 protein levels are further reduced through post-transcriptional regulation mediated by miR172. The reduction in the level of AP2 by SOC1 and miR172 further accelerates the increase in *SOC1* transcription and the floral transition. However, in the short time interval between the initiation of floral transition and the disappearance of AP2 from the SAM, AP2 markedly increases meristem size (Figure 3-11B). Therefore, the doming of the SAM associated with flowering is limited to the early stages of floral transition prior to the removal of AP2 by the actions of SOC1 and miR172. In *soc1* mutants, floral transition and the repression of *AP2* are both delayed, and the time interval in which doming can occur is therefore shifted later. Thus, the mutual repression of these two factors determines the timing of floral transition and ensures that the SAM rapidly increases in size only during the early stages of floral transition.

3.3.2 A quantitative framework to analyse changes in SAM morphology

Doming in Arabidopsis was initially described on the basis of longitudinal meristematic sections (Miksche & Brown, 1965; Vaughan, 1951). The changes in meristem shape have been quantified using different parameters (Jacqmard et al., 2003; Laufs et al., 1998). Moreover, the

changes in the shape of the meristem have been evaluated using the ratio between these parameters (Schlegel et al., 2021), or by adjusting the shape of the meristem to a parabola (Gruel et al., 2016; Laufs et al., 1998), as was previously performed in other species (Romberger & Gregory, 1977). In this study, meristem shape was also captured by directly defining points that delimit the apical layer of the SAM, similar to the approach of Fujiwara et al. (2021) to extract the shape of the RAM (see Material and methods; Supplemental Figure 3-3). The generated parabolas exhibited an optimal fit to the originally defined points, because all the parabolas exhibited R^2 values greater than 0.95 (Supplemental Figure 3-3A). From these fitted parabolas, the SAM height and width could be calculated. This strategy of fitting parabolas to points that were directly defined in the meristem confocal acquisitions yielded higher values of height and width at some time points (Supplemental Figure 3-3B–C). The changes in the inferred height and width from the parabolas followed a similar trend to the directly measured height and width in this chapter, because height exhibited a mean 3.14-fold increase, whereas width exhibited a mean 2.04-fold increase from the beginning of the time course until the doming stage (+7 LD; Supplemental Figure 3-3D–E). The smaller increase in height using this validation strategy compared with the direct measurement of this parameter (i.e. a 3.9-fold change) underlies a difference in mean height at the first time point, because whereas the directly measured mean height at 2 wSD was 13.11 µm, the calculated height from fitted parabolas was on average 19.26 µm. Despite the differences in some values of height and width, the reported changes in meristem morphology by the two strategies were consistent, which indicates that they are both suitable approaches to quantify changes in SAM morphology (Supplemental Figure 3-3F).

3.3.3 AP2 is related to several mechanisms that impact meristem size

AP2 is expressed in the SAM during vegetative development, when it represses *SOC1* transcription, but does not detectably increase meristem size. Doming only occurs in the time interval between the initiation of floral transition and the repression of *AP2*. This observation suggests that the promotion of meristem size by AP2 requires other factors (represented as X

in Figure 3-11) that are induced during floral transition and whose expression depends on SOC1. This mechanism might have parallels with the role of AP2 in increasing floral meristem size (Huang et al., 2017). Towards the end of floral development, the floral-specific MADS-domain transcription factor AGAMOUS (AG) reduces stem cell number in floral meristems by repressing transcription of the homeobox gene *WUS* (Lenhard et al., 2001; Lohmann et al., 2001), whereas AP2 antagonises the effect of AG on stem cells by increasing *WUS* transcription (Huang et al., 2017). In another context, at the end of inflorescence development, when the fruits are fully formed, the inflorescence meristem terminates growth during global proliferative arrest and this is associated with a reduction in *WUS* transcription (Balanzà et al., 2018). However, at this stage, induction of *AP2* from a transgene can reactivate *WUS* expression and SAM growth (Balanzà et al., 2018). Nevertheless, WUS expression is influenced by several meristematic regulators. Despite the positive role of *AP2* in regulating *WUS*, the expression of *WUS* in the RNA-seq data of dissected plant apices of *ap2-12* mutants was comparable to that in Col-0 (Supplemental Figure 3-16A). Whereas *CLV3* expression was lower at 10 LD in *ap2-12* mutants than in Col-0, there was no difference in SAM size between the genotypes at this stage (Supplemental Figure 3-16D). Thus, how AP2 influences this regulatory network will require extensive genetic and phenotypic analysis. The proposed enhancement of AP2 function by transcription factors induced during floral transition could explain why AP2 mainly regulates meristem size at this stage, and why meristem doming is delayed in *soc1* mutants. However, SOC1 was previously shown to reduce expression of enzymes involved in gibberellin biosynthesis and catabolism in the SAM, and this was proposed to influence the rate of meristem doming in *soc1* mutants (Kinoshita et al., 2020). Although AP2 represses SOC1 and therefore might influence GA levels during doming, this is not essential for the promotion of doming by AP2, which also occurs in a *soc1* mutant background. Notably, the extended persistence of AP2 protein at the SAM was reported in this chapter by comparing the spatial protein accumulation pattern of two different genomic insertions of the same reporter (i.e. *AP2::AP2:VENUS #13/ap2-12* vs. *AP2::AP2:VENUS*

#1/ap2-12 soc1-2). These findings could be further supported by comparing two lines carrying the AP2 translational reporter inserted at the same genomic region.

One potential mechanism by which *AP2* might impact meristem size and that is related to the WUS–CLV3 feedback loop is cytokinin signalling (Leibfried et al., 2005). Induction of *AP2* expression at the SAM during global proliferative arrest positively regulates cytokinin responses (Martínez-Fernández et al., 2020). Cytokinin treatment of mature inflorescence meristems caused a domed meristem shape (Merelo et al., 2022), similar to the more domed shape of *rAP2-V* meristems than Col-0 meristems at the 1-cm bolting stage (Sang et al., 2022). Moreover, increased cytokinin content upon mutation of *CYTOKININ OXIDASE 3* (*CKX3*) and *CKX5* causes a larger inflorescence meristem (Bartrina et al., 2011). Notably, in the time course under LD conditions of this chapter, *CYTOCHROME P450 FAMILY 735 SUBUNIT A2* (*CYP735A2*) was upregulated at 12 LD in the RNA-seq data of dissected *ap2-12* apices compared with Col-0 apices (Supplemental Figure 3-16B). *CYP735A2* is closely related to *CYP735A1*, and both encode the cytochrome P450 monooxygenase CYP735A, which is involved in transhydroxylation during trans-zeatin biosynthesis (Takei et al., 2004). Consistent with a positive role of cytokinin in the regulation of meristem size, *cyp735a1 cyp735a2* double mutants exhibit smaller meristems (Kiba et al., 2013), but the relevance of the upregulation of *CYP735A2* in *ap2-12* mutants needs to be further established. A second gene related to cytokinin signalling that was differentially expressed in the RNA-seq data of dissected *ap2* apices was *STM,* which has been reported to induce cytokinin synthesis and was downregulated from 12 LD onwards compared with Col-0 (Supplemental Figure 3-16A; Yanai et al., 2005). This downregulation of *STM* in *ap2-12* mutants, which exhibit smaller meristems upon floral transition, is consistent with the reduced SAM size of knock-down mutants for *STM* (*stm-bum1;* Su et al., 2020). Collectively, the involvement of *AP2* in the various mechanisms that regulate meristem size needs to be further assessed.

An increase in shoot meristem size and in meristem doming have been described in several species during floral transition (Bernier, 1988; Lyndon & Battey, 1985). A correlation between changes in growth rate and the size and arrangement of primordia have been established, with

some exceptions (e.g. neither *Ranuculus* nor *Epilobium* were reported to exhibit a change in growth rate during floral transition). It has been established that during doming, several mechanisms prevent the recruitment of cells into developing primordia, such that they will remain in the meristematic region and thus lead to an enlarged SAM. Typically, the meristem area is defined by considering the primordia at the boundaries of the SAM (as in this dissertation), which means that primordium development is a major determinant of meristem area (reviewed in Kwiatkowska, 2004). In fact, a positive correlation between the rate of organ production and SAM area was previously reported in Arabidopsis (Landrein et al., 2015). In other species, the transition from vegetative to reproductive growth involves an increase in meristem size and accelerated organ production (Erickson & Meicenheimer, 1977; Lyndon, 1978; Meicenheimer, 1979). It would be useful to test the relationship between SAM morphology and the rate of production of aerial organs in Arabidopsis during floral transition.

miR172 positively regulates inflorescence meristem size (Lian et al., 2021), largely by regulating *AP2* (Sang et al., 2022). Results from this study indicate that miR172 also regulates SAM area and morphology during floral transition (see Appendix to this chapter). Furthermore, *AP2* is a major effector of miR172 function, because in most of the performed comparisons, the meristem area and morphology of *ap2-12* mutants during floral transition were similar to those of *mir172a-2 b-3 d-3 ap2-12* mutants. However, under continuous LDs, the meristem area of *mir172a-2 b-3 d-3 ap2-12* mutants was greater than that of *ap2-12* mutants, reaching a maximum difference at 17 LD, when the SAM of *mir172a-2 b-3 d-3 ap2-12* was on average $4.83 \cdot 10^3$ μm^2 larger than *ap2-12* mutants. Consistently, the height and width of *mir172a-2 b-3 d-3 ap2-12* SAMs were greater than those of *ap2-12*, which suggests that the absence of doming of *ap2-12* mutants is recovered to some extent in a *mir172* mutant background. One possible explanation for this is that other *AP2-LIKE* genes are ectopically expressed in *mir172a-2 b-3 d-3 ap2-12* and can suppress the effect of *ap2-12*. *TOE2* was the only *AP2-LIKE* gene that exhibited significant differences in mRNA between *ap2-12* and *mir172a-2 b-3 d-3 ap2-12* dissected plant apices during a time course between 10 LD and 17 LD (Supplemental Figure 4-6). The next chapter of this dissertation describes the characterisation

of the AP2-LIKE transcription factor TOE2. Notably, *soc1-2 ap2-12* double mutant SAMs were higher and wider in comparison with *ap2-12* SAMs at later stages of floral transition. Moreover, *SOC1* is a negative regulator of other *AP2-LIKE* genes (Immink et al., 2012; Tao et al., 2012).

miR172 has been related to the rate of initiation of aerial organs (Ó'Maoiléidigh et al., 2021; Sang et al., 2022). Both *mir172a-2 b-3 d-3* mutants and *rAP2-V* plants exhibit larger inflorescence meristems than Col-0 and produce flowers more rapidly. In fact, the phyllotactic angle of organs initiated form the SAMs of 1-cm bolting *rAP2-V* plants was consistently lower than that of wild-type (Sang et al., 2022). Furthermore, according to the results in this chapter, the rate of organ production was further accelerated when *rAP2-V* was introduced into the *soc1-2* mutant background, which is expected to increase the transcription of *rAP2-V.* The expression of *rAP2-V* should be quantified in the *soc1-2* mutant background and compared with that in Col-0. This, together with a characterisation of the alteration in the rAP2-V protein accumulation pattern and meristem morphology, might provide further evidence for the link between meristem size and plastochron. Moreover, the presented data in Figure 3-4A–C confirmed the intermediate leaf number of *soc1-2 ap2-12* mutants between that of either single mutant (Yant et al., 2010), and suggested that increasing the number of functional *AP2* alleles increases leaf number, which is a consistent trend to the flowering-time of plants carrying AP2 translational reporters (Sang et al., 2022). Importantly, the estimated plastochron from the segregating F2 population of the *soc1-2* × *ap2-12* cross suggests that *AP2* accelerates lateral organ formation (Figure 3-6); however, the mechanism by which *AP2* regulates meristem area and plastochron requires further characterisation.

Domed meristems contain more cells because doming involves cell proliferation (Jacqmard et al., 2003; Kinoshita et al., 2020), which is consistent with an acceleration of the cell cycle (Klepikova et al., 2015). However, doming also involves an increase in meristem cell area and, notably, the decrease in meristem area after the doming stage reflects a decrease in cell area, whereas cell number remains constant (Kinoshita et al., 2020). In the analyses described in this chapter, meristem area and cell number changed consistently over time in all the analysed genotypes (Supplemental Figure 3-17). Therefore, the decreased cell number in *ap2-12* and

the increased cell number in *rAP2-V* meristems compared with Col-0 was interpreted as evidence for a positive regulation of cell proliferation by *AP2* during floral transition, which is consistent with the results at the 1-cm bolting stage (Sang et al., 2022). Nevertheless, at many analysed time points, *ap2-12* and *rAP2-V* meristems exhibited larger cells than Col-0, which is indicative of the complex regulation of cell area (reviewed in D'Ario & Sablowski, 2019 and Sablowski & Carnier Dornelas, 2014). One possibility is that *AP2* also positively regulates cell expansion. This might explain the appearance of larger cells in *rAP2-V* SAMs, whereas in the *ap2-12* mutant, the larger cells might be explained by a reduced cell division rate. Another explanation for the larger cells in *ap2-12* mutant meristems might be compensation syndrome, which consists in an increase in cell area upon reduced cell number due to mutation of a gene that promotes cell proliferation, as occurs in mutants for *AINTEGUMENTA* (*ANT;* Mizukami & Fischer, 2000) or *ANGUSTIFOLIA3* (*AN3;* Horiguchi et al., 2005). Notably, overexpression of *ANT* or *AN3* causes an increase in cell number but not cell size, contrary to *rAP2-V*, which leads to increase in SAM cell size. The regulation of cell proliferation and expansion by *AP2* at the shoot meristem needs to be further characterised.

3.3.4 The regulation of SAM morphology by AP2 is related to the photoperiodic pathway

Previous analyses reported an increase in inflorescence meristem size under LDs when plants were grown under SD conditions (Landrein et al., 2015). Our results showed that meristems from plants that were grown continuously under SD conditions were smaller than those grown under LDs (Figure 3-9). Whereas under SDs, the area of wild-type SAMs increased and reached a value that was comparable to that from doming under continuous LDs, the decrease in SAM area that is characteristic for the end of floral transition was more pronounced (Figure 3-8). These observations suggest that inductive photoperiods, which positively regulate doming (Jacqmard et al., 2003; Kinoshita et al., 2020), enable a mechanism that leads to an increase in SAM area. This is consistent with *SOC1* being one of the earliest responsive genes

under inductive photoperiods at the SAM (Borner et al., 2000; H. Lee et al., 2000; Samach et al., 2000).

In this dissertation, *SOC1* is suggested to accelerate the positive regulation of doming by *AP2* by enabling a mechanism that is labelled as X in the model depicted in Figure 3-11. This reflects the fact that although different mechanisms by which *AP2* can regulate the SAM area have been proposed (Sang et al., 2022; Würschum et al., 2006), it is unclear which of them is regulated by *SOC1.* Although the production of high-throughput data is still a challenge when quantifying SAM morphology due to technical constraints, the proposed strategies in this chapter could be used in combination with existing data to screen for possible candidate regulators of doming downstream of *AP2* and *SOC1*. The list of candidate regulators could be restricted to those genes whose regulatory regions are bound by SOC1 (Immink et al., 2012; Tao et al., 2012). The currently available *AP2*- and *SOC1*-inducible systems (Hyun et al., 2016; Martínez-Fernández et al., 2020), as well as the engineering of domain-specific inducible systems, might be helpful tools with which to validate the candidate regulators of doming. One candidate regulator downstream of the SOC1–AP2 pathway is *TERMINAL FLOWER 1* (*TFL1*), which is an FT-related protein that maintains inflorescence meristem identity and prevents the formation of a terminal flower, as occurs in loss-of-function mutants for this gene (Shannon & Meeks-Wagner, 1991). The *rAP2-V soc1-2* plants exhibited terminal flower-like structures (Figure 3-7), and SOC1 is a positive regulator of *TFL1* (Azpeitia et al., 2021). Understanding how *AP2* and *SOC1* are related to *TFL1* regulation might indicate how the mutual repression between *AP2* and *SOC1* affects the indeterminacy of the SAM.

Doming has been reported in different species and has been proposed to be a hallmark of floral transition. In this chapter, the flowering-time regulator AP2 is shown to be essential for doming. In spite of this, it remains unknown whether doming is solely a consequence of floral transition or whether it is relevant for inflorescence development. No other reports of mutants that undergo floral transition without doming of the SAM were found. Therefore *ap2-12* could represent a valuable tool to characterise different developmental processes related to doming, although the pleiotropic effects of *ap2* mutations increases the difficulty of defining the effects

specifically caused by the absence of doming. Characterising additional mutants that do not undergo doming would be important in distinguishing doming from other developmental processes.

3.3.5 A mutual repression motif that regulates SAM morphology and flowering

A feature of the model presented in this chapter is that the mutual repression of *AP2* and *SOC1* determines the timing of floral transition and SAM doming. This mutual repression occurs by direct binding of either one of the transcription factors to the promoter of the other gene (Immink et al., 2012; Tao et al., 2012; Yant et al., 2010). This type of cross-regulatory motif has been extensively characterized in other developmental processes, such as the response to morphogens during Drosophila embryo development and mammalian neural tube development (Briscoe et al., 2000; Briscoe & Small, 2015; Clyde et al., 2003). The reciprocal repression motif is proposed to sharpen and steepen spatial boundaries in gene expression (Sokolowski et al., 2012). AP2 and SOC1 are expressed in the same spatial pattern throughout the SAM, but show different temporal patterns, with AP2 being expressed during vegetative development and SOC1 in the inflorescence meristem. The mutual repression of SOC1 and AP2 may sharpen the temporal transition from the vegetative to floral state and ensure that there is only a short time interval during which both factors are expressed and AP2 can promote SAM doming. A notable feature of the mutual repression of AP2 and SOC1 is that the balance between both repressive factors is determined by environmental cues, such as daylength. Further characterisation of this mutual repression motif will require mutational analysis of the binding sites of each factor and determination of the location of the motif within the broader gene regulatory network controlling floral transition. Such approaches will facilitate predictive modelling of meristem shape changes and the timing of floral transition.

Table 3-1. Data for the flowering-time experiments described this chapter.

"s.d." = standard deviation.

Experiment	Genoytpe	*N*	Rosette leaf number		Cauline leaf number		Days to bolting	
			Mean	s.d.	Mean	s.d.	Mean	s.d.
Figure 3-4 Supplemental Figure 3-11 LD	Col-0	19	13.4	1.61	3.6	0.61	22.6	2.03
	ap2-12	24	11.2	1.59	2.3	0.57	21.0	1.40
	soc1-2	20	22.6	1.93	5.6	0.95	25.7	1.72
	soc1-2 ap2-12	16	17.4	1.63	3.1	0.81	24.6	1.96
	soc1-2 AP2/ap2-12	44	21.4	1.78	4.8	0.94	25.9	1.38
	soc1-2 AP2/AP2	17	23.3	1.76	6.1	1.03	26.1	1.22
Figure 3-6 Supplemental Figure 3-13 LD	Col-0	21	13.5	1.86	3.9	0.89	21.7	1.90
	soc1-2	20	22.2	1.94	5.35	0.59	24.2	1.14
	ap2-12	21	11.2	1.70	2.62	0.97	19.9	0.94
	soc1-2/soc1-2 ap2-12/ap2-12	20	17.6	3.32	4.05	1.15	24.3	1.03
	soc1-2/soc1-2 AP2/ap2-12	16	18.9	1.75	4.6	0.65	24.6	1.14
	soc1-2/soc1-2 AP2/AP2	19	21.4	1.82	5.8	1.06	25.4	1.46
	SOC1/soc1-2 ap2-12/ap2-12	45	12.0	1.37	2.8	0.58	20.8	0.68
	SOC1/soc1-2 AP2/ap2-12	53	13.1	1.54	3.5	0.64	21.2	1.13
	SOC1/soc1-2 AP2/AP2	40	14.7	1.94	4.7	0.81	21.8	1.62
	SOC1/SOC1 ap2-12/ap2-12	16	11.2	1.50	2.7	0.82	20.4	0.96
	SOC1/SOC1 AP2/ap2-12	33	12.5	1.30	3.5	0.55	20.8	0.99
	SOC1/SOC1 AP2/AP2	20	14.4	2.28	4.6	0.83	21.4	1.15
Figure 3-7 LD	Col-0	24	15.0	2.26	3.5	0.59	28.2	1.24
	rAP2-V	21	17.4	2.23	4.8	1.58	29.9	1.58
	soc1-2	23	26.2	3.06	6.0	0.56	34.5	0.99
	rAP2-V/soc1-2	22	85.9	5.74	51.4	5.61	46.7	2.03
Figure 3-10 SD	Col-0	24	52.2	6.09	7.9	1.02	58.4	3.27
	ap2-12	22	33.4	2.70	5.6	1.18	49.0	3.58
	soc1-2	21	75.9	7.36	14.3	2.37	78.8	6.26
	soc1-2 ap-12	24	39.1	3.90	9.6	1.14	54.1	5.43

3.4 Supplemental figures

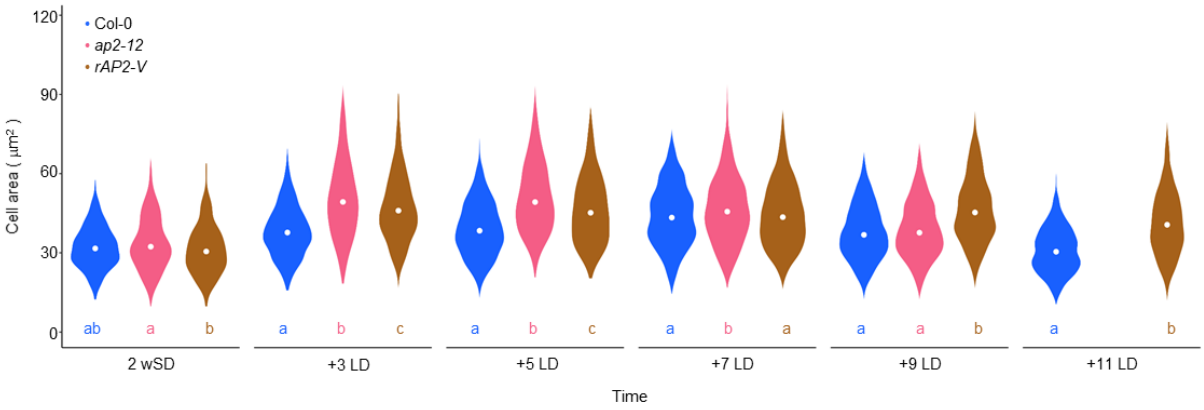

Supplemental Figure 3-1. Changes in cell area in the meristem during the time course in Figure 3-1.

White dots represent the median value for each genotype. Significant intra-time point differences among genotypes were determined via one-way ANOVA, followed by Tukey post-hoc comparisons ($p < 0.05$). Data sets that share a common letter do not differ significantly. $N = 3–4$.

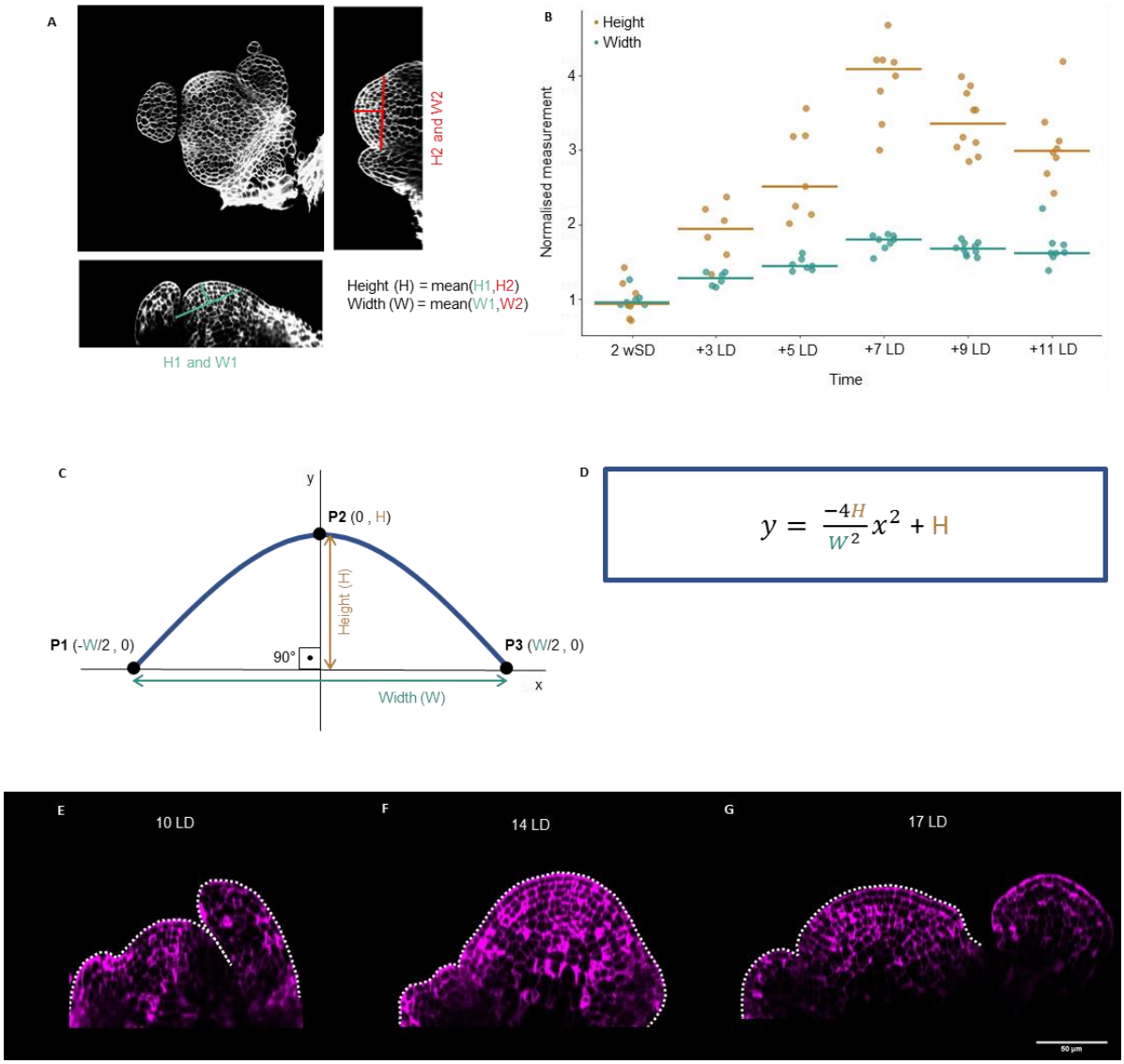

Supplemental Figure 3-2. Method to quantify changes in SAM morphology by measuring height and width of the shoot apical meristem.

(A) Two orthogonal views were generated from each Z-stack. In each orthogonal view, height and width were measured following the specified criteria in materials and methods. The two measurements for each parameter were considered as technical replicates. Therefore, the mean between these values was used for further analysis. (B) Normalised height and width of Col-0 meristems to those at the first time point of the time course shown in Figure 3-2B–C. *N* =12–20. (C–D) Adjustment of the measured height and width to a parabola. (C) Representation of height and width in a Cartesian coordinate system. Note that three points can be placed at the extremes of these measurements, which define a unique parabola. (D) General equation to represent a parabola from measured height and width. (E–F) Col-0 meristems producing (E) rosette leaves, (F) cauline leaves and (G) flowers at their flanks.

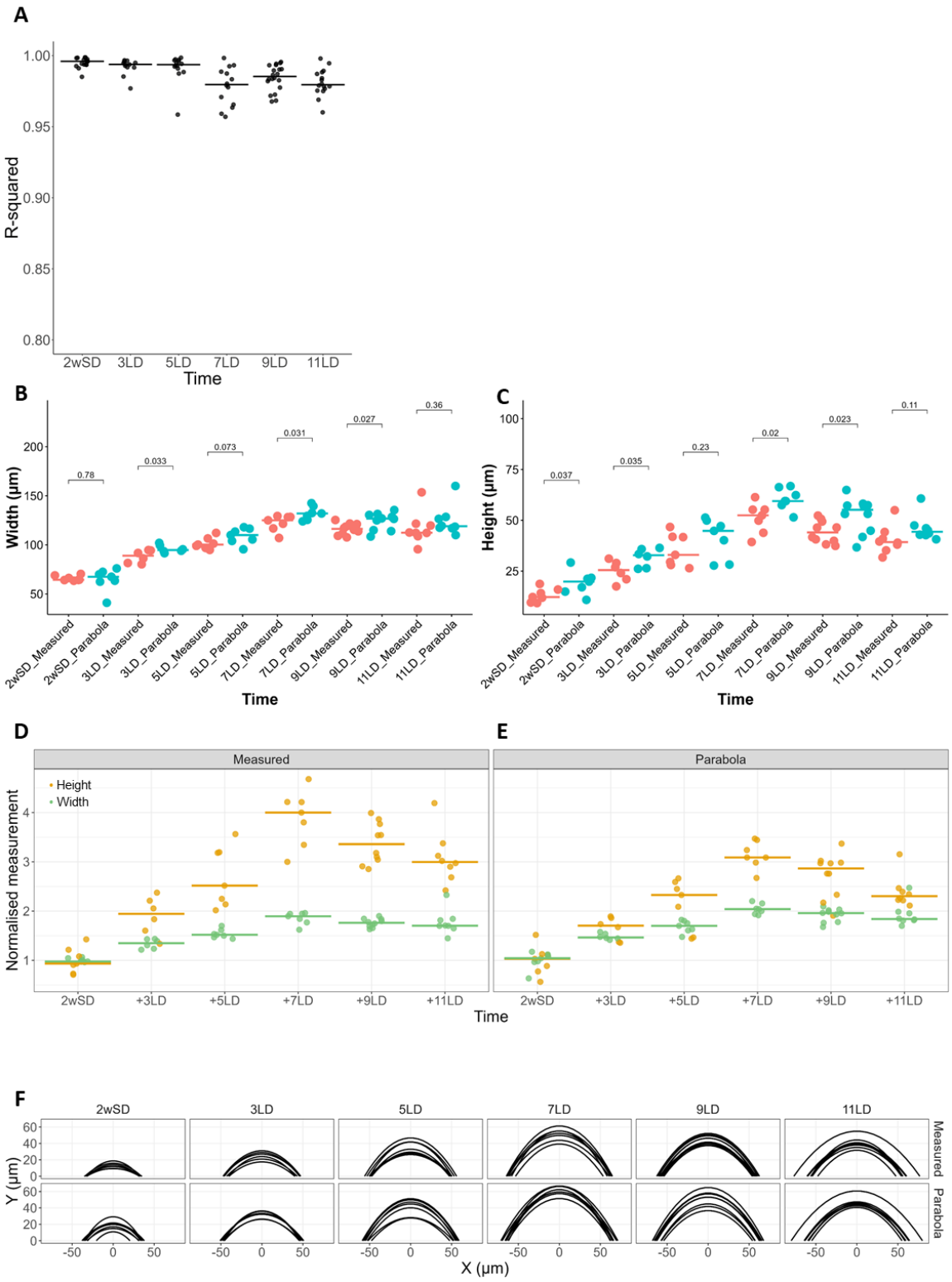

Supplemental Figure 3-3. Validation of the strategy to define the points of the parabola fitted to the shape of Col-0 meristems following a shift between photoperiods.

(A) R^2 values for the curve fitting from the defined points in the orthogonal views of the confocal acquisition. (B–C) Comparison of the values of (B) width and (C) height. Significant intra-time point differences between methods to estimate height and width were determined via Student's *t*-test. The *p*-value is indicated for each comparison. (D–E) Normalised height and width from the values of (D) directly measured parameters or (E) inferred from the parabolas defined by the points in the orthogonal views. (B–E) The horizontal bars represent the median value for each genotype. (B–E) The colour of the dots corresponds to (B–C) method to estimate height and width and (D–E) represented parameter. (F) Inferred parabolas from the estimated height and width from both methods. *N* = 12–20.

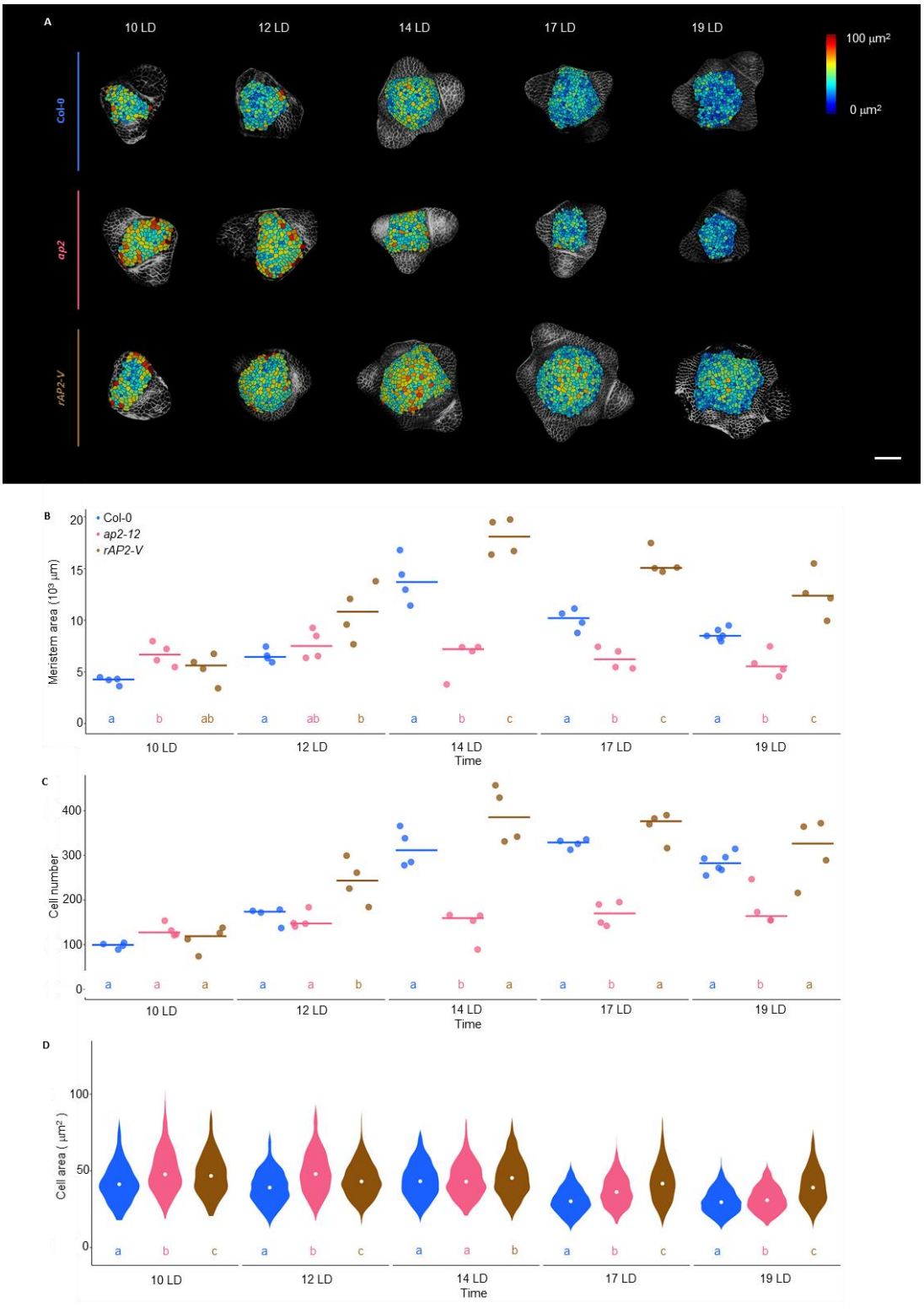

Supplemental Figure 3-4. Segmentation analysis of the shoot apical meristem of Col-0, *ap2-12* and *rAP2-VENUS* under continuous LDs.

(A) Top view of the heatmap quantification of cell area in the meristem region. White asterisks indicate the first time point at which floral primordia were detected in the analysis of the corresponding genotype. Scale bar = 50 µm. *N* = 4. (B–D) Quantification of (B) meristem area, (C) cell number and (D) cell area in the meristem region. The (B–C) horizontal bars and the (D) white dots represent the median value for each genotype. Significant intra-time point differences among genotypes were determined via one-way ANOVA, followed by Tukey post-hoc comparisons ($p < 0.05$). Data sets that share a common letter do not differ significantly. *N* = 4

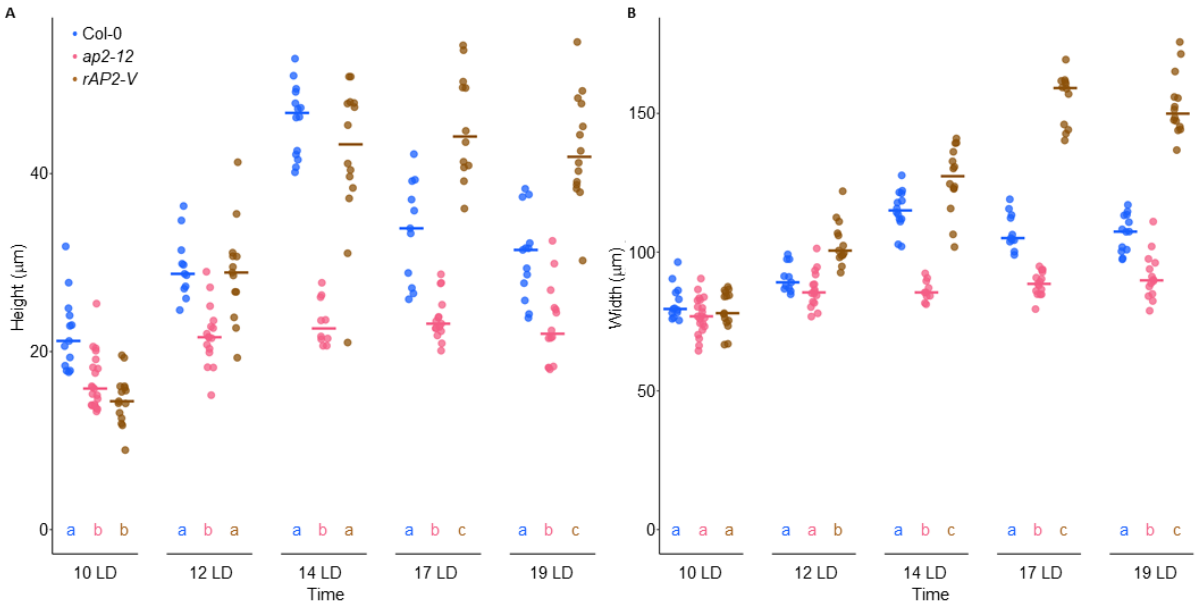

Supplemental Figure 3-5. Measured height and width of the represented meristems in Figure 3-3A.

Measured (A) height and (B) width. The horizontal bars represent the median value for each genotype. Significant intra-time point differences among genotypes were determined via one-way ANOVA, followed by Tukey post-hoc comparisons ($p < 0.05$). Data sets that share a common letter do not differ significantly. $N = 10–21$.

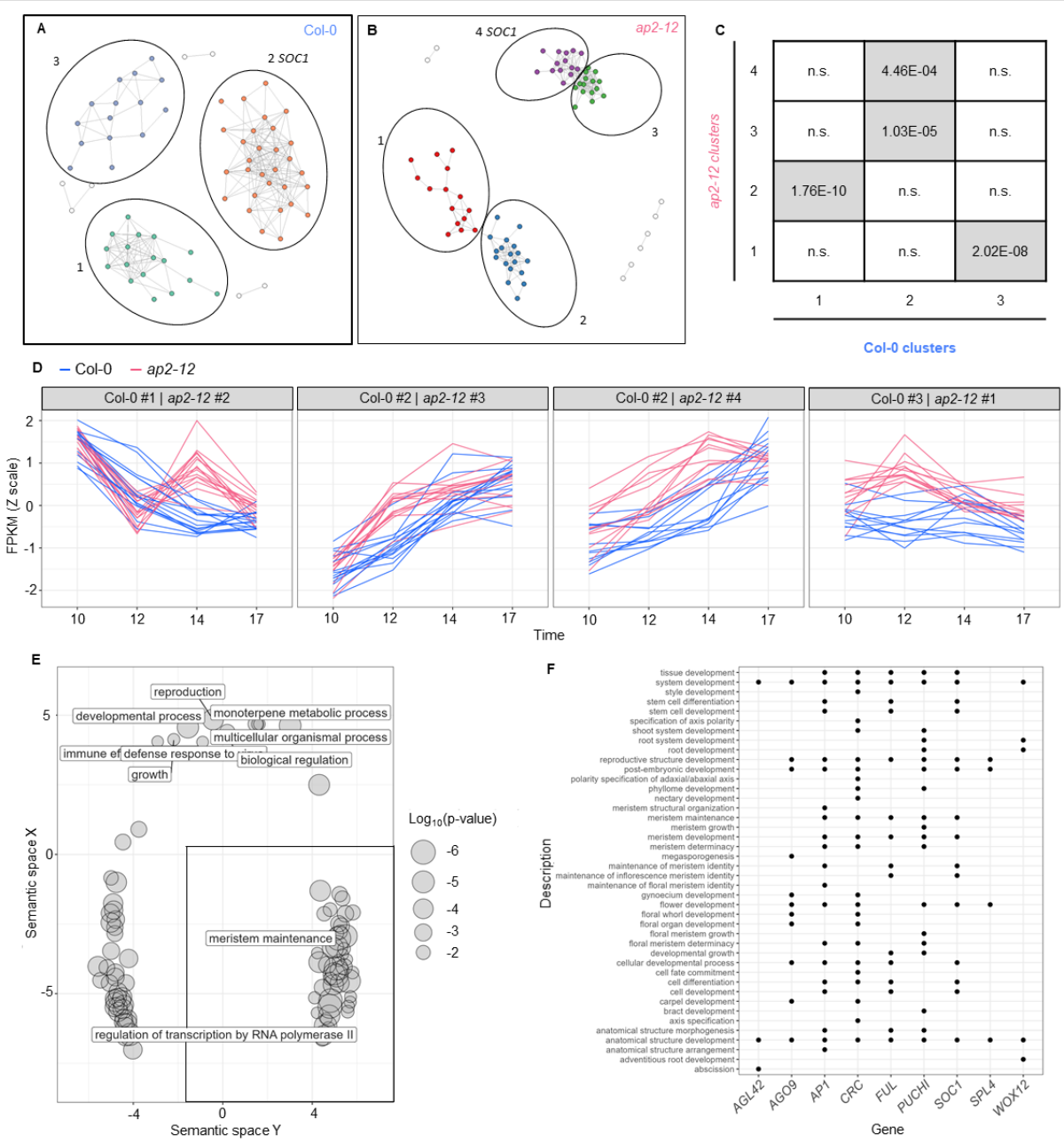

Supplemental Figure 3-6. Co-expression modules during floral transition in dissected apices of Col-0 and *ap2-12*.

(A–D) Co-expression modules among the genes that were differentially expressed between Col-0 and *ap2-12* apices at least one time point during LDs. (A–B) Modules in (A) Col-0 and (B) *ap2-12*. Each node represents one gene. A line connecting two nodes indicates a Pearson correlation coefficient between the expression of these genes greater than 0.85. Co-expression modules smaller than five genes were not considered. Each co-expression module is encircled together with its label. "*SOC1*" indicates the module that includes *SOC1*. (C) Hypogeometric test between Col-0 and *ap2-12* modules. "n.s." indicates lack of significance (*p*-value > 0.05). (D) Expression profiles of the genes in each co-expression module. (E) Revigo visualisation of the enriched gene-ontology (GO)-terms in cluster 4 of the *ap2-12* mutant. (F) Correspondence between genes from cluster 4 and the GO-terms that fall in the proximal semantic space of "meristem maintenance" (represented as a black square in E). Gene symbols: *AGAMOUS-LIKE 42* (*AGL42*); *ARGONAUTE 9* (*AGO9*); *APETALA 1* (*AP1*); *CRABSCLAW* (*CRC*); *FRUITFULL* (*FUL*); *SUPPRESSOR OF OVEREXPRESSION OF CONSTANS 1* (*SOC1*); *SQUAMOSA PROMOTER-BINDING PROTEIN-LIKE 4* (*SPL4*); *WUSCHEL-RELATED HOMEOBOX 12* (*WOX12*).

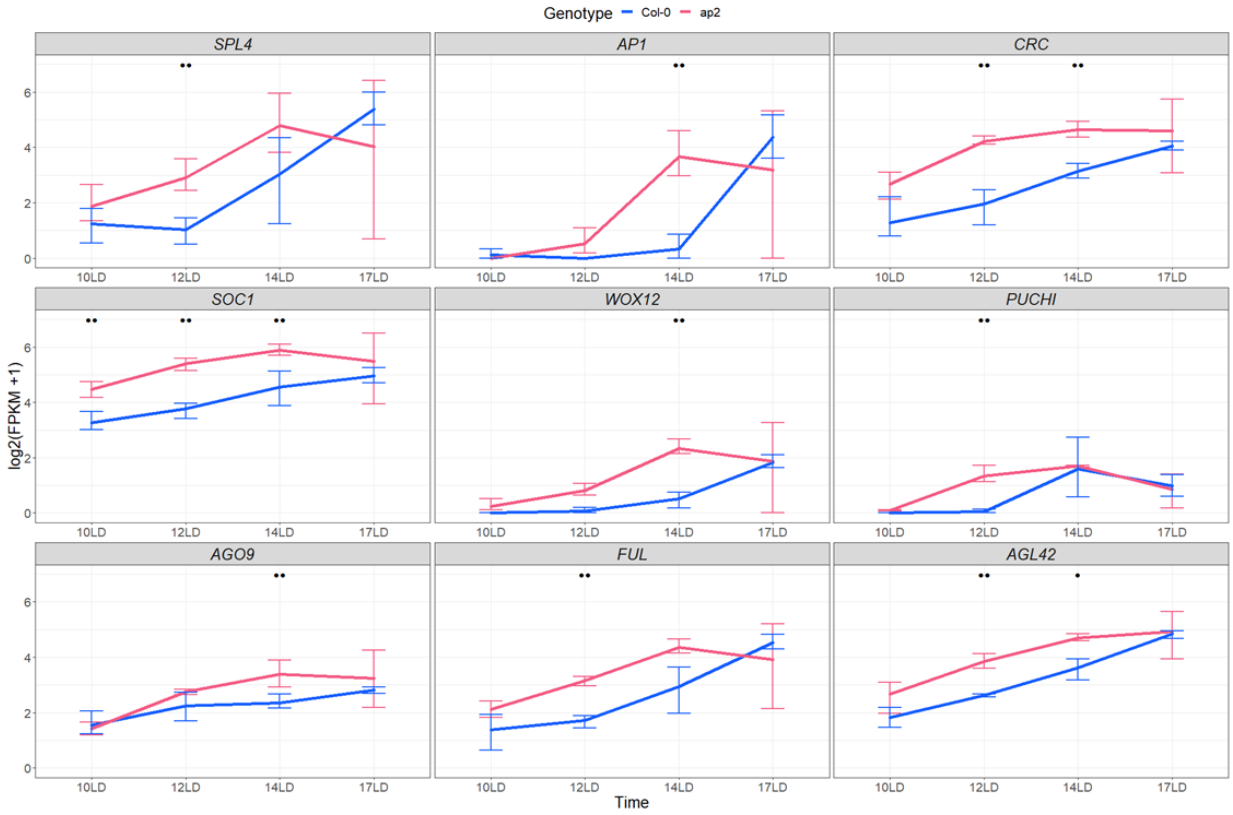

Supplemental Figure 3-7. Expression profile for the genes represented in Supplemental Figure 3-6E in dissected apices of Col-0 and *ap2-12*.

Error bars represent the range between the maximum and minimum values among the three replicates at each time point. Statistically significant differences between Col-0 and *ap2-12* are indicated with * (adjusted *p*-value < 0.05) or ** [adjusted *p*-value < 0.05 and absolute value of $\log_2$(fold change) > 1]. Gene symbols: *AGAMOUS-LIKE 42* (*AGL42*); *ARGONAUTE 9* (*AGO9*); *APETALA 1* (*AP1*); *CRABSCLAW* (*CRC*); *FRUITFULL* (*FUL*); *SUPPRESSOR OF OVEREXPRESSION OF CONSTANS 1 (SOC1); SQUAMOSA PROMOTER-BINDING PROTEIN-LIKE 4* (*SPL4*); *WUSCHEL-RELATED HOMEOBOX 12* (*WOX12*).

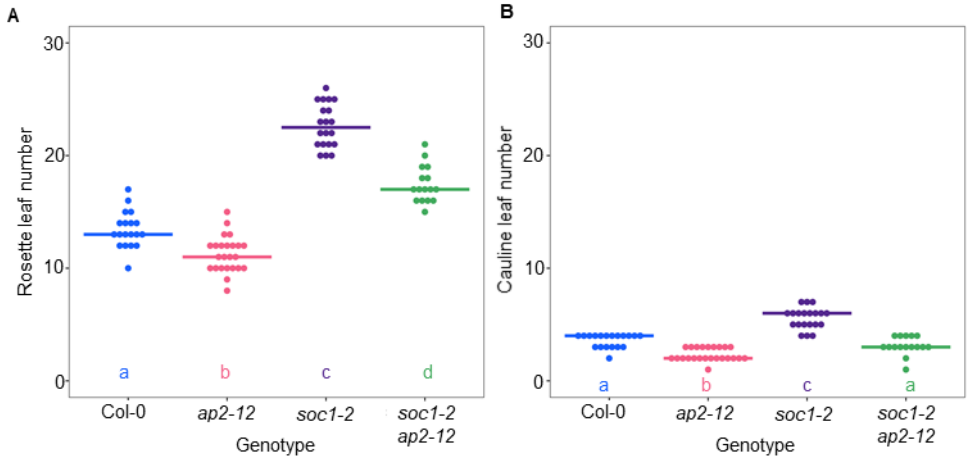

Supplemental Figure 3-8. Flowering time of Col-0, *ap2-12*, *soc1-2* and *soc1-2 ap2-12*.

Flowering time according to (A) rosette and (B) cauline leaf number. The horizontal bars represent the median value for each genotype. Significant differences among genotypes were determined via one-way ANOVA, followed by Tukey post-hoc comparisons ($p < 0.05$). Data sets that share a common letter do not differ significantly. N = 16–24.

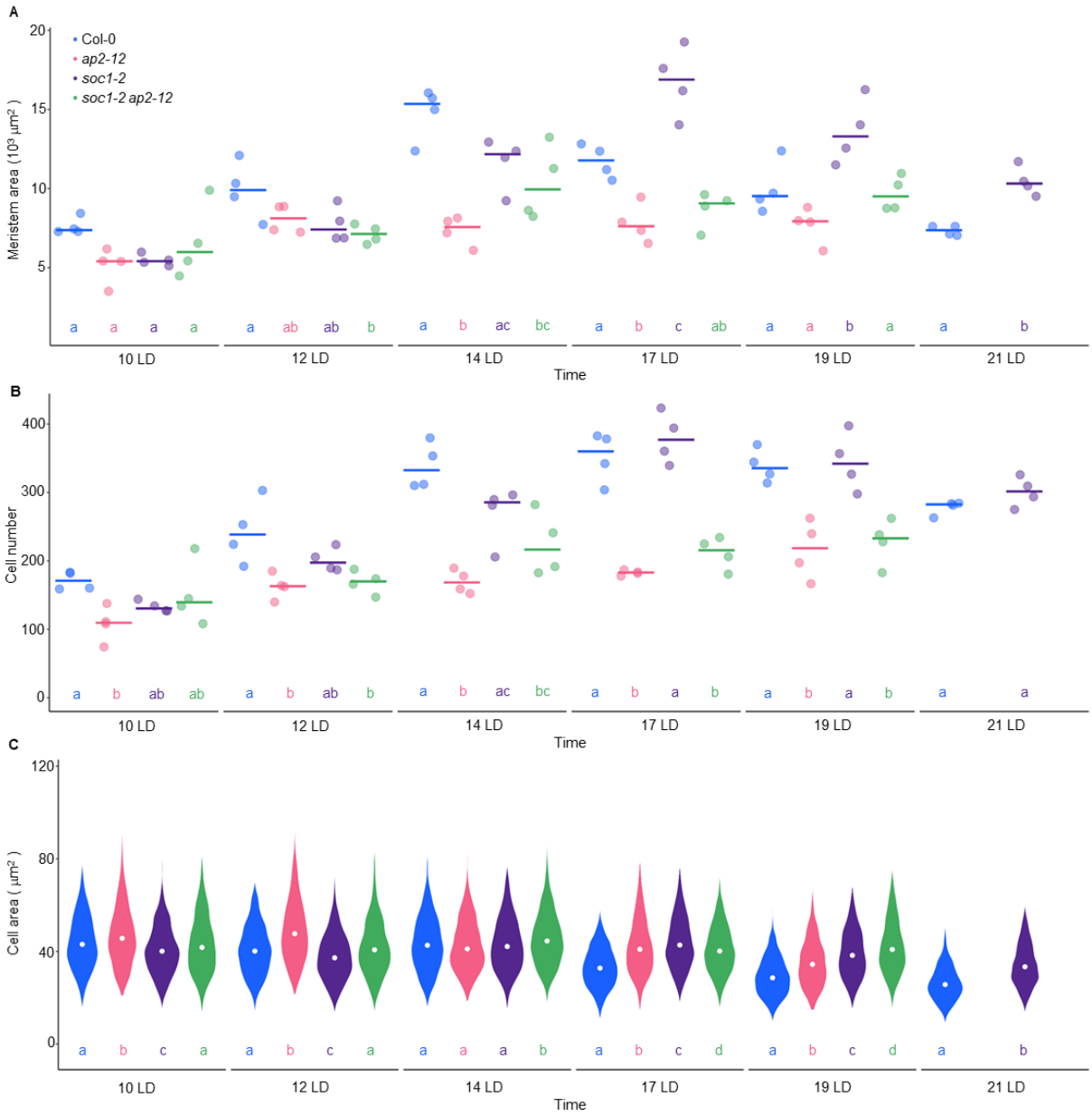

Supplemental Figure 3-9. Quantification of meristem area, cell number and cell area in the meristem region of the analysis shown in Figure 3-4D.

Quantification of (A) meristem area and (B) cell number and (C) cell area. The (A–B) horizontal bars and the (C) white dots represent the median value for each genotype. Significant intra-time point differences among genotypes were determined via one-way ANOVA, followed by Tukey post-hoc comparisons ($p < 0.05$). Data sets that share a common letter do not differ significantly. $N = 4$.

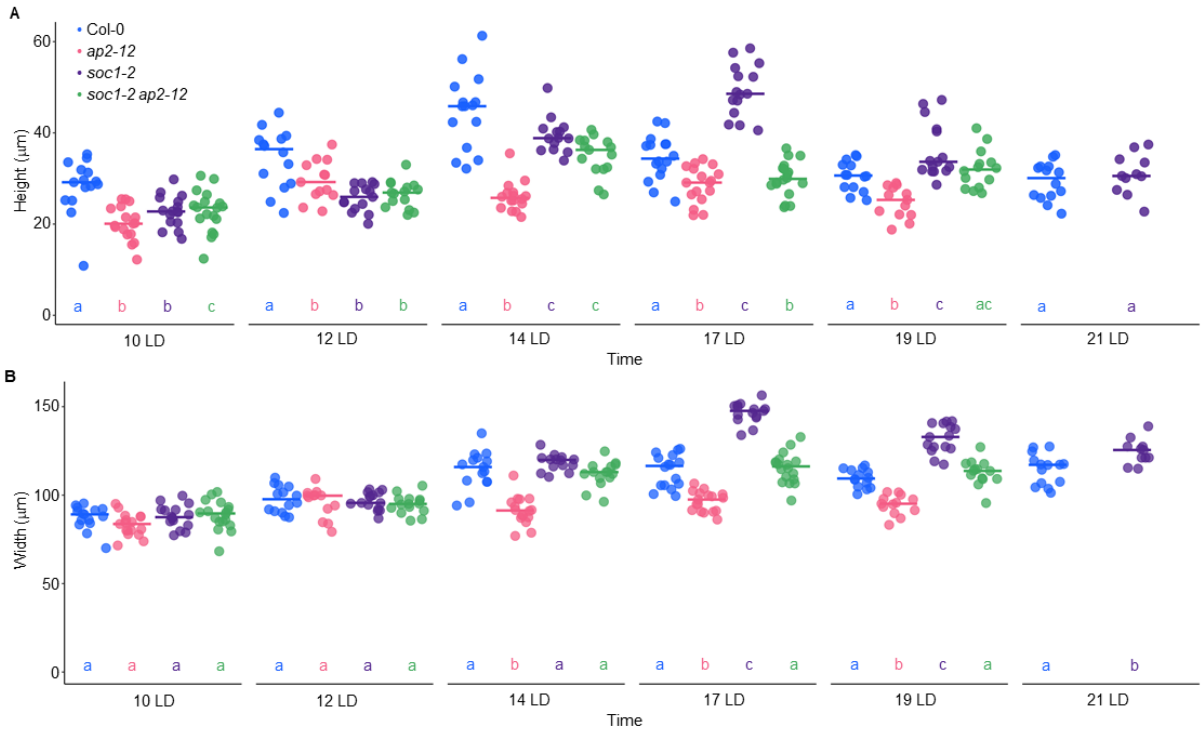

Supplemental Figure 3-10. Measured height and width of the represented meristems in Figure 3-4E.

Measured (A) meristem height and (B) meristem width. The horizontal bars represent the median value for each genotype. Significant intra-time point differences among genotypes were determined via one-way ANOVA, followed by Tukey post-hoc comparisons ($p < 0.05$). Data sets that share a common letter do not differ significantly. $N = 11–18$.

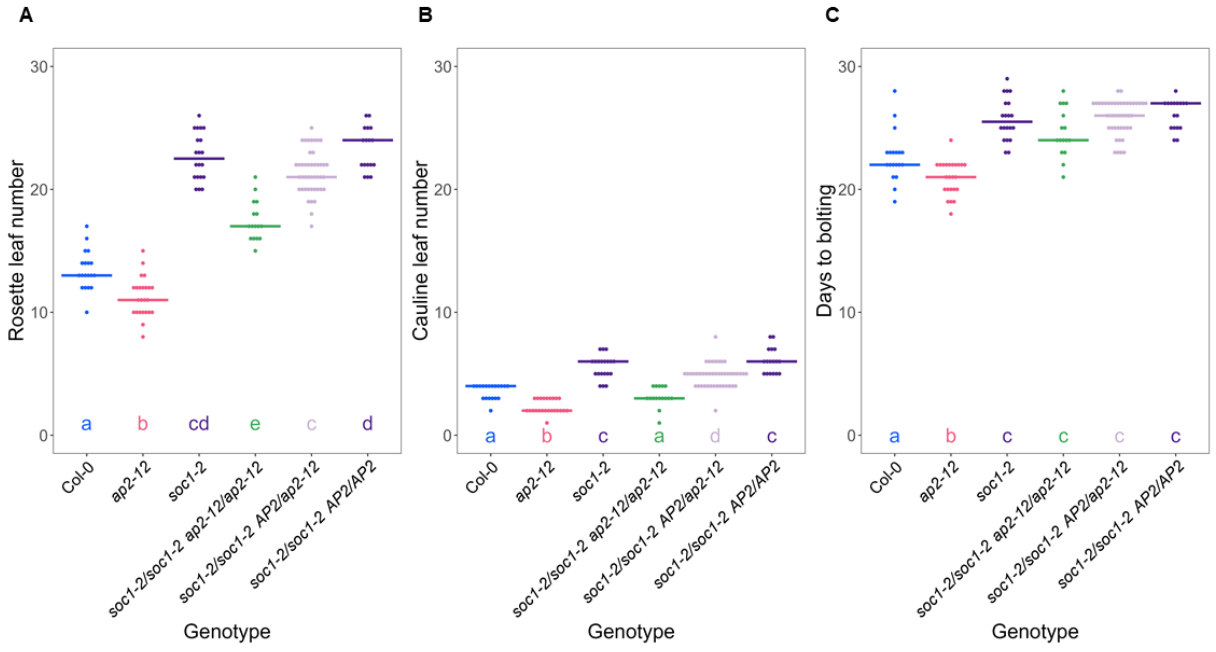

Supplemental Figure 3-11. Flowering time of *soc1-2 ap2-12* and the related segregating lines.

Flowering time was measured by (A) rosette leaf number, (B) cauline leaf number and (C) days to bolting. The horizontal bars represent the median value for each genotype. Significant differences were determined via one-way ANOVA, followed by Tukey post-hoc comparisons ($p < 0,05$). Data sets that share a common letter do not differ significantly. $N = 17–44$.

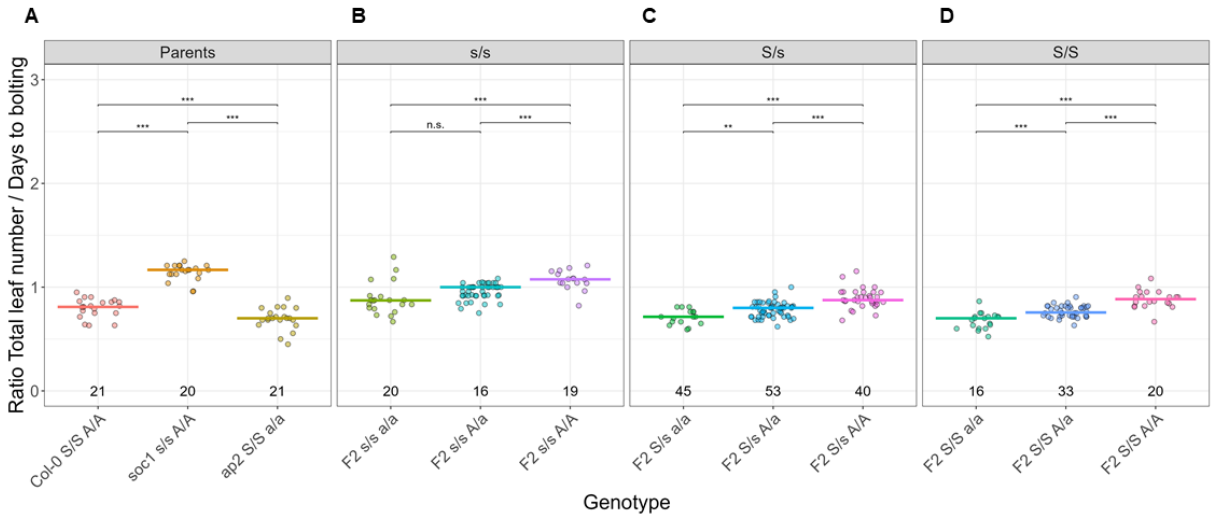

Supplemental Figure 3-12. Estimation of the rate of leaf production as the ratio between total leaf number and days to bolting.

The wild-type (WT) and parental lines are plotted in panel A. The plants are grouped according to their genotype. The horizontal bars represent the median value for each genotype. Immediately above the x axis, the number of samples for each genotype is indicated. The genotype for *SOC1* is represented as S (WT) or s (*soc1-2),* and the genotype for *AP2* is represented as A (WT) or a (*ap2-12)*. Statistical significance between two groups was determined via Student's *t*-tests. Significance ($p < 0.05$) is indicated as *, $p < 0.01$ is indicated as ** and $p < 0.001$ is indicated as ***. ($p > 0.05$) is indicated as n.s. $N = 16–53$.

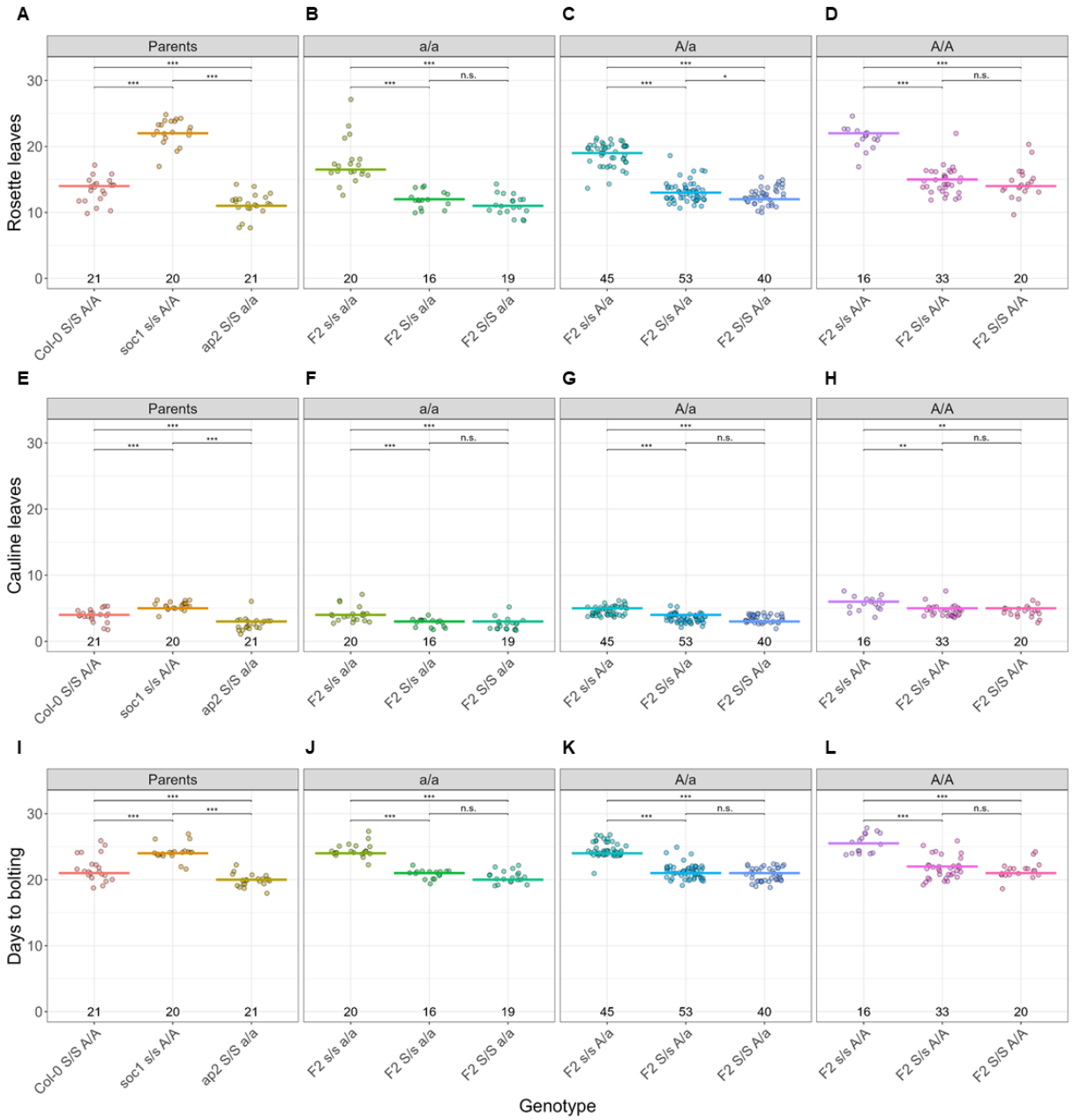

Supplemental Figure 3-13. Data from Figure 3-6 order according to the genotype for *AP2*.

Flowering time measurements of the F2 population from the *soc1-2* × *ap2-12* cross grown under long days in terms of (A–D) rosette leaf number, (E–H) cauline leaf number and (I–L) days to bolting. The wild-type (WT) and parental lines are plotted in panels A, E and I. The plants are grouped according to their genotype. The horizontal bars represent the median value for each genotype. Immediately above the x axis, the number of samples for each genotype is indicated. The genotype for *SOC1* is represented as S (WT) or s (*soc1-2),* and the genotype for *AP2* is represented as A (WT) or a (*ap2-12)*. Statistical significance between two groups was determined via Student's *t*-test. Significance ($p < 0.05$) is indicated as *, $p < 0.01$ is indicated as ** and $p < 0.001$ is indicated as ***. ($p > 0.05$) is indicated as n.s. N = 16–53.

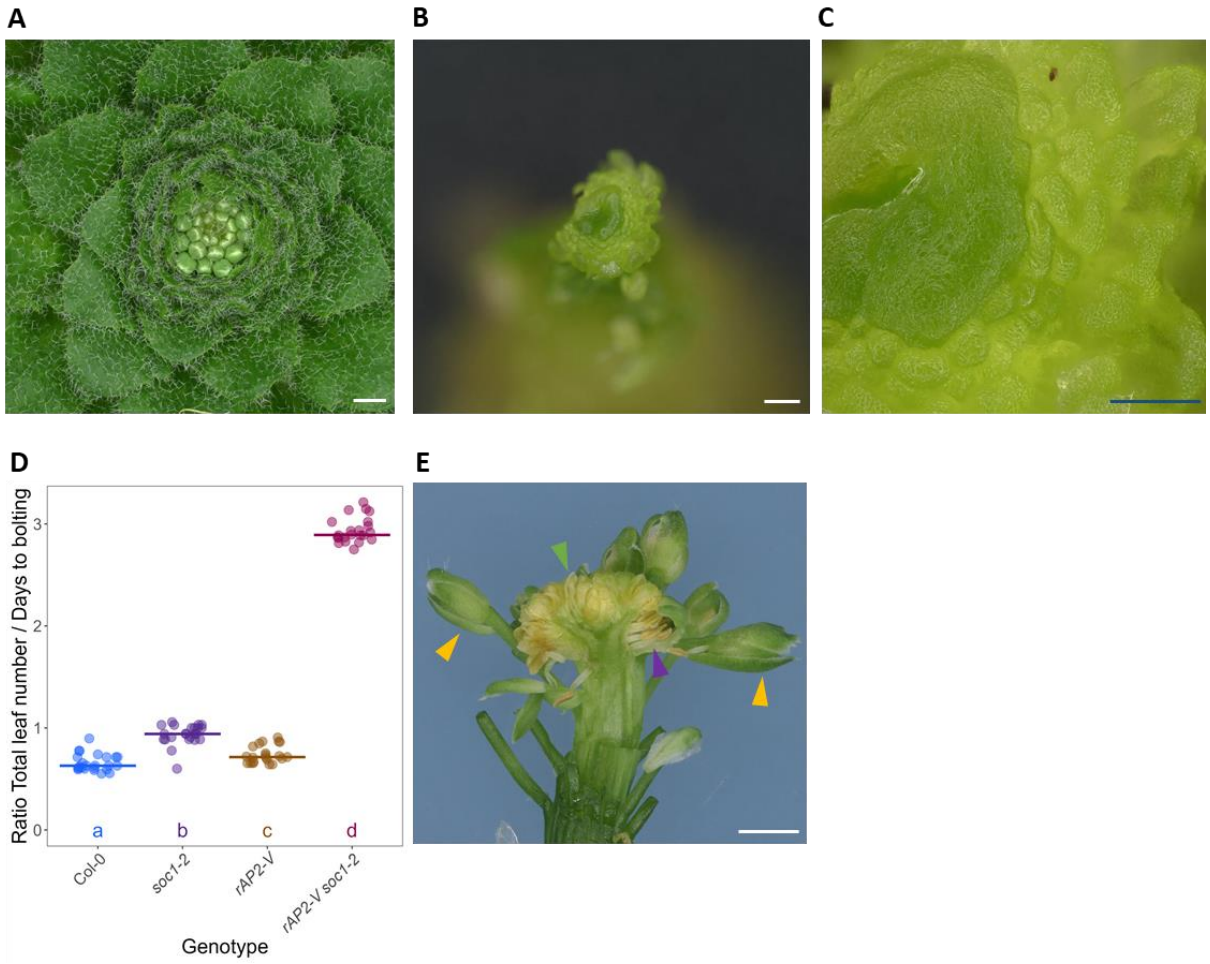

Supplemental Figure 3-14. Inflorescence meristem identity is lost in *rAP2 soc1-2* plants.

(A–C) Photographs of the earliest stages of bolting (48 LD) of an *rAP2-V soc1-2* plant. (A) Top view of the rosette; note the presence of developing flowers. (B–C) Dissected SAM; note the presence of developing stamens in C. (D) Estimation of the rate of leaf production as the ratio between total leaf number and days to bolting. The horizontal bars represent the median value for each genotype. Significant differences were determined via one-way ANOVA, followed by Tukey post-hoc comparisons ($p < 0,05$). Data sets that share a common letter do not differ significantly. $N = 21–24$. (E) Side view a cut section of the terminal flower shown in Figure 3-7I. Note the presence of flowers with subtending bracts (yellow arrowheads), fully developed stamens (purple arrowhead) and a mass of sepalloid tissue (green arrowhead), with the presence of some ovules. White scale bars = 200 µm; blue scale bar = 100 µm.

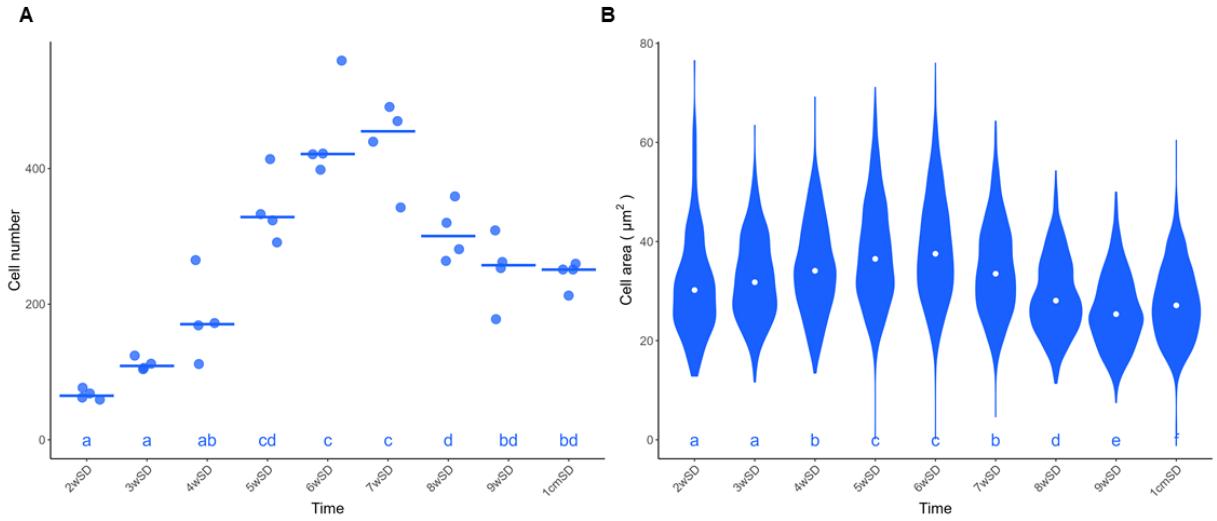

Supplemental Figure 3-15. Changes in cell number and cell area in Col-0 meristems during floral transition under continuous SDs.

The horizontal bars (A) or the white dots (B) represent the median value for each genotype. Significant differences were determined via one-way ANOVA, followed by Tukey post-hoc comparisons ($p < 0,05$). Data sets that share a common letter do not differ significantly. $N = 4$.

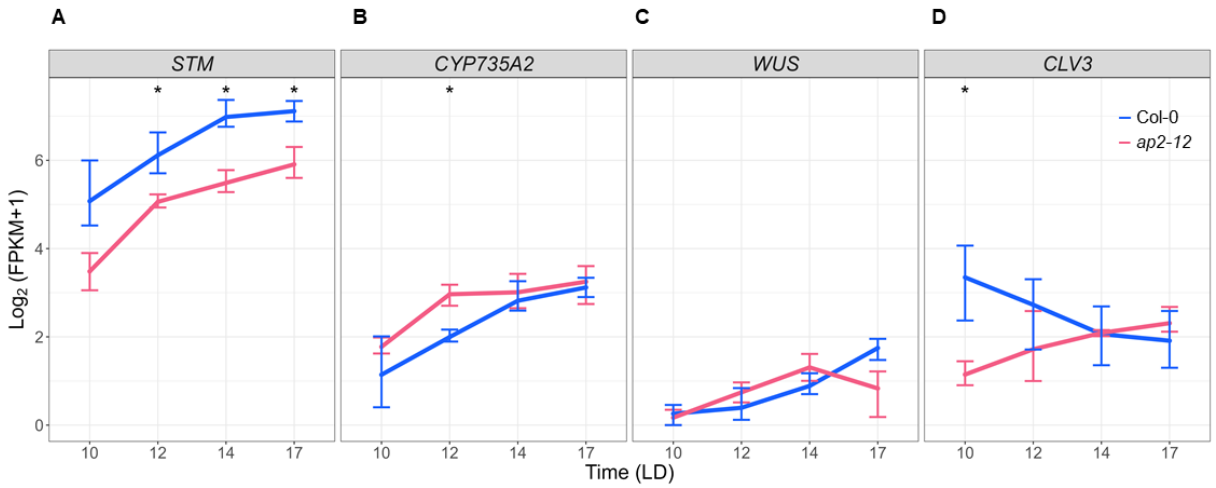

Supplemental Figure 3-16. Expression profiles of selected genes under LDs.

Expression profiles of (A) *STM,* (B) *CYP735A2,* (C) *WUS* and (D) *CLV3* under long days. The gene symbol is given on top of each plot. The colour code corresponds to the genotype and is indicated at the top-right. Error bars represent the range between the maximum and minimum value of three replicates. Statistical differences between Col-0 and *ap2-12* are indicated with * (adjusted *p*-value < 0.05).

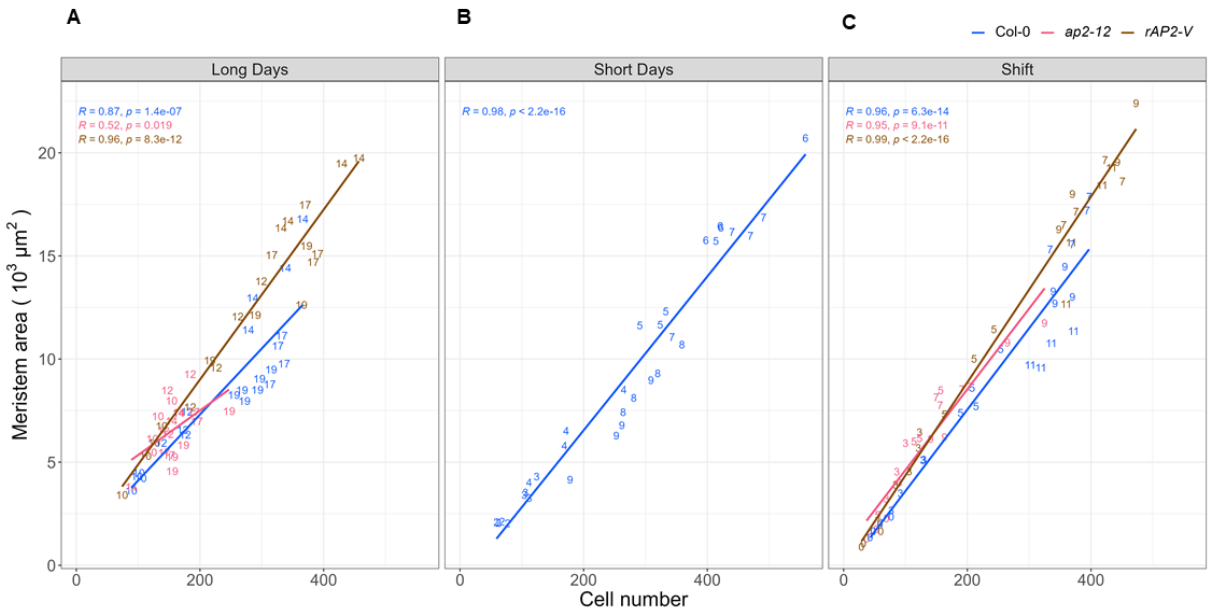

Supplemental Figure 3-17. Correlation between meristem area and cell number in the segmentation analyses of this chapter.

Scatter plots showing the correlation between meristem area and cell number of the SAM of Col-0, *ap2-12* and *rAP2-VENUS* during the time course under (A) continuous long days (LDs), (B) continuous short days (SDs) and (C) during the shift to LDs after 2 weeks under SD conditions. Each number corresponds to one sample and represents (A,C) the number of days in which the plant grew under LD conditions or (B) the number of weeks in which the plant grew under SD conditions. The regression line for each genotype is represented. The colour of the numbers and the regression line correspond to the genotype, and the colour code is indicated at the top-right of panel C. The Pearson correlation coefficient and the *p*-value is indicated for each genotype at the top-left corner of each panel.

Supplemental Table 3-1. List of genes that are differentially expressed in *ap2-12* compared with Col-0 apices during floral transition under LDs.

"n.a." = not assigned, i.e. comparisons that are not statistically significant (adjusted *p*-value > 0.05). "LFC" = Log_2(Fold Change). "LD" = Long days. Adjusted *p*-values are shown.

AGI gene code	Description (NCBI gene)	Symbol	10 LD		12 LD		14 LD		17 LD	
			LFC	*p*-value	LFC	*p*-value	LFC	*p*-value	LFC	*p*-value
AT1G02190	Fatty acid hydroxylase superfamily	*AT1G02190*	n.a.	n.a.	1.04	4.97E-02	n.a.	n.a.	n.a.	n.a.
AT1G02640	Beta-xylosidase 2	*BXL2*	n.a.	n.a.	1.20	4.31E-04	n.a.	n.a.	n.a.	n.a.
AT1G04800	Glycine-rich protein	*AT1G04800*	n.a.	n.a.	n.a.	n.a.	4.57	8.03E-05	n.a.	n.a.
AT1G07730	Disease resistance-responsive (dirigent-like protein) family protein	*AT1G07730*	n.a.	n.a.	6.87	3.18E-05	n.a.	n.a.	n.a.	n.a.
AT1G10070	Branched-chain amino acid transaminase 2	*BCAT-2*	n.a.	n.a.	1.64	1.89E-02	n.a.	n.a.	n.a.	n.a.
AT1G15980	NDH-dependent cyclic electron flow 1	*PNSB1*	n.a.	n.a.	n.a.	n.a.	1.88	4.13E-02	n.a.	n.a.
AT1G18735	ncRNA	*AT1G18735*	n.a.	n.a.	5.33	1.14E-02	n.a.	n.a.	n.a.	n.a.
AT1G19540	NmrA-like negative transcriptional regulator family protein	*AT1G19540*	n.a.	n.a.	1.11	2.34E-03	n.a.	n.a.	n.a.	n.a.
AT1G21360	Glycolipid transfer protein 2	*GLTP2*	n.a.	n.a.	3.30	6.39E-03	n.a.	n.a.	n.a.	n.a.
AT1G31690	Copper amine oxidase family protein	*AT1G31690*	n.a.	n.a.	n.a.	n.a.	2.69	1.95E-04	n.a.	n.a.
AT1G32080	Membrane protein	*LRGB*	n.a.	n.a.	n.a.	n.a.	1.41	8.43E-03	n.a.	n.a.
AT1G33055		*AT1G33055*	n.a.	n.a.	2.51	1.48E-13	n.a.	n.a.	n.a.	n.a.
AT1G43800	Plant stearoyl-acyl-carrier-protein desaturase family protein	*FTM1*	n.a.	n.a.	1.10	3.20E-03	n.a.	n.a.	n.a.	n.a.
AT1G53160	Squamosa promoter binding protein-like 4	*SPL4*	n.a.	n.a.	2.44	2.41E-03	n.a.	n.a.	n.a.	n.a.
AT1G60590	Pectin lyase-like superfamily protein	*AT1G60590*	n.a.	n.a.	n.a.	n.a.	n.a.	n.a.	-1.09	1.22E-08
AT1G62360	KNOX/ELK homeobox transcription factor	*STM*	n.a.	n.a.	-1.02	7.79E-04	-1.47	8.22E-10	-1.10	8.19E-04

AT1G62370	RING/U-box superfamily protein	*AT1G62370*	n.a.	n.a.	n.a.	n.a.	2.13	2.23E-06	n.a.	n.a.
AT1G63050	MBOAT (membrane bound O-acyl transferase) family protein	*LPLAT2*	1.09	1.33E-03	1.02	8.55E-09	1.42	9.70E-15	n.a.	n.a.
AT1G67110	Cytochrome P450. Family 735. Subfamily A. Polypeptide 2	*CYP735A2*	n.a.	n.a.	1.05	5.50E-03	n.a.	n.a.	n.a.	n.a.
AT1G68440	Transmembrane protein	*AT1G68440*	n.a.	n.a.	1.02	3.14E-02	n.a.	n.a.	n.a.	n.a.
AT1G69120	K-box region and MADS-box transcription factor family protein	*AP1*	n.a.	n.a.	n.a.	n.a.	4.81	3.96E-02	n.a.	n.a.
AT1G69180	Plant-specific transcription factor YABBY family protein	*CRC*	n.a.	n.a.	2.37	1.87E-10	1.54	1.31E-06	n.a.	n.a.
AT1G70290	Trehalose-6-phosphatase synthase S8	*TPS8*	n.a.	n.a.	1.12	2.41E-03	n.a.	n.a.	n.a.	n.a.
AT1G78500	Terpenoid cyclases family protein	*AT1G78500*	n.a.	n.a.	n.a.	n.a.	n.a.	n.a.	-2.02	2.41E-02
AT2G02710	PAS/LOV protein B	*PLPB*	n.a.	n.a.	1.08	1.17E-03	n.a.	n.a.	n.a.	n.a.
AT2G04160	Subtilisin-like serine endopeptidase family protein	*AIR3*	n.a.	n.a.	n.a.	n.a.	4.93	3.02E-16	n.a.	n.a.
AT2G05812	ncRNA	*AT2G05812*	n.a.	n.a.	8.47	2.21E-14	n.a.	n.a.	n.a.	n.a.
AT2G15880	Leucine-rich repeat (LRR) family protein	*AT2G15880*	n.a.	n.a.	1.44	3.20E-03	n.a.	n.a.	n.a.	n.a.
AT2G18700	Trehalose phosphatase/synthase 11	*TPS11*	n.a.	n.a.	1.20	3.04E-04	n.a.	n.a.	n.a.	n.a.
AT2G19590	ACC oxidase 1	*ACO1*	n.a.	n.a.	1.44	3.75E-09	n.a.	n.a.	n.a.	n.a.
AT2G20670	Sugar phosphate exchanger. Putative (duf506)	*AT2G20670*	n.a.	n.a.	1.16	7.24E-03	n.a.	n.a.	n.a.	n.a.
AT2G26150	Heat shock transcription factor A2	*HSFA2*	n.a.	n.a.	-2.66	1.23E-03	n.a.	n.a.	n.a.	n.a.
AT2G26400	Acireductone dioxygenase 3	*ARD3*	n.a.	n.a.	1.07	6.60E-03	n.a.	n.a.	n.a.	n.a.
AT2G28120	Major facilitator superfamily protein	*AT2G28120*	n.a.	n.a.	1.47	3.83E-02	n.a.	n.a.	n.a.	n.a.
AT2G31085	CLAVATA3/ESR-RELATED 6	*CLE6*	n.a.	n.a.	2.10	1.15E-02	n.a.	n.a.	n.a.	n.a.

AT2G39380	exocyst subunit exo70 family protein h2	*EXO70H2*	n.a.	n.a.	6.09	2.34E-03	8.07	3.10E-10	n.a.	n.a.
AT2G45660	AGAMOUS-like 20	*AGL20*	1.09	4.54E-02	1.61	5.60E-11	1.15	5.03E-03	n.a.	n.a.
AT3G01500	Carbonic anhydrase 1	*CA1*	n.a.	n.a.	n.a.	n.a.	5.25	1.48E-33	n.a.	n.a.
AT3G05730	Defensin-like protein	*AT3G05730*	n.a.	n.a.	n.a.	n.a.	1.33	1.70E-02	n.a.	n.a.
AT3G12580	Heat shock protein 70	*HSP70*	-7.93E-06	3.46E-03	-2.47	2.68E-06	n.a.	n.a.	n.a.	n.a.
AT3G15450	Aluminum induced protein with YGL and LRDR motifs	*AT3G15450*	n.a.	n.a.	1.68	4.52E-03	n.a.	n.a.	n.a.	n.a.
AT3G16360	HPT phosphotransmitter 4	*AHP4*	n.a.	n.a.	n.a.	n.a.	-1.40	3.37E-03	n.a.	n.a.
AT3G16660	Pollen Ole e 1 allergen and extensin family protein	*AT3G16660*	n.a.	n.a.	n.a.	n.a.	2.18	8.35E-03	n.a.	n.a.
AT3G16670	Pollen Ole e 1 allergen and extensin family protein	*AT3G16670*	n.a.	n.a.	n.a.	n.a.	7.05	2.20E-39	n.a.	n.a.
AT3G22435		*AT3G22435*	6.90	6.51E-06	n.a.	n.a.	n.a.	n.a.	n.a.	n.a.
AT3G26200	Cytochrome P450. family 71. subfamily B. polypeptide 22	*CYP71B22*	n.a.	n.a.	n.a.	n.a.	1.90	3.89E-02	n.a.	n.a.
AT3G26250	Cysteine/Histidine-rich C1 domain family protein	*AT3G26250*	9.25	3.50E-27	9.26	1.02E-25	9.52	4.29E-24	10.09	1.38E-27
AT3G28500	60S acidic ribosomal protein family	*AT3G28500*	n.a.	n.a.	n.a.	n.a.	2.18	3.45E-03	n.a.	n.a.
AT3G29633		*AT3G29633*	3.65	3.24E-02	n.a.	n.a.	n.a.	n.a.	n.a.	n.a.
AT3G45140	Lipoxygenase 2	*LOX2*	n.a.	n.a.	n.a.	n.a.	1.61	2.46E-02	n.a.	n.a.
AT3G52840	Beta-galactosidase 2	*BGAL2*	n.a.	n.a.	1.11	6.83E-03	n.a.	n.a.	n.a.	n.a.
AT3G58120	Basic-leucine zipper (bZIP) transcription factor family protein	*BZIP61*	n.a.	n.a.	n.a.	n.a.	1.20	5.03E-03	n.a.	n.a.
AT3G62950	Thioredoxin superfamily protein	*AT3G62950*	n.a.	n.a.	1.70	3.59E-02	n.a.	n.a.	n.a.	n.a.
AT4G01525	SADHU non-coding retrotransposon 5-1	*SADHU5-1*	2.87	1.74E-19	2.33	3.31E-20	2.15	7.09E-21	1.74	4.84E-13

AT4G03060	Alkenyl hydroxalkyl producing 2	*AOP2*	n.a.	n.a.	-1.01	3.30E-10	-0.96	1.10E-02	n.a.	n.a.
AT4G04223	ncRNA	*AT4G04223*	n.a.	n.a.	n.a.	n.a.	-3.46	8.43E-03	n.a.	n.a.
AT4G08290	Nodulin mtn21 /eama-like transporter family protein	*UMAMIT20*	n.a.	n.a.	1.04	4.52E-05	n.a.	n.a.	n.a.	n.a.
AT4G15160	Bifunctional inhibitor/lipid-transfer protein/seed storage 2S albumin superfamily protein	*AT4G15160*	n.a.	n.a.	1.08	3.39E-07	n.a.	n.a.	n.a.	n.a.
AT4G15320	Cellulose synthase-like B6	*CSLB06*	n.a.	n.a.	n.a.	n.a.	-1.81	6.09E-03	n.a.	n.a.
AT4G15490	UDP-Glycosyltransferase superfamily protein	*UGT84A3*	n.a.	n.a.	n.a.	n.a.	1.84	5.23E-03	n.a.	n.a.
AT4G16260	Glycosyl hydrolase superfamily protein	*AT4G16260*	n.a.	n.a.	2.44	3.20E-03	n.a.	n.a.	n.a.	n.a.
AT4G22495		*AT4G22495*	n.a.	n.a.	2.81	4.92E-02	n.a.	n.a.	n.a.	n.a.
AT4G24110	NADP-specific glutamate dehydrogenase	*AT4G24110*	n.a.	n.a.	1.16	3.19E-02	n.a.	n.a.	n.a.	n.a.
AT4G24150	Growth-regulating factor 8	*GRF8*	n.a.	n.a.	n.a.	n.a.	2.04	3.37E-03	n.a.	n.a.
AT4G26150	Cytokinin-responsive gata factor 1	*CGA1*	n.a.	n.a.	-1.35	1.75E-02	n.a.	n.a.	n.a.	n.a.
AT4G26530	Aldolase superfamily protein	*FBA5*	n.a.	n.a.	n.a.	n.a.	3.48	1.80E-05	n.a.	n.a.
AT4G27450	Aluminum induced protein with YGL and LRDR motifs	*AT4G27450*	n.a.	n.a.	1.79	2.06E-24	0.81	1.42E-04	n.a.	n.a.
AT4G33070	Thiamine pyrophosphate dependent pyruvate decarboxylase family protein	*AT4G33070*	n.a.	n.a.	2.76	2.00E-11	n.a.	n.a.	n.a.	n.a.
AT4G34065	Pseudogene of AT5G06265	*AT4G34065*	n.a.	n.a.	n.a.	n.a.	-2.32	7.05E-03	n.a.	n.a.
AT4G35770	Rhodanese/Cell cycle control phosphatase superfamily protein	*SEN1*	n.a.	n.a.	2.63	1.84E-07	n.a.	n.a.	n.a.	n.a.
AT4G36030	Armadillo repeat only 3	*ARO3*	7.64	2.96E-03	n.a.	n.a.	n.a.	n.a.	n.a.	n.a.
AT4G36430	Peroxidase superfamily protein	*AT4G36430*	n.a.	n.a.	2.60	3.20E-03	n.a.	n.a.	n.a.	n.a.

AT4G36920	Integrase-type DNA-binding superfamily protein	*AP2*	-2.22	3.50E-27	-1.77	7.99E-35	-1.86	8.55E-19	n.a.	n.a.
AT4G37980	Cinnamyl alcohol dehydrogenase 7	*ELI3-1*	n.a.	n.a.	n.a.	n.a.	2.72	4.60E-02	n.a.	n.a.
AT4G38820		*AT4G38820*	n.a.	n.a.	5.99	2.56E-03	n.a.	n.a.	n.a.	n.a.
AT4G39480	cytochrome p450. family 96. subfamily a. polypeptide 9	*CYP96A9*	n.a.	n.a.	n.a.	n.a.	1.58	1.70E-02	n.a.	n.a.
AT4G39675		*AT4G39675*	n.a.	n.a.	5.76	2.56E-03	n.a.	n.a.	n.a.	n.a.
AT5G01540	lectin receptor kinase a4.1	*LECRKA4.1*	n.a.	n.a.	6.54	4.93E-04	n.a.	n.a.	n.a.	n.a.
AT5G05440	polyketide cyclase/dehydrase and lipid transport superfamily protein	*PYL5*	n.a.	n.a.	1.06	2.29E-02	n.a.	n.a.	n.a.	n.a.
AT5G14565	ath-mir398c	*ATH-MIR398C*	n.a.	n.a.	5.45	2.70E-02	n.a.	n.a.	n.a.	n.a.
AT5G14740	carbonic anhydrase 2	*CA2*	n.a.	n.a.	n.a.	n.a.	2.67	1.80E-05	n.a.	n.a.
AT5G17810	WUSCHEL related homeobox 12	*WOX12*	n.a.	n.a.	n.a.	n.a.	2.83	5.49E-04	n.a.	n.a.
AT5G18560	Integrase-type DNA.-binding superfamily protein	*PUCHI*	n.a.	n.a.	4.56	1.02E-03	n.a.	n.a.	n.a.	n.a.
AT5G19120	Eukaryotic aspartyl protease family protein	*AT5G19120*	n.a.	n.a.	1.31	8.33E-06	n.a.	n.a.	n.a.	n.a.
AT5G20250	Raffinose synthase family protein	*DIN10*	n.a.	n.a.	1.96	2.50E-10	n.a.	n.a.	n.a.	n.a.
AT5G21150	Argonaute family protein	*AGO9*	n.a.	n.a.	n.a.	n.a.	1.06	1.70E-02	n.a.	n.a.
AT5G22920	CHY-type/CTCHY-type/RING-type Zinc finger protein	*AT5G22920*	n.a.	n.a.	1.12	1.44E-06	n.a.	n.a.	n.a.	n.a.
AT5G38420	Ribulose bisphosphate carboxylase (small chain) family protein	*RBCS2B*	n.a.	n.a.	n.a.	n.a.	2.52	1.57E-02	n.a.	n.a.
AT5G38430	Ribulose bisphosphate carboxylase (small chain) family protein	*RBCS1B*	n.a.	n.a.	n.a.	n.a.	1.37	3.37E-03	n.a.	n.a.
AT5G38710	Methylenetetrahydrofolate reductase family protein	*AT5G38710*	n.a.	n.a.	1.14	9.13E-05	n.a.	n.a.	n.a.	n.a.

AT5G44480	NAD(P)-binding Rossmann-fold superfamily protein	*DUR*	n.a.	n.a.	n.a.	n.a.	-1.03	4.25E-02	n.a.	n.a.
AT5G44620	Cytochrome P450. Family 706. Subfamily A. Polypeptide 3	*CYP706A3*	n.a.	n.a.	1.01	3.47E-02	n.a.	n.a.	n.a.	n.a.
AT5G45340	Cytochrome P450. Family 707. Subfamily A. Polypeptide 3	*CYP707A3*	n.a.	n.a.	1.79	1.15E-04	n.a.	n.a.	n.a.	n.a.
AT5G49360	Beta-xylosidase 1	*BXL1*	n.a.	n.a.	1.39	3.24E-06	n.a.	n.a.	n.a.	n.a.
AT5G52640	Heat shock-like protein	*HSP90.1*	n.a.	n.a.	-1.39	3.78E-04	n.a.	n.a.	n.a.	n.a.
AT5G55930	Oligopeptide transporter 1	*OPT1*	n.a.	n.a.	n.a.	n.a.	2.35	1.16E-02	n.a.	n.a.
AT5G56870	Beta-galactosidase 4	*BGAL4*	n.a.	n.a.	2.10	2.56E-03	n.a.	n.a.	n.a.	n.a.
AT5G60910	AGAMOUS-like 8	*AGL8*	n.a.	n.a.	1.63	4.31E-04	n.a.	n.a.	n.a.	n.a.
AT5G62165	AGAMOUS-like 42	*AGL42*	n.a.	n.a.	1.22	5.55E-03	0.92	3.32E-02	n.a.	n.a.
AT5G63160	BTB and TAZ domain protein 1	*BT1*	n.a.	n.a.	1.06	3.11E-03	n.a.	n.a.	n.a.	n.a.
AT5G65730	Xyloglucan endotransglucosylase/hydrolase 6	*XTH6*	n.a.	n.a.	n.a.	n.a.	1.53	2.41E-05	n.a.	n.a.
AT5G67180	Target of early activation tagged (EAT) 3	*TOE3*	n.a.	n.a.	n.a.	n.a.	1.01	8.43E-03	n.a.	n.a.

Supplemental Table 3-2. Differentially expressed genes in Col-0 apices at 10 LD vs. 14 LD and in Col-0 vs. *ap2-12* apices at 14 LD.

This list corresponds to the overlap of two of the three data sets represented in Figure 3-3B. "LFC" = Log_2(Fold Change). "LD" = Long days. Adjusted *p*-values are shown.

AGI gene code	Description (NCBI gene)	Symbol	Col-0 10 LD vs. 14 LD		Col-0 vs. *ap2-12* 14 LD	
			LFC	Ajusted *p*-value	LFC	Ajusted *p*-value
AT1G04800	Glycine-rich protein	*AT1G04800*	-5.89	2.49E-06	4.57	8.03E-05
AT1G15980	NDH-dependent cyclic electron flow 1	*PNSB1*	-4.05	4.48E-05	1.88	4.13E-02
AT1G31690	Copper amine oxidase family protein	*AT1G31690*	-3.71	6.27E-04	2.69	1.95E-04
AT1G32080	Membrane protein	*LRGB*	-3.08	8.41E-05	1.41	8.43E-03
AT1G62360	KNOX/ELK homeobox transcription factor	*STM*	1.62	4.62E-04	-1.47	8.22E-10
AT1G69180	Plant-specific transcription factor YABBY family protein	*CRC*	1.72	1.05E-02	1.54	1.31E-06
AT2G04160	Subtilisin-like serine endopeptidase family protein	*AIR3*	-3.71	3.36E-04	4.93	3.02E-16
AT2G45660	AGAMOUS-like 20	*AGL20*	1.21	5.41E-03	1.15	5.03E-03
AT3G01500	Carbonic anhydrase 1	*CA1*	-6.55	4.98E-06	5.25	1.48E-33
AT3G05730	Defensin-like protein	*AT3G05730*	-1.05	2.93E-02	1.33	1.70E-02
AT3G45140	Lipoxygenase 2	*LOX2*	-3.16	3.40E-05	1.61	2.46E-02
AT3G58120	Basic-leucine zipper (bZIP) transcription factor family protein	*BZIP61*	-1.86	1.28E-05	1.20	5.03E-03
AT4G01525	SADHU non-coding retrotransposon 5-1	*SADHU5-1*	1.28	7.55E-04	2.15	7.09E-21
AT4G26530	Aldolase superfamily protein	*FBA5*	-3.91	8.50E-09	3.48	1.80E-05
AT4G34065	Pseudogene of AT5G06265	*AT4G34065*	1.24	2.92E-02	-2.32	7.05E-03
AT4G37980	Cinnamyl alcohol dehydrogenase 7	*ELI3-1*	-2.90	7.11E-03	2.72	4.60E-02
AT5G14740	Carbonic anhydrase 2	*CA2*	-4.57	2.45E-09	2.67	1.80E-05
AT5G38420	Ribulose bisphosphate carboxylase (small chain) family protein	*RBCS2B*	-4.49	5.02E-05	2.52	1.57E-02
AT5G38430	Ribulose bisphosphate carboxylase (small chain) family protein	*RBCS1B*	-3.70	1.41E-04	1.37	3.37E-03

3.5 Appendix to Chapter 3: miR172 controls SAM size by regulating AP2 during floral transition

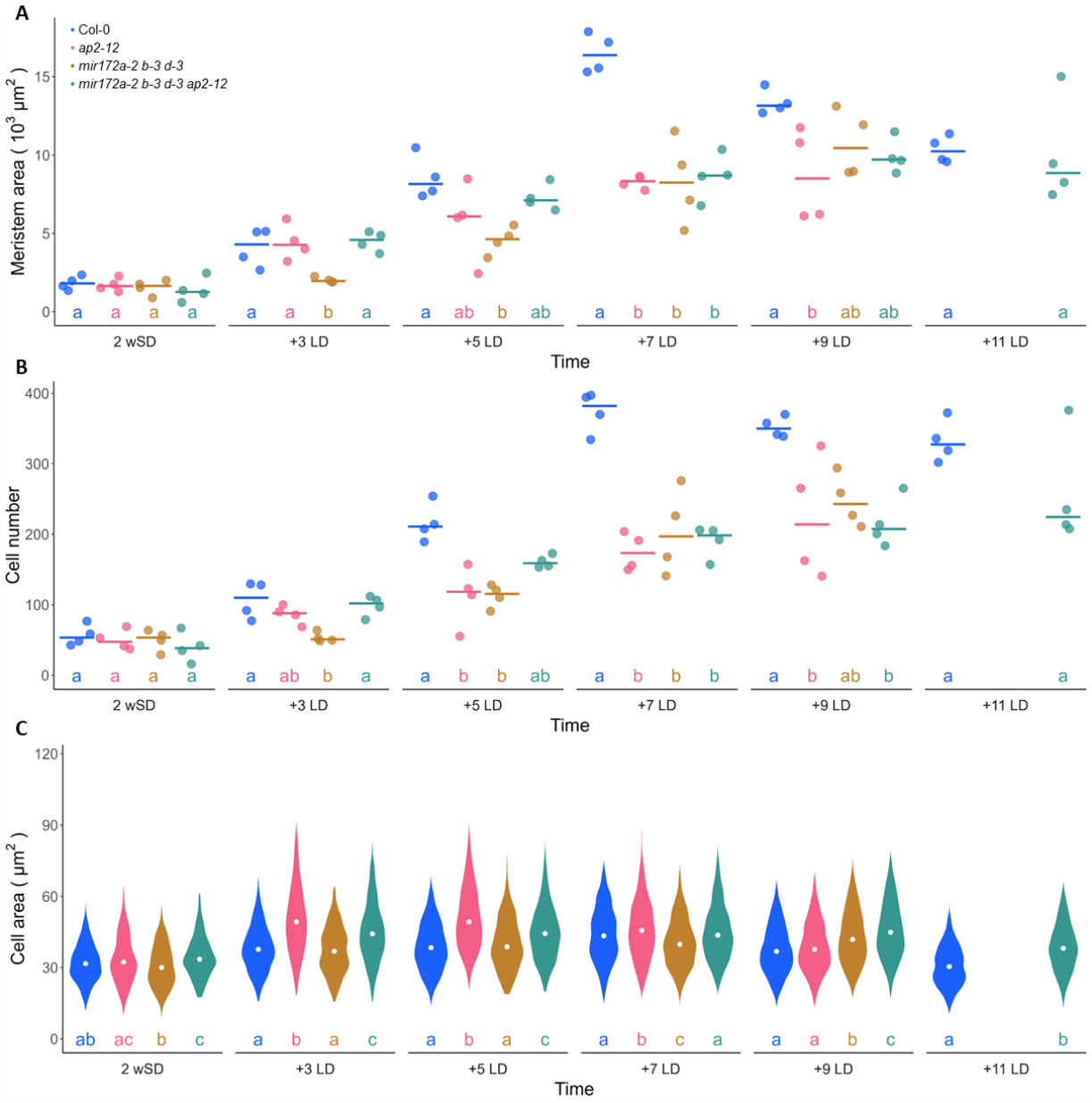

Appendix Figure 3-1. Segmentation analysis of the shoot apical meristems of Col-0, *ap2-12, mir172a-2 b-3 d-3* and *mir172a-2 b-3 d-3 ap2-12* plants grown for 2 weeks under short day (SD) conditions and then transferred to long day (LD) conditions.

Quantification of (A) meristem area and (B) cell number and (C) cell area in the meristem region. The (a–b) horizontal bars and the (c) white dots represent the median value for each genotype. Significant intra-time point differences among genotypes were determined via one-way ANOVA, followed by Tukey post-hoc comparisons ($p < 0.05$). Data sets that share a common letter do not differ significantly. The colour of the dots and the letters correspond to the genotype, and the colour code is indicated at the top-left of panel A. $N = 4$.

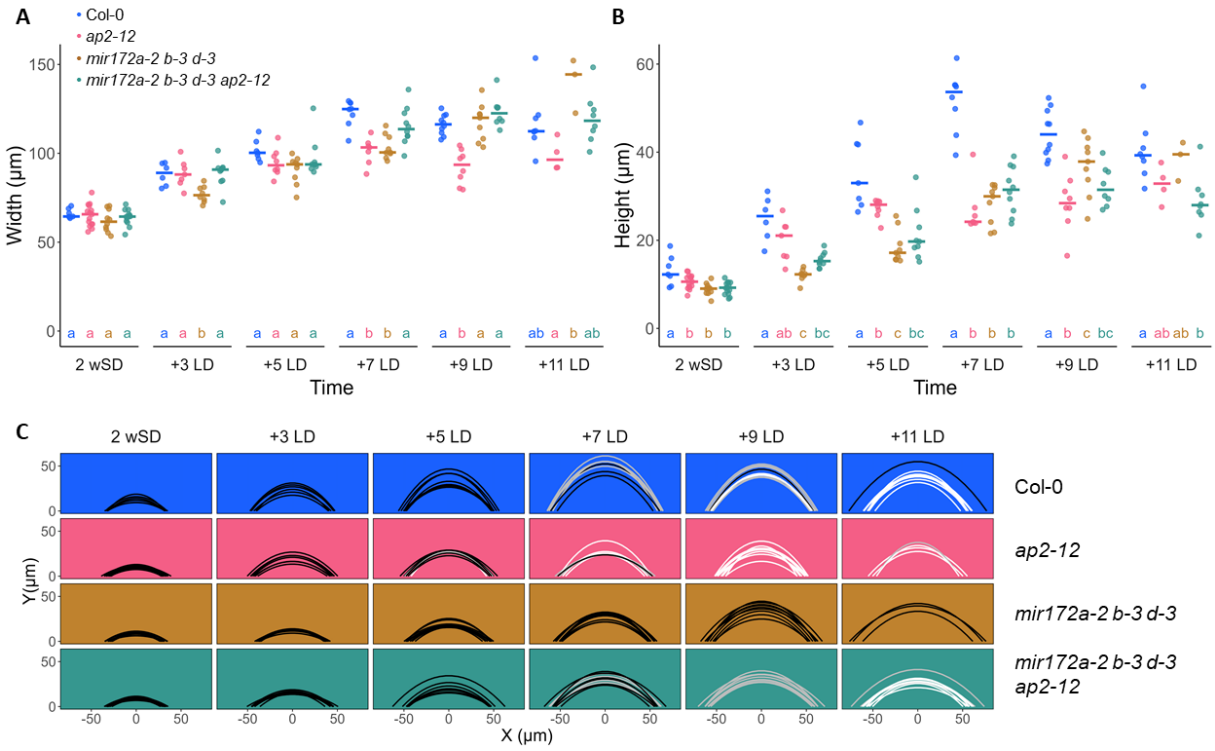

Appendix Figure 3-2. Morphological changes of the shoot apical meristems of Col-0, *ap2-12, mir172a-2 b-3 d-3* and *mir172a-2 b-3 d-3 ap2-12* plants grown for 2 weeks under short day (SD) conditions and then transferred to long day (LD) conditions.

(A–B) Measurement of (a) width and (b) height of the shoot apical meristem (SAM) of plants grown for 2 weeks in short days (SDs) then transferred to long days (LDs) for 3 to 11 days. The horizontal bars represent the median value for each genotype. Significant intra-time point differences among genotypes were determined via one-way ANOVA, followed by Tukey post-hoc comparisons ($p < 0.05$). Data sets that share a common letter do not differ significantly. The colour of the dots and the letters correspond to the genotype, and the colour code is indicated at the top-left of panel b. (C) SAM morphology adjusted to parabolas generated by the measurements in A–B. The parabolas are coloured according to the identity of primordia that were formed at the SAM periphery, and the colour code is indicated at the bottom of panel C. *N* = 3–15.

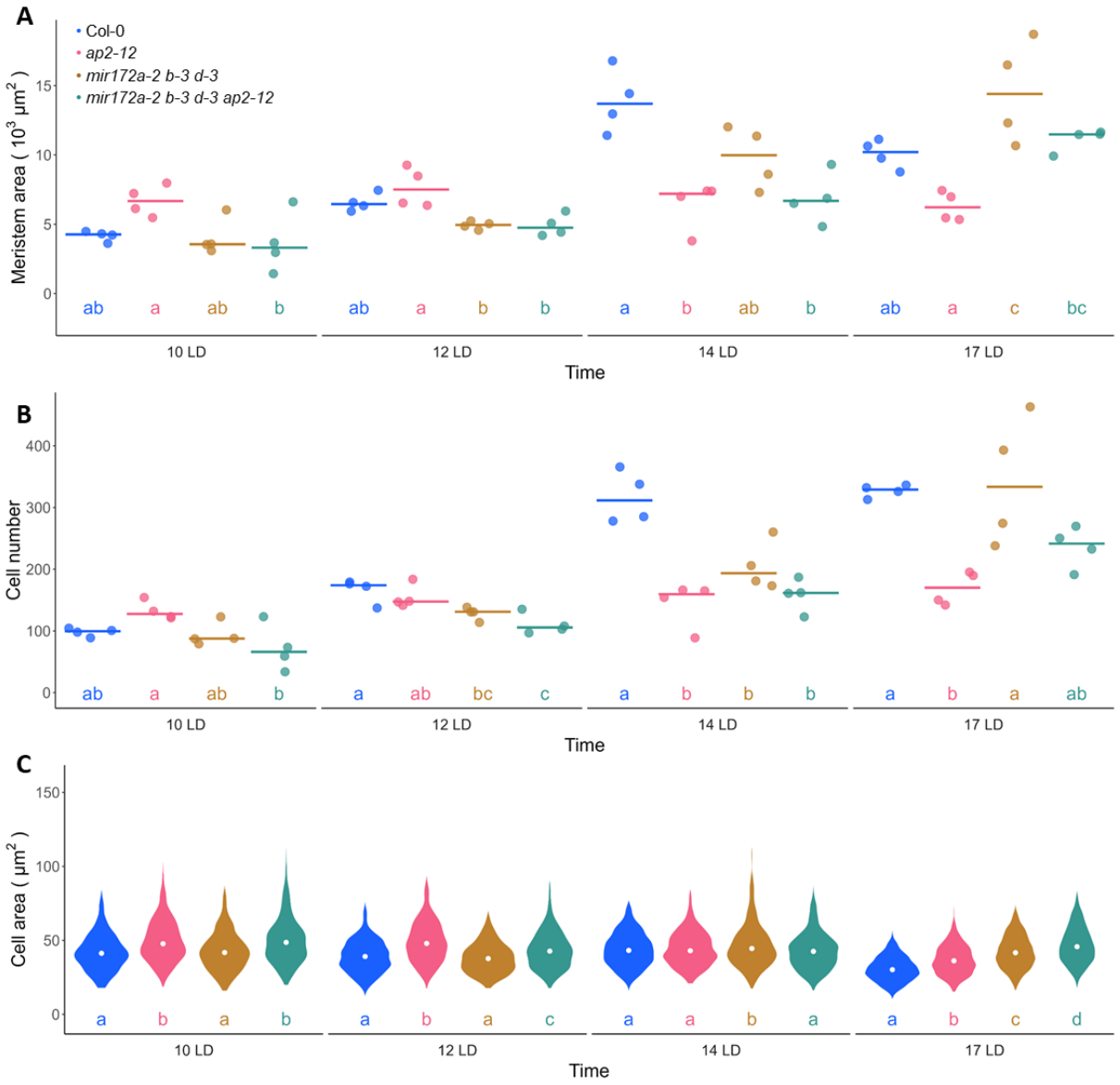

Appendix Figure 3-3. Segmentation analysis of the shoot apical meristem of Col-0, *ap2-12*, *mir172a-2 b-3 d-3* and *mir172a-2 b-3 d-3 ap2-12* plants grown under continuous long days (LDs).

Quantification of (A) meristem area, (B) meristem cell number and (C) meristem cell area. The (A–B) horizontal bars and the (C) white dots represent the median value for each genotype. Significant intra-time point differences among genotypes were determined via one-way ANOVA, followed by Tukey post-hoc comparisons ($p < 0.05$). Data sets that share a common letter do not differ significantly. The colour of the dots and the letters correspond to the genotype, and the colour code is indicated at the top-left of panel A. $N = 4$.

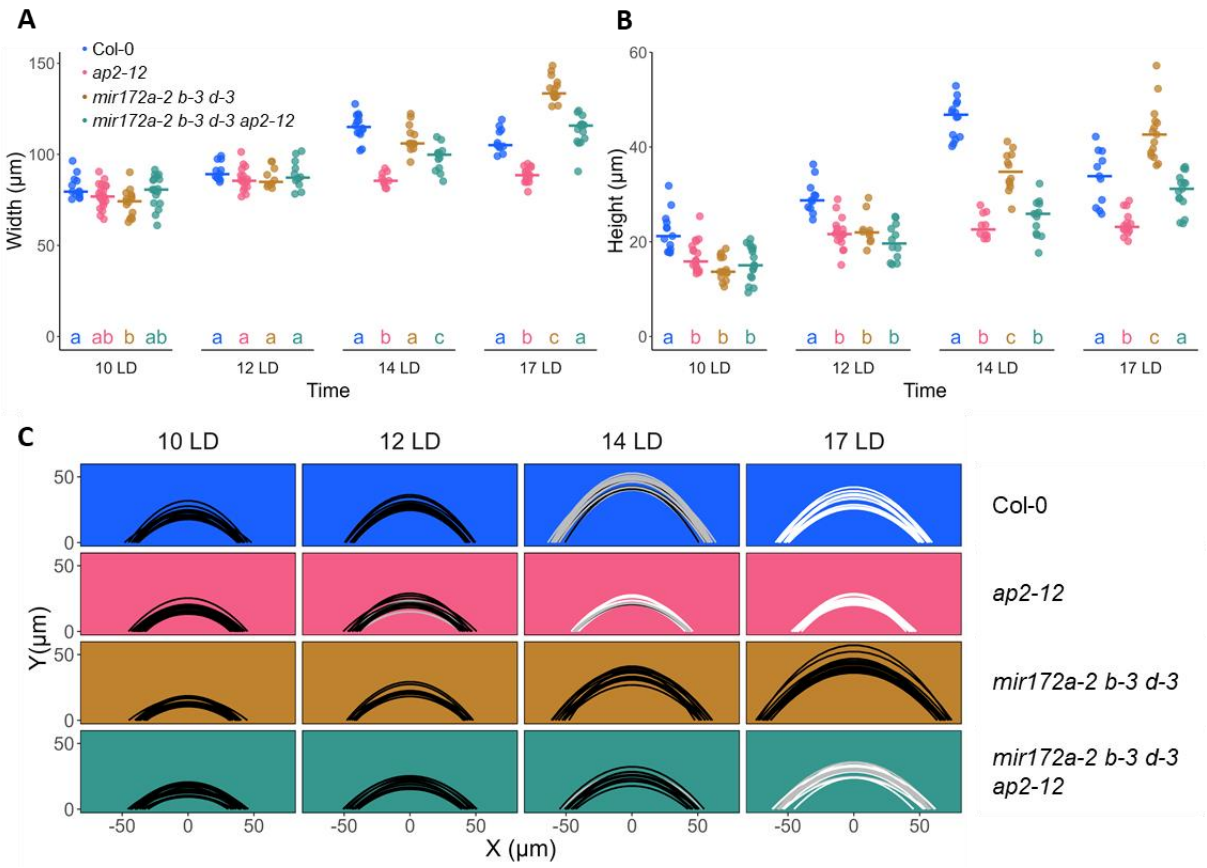

Appendix Figure 3-4. Changes in the morphology of the shoot apical meristem of Col-0, *ap2-12*, *mir172a-2 b-3 d-3* and *mir172a-2 b-3 d-3 ap2-12* plants grown under continuous long days (LDs).

(A–B) Measurement of (A) width and (B) height of the shoot apical meristem (SAM) under continuous LDs. The horizontal bars represent the median value for each genotype. Significant intra-time point differences among genotypes were determined via one-way ANOVA, followed by Tukey post-hoc comparisons ($p < 0.05$). Data sets that share a common letter do not differ significantly. The colour of the dots and the letters correspond to the genotype, and the colour code is indicated at the top-left of panel B. (C) SAM morphology adjusted to parabolas generated by the measurements in A–B. The parabolas are coloured according to the identity of primordia that were formed at the SAM periphery, and the colour code is indicated at the bottom of panel C. N = 10–21.

4 Characterisation of the APETALA2-LIKE transcription factor TARGET OF EAT 2

4.1 Introduction

miR172 is a positive regulator of flowering time under LDs and SDs (Lian et al., 2021; Ó'Maoiléidigh et al., 2021). In the second chapter of this dissertation, results on the relationship between miR172 and the photoperiodic pathway are presented and suggest that although the regulation of flowering time by *MIR172* and *AP2-LIKE* genes is influenced by inductive photoperiods, these genes also regulate flowering time in a photoperiod-independent manner. In other words, miR172 function is not only dependent on the activity of *FT/TSF*, but instead, its activity at the SAM during floral transition also promotes flowering independently of *FT*/*TSF* activity.

In the experiments described in this chapter, the involvement of *MIR172* genes in the regulation of flowering time was analysed by comparing the transcriptome profile of dissected plant apices from Col-0 and *mir172a-2 b-3 d-3* mutants. In particular, the analysis focused on changes in expression of the *AP2-LIKE* genes. Because the mRNA level of *TOE2* was constant over time in *mir172a-2 b-3 d-3* but progressively decreased in Col-0, suggesting negative regulation of *TOE2* mRNA by miR172, *TOE2* was selected for further analysis and characterisation.

The flowering time of *mir172a-2 b-3 d-3 toe2-1* mutants was measured to analyse whether *TOE2* functions downstream of miR172 in the regulation of flowering time under SDs. A translational reporter for TOE2 was also generated and its spatial pattern of expression was characterised under SDs and LDs. In addition, *FT/TSF* and *SPL4* were analysed as potential functional effectors of *TOE2* in the regulation of flowering time. Moreover, the genetic relationship between *TOE2* or *SPL4* and *AP2* in the control of flowering time was studied.

4.2 Results

4.2.1 The repression of TOE2 by miR172 under SD contributes to the promotion of flowering time

The data presented in Chapter 2 suggested that miR172 regulates flowering time in LDs and SDs, and can act independently of *FT*, a major effector of the photoperiodic pathway. This result is consistent with the hypothesis that the function of miR172 at the SAM contributes to the regulation of flowering time. To determine which are the main genes downstream of miR172 at the SAM, a global transcriptome analysis from SAM-enriched plant apices of Col-0 and *mir172a-2 b-3 d-3* was performed under continuous LDs and SDs. By the end of the LD time course, floral primordia were detected only at the periphery of Col-0 SAMs (Figure 4-1A). Moreover, under SD, Col-0 had developing cauline leaves at the flanks of the SAM, in contrast to *mir172a-2 b-3 d-3* plants (Figure 4-1B). The difference in flowering time between the two genotypes was further confirmed by the temporal expression patterns of the flowering markers *AP1, FUL* and *SPL4,* which are the three flowering-related genes whose expression in Col-0 changed the most during floral transition (Supplemental Figure 4-1; Table 4-1). Although the expression of these three genes changed in Col-0 during both LD and SD time courses, only *FUL was* significantly upregulated during the analysed time courses in *mir172a-2 b-3 d-3* mutants (Figure 4-1C–F). Taken together, this confirms that *mir172a-2 b-3 d-3* flowered later than Col-0 in the experimental conditions used.

Consistent with previous reports (Mathieu et al., 2009; Schmid et al., 2003; Schwab et al., 2005), mRNA from all the *AP2-LIKE* genes was detected in plant apices during floral transition (Supplemental Figure 4-2). However, contrary to expectation, not all the *AP2-LIKE* gene mRNAs exhibited changes in abundance over time. In fact, under continuous LDs, only the mRNA levels of *SMZ* and *SNZ* decreased significantly (Table 4-2) and under SDs, only the mRNA levels of *SMZ, SNZ* and *TOE2* decreased significantly. I consider these observations to indicate a complex regulation of *AP2-LIKE* gene expression, which involves differential transcriptional regulation of different members of the family as well as translational inhibition

by miR172 (as was reported for *AP2* in Chen, 2004), which could not be detected via RNA-Seq.

Table 4-1. Differentially expressed genes related to flowering in apices of Col-0 during floral transition under LDs and SDs.

This list corresponds to the overlap of the three data sets presented in Supplemental Figure 4-1. Gene expression was compared in long day (LD) time course (10 LD vs. 17 LD) and in the short day (SD) time course (3 wSD vs. 6 wSD). Gene Symbols: *GIBBERELLIN 2-OXIDASE 6 (GA2OX1); GIBBERELLIN 3-OXIDASE 1 (GA3OX1); SQUAMOSA PROMOTER-BINDING PROTEIN-LIKE 4 (SPL4); RGA-LIKE1 (RGL1); MICRORNA157 (MIR157); APETALA1 (AP1); GIBBERELLIN 2-OXIDASE 1 (GA2OX1); SQUAMOSA PROMOTER-BINDING PROTEIN-LIKE 3 (SPL3); SCHNARCHZAPFEN (SNZ); ABA-RESPONSIVE KINASE SUBSTRATE 3 (AKS3); WRKY DNA-BINDING PROTEIN 12 (WRK12); SUPPRESSOR OF OVEREXPRESSION OF CONSTANS 1 (SOC1); TB1,CYC,PCF (TCP) DOMAIN PROTEIN 13 (TCP13); TCP DOMAIN PROTEIN 4 (TCP4); TCP DOMAIN PROTEIN 18 (TCP18); MICRORNA319A (MIR319A); GNC-LIKE (GNL); TARGET OF FLC AND SVP 1 (TFS1); FD (FD); TERMINAL FLOWER 1 (TFL1); TCP DOMAIN PROTEIN 17 (TCP17); GATA,NITRATE-INDUCIBLE,CARBON METABOLISM-INVOLVED (GNC); TCP DOMAIN PROTEIN 5 (TCP5)*

AGI gene code	Symbol	Long Days (10 LD vs. 17 LD)			Short Days (3 wSD vs. 6 wSD)		
		Log_2(Fold Change)	Ajusted *p*-value	Ranking	Log_2(Fold Change)	Ajusted *p*-value	Ranking
AT1G02400	*GA2OX6*	-1.29	3.04E-02	16	-3.85	1.24E-10	21
AT1G15550	*GA3OX1*	1.67	2.62E-07	8	1.72	1.52E-08	9
AT1G53160	***SPL4***	**4.80**	**7.05E-16**	**2**	**4.81**	**8.70E-16**	**3**
AT1G66350	*RGL1*	1.08	1.41E-04	13	1.60	1.51E-07	11
AT1G66783	*MIR157A*	-2.58	7.39E-05	21	-6.34	6.04E-19	24
AT1G69120	***AP1***	**8.19**	**3.38E-17**	**1**	**5.39**	**3.86E-03**	**2**
AT1G78440	*GA2OX1*	-1.39	4.12E-02	17	-1.03	4.49E-02	14
AT2G33810	*SPL3*	2.41	1.51E-08	6	2.26	1.62E-06	8
AT2G39250	*SNZ*	-4.44	4.89E-06	24	-6.28	5.35E-09	23
AT2G42280	*AKS3*	-1.25	4.61E-05	15	-2.25	3.11E-08	16
AT2G44745	*WRKY12*	1.47	3.13E-03	10	1.72	1.61E-12	10
AT2G45660	*SOC1*	1.67	8.08E-07	9	3.09	1.09E-11	5
AT3G02150	*TCP13*	-1.84	1.86E-02	19	-2.25	3.37E-03	17
AT3G15030	*TCP4*	-1.76	5.94E-03	18	-2.32	2.72E-12	18
AT3G18550	*TCP18*	2.82	2.98E-04	5	4.03	9.09E-07	4
AT4G23713	*MIR319A*	1.20	5.91E-03	11	1.16	5.37E-06	13
AT4G26150	*GNL*	-2.94	3.19E-04	23	-3.45	6.67E-07	20
AT4G34400	*TFS1*	3.03	3.53E-07	4	2.49	4.60E-25	7
AT4G35900	*FD*	1.12	1.72E-02	12	1.27	9.93E-08	12
AT5G03840	*TFL1*	1.99	7.63E-03	7	2.59	6.99E-10	6
AT5G08070	*TCP17*	-1.88	2.02E-02	20	-2.36	3.98E-03	19
AT5G56860	*GNC*	-2.83	3.13E-04	22	-4.01	4.15E-09	22
AT5G60910	***FUL***	**3.68**	**8.52E-12**	**3**	**6.01**	**1.00E-17**	**1**
AT5G60970	*TCP5*	-1.21	1.83E-02	14	-1.96	1.78E-05	15

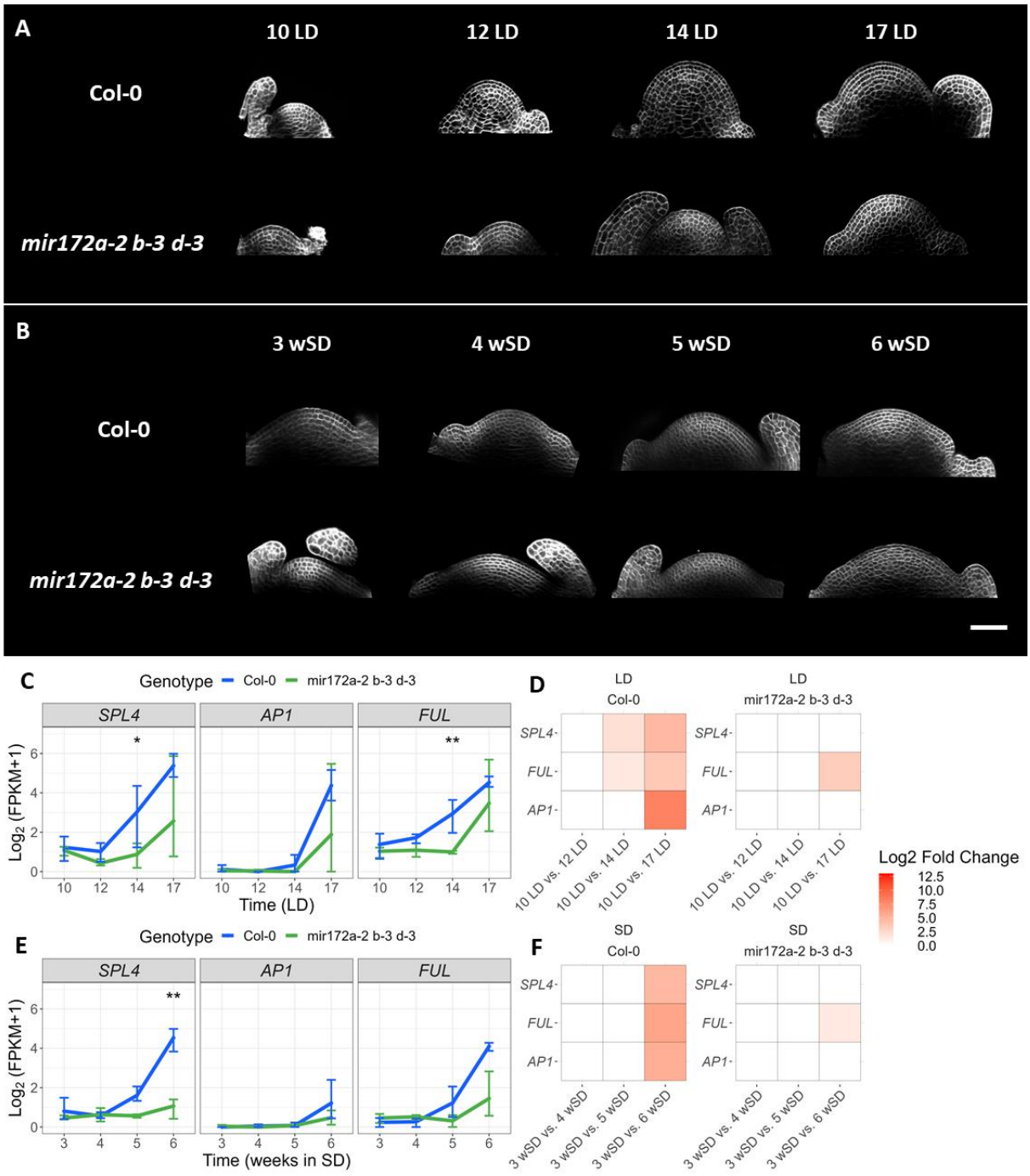

Figure 4-1. Comparative global expression analysis to understand the role of miR172 at the SAM during floral transition.

(A–B) Confocal images for the samples used for the RNA-Seq time course under (A) LDs and (B) SDs. The age of the plants is indicated at the top of each panel of images. The genotype of each plant is indicated on the left part of each row of images. Scale bar = 50 µm. (C–F) Transcriptome profiling of the flowering marker genes *SQUAMOSA-PROMOTER BINDING PROTEIN-LIKE 4* (*SPL4*), *APETALA1* (*AP1*) and *FRUITFULL* (*FUL*) under (C–D) LDs and (E–F) SDs. (C,E) Expression of flowering marker genes over time in Col-0 and *mir172a-2 b-3 d-3* under (C) LDs and (E) SDs. Error bars represent the range between the maximum and minimum values for the three replicates at each time point. Statistically significant differences between Col-0 and *mir172a-2 b-3 d-3* are indicated with * (adjusted *p*-value < 0.05) or ** [adjusted *p*-value < 0.05 and absolute value of $\log_2$(fold change) > 1. (D,F) Heatmaps showing the $\log_2$(fold change) in gene expression of *AP1, SPL4* and *FUL* by comparing expression at each time point of each time course with that at the first time point under (D) LDs and (F) SDs.

Table 4-2. Change in expression of *AP2-LIKE* genes in dissected plant apices of Col-0, *ap2-12*, *mir172a-2 b-3 d-3* and *mir172a-2 b3 d-3 ap2-12* mutants during a LD or SD time course.

Comparisons in gene expression between the first and last time points of the performed RNA-Seq time courses. The coloured comparisons are those that are statistically significant (adjusted *p*-value < 0.05). A downregulation in mRNA level is highlighted in blue; an upregulation in mRNA level is highlighted in red. Gene symbols: *APETALA2* (*AP2*)*; TARGET OF EAT* (*TOE*)*; SCHNARCHZAPFEN* (*SNZ*)*; SCHLAFMÜTZE* (*SMZ*).

AGI gene code	Symbol	Col-0				*ap2-12*			
		10 LD vs. 17 LD		3 wSD vs. 6 wSD		10 LD vs. 17 LD		3 wSD vs. 6 wSD	
		Log_2 (Fold Change)	Ajusted *p*-value	Log_2 (Fold Change)	Ajusted *p*-value	Log_2 (Fold Change)	Ajusted *p*-value	Log_2 (Fold Change)	Ajusted *p*-value
AT4G36920	*AP2*	0.42	0.05	0.28	0.18	1.44	1.84E-03	-0.41	0.15
AT2G28550	*TOE1*	0.12	0.64	-0.10	0.76	-0.01	0.98	-0.62	0.01
AT5G60120	*TOE2*	-0.38	0.22	-1.07	4.71E-07	-0.08	0.82	-1.79	7.84E-14
AT5G67180	*TOE3*	0.24	0.47	0.65	0.10	0.00	0.99	2.24	1.95E-22
AT2G39250	*SNZ*	-4.44	4.89E-06	-6.28	5.35E-09	-3.80	2.15E-19	0.26	0.61
AT3G54990	*SMZ*	-0.80	0.04	-1.78	1.10E-06	-0.46	0.07	-2.74	5.08E-17
AGI	Symbol	*mir172a-2 b-3 d-3*				*mir172a-2 b-3 d-3 ap2-12*			
		10 LD vs. 17 LD		3 wSD vs. 6 wSD		10 LD vs. 17 LD		3 wSD vs. 6 wSD	
		Log_2 (Fold Change)	Ajusted *p*-value	Log_2 (Fold Change)	Ajusted *p*-value	Log_2 (Fold Change)	Ajusted *p*-value	Log_2 (Fold Change)	Ajusted *p*-value
AT4G36920	*AP2*	0.29	0.41	0.38	0.08	0.52	0.04	0.67	0.01
AT2G28550	*TOE1*	0.38	0.01	0.03	0.90	0.44	0.02	0.08	0.67
AT5G60120	*TOE2*	-0.20	0.57	-0.09	0.72	0.06	0.78	0.19	0.30
AT5G67180	*TOE3*	1.10	0.03	-0.02	0.96	0.51	0.08	0.37	0.25
AT2G39250	*SNZ*	-3.77	1.82E-14	-0.41	0.19	-3.23	8.44E-05	-3.67	2.75E-09
AT3G54990	*SMZ*	-0.37	0.34	-2.00	2.64E-06	-0.32	0.30	-2.01	1.56E-09

During floral transition, *MIR172* genes are expressed and miR172 accumulates at the SAM (Lian et al., 2021; Ó'Maoiléidigh et al., 2021; Wollmann et al., 2010). To confirm the involvement of miR172 in the regulation of *AP2-LIKE* gene expression, the expression levels of *AP2-LIKE* genes in *mir172a-2 b-3 d-3* triple mutants were compared with those in Col-0 at each time point of the analysis. Most of the temporal patterns of expression of the *AP2-LIKE* genes were comparable in Col-0 and *mir172a-2 b-3 d-3* (Figure 4-2A–B). This is consistent with the repression of *AP2-LIKE* gene expression by miR172 via translational inhibition, which cannot be detected via RNA-Seq. Nevertheless, the decrease in expression of *SNZ* under LDs

was delayed in the triple mutant, as shown by the higher *SNZ* mRNA level in *mir172a-2 b-3 d-3* than in Col-0 at 14 LD (Figure 4-2A). Moreover, there was no significant change in *TOE2* mRNA in *mir172a-2 b-3 d-3* under SDs in contrast to the decrease in *TOE2* mRNA observed in Col-0, which resulted in a higher level of *TOE2* mRNA in *mir172a-2 b-3 d-3* than in Col-0 at 5 wSD and 6 wSD (Figure 4-2B–C). Importantly, the cleavage of *TOE2* mRNA by miR172 was demonstrated *in vitro* by Schwab et al., 2005. Therefore, the repression by miR172 of *SNZ* mRNA under LDs, and *TOE2* mRNA under SDs, is likely to be important for flowering time regulation.

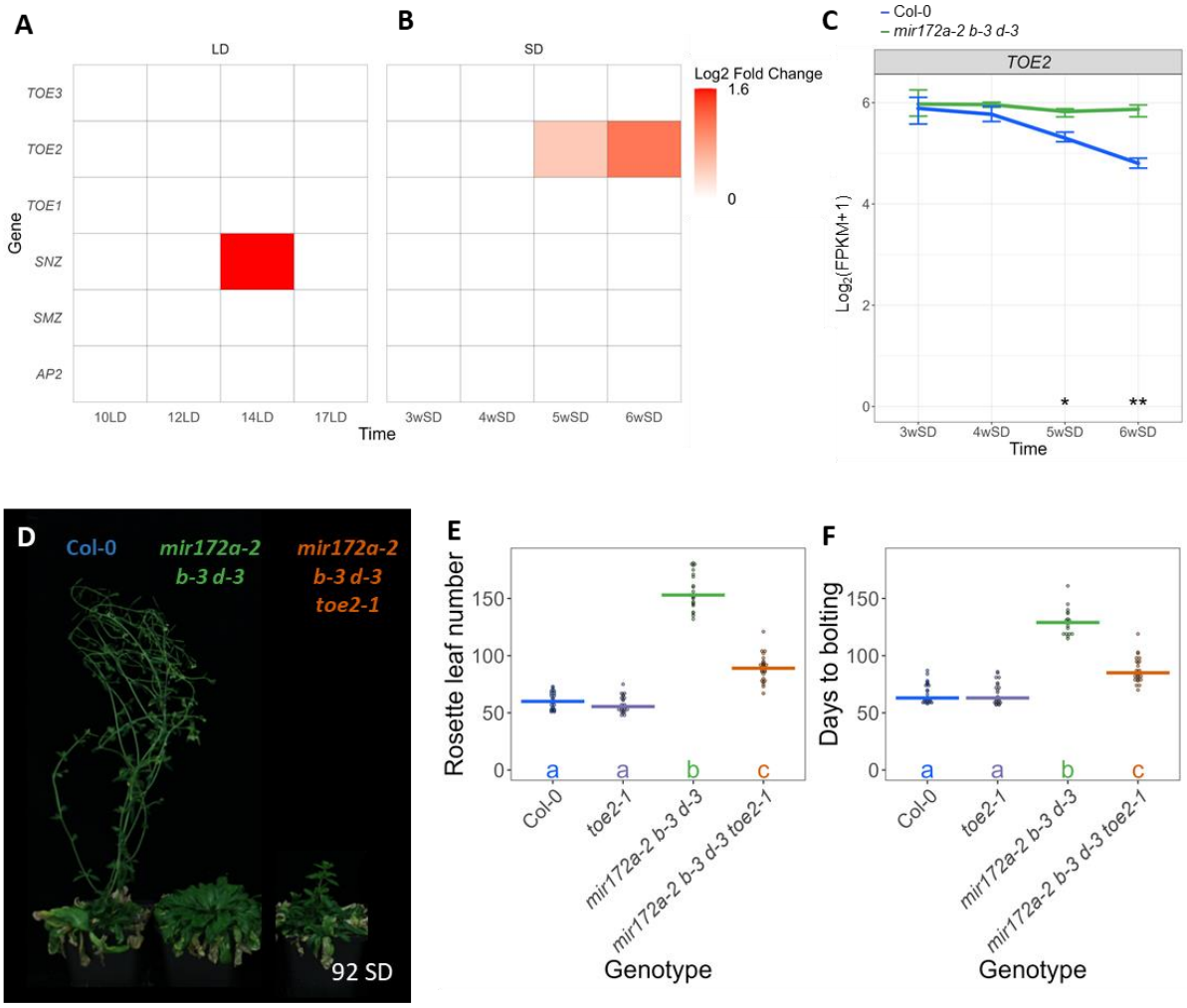

Figure 4-2. *TOE2* is a major target of miR172 in the regulation of flowering time under SD.

(A–C) Transcriptome profiling of the *AP2-LIKE* genes at the SAM. (A–B) Heatmaps showing the $\log_2$(fold change) in normalised gene expression of the *AP2-LIKE* genes in apices of *mir172a-2 b-3 d-3* mutants compared with Col-0 at each time point of the analysis under (A) LDs and (B) SDs. The colour code of the plotted values is depicted at the right part of the panel. (C) Expression of *TOE2* over time in Col-0 and *mir172a-2 b-3 d-3* under SD. Error bars represent the range between the maximum and minimum values among the three replicates at each time point. Statistically significant differences between Col-0 and *mir172a-2 b-3 d-3* are indicated with * (adjusted *p*-value < 0,05) or ** [adjusted *p*-value < 0.05 and absolute value of $\log_2$(fold change) > 1]. (See next page)

(D–F) Flowering-time of *mir172a-2 b-3 d-3 toe2-1* under SDs. (D) Photographs of 92-day-old plants from the flowering-time experiment in SDs. The genotype of each plant is indicated at the top. (E–F) Flowering-time measurements in terms of (E) rosette leaf number and (F) days to bolting. The horizontal bars correspond to the median of each genotype. Significant differences were determined via one-way ANOVA, followed by Tukey post-hoc comparisons ($p < 0.05$). Letters shared by data sets indicate no significant differences. $N = 22–25$.

To evaluate whether the repression of *TOE2* by miR172 under SDs contributes to the regulation of flowering time, the flowering time of the *mir172a-2 b-3 d-3 toe2-1* quadruple mutant was measured under the same conditions. The *toe2-1* mutant flowered slightly earlier than Col-0, as shown by a mean reduction in rosette leaf number of 3.15 and in days to bolting of 0.56 (Figure 4-2D–F). Although *mir172a-2 b-3 d-3 toe2-1* quadruple mutants flowered later than Col-0, *mir172a-2 b-3 d-3 toe2-1* produced on average 67 fewer rosette leaves and bolted 42 days earlier than *mir172a-2 b-3 d-3* mutants, which indicates that the introduction of the *toe2-1* mutation into the *mir172a-2 b-3 d-3* mutant background led to a partial recovery of the late-flowering phenotype of *mir172a-2 b-3 d-3*. This result suggests that the negative regulation of flowering time by *TOE2* becomes more relevant upon *mir172a-2 b-3 d-3* mutation. Moreover, these results indicate that the repression of *TOE2* by miR172 under SD promotes floral transition.

4.2.2 TOE2 accumulates at the periphery of the SAM during early stages of floral transition

To analyse whether TOE2 protein accumulates at the SAM during floral transition, a *TOE2::TOE2:mScarlet:2HA* reporter was generated and transformed into the *toe2-1* mutant background (Supplemental Figure 4-3). Meristems of plants carrying this construct and grown under SDs were dissected and imaged by confocal microscopy in a time window that included the time points used for RNA-Seq. The TOE2-mScarlet-2HA reporter accumulated in young developing leaves of vegetative meristems (i.e. 2 wSD and 3 wSD) and early transitioning meristems (i.e. 4 wSD; Figure 4-3A). In some confocal images, TOE2-mScarlet-2HA accumulation was detected at the periphery of the SAM, specifically at developing lateral organ primordia (Figure 4-3A–B). At 5 wSD, TOE2-mScarlet-2HA was detectable in leaves, but at a lower intensity, consistent with the reduction in *TOE2* mRNA in Col-0 at this time point (Figure 4-2C). At 6 wSD, TOE2-mScarlet-2HA protein was hardly detectable at the SAM. Notably,

TOE2-mScarlet-2HA accumulated in developing flowers, at the boundaries between young sepals (Figure 4-3C), which is consistent with the previously reported expression of *TOE2* in flowers (Jung et al., 2007). Taken together, these data show that TOE2 accumulates at the SAM during floral transition under SDs and the temporal pattern of expression recapitulates the reduction in *TOE2* expression observed via RNA-Seq.

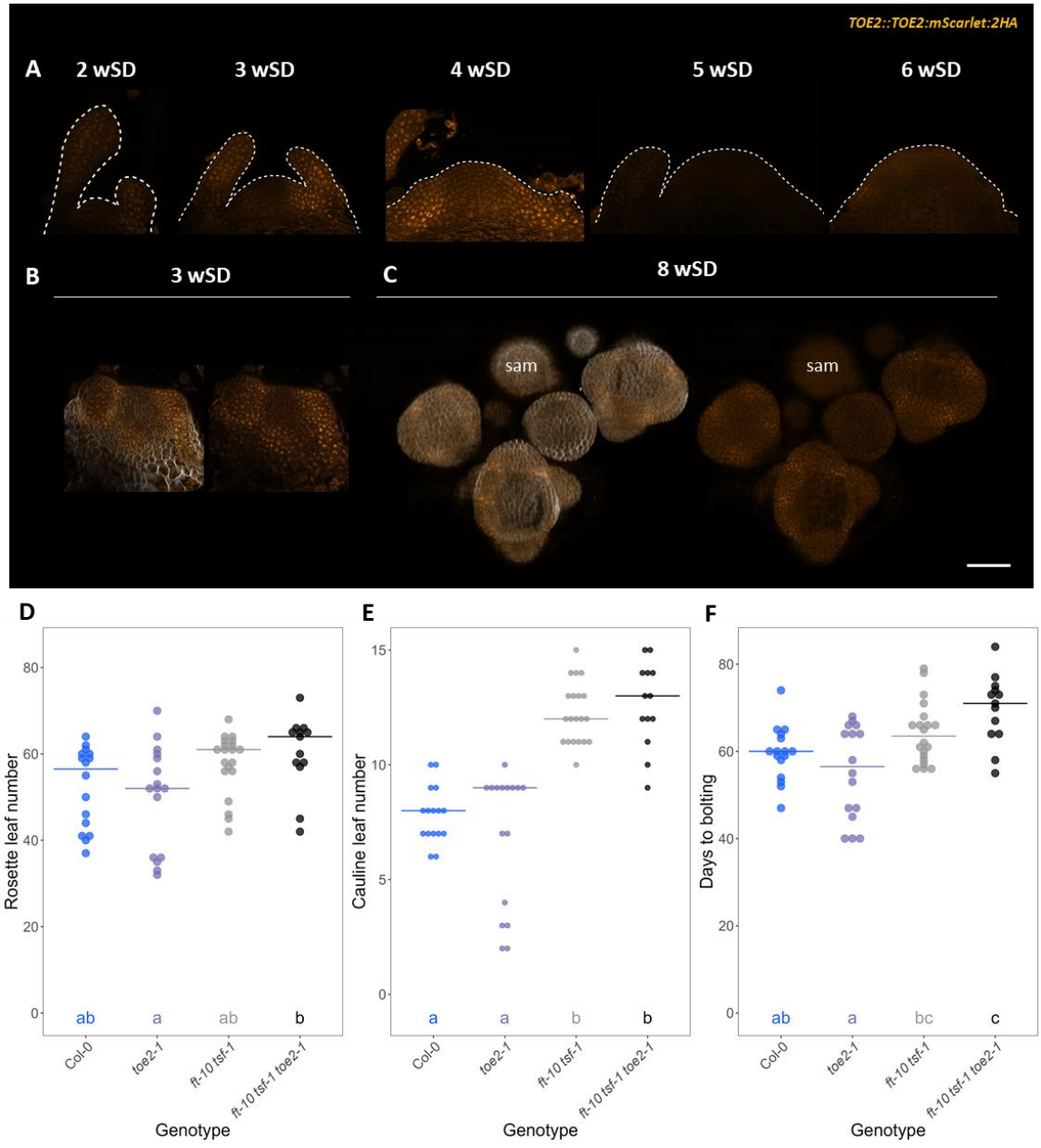

Figure 4-3. *TOE2* accumulates at developing organs at the periphery of the SAM.

(A–C) Spatial pattern of expression of *TOE2::TOE2:mScarlet:2HA* in plant apices during a time course under continuous SDs. (A) Lateral views of the SAM. The shape of the meristem and its peripheral organs is indicated with a dotted white line. (B–C) Top views of the SAM and the developing organs at the SAM periphery at (B) 3 wSD and (C) 8 wSD. The images on the left of panels B and C are merged images of the Renaissance and mScarlet channels; the images on the right represent only the mScarlet channel. The location of the SAM in C is indicated with “sam”. Scale bar = 50 µm. (See next page)

(D–F) Flowering-time measurements of *ft-10 tsf-1 toe2-1* under SDs in terms of (D) rosette leaf number, (E) cauline leaf number and (F) days to bolting. The horizontal bars correspond to the median of each genotype. Statistically significant differences were determined via one-way ANOVA, followed by Tukey post-hoc comparisons ($p < 0.05$). A common letter among data sets indicates no significant differences. $N = 13–20$.

Previous studies reported that *TOE1* and *TOE2* are negative regulators of *FT* and that ectopic *FT* expression in *toe1 toe2* plants in SDs might be the basis for the early flowering of this double mutant (B. Zhang et al., 2015). To analyse whether the slight decrease in flowering time caused by the *toe2-1* mutation is dependent on the activity of *FT* and *TSF,* the flowering time of the *ft-10 tsf-1 toe2-1* triple mutant was measured under SDs. Consistent with the flowering-time analysis described earlier (Figure 4-2F), *toe2-1* exhibited a comparable leaf number and bolted similarly to Col-0 (Figure 4-3D–F). Moreover, the introduction of *toe2-1* mutation into the *ft-10 tsf-1* mutant background did not affect leaf number (Figure 4-3D–E). Whereas *ft-10 tsf-1* mutants bolted 5.6 days later than Col-0, due to the increased variability in flowering time in this analysis, this slight difference was not statistically significant. Notably, introduction of the *toe2-1* mutation into the *ft-10 tsf-1* double mutant background enhanced the slightly late-bolting phenotype of *ft-10 tsf-1*, because *ft-10 tsf-1 toe2-1* triple mutants bolted on average 10.5 days later than Col-0, although this was not statistically significant. Nevertheless, the slightly later-bolting phenotype of *ft-10 tsf-1 toe2-1* might indicate that *TOE2* can impact flowering time in the absence of functional *FT*/*TSF.*

4.2.3 SQUAMOSA PROMOTER BINDING PROTEIN-LIKE 4 (SPL4) is a candidate regulator of flowering time downstream of TOE2

To define potential *FT/TSF*-independent functions of *TOE2* in the regulation of flowering time at the SAM, the RNA-Seq data for Col-0 and *mir172a-2 b-3 d-3* mutants was compared to identify genes that were co-expressed with *TOE2* during floral transition under SDs (Figure 4-4A). The list of DEGs in Col-0 from the comparison 3 wSD vs. 6 wSD was cross-referenced to the list of DEGs at 6 wSD between Col-0 and *mir172a-2 b-3 d-3* mutants, which are two lists that included *TOE2*. Moreover, genes whose expression was correlated with that of *TOE2* in Col-0 with a Pearson's correlation coefficient greater than 0.85 were compared with genes in the previous overlap. This yielded 11 candidate genes (Table 4-3). However, most of these

genes exhibited significant changes in expression in *mir172a-2 b-3 d-3* at 6 wSD compared to 3 wSD, which was not the case for *TOE2.* Therefore, the genes for which no changes in expression in *mir172a-2 b-3 d-3* mutants were observed during the SD time course were selected, and resulted in three candidate genes (Figure 4-4B): *SPL4, TCP (TB1, CYC, PCF) DOMAIN PROTEIN 1* (*TCP1*) and *HOMEOBOX PROTEIN 29* (*HB29*)*/ZINC FINGER HOMEODOMAIN 11* (*ZHDF11*)*.* Similar to the expression of *TOE2*, the expression of these three candidate genes changed significantly during floral transition under SD, leading to differential expression levels when comparing their expression in Col-0 vs. *mir172a-2 b-3 d-3* at 6 wSD.

Table 4-3. Genes whose expression correlated with that of *TOE2* during SDs in Col-0 and *mir172a-2 b-3 d-3* plant apices.

The expression profiles of these genes are shown in Supplemental Figure 4-4.

AGI gene code	Description	Symbol
AT1G13470	Hypothetical protein (Domain of Unknown Function; DUF126)	*AT1G13470*
AT1G33840	LURP-one-like protein (DUF567)	*AT1G33840*
AT1G53160	Squamosa promoter binding protein-like 4	*SPL4*
AT1G67260	TCP family transcription factor	*TCP1*
AT1G69600	Zinc finger homeodomain 11	*ZFHD11*
AT2G43480	Peroxidase superfamily protein	*AT2G43480*
AT5G05890	UDP-Glycosyltransferase superfamily protein	*AT5G05890*
AT5G44620	Cytochrome P450, family 706, subfamily A, polypeptide 3	*CYP706A3*
AT5G44630	Terpenoid cyclases/Protein prenyltransferases superfamily protein	*AT5G44630*
AT5G55440	F-box protein, putative (DUF295)	*AT5G55440*
AT5G60120	Target of early activation tagged (EAT) 2	*TOE2*

Among the three candidate genes, only *SPL4* has previously been implicated in the regulation of flowering time, together with its closely related paralogues *SPL3* and *SPL5* (Jung et al., 2016; Torti et al., 2012)*.* Moreover, *SPL4* was one of the flowering marker genes that exhibited one of the greatest changes in expression in Col-0 during floral transition (Figure 4-1). To confirm the involvement of *SPL4* in the regulation of floral transition, the flowering time of the *spl4* mutant was measured under SD conditions. The bolting time and time to opening of the first flower were similar in *spl4* and Col-0 (Figure 4-4E–F). However, *spl4* mutants exhibited on

average of 5.4 more rosette leaves and 5.5 more cauline leaves than Col-0 (Figure 4-4C–D).

These results indicate that *SPL4* is a positive regulator of floral transition under SDs.

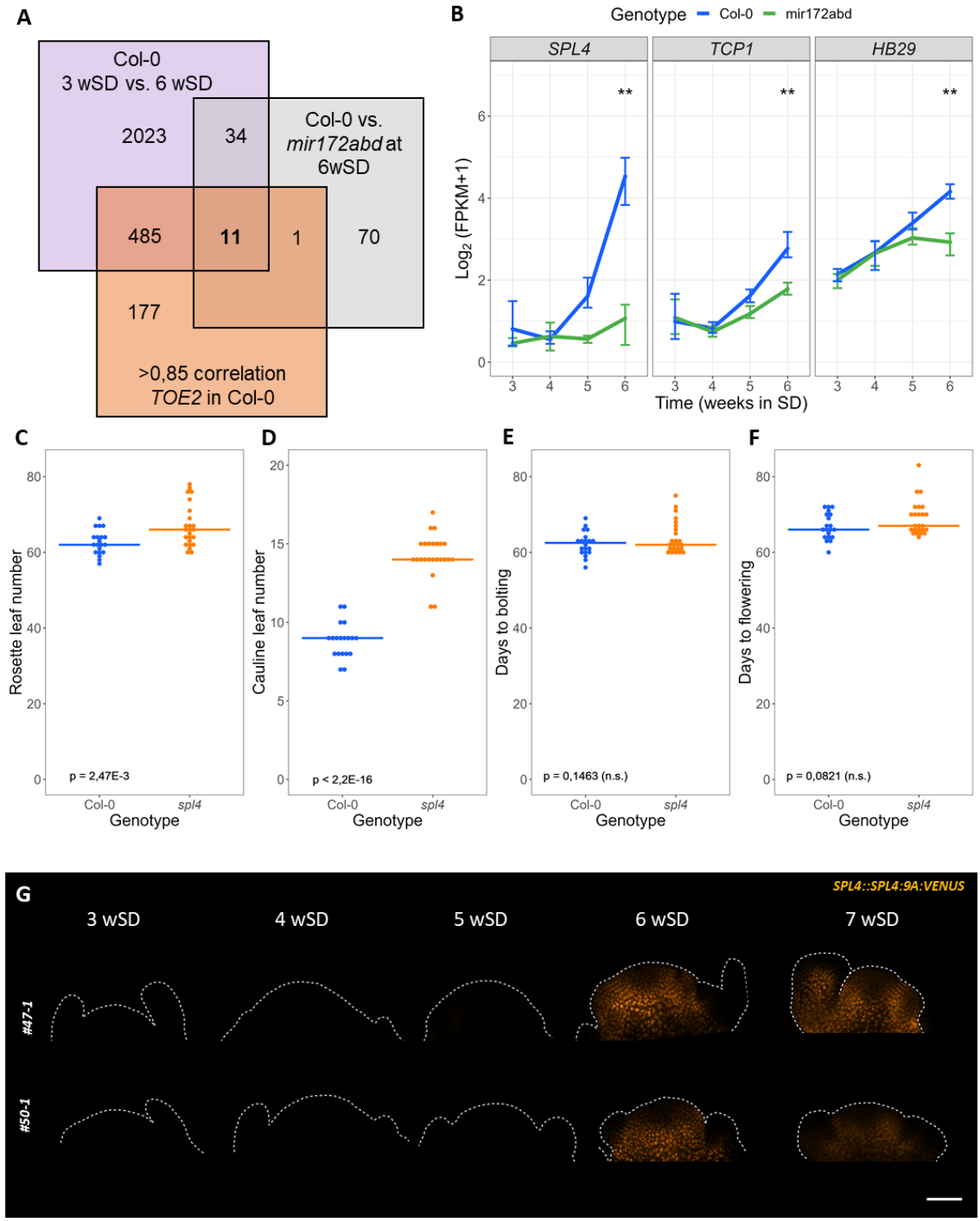

Figure 4-4. *SPL4* expression negatively correlates with *TOE2* expression at the SAM.

(A) Venn diagram depicting the overlap between the list of differentially expressed genes (DEGs) in Col-0 comparing 3 wSD vs. 6 wSD, the list of DEGs at 6 wSD comparing Col-0 vs. *mir172a-2 b-3 d-3* and the list of genes whose expression had a Pearson's correlation with that of *TOE2* expression in Col-0 greater than 0.85 (see next page).

(B) Selection of three genes from the overlap between the three sets in A, whose expression did not significantly change in *mir172a-2 b-3 d-3* when comparing 3 wSD vs. 6 wSD. The gene symbol is represented on top of each plot. Error bars represent the range between the maximum and minimum value for each of the three replicates. Statistically significant differences between Col-0 and *mir172a-2 b-3 d-3* are indicated with * (adjusted *p*-value < 0.05) or ** (adjusted *p*-value < 0.05 and absolute value of $\log_2$(fold change > 1). (C–D) Flowering-time measurements for *spl4* mutants under SDs, in terms of (C) rosette leaf number, (D) cauline leaf number, (E) days to bolting and (F) days until first open flower. The horizontal bars correspond to the median of each genotype. Statistical significance was assessed by Student's *t*-test. The *p*-value is indicated at the lower left corner of each plot. *N* = 20–24. (G) Spatial pattern of translational reporters of SPL4 (*SPL4::SPL4:9A:VENUS)* at the SAM during a time course under SDs. The genotypes are indicated at the left of each row of images. The shape of the SAM is indicated by a white dotted line. Scale bar = 50 µm.

During floral transition, *SPL4* is expressed at the base of the SAM (Torti et al., 2012). To analyse the accumulation of SPL4 protein at the SAM, the spatial pattern of the SPL4::SPL4:9A:VENUS reporter was analysed via confocal microscopy during a SD time course. Consistent with the pattern of *SPL4* mRNA expression by RNA-Seq, no accumulation of SPL4-VENUS was detected in vegetative meristems (Figure 4-4G). At 5 wSD, weak signal was detected at the periphery of the SAM, specifically at positions of incipient lateral organs (Supplemental Figure 4-5). Also, expression of SPL4-VENUS was observed throughout the SAM at the inflorescence stage, with a higher level of expression at the basal regions of the SAM and in the developing flowers. Taken together, these results suggest that *SPL4* may promote floral transition at the SAM.

4.2.4 AP2-LIKE transcription factors delay flowering time in part by repressing SPL4 expression

The *mir172a-2 b-3 d-3 ap2-12* mutants flower earlier than *mir172a-2 b-3 d-3,* which indicates that miR172 positively regulates flowering time at least partially by targeting AP2 (Ó'Maoiléidigh et al., 2021). However, *mir172a-2 b-3 d-3 ap2-12* mutants flower later than *ap2-12* mutants, suggesting that the upregulation of other *AP2-LIKE* transcription factors in *mir172a-2 b-3 d-3 ap2-12* probably contributes to late flowering. Therefore, *ap2-12* and *mir172a-2 b-3 d-3 ap2-12* mutants were included in the RNA-Seq analysis under SD. In *ap2-12*, some differences were detected in the expression profiles of the *AP2-LIKE* genes that showed a significant change in mRNA levels in Col-0 during the time course under SDs (i.e. *SMZ, SNZ and TOE2;* Supplemental Figure 4-2). A more rapid decrease in *SMZ* mRNA was detected in *ap2-12* mutants in comparison with Col-0: *SMZ* mRNA levels decreased from 3 wSD to 6 wSD by 2.7 fold in *ap2-12*, whereas it decreased by 1.8 fold in Col-0 (Table 4-2).

This difference was similar to the observed change in *TOE2* mRNA levels, which decreased from 3 wSD to 6 wSD by 1.1 fold in Col-0 and by 1.8 fold in *ap2-12* mutants. Notably, *SNZ* mRNA was higher in *ap2-12* mutants by 2.2 fold at 6 wSD (Supplemental Figure 4-2). This might indicate that *AP2* impacts the expression of other *AP2-LIKE* genes. Consistent with the regulation of *AP2-LIKE* genes by AP2, *TOE3* mRNA was increased in *ap2-12* at most of the time points of the SD time course in comparison with Col-0. Notably, AP2 is able to bind to *TOE3* promoter regions and was proposed to be a negative regulator of *TOE3* expression (Yant et al., 2010). Although these results suggest a complex relationship among *AP2-LIKE* genes during floral transition, the observed rapid decrease in mRNA levels of *SMZ* and *TOE2* in *ap2-12* is consistent with early flowering of *ap2-12*.

Considering the regulation of *AP2-LIKE* gene expression by *AP2* and miR172, the basis for the flowering time of *mir172a-2 b-3 d-3 ap2-12* mutants might be rather complex. However, the expression level of *TOE2* remained constant in *mir172a-2 b-3 d-3 ap2-12* plants and was comparable to that in *mir172a-2 b-3 d-3* (Figure 4-5A). This suggests that persistent *TOE2* expression might contribute to the late flowering of *mir172a-2 b-3 d-3 ap2-12*. To analyse whether *TOE2* contributes to the late flowering of *mir172a-2 b-3 d-3* mutants, the flowering time of *mir172a-2 b-3 d-3 ap2-12 toe1-2* quintuple mutants was measured. On average, the *mir172a-2 b-3 d-3 ap2-12* mutant produced 45 fewer rosette leaves and bolted 20.5 days earlier than *mir172a-2 b-3 d-3* (Figure 4-5C–D). Importantly, the reduction in flowering time of *mir172a-2 b-3 d-3 toe2-1* compared to *mir172a-2 b-3 d-3* was more extreme than that of *mir172a-2 b-3 d-3 ap2-12* compared with *mir172a-2 b-3 d-3*, because *mir172a-2 b-3 d-3 toe2-1* produced 22 rosette leaves fewer and bolted 21.5 days earlier than *mir172a-2 b-3 d-3 ap2-12*. Because *ap2-12* produced fewer leaves than *toe2-1*, *AP2* has a greater affect than *TOE2* in the repression of flowering time in Col-0; however, upon *mir172a-2 b-3 d-3* mutation this situation is reversed.

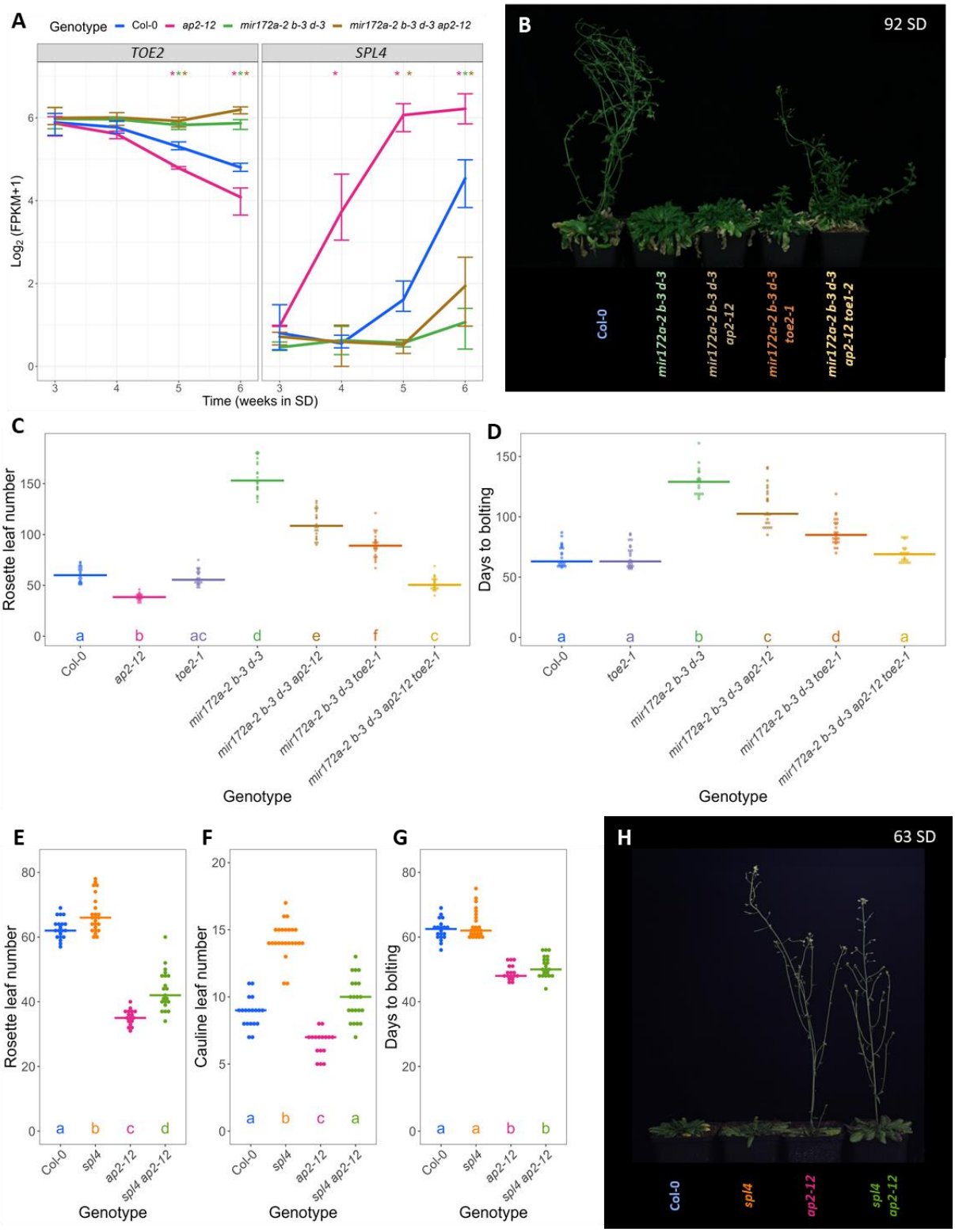

Figure 4-5. The persistence of *TOE2* expression in *mir172a-2 b-3 d-3 ap2-12* leads to late flowering.

(A) Expression profiles of *TOE2* and *SPL4* in plant apices of Col-0, *ap2-12*, *mir172a-2 b-3 d-3* and *mir172a-2 b-3 d-3 ap2-12* mutants under SDs. The gene is shown on top of each plot. Error bars represent the range between the maximum and minimum value among the three replicates at each time point. Statistically significant differences between Col-0 and the rest of genotypes are indicated with * (adjusted *p*-value < 0.05) or ** [adjusted *p*-value < 0.05 and absolute value of $\log_2$(fold change > 1] following the colour code at the top of the panel. (B–H) Flowering-time analysis of (B–D) *mir172a-2 b-3 d-3 ap2-12 toe2-1* (*N* = 22–24) and (E–H) *spl4 ap2-12* (*N* = 17–24) under SDs. (B) Photograph of 92-day-old plants grown in SDs used in the flowering time analysis. The genotype of each plant is indicated at the top. (See next page)

(C–D) Flowering time measurements of *mir172a-2 b-3 d-3 ap2-12 toe2-1* in terms of (C) rosette leaf number and (D) days to bolting. (E–G) Flowering-time measurements of *spl4 ap2-12* in terms of (E) rosette leaf number, (F) cauline leaf number and (G) days to bolting. The horizontal bars correspond to the median of each genotype. Statistically significant differences were determined via one-way ANOVA, followed by Tukey post-hoc comparisons ($p < 0.05$). A common letter among data sets indicate no significant differences. (H) Photograph of 63-day-old plants grown in SDs used for the flowering time analysis.

The rosette leaf number and bolting time of *mir172a-2 b-3 d-3 ap2-12 toe1-2* mutants were similar to those of Col-0. The introduction of the *toe2-1* mutation further rescued the late-flowering phenotype of *mir172a-2 b-3 d-3 ap2-12* mutants, which suggests that the persistence of *TOE2* expression in apices of *mir172a-2 b-3 d-3 ap2-12* mutants leads to late flowering. Importantly, *ap2-12* mutants exhibited on average 13.1 fewer rosette leaves than the higher-order *mir172a-2 b-3 d-3 ap2-12 toe2-1* mutant*,* which indicates that *ap2-12* mutants flowered earlier than *mir172a-2 b-3 d-3 ap2-12 toe2-1.* This might be caused by ectopic expression of other *AP2-LIKE* genes in *mir172a-2 b-3 d-3 ap2-12 toe2-1.* Taken together, these results demonstrate that *AP2* and *TOE2* function redundantly in negatively regulating flowering time, particularly in *mir172* mutant backgrounds.

The expression of *SPL4* increased progressively under SDs in parallel with the reduction of *TOE2* expression. To analyse whether this inverse relationship between the change in *TOE2* and *SPL4* expression was also observed in *ap2-12* and *mir172a-2 b-3 d-3* mutants, the expression of *SPL4* was analysed in the RNA-Seq data. Expression of *SPL4* increased rapidly over time in *ap2-12* mutants, which is consistent with the early flowering of this mutant (Figure 4-5A). This effect might represent direct regulation of *SPL4* by AP2, because AP2 binds to the regulatory region of *SPL4* in inflorescences (Yant et al., 2010). In the late-flowering *mir172a-2 b-3 d-3* and *mir172a-2 b-3 d-3 ap2-12* mutants, the expression level of *TOE2* remained constant, and as expected, the level of *SPL4* was comparable in both mutants and remained low at 6 wSD. These results suggest that TOE2 might repress *SPL4* in *mir172a-2 b-3 d-3 ap2-12* plants. Although *TOE2* expression remained constant over time in *mir172a-2 b-3 d-3* mutants, a 1.8-fold increase in *TOE2* was observed in *mir172a-2 b-3 d-3 ap2-12* mutants. These results suggest that the action of *AP2* and *TOE2* converge in the repression of *SPL4* expression.

To analyse whether the early upregulation of *SPL4* in *ap2-12* mutants contributes to the regulation of flowering time, the flowering time of the *spl4 ap2-12* double mutant was measured under SD (Figure 4-5E–H). The *spl4 ap2-12* mutant bolted at a comparable time to *ap2-12*. Although SPL4 does not seem to contribute to the early bolting of *ap2-12*, a partial recovery of the reduced leaf number of *ap2-12* was observed for *spl4 ap2-12*, which produced on average 8.4 more rosette leaves than *ap2-12*. Moreover, an increase of 3.2 cauline leaves for the *spl4 ap2-12* double mutant compared with *ap2-12* was observed. On one hand, this suggests that the upregulation of *SPL4* in *ap2-12* leads to a decrease in leaf number, which has a larger relative effect in cauline leaf number than rosette leaf number, because the cauline leaf number of *spl4 ap2-12* was comparable to that of Col-0 whereas *spl4 ap2-12* still produced many fewer rosette leaves than Col-0. On the other hand, an increase in *AP2* mRNA in *spl4* might contribute to the increase in leaf number. This experiment suggests that the relationship between *AP2-LIKE* genes and *SPL4* affects leaf number rather than bolting.

4.2.5 TOE2 does not delay flowering of ft tsf mutants under LDs

The *toe2-1* mutant produced slightly fewer leaves and bolted slightly earlier than Col-0 under LDs (Figure 2-1). Moreover, the decrease in *TOE2* mRNA level in Col-0 plant apices that was observed during the SD time course was not detectable under LDs (Table 4-2). To analyse the pattern of TOE2 protein accumulation at the SAM, the spatial pattern of TOE2-mScarlet-2HA expression was determined along a time course during continuous LDs via confocal microscopy. Consistent with data for SD conditions, TOE2 was not expressed in the central region of the SAM, but was present in developing leaves, even at young stages (Figure 4-6A). Moreover, TOE2 accumulation was detected in developing axillary meristems, but not in young developing flowers. These results indicate that the TOE2 accumulation pattern in plant apices is similar under LD and SD.

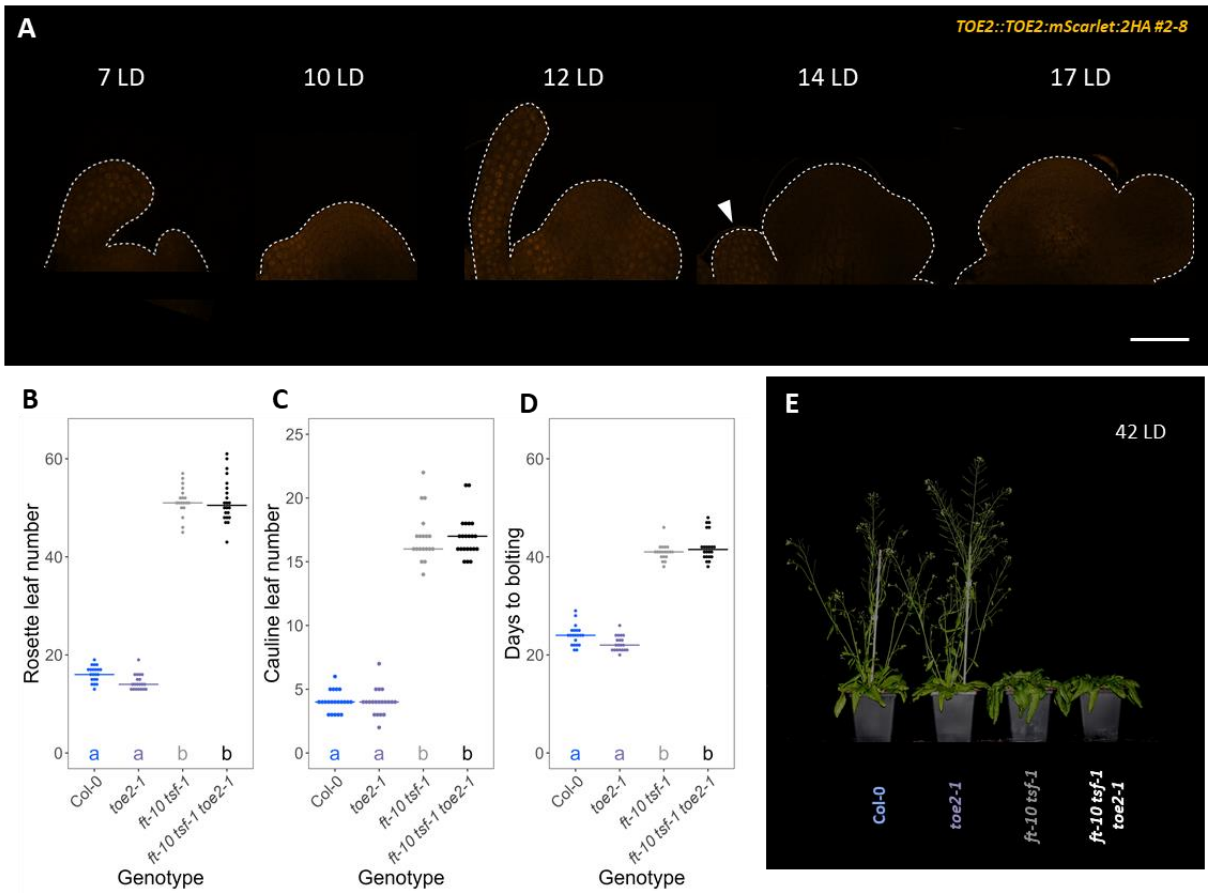

Figure 4-6. *TOE2* regulates flowering time under LDs through *FT/TSF.*

(A) Spatial expression pattern of the translational reporter TOE2 (*TOE2::TOE2:mScarlet:2HA*) at the SAM during a time course under LDs. The shape of the SAM is indicated by a white dotted line. Scale bar = 50 µm. The arrowhead indicates an axillary meristem, where TOE2-mScarlet-2HA accumulation could be detected. (B–D) Flowering-time measurements in terms of (B) rosette leaf number, (C) cauline leaf number and (D) days to bolting. The horizontal bars correspond to the median of each genotype. Significant differences were determined via one-way ANOVA, followed by Tukey post-hoc comparisons ($p < 0.05$). A common letter between two groups indicate no statistically significant differences. (E) Photograph of 42-day-old plants grown in LDs used for the flowering time analysis. *N* = 19–22.

TOE2 has been proposed to negatively impact *FT* expression. To explain how *TOE2* regulates flowering time via *FT/TSF,* the flowering time of *ft-10 tsf-1 toe2-1* triple mutants was measured. Combination of the *ft-10 tsf-1* mutations with *toe2-1* in the triple *ft-10 tsf-1 toe2-1* mutant resulted in a similar leaf number and bolting time to *toe2-1* (Figure 4-6B–E). These data suggest that under continuous LD, the slight early flowering of toe2 mutants requires *FT/TSF*.

4.2.6 SPL4 is a negative regulator of cauline leaf number under SDs and LDs

In previous sections in this chapter, the function of *SPL4* in the regulation of flowering time was analysed under SD. Because *SPL4* expression is induced under LD conditions (Torti et al., 2012), the pattern of SPL4 accumulation at the SAM was determined via confocal microscopy

using the same reporter line as used in Figure 4-4G. Consistent with its expression pattern in SDs, SPL4-VENUS was not detected in vegetative meristems (Figure 4-7A). However, the onset of SPL4-VENUS expression occurred in early transitioning meristems (10 LD) as foci of expression at the basal region of the meristems. From 12 LDs onwards, these foci expanded to form a band that also included the meristem periphery. Moreover, SPL4-VENUS was detectable in the apical regions of the meristem, but at a lower intensity, consistent with the pattern of mRNA accumulation observed by *in-situ* hybridisation (Torti et al., 2012). At later stages, SPL4-VENUS persisted at the SAM, and accumulated at the basal part of floral primordia. These results suggest that the pattern of SPL4 protein accumulation at the SAM during floral transition is the same as that of *SPL4* mRNA expression.

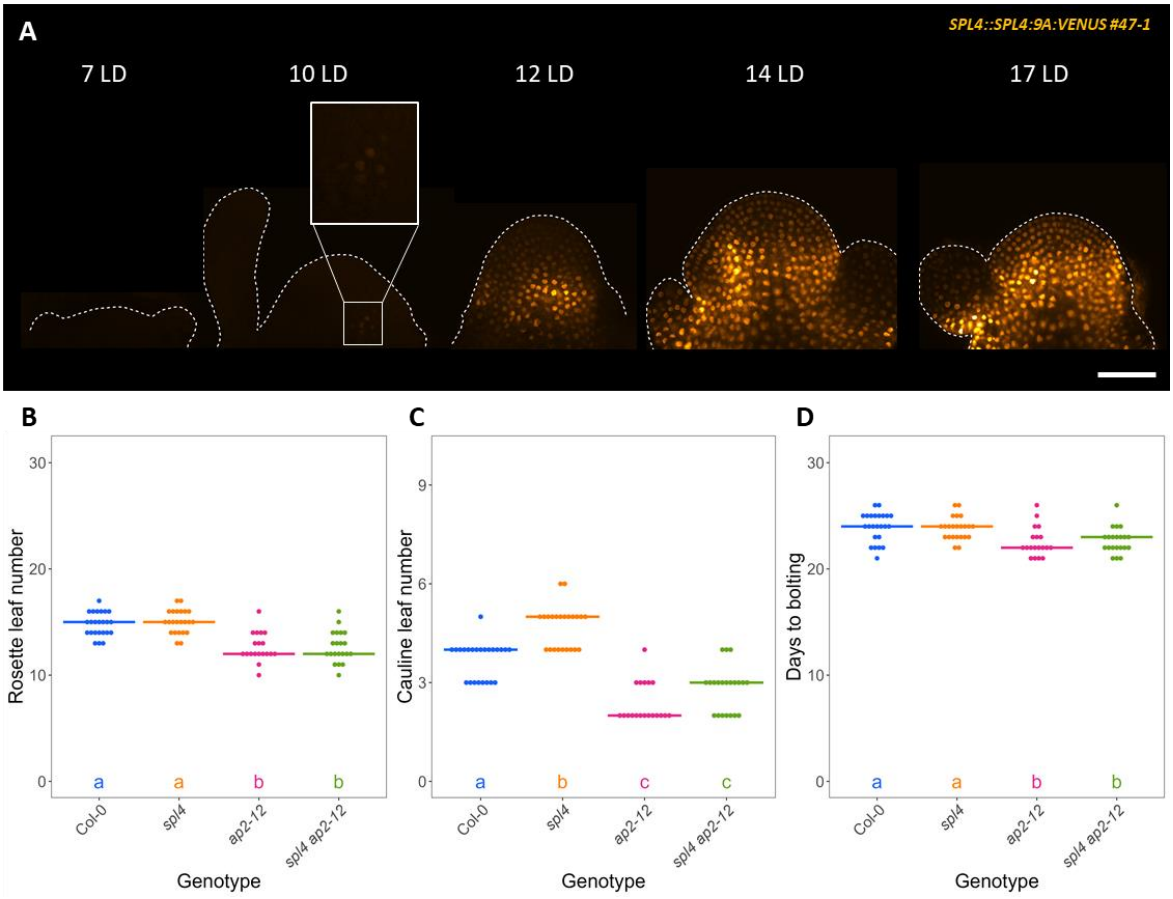

Figure 4-7. SPL4 accumulates at the SAM during floral transition under continuous LDs and is a negative regulator of cauline leaf number.

(A) Spatial expression pattern of the translational reporter SPL4 (*SPL4::SPL4:9A:VENUS)* at the SAM during a time course under LDs. The shape of the SAM is indicated by a white dotted line. Scale bar = 50 µm. (B–E) Flowering-time measurements of *spl4 ap2-12.* (B–D) Flowering time measurements in terms of (B) rosette leaf number, (C) cauline leaf number and (D) days to bolting. The horizontal bars correspond to the median of each genotype. Significant differences were determined via one-way ANOVA, followed by Tukey post-hoc comparisons ($p < 0.05$). A common letter between two groups indicate no statistically significant differences. N = 19–24.

Under LDs, *ap2-12* mutants are early flowering (Figure 2-1. The *ap2-12, toe1-2* and *toe2-1* mutants are early flowering under LDs.). Moreover, *SPL4* was upregulated earlier in *ap2-12* apices than in wild-type apices (Supplemental Figure 3-7Supplemental Figure 3-7. Expression profile for the genes represented in Supplemental Figure 3-6E in dissected apices of Col-0 and *ap2-12*.). To analyse whether this rapid *SPL4* upregulation leads to the early flowering of *ap2-12* mutants, the flowering time of *spl4 ap2-12* mutants was measured under LD. The leaf number and days to bolting of *spl4 ap2-12* mutants were comparable to those of *ap2-12* mutants (Figure 4-7B–D). This suggests that the rapid upregulation of *SPL4* in *ap2-12* mutants correlates with early flowering and might have other functional implications in addition to the regulation of bolting time or leaf number. Nevertheless, in previous sections, the possibility that *SPL4* might regulate *AP2* and determine the number of cauline leaves arose because the number of cauline leaves of *spl4 ap2-12* was intermediate between that of *spl4* and *ap2-12* single mutants under SDs. Because the mean decrease of 1.3 cauline leaves shown by *ap2-12* in comparison to Col-0 was epistatic to the mean increase of 1.0 cauline leaf shown by *spl4* in comparison with Col-0 (i.e. the *spl4 ap2-12* mutant produced the same number of cauline leaves as *ap2-12*), this suggests that *SPL4* might reduce cauline leaf number by reducing *AP2* activity.

4.3 Discussion

4.3.1 The regulation of AP2-LIKE gene expression is complex

Upon floral induction, miR172 accumulates at the SAM (Wollmann et al., 2010) and this is consistent with the expression of *MIR172* genes at the SAM (Lian et al., 2021; Ó'Maoiléidigh et al., 2021). To analyse the effect of miR172 at the SAM, the global transcriptome of apices of *mir172a-2 b-3 d-3* was compared with that of Col-0. The mRNA levels of *AP2-LIKE* genes in dissected apices of *mir172a-2 b-3 d-3* did not differ significantly from those in Col-0, except that for *SNZ* under LDs and *TOE2* under SDs. Therefore, the mRNA level of some but not all *AP2-LIKE* genes decreased during floral transition in the analysed material, consistent with previous reports (Mathieu et al., 2009; Schwab et al., 2005). Some of these genes described

in previous studies showed only minor changes in mRNA level over the floral transition, such as *AP2* (Schwab et al., 2005). Mathieu et al., (2009) showed that the expression of all *AP2-LIKE* genes decreased to differing degrees, except for that of *TOE3.* However, *SNZ* showed the smallest decrease in mRNA level among *AP2-LIKE* genes, whereas in the time course under LDs presented in this chapter, *SNZ* was among the genes that showed the greatest change in expression. Despite the experimental differences in the published time courses cited above (i.e. the time course of Mathieu et al., (2009) was a shift between different photoperiod conditions) and the differences in the technologies used for transcriptome profiling (i.e. RNA-seq via microarrays), these reports suggest that not all the *AP2-LIKE* gene mRNA levels decrease at the SAM during floral transition. One possible explanation for this is the method used to dissect plant apices, which might also include young developing organs and stem tissue that might express *AP2-LIKE* genes. To eliminate the possibility that mRNA of *AP2-LIKE* genes expressed in developing organs confounded the quantification of *AP2-LIKE* gene expression at the SAM, *in situ* hybridisations to detect the mRNA from *AP2-LIKE* genes could be performed during floral transition. Moreover, although some *AP2-LIKE* gene transcripts are cleaved by miR172 (Schwab et al., 2005), Chen, (2004) suggested that the main mechanism of *AP2* repression by miR172 is translational inhibition, which would not have been detected by the RNA-Seq time course experiments in this study. The absence of observed changes in mRNA levels of most *AP2-LIKE* genes in dissected plant apices despite the presence of miR172 is therefore most probably the result of translational inhibition in the regulation of *AP2-LIKE* expression. Characterizing the level of AP2-LIKE proteins using translational reporters would test this possibility.

4.3.2 The relationship between TOE2 and FT/TSF is influenced by photoperiod

Because *TOE2* was the only downregulated *AP2-LIKE* gene in *mir172a-2 b-3 d-3* in comparison with Col-0 under SDs, it was selected for further study. One aim of the experiments in this chapter was to characterise the function of *TOE2* in the regulation of flowering time. The *mir172a-2 b-3 d-3 toe2-1* mutant flowered earlier than *mir172a-2 b-3 d-3*. However, the *toe2-*

1 mutation did not affect flowering time in Col-0 background under SDs, because in the experiments described in this chapter, no statistically significant differences in leaf number and bolting time were observed between *toe2-1* and Col-0. This suggests that *TOE2* loss of function contributes to flowering-time regulation in the *mir172a-2 b-3 d-3* mutant background, whereas in wild type, *TOE2* either has no role in flowering control or functions redundantly with other members of the *AP2-LIKE* family.

Using the newly constructed translational fusion for TOE2, no accumulation of TOE2-mScarlet-2HA was observed in the central regions of the SAM, but TOE2 was detected in developing organs, even in extremely young primordia. This pattern is consistent with the RNA-seq, because although the material used for RNA-Seq was enriched for meristematic tissue, it also included young developing lateral organ primordia. Considering this pattern of TOE2 protein accumulation, the relationship between *TOE2* and *FT/TSF* was further analysed, because previous studies have implicated *TOE1* and *TOE2* in the regulation of *FT/TSF* (Du et al., 2020; Zhai et al., 2015; B. Zhang et al., 2015). Initial flowering-time results for the *ft-10 tsf-1 toe2-1* mutant under SDs suggest that *toe2-1* mutation enhances the mild late-bolting phenotype of *ft-10 tsf-1.* However, integrating this result with previous data is difficult because *FT* ectopic expression was previously described in *toe1 toe2* double mutants (B. Zhang et al., 2015). Furthermore, no available data support a direct regulation of *FT* by *TOE2*, although TOE1 was reported to bind to *FT* regulatory regions (B. Zhang et al., 2015). The link between *TOE2* and *FT* expression was proposed to involve the interaction of TOE2 with CRY receptors, but this interaction occurs in a blue light-dependent manner, and thus might be expected to be more relevant under LDs (Du et al., 2020). In this study, *ft-10 tsf-1* was epistatic to *toe2-1* in terms of flowering time, suggesting that the potential involvement of *TOE2* in the regulation of flowering time under LDs requires functional *FT/TSF.* Therefore, although it is plausible to also suggest a mechanism that relates *FT/TSF* and *TOE2* functions under SD conditions, this requires further confirmation and it would be important to test whether ectopic *FT/TSF* expression occurs in *toe2-1* mutants under SDs.

4.3.3 *AP2-LIKE* genes and *SPL4* genetically interact in the regulation of flowering time

The earlier flowering of *mir172a-2 b-3 d-3 ap2-12* in comparison with *mir172a-2 b-3 d-3* was considered to reflect the repression of *AP2* expression by miR172 (Ó'Maoiléidigh et al., 2021). In this chapter, this strategy was used to test the relevance of *TOE2* repression by miR172 in the regulation of flowering time under SDs. In the experiment to measure the flowering time of *mir172a-2 b-3 d-3 ap2-12 toe2-1,* the genotypes *mir172a-2 b-3 d-3 ap2-12* and *mir172a-2 b-2 d-3 toe2-1* were included as controls. The results demonstrated that *mir12a-2 b-3 d-3 toe2-1* was earlier flowering than *mir172a-2 b-3 d-3 ap2-12* under SDs. Notably, *ap2-12* was earlier flowering than *toe2-1.* This suggests that in wild type, the repression of flowering time by *AP2* is greater than that by *TOE2*, whereas in *mir172a-2 b-3 d-3*, the opposite is true. Because *TOE2* is downregulated more rapidly in plant apices of *ap2-12* mutants in comparison with Col-0, it would be relevant to understand better the genetic relationship between *AP2* and *TOE2* by measuring the flowering time of *ap2-12 toe2-1* mutants under SDs. It would also be interesting to determine where and when TOE2 is expressed in *mir172a-2 b-3 d-3,* either by introducing the *TOE2::TOE2:mScarlet:2HA* transgene into the *mir172a-2 b-3 d-3* background or by generating a *TOE2::rTOE2:mScarlet:2HA* line.

A relatively high level of *TOE2* mRNA persisted in *mir172a-2 b-2 d-3* and *mir172a-2 b-3 d-3 ap2-12* mutants for longer than in wild type, and the genetic analyses presented in this chapter suggest that this contributes to the observed later flowering of these mutants in comparison with wild type. Therefore, because no *FT/TSF* expression is expected in Col-0 under SDs, it is unlikely that the late flowering of *mir172a-2 b-3 d-3* and *mir172a-2 b-3 d-3 ap2-12* mutants caused by *TOE2* is mediated by repression of *FT/TSF.* For this reason, candidate genes were identified whose expression changed in the RNA-Seq in a way that correlated with that of *TOE2*. This filtering strategy yielded three candidate genes, whose expression negatively correlated to the one of *TOE2* in Col-0 under SDs: *SPL4, HB29* and *TCP1*. The effect of *HB29* and *TCP1* on flowering time has not been thoroughly tested by genetics. The leaf number of

hb29 mutants is comparable to that of wild type under LDs (Elfving et al., 2011), but no available data test the involvement of *HB29* or *TCP1* with the regulation of flowering time under SDs. Therefore, it would be relevant to measure the flowering time of *hb29* and the available *TCP1* gain-of-function lines (Y. Gao et al., 2015) under SDs.

Due to the induction of *SPL4* expression during floral transition (Torti et al., 2012) and the availability of translational fusion marker lines in the group, *SPL4* was selected as a suitable candidate gene that might function downstream of *TOE2*. Notably, in *Arabis alpina,* a perennial relative of Arabidopsis*, AaTOE2* has been shown to negatively regulate the expression of *AaSPL5* (Zhou et al., 2021). In the analyses of this chapter, although the *spl4* loss-of-function mutant flowered later than wild type under SDs, the pattern of SPL4 protein accumulation did not overlap substantially with that of TOE2, and neither did the previously reported pattern of *SPL4* mRNA at the SAM according to *in-situ* hybridisation (Torti et al., 2012). The *in situ* hybridization showed that *SPL4* is expressed during the later stages of floral transition in a band at the basal part of the meristem that comprises the rib meristem and the peripheral zone. The potential relationship between *TOE2* and *SPL4* in regulating flowering time needs to be further examined. For this, the flowering time of the double mutant *spl4 toe2-1* should be measured under SDs, and expression of the translational marker of SPL4 tested in the *toe2* mutant by confocal microscopy. Moreover, the genetic relation between *AP2* and *TOE2* should be explored by measuring the flowering time of the *ap2-12 toe2-1* double mutant and characterising the spatial pattern of expression of the translational marker of AP2 in the *toe2* mutant background by confocal microscopy, as well as that of *TOE2* in the *ap2* mutant background.

The relationship between *AP2* and *SPL4* has been previously reported, and AP2 can directly bind the regulatory region of *SPL4* and repress its expression (Yant et al., 2010). However, the comparable cauline leaf number of *spl4 ap2-12* and *ap2-12* mutants under LDs suggests that the greater number of cauline leaves produced by *spl4* might be mediated by *AP2.* Moreover, the comparable flowering time of *spl4* and *ap2-12* mutants suggest that the proposed repression of *SPL4* by AP2 under LDs does not substantially affect flowering time. One

possible mechanism for this might be the activation of *FUL* by *SPL4* (Xie et al., 2020), which could lead to the repression of *AP2* expression (Yant et al., 2010). However, the intermediate phenotype of *spl4 ap2-12* in terms of rosette and cauline leaf number under SDs suggests that the mutual repression of *AP2* and *SPL4* (where the repression of *AP2* by *SPL4* would be mediated by *FUL*) regulates rosette and cauline leaf number. Notably, whereas the suggested mutual repression motif between *AP2* and *SPL4* would impact on cauline leaf number, in terms of rosette leaf number, the repression of *SPL4* by *AP2* is possibly more relevant than the repression of *AP2* by *SPL4*, because the rosette leaf number of *spl4 ap2-12* was more similar to *ap2-12* rather than *spl4* and *SPL4* is not expressed in vegetative development of wild-type plants. All in all, these data suggest that *SPL4* activity reduces cauline leaf number under LDs and SDs, and may achieve this by repressing *AP2*.

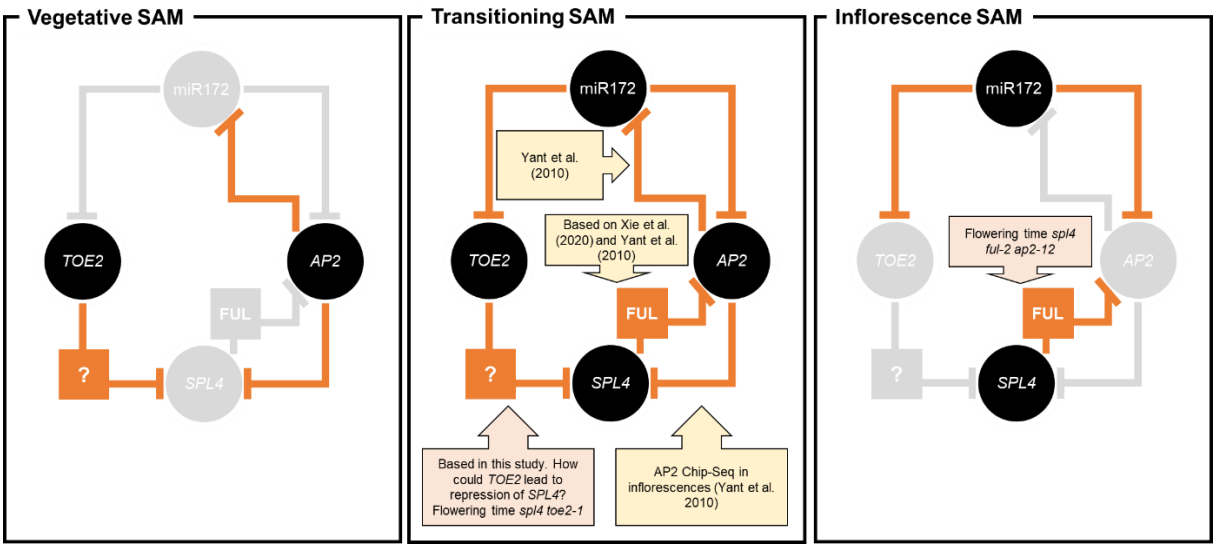

Figure 4-8. Genetic relationships between *MIR172, AP2, TOE2* and *SPL4*.

The genetic relationships between *FT/TSF, MIR172* and *AP2-LIKE* are represented as positive regulation (green) or negative regulation (orange). A box with a question mark shows that a relationship requires further confirmation. An orange box containing "FUL" indicates that the marked genetic relationship is dependent on the action of *FUL*. The observations in which these relationships are based are placed in yellow text boxes. Experimental suggestions to confirm the represented relationships are contained within orange text boxes.

Collectively, the aim of the experiments described in this chapter was to identify the genetic relationships among *MIR172, AP2, TOE2* and *SPL4* at the SAM in the regulation of flowering time (Figure 4-8). Although data are presented that show the function of *TOE2* downstream of miR172 in the regulation of flowering time, further experiments should address the mechanism of action of *TOE2* in wild type and upon *mir172a-2 b-3 d-3* mutation.

Table 4-4. Data for the flowering-time experiments described this chapter.

"s.d." = standard deviation. "n.a." = not applicable, i.e., such measurements were not performed.

[a]Five *mir172a-2 b-3 d-3* plants did not bolt in this analysis.

[b]These plants were grown in parallel to the experiment in (Figure 2-1).

[c]These plants were grown in parallel to the experiment in (Figure 2-2).

Experiment	Genoytpe	*n*	Rosette leaf number		Cauline leaf number		Days to bolting		Days until first open flower	
			Mean	s.d.	Mean	s.d.	Mean	s.d.	Mean	s.d.
Figure 4-2 Figure 4-5 SD	Col-0	23	60.7	7.36	n.a.	n.a.	67.5	8.88	n.a.	n.a.
	ap2-12	22	38.6	3.19	n.a.	n.a.	n.a.	n.a.	n.a.	n.a.
	toe2-1	24	57.5	7.09	n.a.	n.a.	67.0	9.38	n.a.	n.a.
	mir172a-2 b-3 d-3	24	156.0	15.30	n.a.	n.a.	129.5[a]	11.4	n.a.	n.a.
	mir172a-2 b-3 d-3 toe2-1	22	111.0	14.00	n.a.	n.a.	109.0	16.7	n.a.	n.a.
	mir172a-2 b-3 d-3 ap2-12	24	89.0	12.00	n.a.	n.a.	87.5	11.3	n.a.	n.a.
	mir172a-2 b-3 d-3 ap2-12 toe1-2	24	51.7	6.29	n.a.	n.a.	69.7	7.11	n.a.	n.a.
Figure 4-3 SD[b]	Col-0	15	51.5	9.12	7.8	1.26	58.6	5.14	71.1	5.41
	toe2-1	13	52.3	11.60	7.9	2.14	58.2	9.42	69.2	8.69
	ft-10 tsf-1	20	57.8	7.07	12.2	1.33	64.2	6.97	n.a.	n.a.
	ft-10 tsf-1 toe2-1	14	60.3	8.64	12.6	1.85	69.1	7.88	n.a.	n.a.
Figure 4-5 SD	Col-0	20	62.6	3.22	8.8	1.12	62.2	3.16	66.8	3.47
	spl4	24	67.0	5.56	14.3	1.33	63.9	4.29	69.0	4.53
	ap2-12	17	35.2	2.39	6.6	0.96	49.1	2.33	n.a	n.a.
	spl4 ap2-12	21	43.6	6.20	9.8	1.63	50.9	3.22	n.a	n.a.
Figure 4-6 LD[c]	Col-0	21	16.1	1.59	4.1	0.81	24.0	2.05	31.5	1.72
	toe2-1	20	14.4	1.57	4.0	1.03	22.3	1.53	30.2	1.74
	ft-10 tsf-1	19	51.4	3.00	16.9	1.94	40.9	1.65	n.a	n.a.
	ft-10 tsf-1 toe2-1	22	51.5	4.50	17.0	1.62	42.1	2.86	n.a	n.a.
Figure 4-7 LD	Col-0	24	14.8	1.10	3.7	0.55	24.0	1.37	27.8	1.36
	spl4	23	15.0	1.11	4.7	0.64	23.8	1.07	28.1	1.16
	ap2-12	19	12.6	1.34	2.4	0.59	22.5	1.39	n.a.	n.a.
	spl4 ap2-12	21	12.7	1.46	2.8	0.68	22.7	1.20	n.a.	n.a.

4.4 Supplemental figures

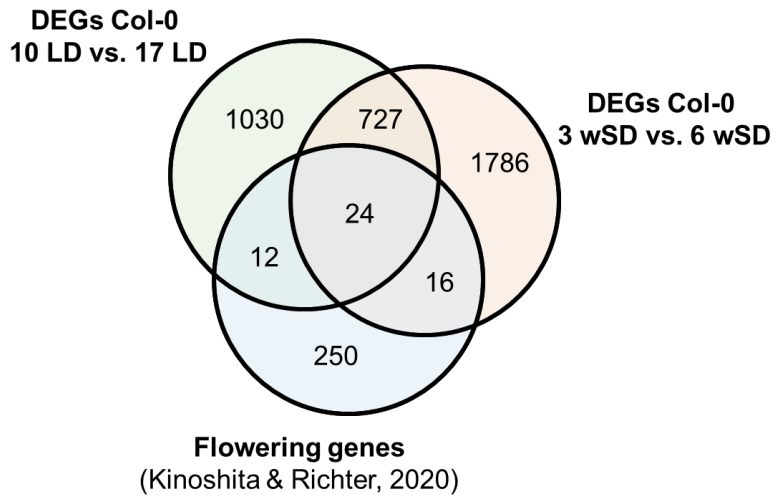

Supplemental Figure 4-1. Filtering to identify flowering marker genes in the RNA-seq experiments.

Venn diagram showing the overlap between the list of differentially expressed genes (DEGs) in Col-0 when comparing 10 LD vs. 17 LD, DEGs in Col-0 when comparing 3 wSD vs. 6 wSD, and the list of flowering genes available in Kinoshita & Richter, (2020). Information about the 24 genes present in all three data sets are provided in Table 4-1.

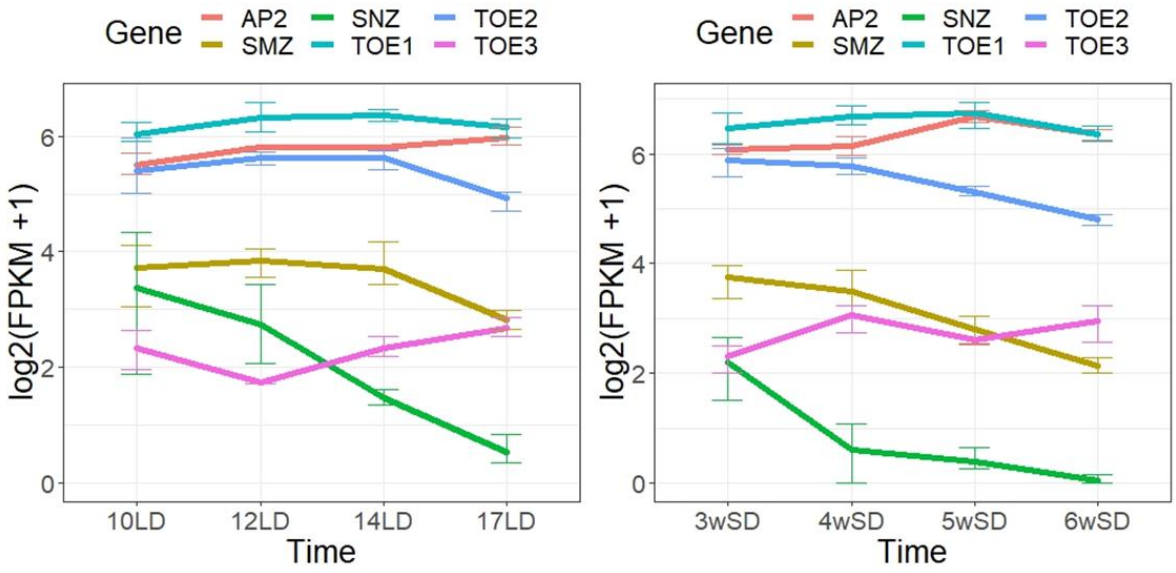

Supplemental Figure 4-2. Temporal expression pattern of the *AP2-LIKE* genes in Col-0 apices from RNA-seq data.

Expression profiles of *AP2-LIKE* genes in dissected plant apices of Col-0 under LDs (left) and SDs (right). The colours represent the different genes indicated at the top of the panel. Error bars represent the range between the maximum and minimum values for the three replicates at each time point.

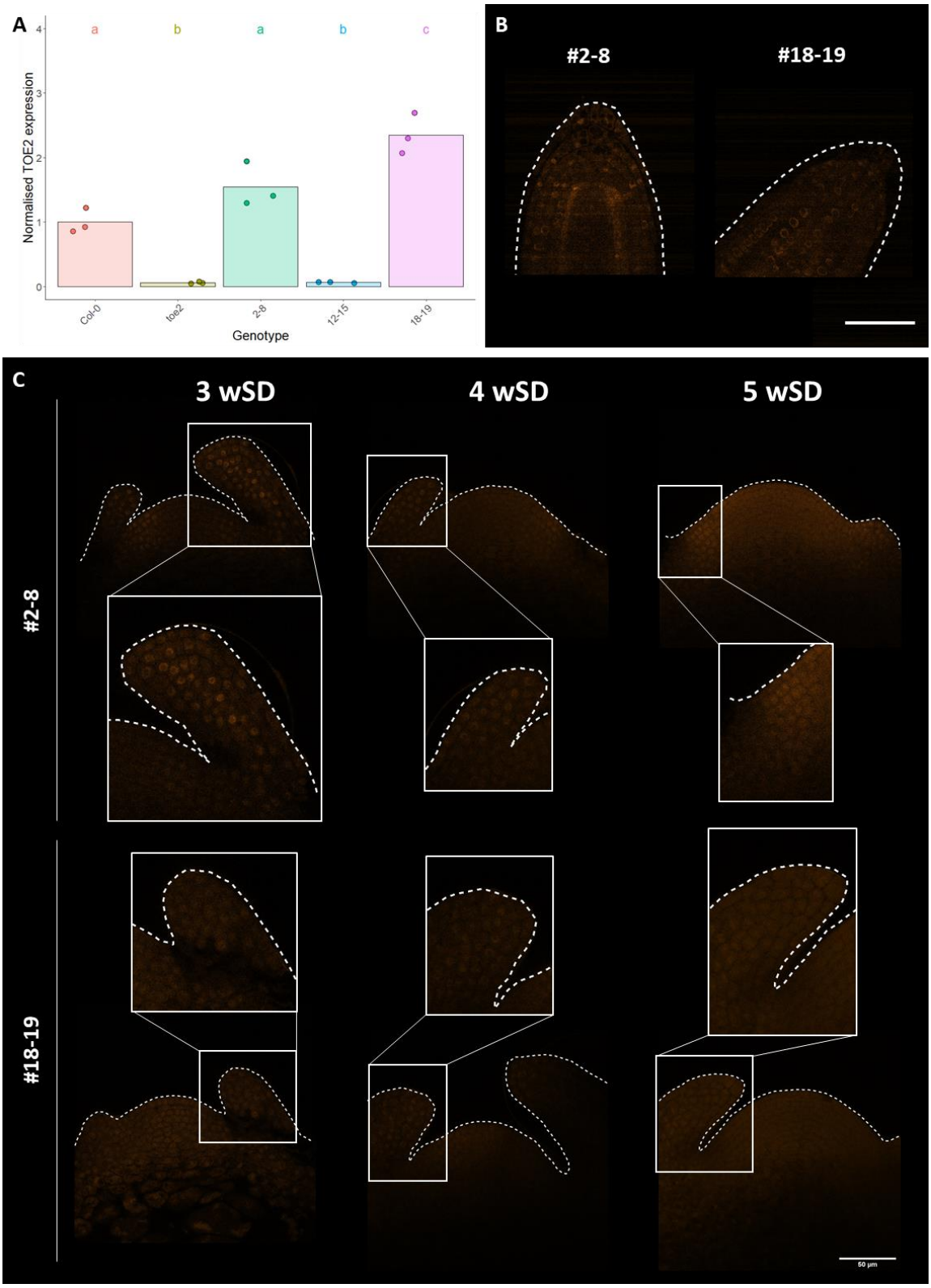

Supplemental Figure 4-3. Expression of the TOE2 translational fusion construct.

(A) Quantification of *TOE2* expression by RT-PCR and normalized to the expression of *PEROXIN4* in 4-day-old seedlings grown in LDs, when *TOE2* expression in roots is expected to be present (Jung et al., 2007) The columns represent the mean of values from three replicates, whose individual values are shown. The genotypes used were T3 homozygous lines. (B) Pattern of TOE2-mScarlet-2HA accumulation in 7-day-old roots grown in LDs. (C) Time course of TOE2 translational reporters under continuous SDs to validate the consistency of the accumulation pattern. Scale bar = 50 µm. The shape of the root or shoot meristem and their lateral organs is indicated with a dotted white line.

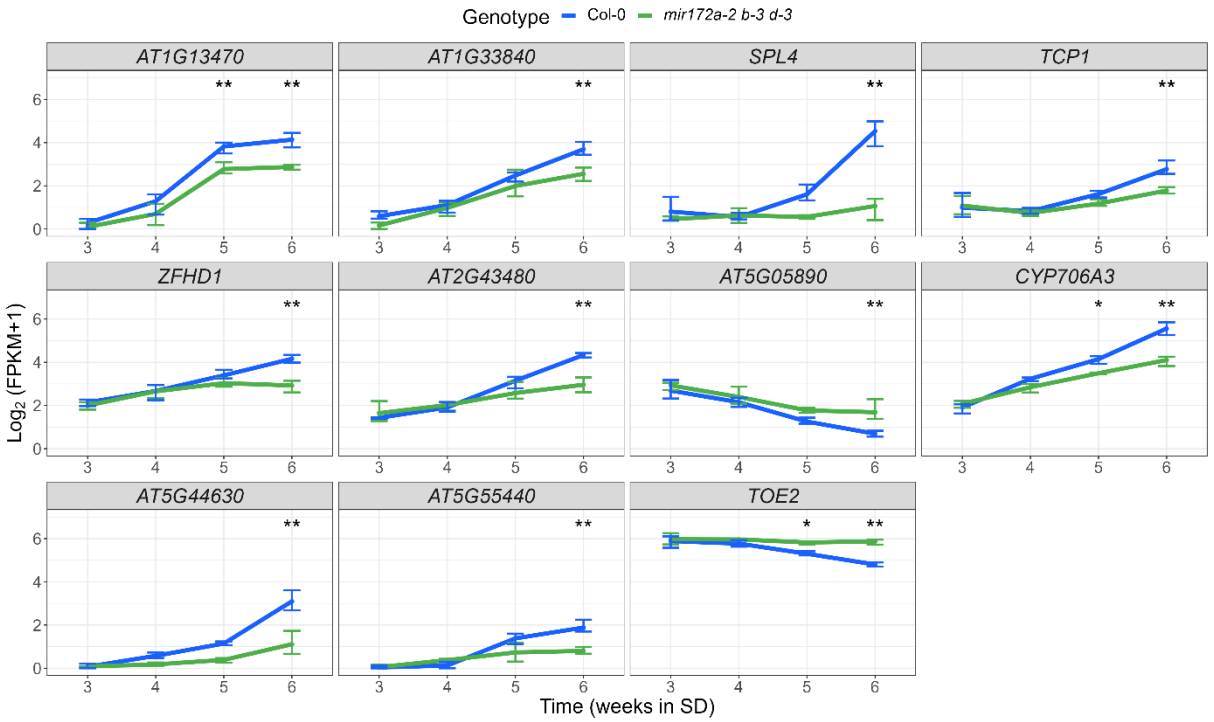

Supplemental Figure 4-4. Expression profiles of the 11 genes that are present in the three sets of the Venn diagram in Figure 4-4A.

(A) Expression profiles of 11 candidate genes in dissected plant apices of Col-0 and *mir172a-2 b-3 d-3* mutants under SD. The AGI gene symbol/gene name is provided on top of each plot. The colour code corresponds to the genotype indicated at the top of the panel. Error bars represent the range between the maximum and minimum value among the three replicates at each time point for plants grown in SDs. Statistically significant differences between Col-0 and *mir172a-2 b-3 d-3* are indicated with * (adjusted *p*-value < 0.05) or ** [adjusted *p*-value < 0.05 and absolute value of $\log_2$(fold change) > 1].

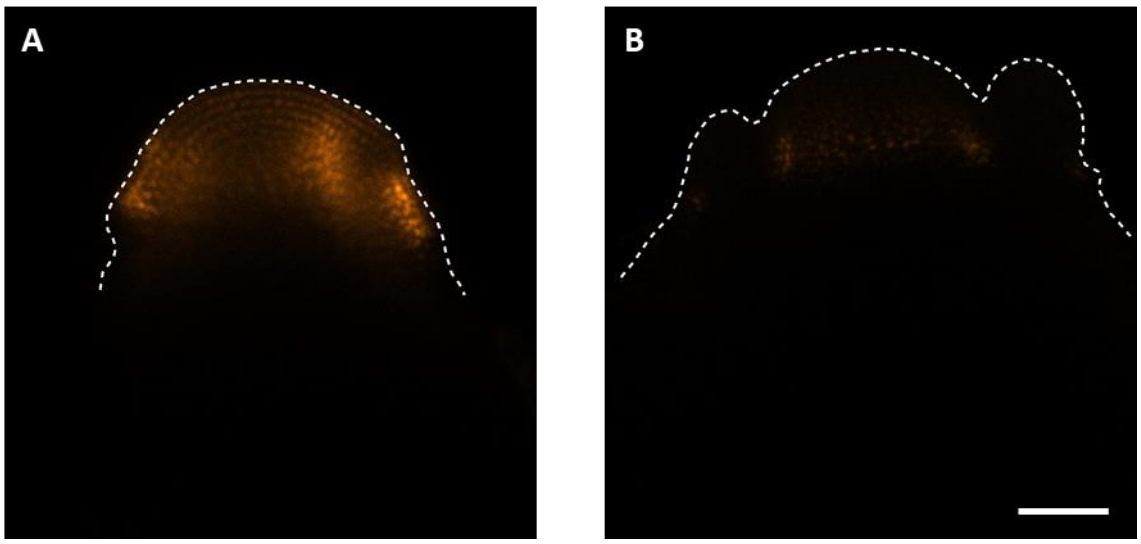

Supplemental Figure 4-5. Confocal images at 5 wSD shown in Figure 4-4 with reduced scale of the look up table.

(A) Line #47-1 and (B) line #50-1. Scale bar: 50 µm. The shape of the meristem and its lateral organs is indicated with a dotted white line.

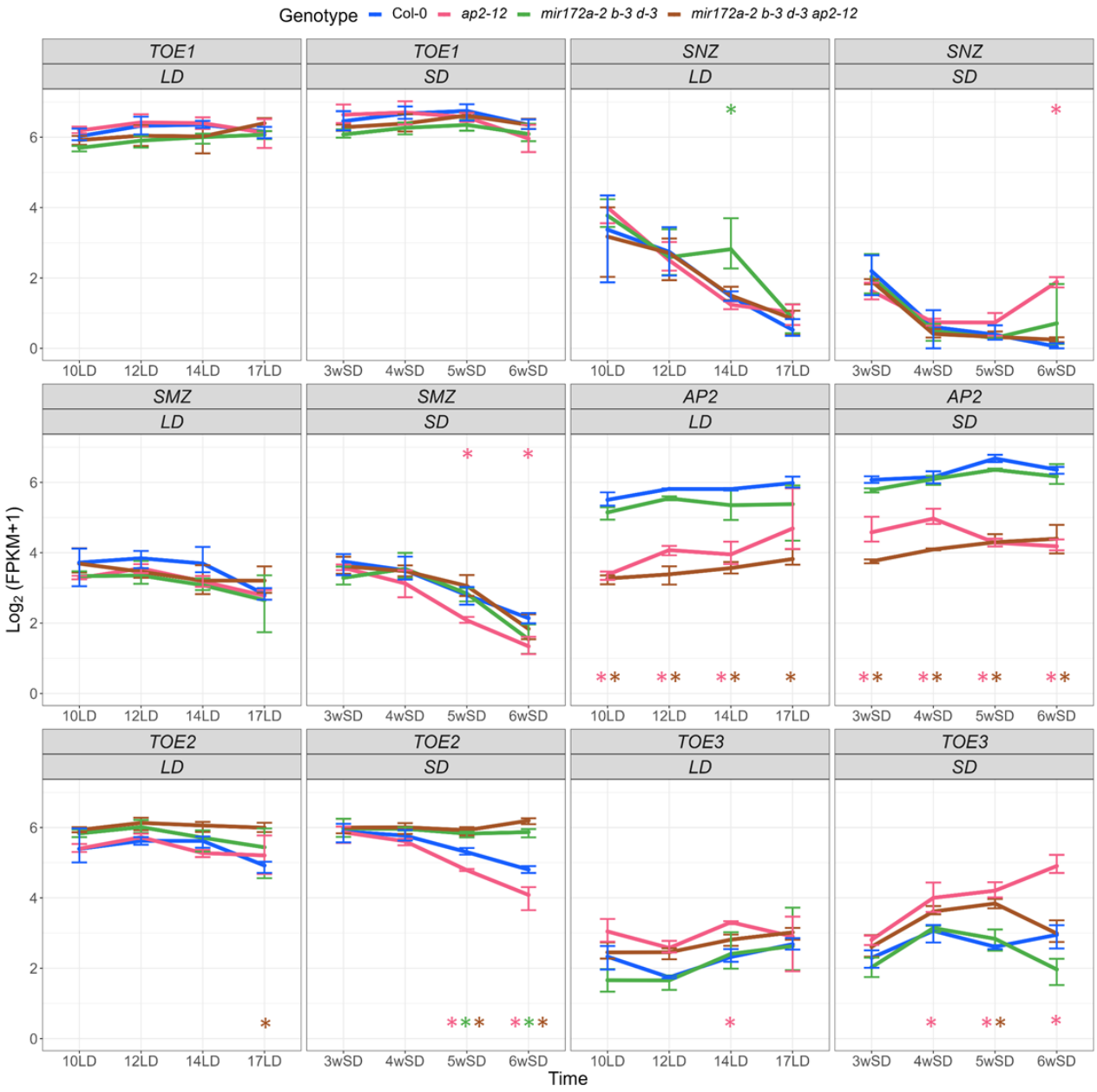

Supplemental Figure 4-6. Expression profile of the *AP2-LIKE* genes during LD and SD time courses.

Expression profiles of *AP2-LIKE* genes in dissected plant apices of Col-0, *ap2-12*, *mir172a-2 b-3 d-3* and *mir172a-2 b-3 d-3 ap2-12* mutants under LDs and SDs. The gene symbol and time course (LD or SD) are represented above each plot. The colour code corresponds to the genotype and is indicated at the top of the panel. Error bars represent the range between the maximum and minimum values among the three replicates at each time point. Statistically significant differences between Col-0 and the other genotypes are indicated with * (adjusted *p*-value < 0.05) following the colour code at the top of the panel.

5 General discussion

The relationship between the photoperiodic pathway and *MIR172* genes in the context of the gene regulatory network that controls flowering time is explored in Chapter 2 of this dissertation. The flowering times of the single *ap2-like* mutants were compared, which showed that *AP2, TOE1* and *TOE2* are the main repressors of flowering time among the *AP2-LIKE* genes under LDs. *AP2* was the only *AP2-LIKE* gene that significantly affected flowering time under SDs, and the only one that negatively regulated the number of cauline leaves under LDs and SDs. The flowering-time analyses of higher-order mutants that were impaired in the function of the main effectors of the photoperiodic pathway (*ft-10 tsf-1* or *fd-3*) and that also contained either mutations of the *MIR172* or *AP2-LIKE* genes revealed that whereas the regulation of flowering time by the *MIR172* or *AP2-LIKE* genes is influenced by the photoperiodic pathway, they also regulate flowering independently of the photoperiodic pathway.- The characterisation of the spatial patterns of expression of *MIR172* genes in Col-0 and *ft-10 tsf-1* backgrounds indicated that the photoperiodic pathway positively regulates *MIR172* expression at the SAM. Moreover, *FT/TSF* are essential for the expression of *MIR172D* in roots. Collectively, these results confirm a relationship between the photoperiodic pathway and *MIR172* genes, and together with previous work suggest that the miR172/AP2-LIKE module acts both upstream and downstream of FT/TSF (Du et al., 2020; Jung et al., 2007; Mathieu et al., 2009; Ó'Maoiléidigh et al., 2021; B. Zhang et al., 2015).

The function of *AP2* in regulating inflorescence meristem size was characterised during floral transition in Chapter 3. Confocal and computational analyses showed that *AP2* is a positive regulator of meristem size. Furthermore, quantitative morphology analyses demonstrated that *AP2* is essential for increases in meristem height and width during floral transition that contribute to meristem doming. The relationship between *AP2* and *SOC1* was characterised in the SAM during floral transition. Confocal microscopy demonstrated that both genes mutually repress each other's expression at this stage of development, which impacts on their respective protein levels in the meristem. *SOC1* was identified to be a major regulator of

flowering time downstream of *AP2*. Moreover, the results suggest that *SOC1* triggers a mechanism that accelerates the positive regulation of meristem doming by *AP2.* Flowering-time analyses of *ap2-12* and *rAP2-V* plants and related higher-order mutants indicated that *AP2* accelerates the rate of leaf production. Furthermore, the involvement of miR172 in the regulation of SAM area was shown to occur in an AP2-dependent manner. Taken together, these results indicate that floral transition and SAM doming are influenced by common regulators that couple these two processes.

Global transcriptome profiling via RNA-Seq was used to characterise potential mechanisms by which miR172 regulates flowering time at the SAM and was described in Chapter 4. The mRNA level of *TOE2* remained constant in *mir172a-2 b-3 d-3* triple mutants, whereas in wild-type plants the mRNA of this gene decreased during floral transition. Furthermore, flowering-time analyses showed that *TOE2* was a major negative regulator of flowering of the *mir172a-2 b-3 d-3* mutant under SDs. A translational reporter for TOE2 was generated and its spatial accumulation pattern revealed that TOE2 is preferentially present at the periphery of the SAM, and especially in young leaf primordia. The potential mechanisms by which *TOE2* negatively regulates flowering time under SDs were studied. The analyses under SDs in this dissertation suggest that *TOE2* regulates flowering time independently from *FT/TSF*, although the effect was small, and that it negatively regulates the expression of *SPL4*. Furthermore, the relationship between *TOE2* and *AP2* was dissected, and the results suggest that the function of these two genes converge on the negative regulation of *SPL4.* The relationship between *FT/TSF* and *TOE2*, as well as *AP2* and *SPL4*, were studied under continuous LDs. The data showed that the spatial pattern of TOE2 protein at the SAM in LDs is comparable with the one in SDs. Moreover, flowering-time analyses suggested that the regulation of flowering time under LDs by *TOE2* involves *FT/TSF* and that the early upregulation of *SPL4* upon *ap2-12* mutation is not relevant for flowering-time regulation. Taken together, TOE2 and AP2 appear to have spatially distinct roles in flowering with TOE2 acting mainly in leaves and AP2 in the SAM, but both negatively regulate *SPL4* transcription.

FT/TSF were found to be positive regulators of *MIR172* transcription at the SAM and of *MIR172D* in roots. Previous reports indicated that miR172 is a positive regulator of *FT/TSF* in leaves (Ó'Maoiléidigh et al., 2021), which is consistent with the repression of *FT* by some AP2-LIKE transcription factors (Mathieu et al., 2009; B. Zhang et al., 2015). These observations suggest that there are certain tissues where *FT/TSF* positively regulate *MIR172* expression, whereas in other tissues *MIR172* positively regulates *FT/TSF* expression. Future analyses should aim to characterise these relationships in different plant tissues and at different developmental stages, to examine the existence of systemic signalling of *FT/TSF, MIR172* and *AP2-LIKE* genes.

AP2 was shown to be a positive regulator of SAM area and doming during floral transition. Studying the relationship between *AP2* function during floral transition and other mechanisms previously shown to regulate meristem size would be of interest. Characterizing in more detail the regulation of lateral organ production by *AP2* during floral transition would be important as this may contribute to its role in controlling meristem size. Furthermore, although the analyses here indicate that *AP2* is a positive regulator of cell proliferation at the SAM, the mechanism by which this occurs needs to be established.

The results in the fourth chapter suggest that *TOE2* and *AP2* converge on the regulation of *SPL4.* The relationship between *TOE2* and *SPL4* should be confirmed by flowering-time analyses and confocal imaging of the *SPL4* translational reporter in the *toe2-1* mutant background. In addition to that, it should be checked whether *SPL4* mRNA levels are higher in the *ap2-12 toe2-1* double mutant. Moreover, the relevance of *TOE2* downregulation by miR172 under SDs could be confirmed by introducing the TOE2 translational reporter into the *mir172a-2 b-3 d-3* mutant background, or via the generation of an rTOE2 reporter (see Materials and methods).

The experiments in this dissertation studied the positive regulation of flowering time by miR172 and its functions in the SAM during floral transition. Firstly, the involvement of *MIR172* genes in the gene regulatory network that controls flowering at the SAM was analysed, and the TOE2

transcription factor was characterised. Secondly, changes in meristem morphology at floral transition were found to be promoted by *AP2*. This confirms that the organisation of the SAM is linked to floral transition because both are regulated by common proteins.

6 Materials and methods

6.1 Plant material and growth conditions

6.1.1 Plant material

All plants in this study were *Arabidopsis thaliana* Columbia-0 (Col-0) background (Table 6-1). Therefore, this ecotype was used as a reference control (wild type).

Table 6-1. Plant material used in this study.

Mutant/transgenic line	Reference
ap2-12	Yant et al., 2010
toe1-2	Aukerman & Sakai, 2003
toe2-1	Aukerman & Sakai, 2003
toe3-1	Yant et al., 2010
smz-2	Mathieu et al., 2009
snz-1	Mathieu et al., 2009
ft-10	Torti et al., 2012
ft-10 tsf-1	Torti et al., 2012
ft-10 tsf-1 ap2-12	This study.
mir172a-2 b-3 d-3	Ó'Maoiléidigh et al., 2021
mir172a-2 b-3 c-1 d-3 e-1	Ó'Maoiléidigh et al., 2021
ft-10 mir172a-2 b-3 d-3	This study.
fd-3	Jang et al., 2009
fd-3 mir172a-2 b-3 d-3	This study.
fd-3 mir172a-2 b-3 c-1 d-3 e-1	This study.
MIR172A::NVG 12.5/Col-0	Ó'Maoiléidigh et al., 2021
MIR172B::NVG 11.3/Col-0	Ó'Maoiléidigh et al., 2021
MIR172D::NVG 4.4/Col-0	Ó'Maoiléidigh et al., 2021
MIR172A::NVG 12.5/ft-10 tsf-1	This study.
MIR172B::NVG 11.3/ft-10 tsf-1	This study.
MIR172D::NVG 4.4/ft-10 tsf-1	This study.
AP2::AP2:VENUS #1/ap2-12	Ó'Maoiléidigh et al., 2021
AP2::rAP2:VENUS #A6/Col-0 (rAP2)	Sang et al., 2022
rAP2/ap2-12	Sang et al., 2022
soc1-2	Lee et al., 2000
soc1-2 ap2-12	Published in Yant et al., 2010 but recreated in this study.
AP2::AP2:VENUS #1/ap2-12 soc1-2	This study.

SOC1::SOC1:GFP/soc1-2	Immink et al., 2012
SOC1::SOC1:GFP/soc1-2 ap2-12	This study.
mir172a-2 b-3 d-3 ap2-12	Ó'Maoiléidigh et al., 2021
mir172a-2 b-3 d-3 toe2-1	This study.
mir172a-2 b-3 d-3 toe2-1 ap2-12	This study.
ft-10 tsf-1 toe2-1	This study.
TOE2::TOE2:mScarlet:2HA #2.8/toe2-1	This study.
TOE2::TOE2:mScarlet:2HA #12.15/toe2-1	This study.
TOE2::TOE2:mScarlet:2HA #18.19/toe2-1	This study.
SPL4::SPL4:9A:VENUS #47-1-1/Col-0	Generated in the group by Kerstin Luxa and Coral Vincent.
SPL4::SPL4:9A:VENUS #50-1-2/Col-0	Generated in the group by Kerstin Luxa and Coral Vincent.
rAP2/soc1-2	This study.
spl4	Generated in the group by Youbong Hyun.
spl4 ap2-12	This study.

6.1.2 Growth conditions

Plants were grown on soil under controlled conditions of SDs (8 h light/16 h dark) or LDs (16 h light/8 h dark). Seeds were sown directly on soil and were stratified for 2 to 3 days in the dark at 4°C and were then transferred to LD- or SD-growth chambers at 21°C, or to the greenhouse.

For germination on agar plates, seeds were firstly sterilised in a fume hood for 2–3 h via exposure to chlorine gas resulting from mixing 100 mL NaOCl (12% Cl) and 4 mL 37% HCl.

6.1.3 Phosphinotricin (PPT) resistance assay

The identification of PPT-resistant plants was performed on agar plates with Murashige & Skoog (MS) medium containing PPT: plants were either directly germinated on the plates or adult leaves were placed on the surface of the medium.

For germination on agar plates, seeds were first sterilised via chlorine gas and were then sown on agar plates (8 g L^{-1} Phytoagar from Duchefa Biochemie, the Netherlands) with 1× MS medium supplemented with 2% (w/v) sucrose and 15 mg mL^{-1} PPT. After stratification for 2 days in the dark at 4°C, plants were grown in continuous light at 21°C for at least 10 days.

The assay using leaf material was performed as in Ó'Maoiléidigh et al. (2021), but using 1× MS medium containing 15 mg mL^{-1} PPT (without sucrose), and placing the plates with leaves in continuous light at 21°C for at least 5 days.

6.2 Molecular cloning

The strategy used to generate a *TOE2::TOE2:mScarlet:2HA* marker line and the corresponding miR172-resistant version is summarised in Figure 6-1. The constructs generated in this study are listed in Table 6-2. The sequence fidelity of all the generated constructs was confirmed via Sanger sequencing. All the oligonucleotides used in this section are listed in Table 6-17, Table 6-18 and Table 6-20.

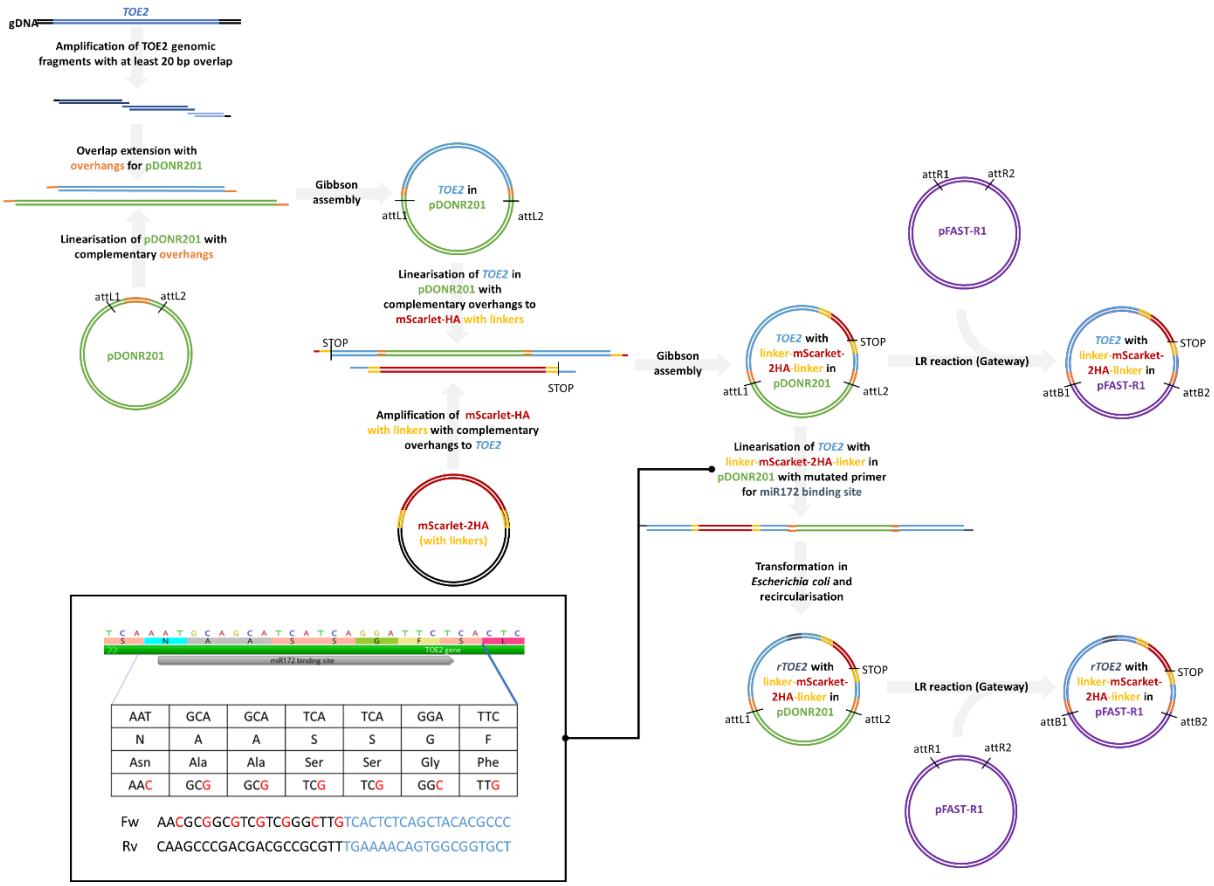

Figure 6-1. Generation of translational reporters for TOE2.

Schematic diagram that summarises the strategy used to generate a translational reporter for TOE2 and a miR172-resistant version of TOE2 (rTOE2). The square panel displays the primers used to generate rTOE2; these primers contained synonymous mutations and were expected to bind to the flanking region of the miR172-binding site.

6.2.1 Polymerase Incomplete Primer Extension (PIPE) cloning

PIPE cloning relies on the incomplete extension products generated during a PCR (Klock & Lesley, 2009). Short overlapping sequences are introduced to the end of the products via PCR involving primers that allow complementarity with a vector that has been amplified via PCR, which generates complementary ends to those of the insert of interest.

Table 6-2. Plasmids used in this study.

Name	Description	Resistance
pDONR201	Gateway® donor vector with attP1 and attP sites and a kanamycin resistance marker	Kanamycin
pFAST-R01	Gateway® destination vector with attR1 and attR2 sites, a spectinomycin resistance marker, and red fluorescent protein (RFP) under the regulation of a seed-specific promoter (*OLEOSIN1).*	Spectinomycin
mScarlet:2HA **pGEM T Easy**	pGEM T Easy vector containing the coding sequence for mScarlet, flanked by two linkers, and with a 2HA tag at the N-terminus.	Ampicillin/ Carbamycin
TOE2::TOE2 **pDONR201**	pDONR201 vector containing the genomic region of *TOE2.*	Kanamycin
TOE2::TOE2:mScarlet:2HA **pDONR201**	pDONR201 vector containing the genomic region of *TOE2.* In this vector, the encoded TOE2 protein contains mScarlet and a 2HA tag at the N-terminus.	Kanamycin
TOE2::TOE2:mScarlet:2HA **pFAST-R01**	pFAST-R01 vector containing the genomic region of *TOE2.* In this vector, the encoded TOE2 protein contains mScarlet and a 2HA tag at the N-terminus.	Spectinomycin
TOE2::TOE2:mScarlet:2HA **pDONR201**	pDONR201 vector containing the genomic region of *TOE2.* In this vector, the encoded TOE2 protein is miR172 resistant and contains mScarlet and a 2HA tag at the N-terminus.	Kanamycin
TOE2::TOE2:mScarlet:2HA **pFAST-R01**	pFAST-R01 vector containing the genomic region of *TOE2.* In this vector, the encoded TOE2 protein is miR172 resistant and contains mScarlet and a 2HA tag at the N-terminus.	Spectinomycin

The genomic region of *TOE2*, consisting of 8.6 kb, was divided into three regions, and each region was amplified by PCR using high-fidelity DNA polymerase PrimeStar® GXL (Takara, Japan; see Table 6-3 and Table 6-4) and genomic DNA extracted from Col-0 via the BioSprint DNA Plant Kit (Qiagen, the Netherlands). The primer pairs for each amplification yielded overlapping ends of the amplicons between each flanking region. After confirming successful PCR amplication by electrophoresing 5 µL of each amplicon on a 1.0% agarose gel, the PCR product was purified using the NucleoSpin® Gel and PCR Clean-up Kit (Macherey-Nagel, Germany). The three amplified regions were then mixed and used to perform overlap extension PCR (Table 6-6). Importantly, the primers at the flanks of regions 1 and 3 were complementary to the ends of the linearised pDONR201 vector. The genomic region of *TOE2* amplified in this way was inserted into the pDONR201 vector via Gibson assembly using the NEBuilder HiFi DNA Assembly Cloning Kit (NEB, USA). The resulting construct from the Gibson assembly was transformed in *Escherichia coli.*

Table 6-3. PCR mix with PrimeSTAR® DNA Polymerase.

PCR component	Volume (µL)
PrimeSTAR® GXL 5× Buffer	10.0
Special dNTP Mix	4.0
PrimeSTAR® GXL DNA Polymerase	2.0
Forward primer 10 µM	1.5
Reverse primer 10 µM	1.5
DNA template (at least 20 ng)	[Variable]
dH_2O	up to 50 µL

Table 6-4. PCR program with PrimeSTAR® GXL.

Information about annealing temperature is shown in Table 6-5.

Step	Temperature (°C)	Time
1	98	30 s
2	98	10 s
3	[Variable] Annealing temperature	30 s
4	68	1 min kb^{-1}
15 cycles, loop to step 2		
5	10	Hold

The NEBuilder HiFi DNA Assembly Cloning Kit was also used to generate a construct that encodes TOE2 fused with mScarlet and a 2-HA tag at the N-terminal region (i.e., sequences encoding mScarlet and 2-HA were inserted into the pDONOR201 vector that already contained the genomic region of *TOE2*).

Table 6-5. Annealing temperature for PCR reactions using PrimeSTAR® DNA polymerase.

Reaction		Primers	Annealing temperature (°C)
Cloning *TOE2* in pDONR201	Region 1 *TOE2*	EB67 + EB68	63
	Region 2 *TOE2*	EB69 + EB70	61
	Region 3 *TOE3*	EB71 + EB72	61
	Overlap extension	EB43 + EB44	54
Cloning mScarlet in pDONR201 with *TOE2*	Linearisation mScarlet	EB98 + EB99	60
	Linearisation pDONR201 with *TOE2*	EB100 + EB101	60
Generation of *rTOE2*		EB115 + EB143	50

Table 6-6. PCR mix for overlapping extension.

PCR component	Volume (µL)
PrimeSTAR® GXL 5× Buffer	10.0
Special dNTP Mix	4.0
PrimeSTAR® GXL DNA Polymerase	2.0
Forward primer 10 µM	1.5
Reverse primer 10 µM	1.5
DNA template (at least 20 ng)	5.0
dH_2O	26.0

6.2.2 Chemical transformation of *E. coli*

Vectors were transformed into C3019H 10-β competent cells (NEB, USA) via chemical transformation. For this, 10-β cells were thawed on ice for 5 min and 2 µL of the desired DNA was added to the tube with cells for 15 min. Cells were heat shocked at 42°C for 30 sec and were then incubated for 10 min on ice. The cells were grown in 500 µL SOC outgrowth medium (NEB, USA) at 37°C for 1 h with shaking at 180 rpm. Finally, 50 µL and 450 µL of the cell suspension was plated on separate agar plates containing lysogeny broth (LB) medium (40 g

L^{-1} LB-Medium from Carl Roth, Germany) for with the appropriate antibiotic (i.e. kanamycin or streptomycin) to select positive colonies. The plates were incubated overnight at 37°C.

6.2.3 Colony PCR

After overnight incubation, colonies were picked from LB plates using sterile pipette tips and the bacteria were resuspended in 19.25 µL dH_2O to be used for PCR (see Table 6-7) and in parallel, the tip was then used to inoculate 5 mL LB medium containing the suitable antibiotic for selection. The LB cultures were stored at 4°C, whereas the 19.25 µL of cell suspension were incubated at 95°C for 7 min. The PCR master mix (Table 6-7) was then added to the 19.25 µL cell suspension in water to perform a PCR using Taq DNA polymerase (Invitrogen/ThermoFisher, USA; see program in Table 6-8). The LB tubes corresponding to the positive colonies were incubated overnight at 37°C with shaking at 180 rpm. Plasmid DNA was then extracted using the NucleoSpin® Plasmid Mini Kit (Macherey-Nagel, Germany).

Table 6-7. Mix for colony PCR.

PCR component	Volume (µL)
10× Buffer	2,5
$MgCl_2$	0.75
dNTP 10 mM	0.5
Forward primer 10 µM	1.0
Reverse primer 10 µM	1.0
Taq polymerase (6 U $µL^{-1}$ Invitrogen)	0.1
dH_2O	19.15

Table 6-8. Program for PCR with Invitrogen Taq

Step	Temperature (°C)	Duration
1	98	3 min
2	98	45 s
3	54	45 s
4	72	1 kb min^{-1}
30 cycles; loop to step 2		
5	72	2 min
6	10	Hold

6.2.4 Gateway LR reactions

The inserts that were included in the pDONR201 vectors were transferred to the expression vector pFAST-R01 using the Invitrogen LR Clonase II (ThermoFisher, USA) according to the manufacturer's instructions. The LR reactions were incubated for at least 2 h.

6.2.5 Generation of miR172-resistant TOE2 (rTOE2)

To aim for an *rTOE2*-containing vector, the pDONR201 that contained *TOE2::TOE2:mScarlet:2HA* was linearised via PCR using the PrimeStar GXL polymerase, using the program and protocols described in section 6.2.1, and using primers that contained a synonymous mutation within the miR172-binding site. Afterwards, the PCR product was purified using the NucleoSpin® Plasmid Mini Kit and 2 µL of the purified product was transformed directly into *E. coli*, as outlined in section 6.2.2.

6.3 Generation of plant transgenic lines

6.3.1 Agrobacterium tumefaciens transformation

Electrocompetent cells (100 µL) of *Agrobacterium tumefaciens* strain GV3101 (pSOUP) were transformed with 50–100 ng plasmid via electroporation in 0.1-cm cuvettes, with a 2.2 kV pulse. Subsequently, bacteria were incubated in 450 µL LB medium at 28°C with shaking at 180 rpm for 2 h. Then, 50 µL and 350 µL of the culture were separately plated onto LB/agar plates that contained the relevant antibiotics for selection (i.e. rifampicin, tetracycline, gentamycin, spectinomycin). Colony PCRs were performed similarly to those for *E. coli,* as described in section 6.2.3.

6.3.2 Plant transformation

Mutant *toe2-1* plants that possessed a few open flowers were transformed via floral dipping. A 2-mL pre-culture in LB containing the relevant antibiotics (see section 6.3.1) of *TOE2::TOE2:mScarlet:2HA* in pFAST-R01 was grown overnight at 28°C with shaking at 180 rpm. The next day, the pre-culture was transferred into a 1-L flask containing 250 mL LB and

the same antibiotics, and was grown overnight at 28°C with shaking at 180 rpm. Plants were transformed by floral dipping when the optical density of the culture at 600 nm was 0.7–1.0. For transformation, plants were dipped for 1 min into a solution consisting off the 250-mL culture and 250 mL 20% (w/v) sucrose with 0.1% (v/v) Silwet® Gold (Spiess-Urania, Germany). After transformation, plants were covered with plastic bags and kept overnight in the dark at room temperature.

6.3.3 Selection of transgenic lines

Screening of transgenic plants was performed using fluorescence microscopy to detect RFP accumulation at the seed coat as a marker of the presence of the transgene. Thirty RFP-containing seeds were germinated. The progeny of each of the 30 T1 plants was harvested and at least 150 seeds were screened to check whether there was a 3:1 segregation of the presence of RFP, as an indication of a single insertion event of the transgene during floral dipping. Four lines exhibited a 3:1 segregation of RFP accumulation at the seed coat. Then, between 10 and 15 RFP-expressing seeds were germinated and the progeny of each T2 plant was collected separately to constitute different T3 lines. Seeds from each T3 line were screened to distinguish between lines that were homozygous (100% RFP-containing seeds) or heterozygous (75% RFP-containing seeds).

6.4 DNA extraction and genotyping

Genotyping was performed after DNA extraction either via Edward's buffer (Edwards et al., 1991) in 1.5-mL tubes, or via RLT buffer using the Biosprint 96 Kit (Qiagen, the Netherlands) according to the manufacturer's instructions, to obtain 100 µL or 200 µL of sample DNA.

Table 6-9. Primers and conditions for genotyping PCRs.

See standard PCR program in Table 6-11.

Gene	Allele	Primers	Annealing temperature (°C)	Elongation time	Number of cycles
AP2	*WT*	EB07 + EB08	50	90 s	35
	ap2-12	B163 + EB08	56	90 s	35
	AP2-VENUS vs. AP2 WT	EB08 + EB141	52	90 s	32
TOE1	*WT*	B164 + B165	60	1 min	35
	toe1-2	B163 + B165	54	45 s	35
TOE2	*WT*	B166 + B167	57	1 min	35
	toe2-1	B163 + B166	52	1 min	30
TOE3	*WT*	EB04 + EB05	59	1 min	35
	toe3-1	EB04 + EB06	57	1 min	35
SMZ	*WT*	EB01 + EB02	57	1 min	35
	smz-2	B163 + EB01	57	1 min	35
SNZ	*WT*	B161 + B162	57	90 s	35
	snz-1	B163 + B161	57	90 s	35
FT	*WT*	EB12 + EB13	50	150 s	35
	ft-10	EB11 + EB12	50	150 s	35
TSF	*WT*	EB14 + EB15	55	120 s	32
	WT vs. tsf-1	EB14 + EB15 + EB16	55	90 s	32
FD	*WT*	EB09 + EB10	55	90 s	32
	fd-3	EB10 + B163	55	90 s	32
SOC1	*WT*	EB40 + EB41	58	1 min	35
	soc1-2	EB41 + EB42	58	1 min	35
	SOC1-GFP vs. SOC1 WT	EB40 + EB120	60	110 s	32
SPL4	*WT*	EB18 + EB20	50	30 s	30
	spl4	EB19 + EB20	50	30 s	30
MIR172A	*WT vs. mir172a-2*	oDM277 + oDM278	56	30 s	35
MIR172B	*WT vs. mir172b-3*	oDM199 + oDM200	50	1 min	35
MIR172C	*WT vs. mir172c-1*	oDM194 + oDM195	56	30 s	35
MIR172D	*WT vs. mir172d-3*	oDM247 + oDM248	56	30 s	35
MIR172E	*WT vs. mir172e-1*	oDM251 + oDM252	56	30 s	35

6.4.1 Edward's DNA extraction

DNA was extracted from one or two young leaves that had visible petioles. The tissue was ground in 1.5-mL tubes containing two tungsten beads and 390 µL extraction buffer (200 mM Tris-HCl pH 7.5–8.0 250 mM NaCl, 25 mM EDTA) using a TissueLyser II (Qiagen, the Netherlands) and performing two rounds of 1 min at 30 Hz. Subsequently, 10 µL 20% (w/v) SDS was added to the sample and after mixing, samples were centrifuged for 3 min at 14,000 rpm. he supernatant (300 µL) was transferred to a fresh 1.5-mL tube containing 300 µL isopropanol. After mixing, samples were centrifuged for 5 min at 14,000 rpm. The supernatant was removed and the samples were washed with 0.85 mL 70% (v/v) ethanol. After centrifuging for 3 min at 14,000 rpm, the supernatant was removed and the pellets were dried using a SpeedVac at 30°C for at least 30 min and were resuspended in 100 µL dH_2O.

6.4.2 Genotyping PCRs

To genotype mutant lines obtained from the Nottingham Arabidopsis Stock Centre (NASC), one PCR to detect the presence of the wild-type allele and another one for the mutant allele were performed using the oligonucleotides listed in Table 6-16. The DNA was amplified using GoTaq® polymerase (Promega, USA) by preparing the master mix as indicated in Table 6-10, and using the program from Table 6-11. The annealing temperature, elongation time and number of cycles for each reaction are listed in Table 6-9.

Table 6-10. Mix for genotyping PCR.

PCR component	Volume (µL)
5X Green GoTaq® Reaction Buffer	2.0
25 mM $MgCl_2$	1.0
10 mM dNTPs	0.4
Forward primer (10 µM)	0.4
Reverse primer (10 µM)	0.4
GoTaq® (5U μL^{-1})	0.05
dH2O	2.75
Genomic DNA	3.0

To genotype *mir172d-3*, a digestion with *Pst*I (NEB, USA) was required. The digestion was performed by mixing the 10 µL PCR product, 0.3 µL *Pst*I (NEB, USA) and 1.15 µL Buffer 3.1 (NEB, USA). The mix was incubated for 3 h at 37°C and the digestion products were visualised by electrophoresis on a 3.0% (w/v) agarose gel containing ethidium bromide.

Table 6-11. Standard genotyping PCR program.

Step	Temperature (°C)	Time
1	95	2 min
2	95	30 s
3	[Variable 1] Annealing temperature	30 s
4	72	[Variable 2] Time of elongation
[Variable 3] Number of loops to step number 2		
5	72	10 min
6	4	Hold

6.5 RNA extraction, qRT-PCR and transcriptome analyses

6.5.1 Harvesting of material

For RNA-sequencing, the shoot apices of Col-0, *mir172a-2 b-3 d-3*, *ap2-12* and *mir172a-2 b-3 d-3* and *mir172a-2 b-3 d-3 ap2-12* mutants were dissected under a stereomicroscope at 10, 12, 14 and 17 days in LD conditions and at 3, 4, 5 and 6 weeks in SD conditions. For each genotype and time point, 10 to 12 apices were harvested for each of three biological replicates.

For the qRT-PCR to validate the mutant status of the *toe3-1* allele, a total of six main and secondary inflorescences were harvested from 28-old plants grown in LDs for each of three biological replicates.

For the qRT-PCR to evaluate the expression of *TOE2::TOE2:mScarlet:2HA,* whole seedlings were grown for 4 LD on half-strength MS agar plates and were harvested as three independent biological replicates. The material was harvested directly into sterile tubes in liquid nitrogen, and was then frozen at -80°C.

6.5.2 RNA extraction

Total RNA was extracted using the RNeasy Plant Mini Kit (Qiagen, the Netherlands). Following the manufacturer's instructions (Quick-Start Protocol from March 2016), the harvested material was disrupted using a TissueLyser II (Qiagen, the Netherlands). The extracted material was eluted in 31 µL RNase-free water and the RNA concentration was measured via a NanoDrop 1000 spectrophotometer (Thermo Scientific, USA). The RNA samples were treated with TURBO™ DNase (Invitrogen) to remove contaminating DNA. Samples were diluted with RNAse-free water to a concentration lower than 200 ng μL^{-1}, then 44 µL of RNA was added to 5 µL 10× TURBO™ buffer and 1 µL of TURBO™ DNase (2U), and the mixture was incubated for 30 min at 37°C. The treated RNA was then extracted using the RNA Clean & Concentrator kit (Zymo Research, USA) according to the manufacturer's instructions. The purified RNA was eluted in 21 µL DNase/RNase-free water and the RNA concentration was measured using a NanoDrop 1000 spectrophotometer.

cDNA was synthesised using the SuperScript™ IV First-Strand cDNA Synthesis Reaction (Thermo Fisher, USA) according to the manufacturer's instructions. Following reverse transcription, 75 µL of sterile, RNA-free water was added.

Table 6-12. Master mix for qRT-PCR.

Reagent	Volume (µL)
iQ™ SYBR© Green Supermix (Bio-Rad, USA)	6.0
dH_2O	3.4
Forward primer (10 µM)	0.3
Reverse primer (10 µM)	0.3
cDNA	2.0

6.5.3 qRT-PCR

To perform RT-PCR, the master mix was prepared as shown in Table 6-12. The relative transcript abundance was determined with a Roche LightCycler© 480 system using the program in Table 6-13. At least three biological replicates were included in each experiment

and three technical replicates for each reaction were performed. All the primers used for qRT-PCR are listed in Table 6-19.

Table 6-13. PCR program for qRT-PCR.

Step	Temperature (°C)	Duration
1	95	3 min
2	95	10 s
3	60	40 s
Plate read. Then loop to step 2. 40 cycles.		
4 (Melting curve)	55 to 95	10 s/1°C.

6.5.4 qRT-PCR analysis

Normalised gene expression was calculated via the ΔΔCt method. First, the expression of the gene of interest (GOI) was normalised in each sample to the expression of the housekeeping gene *PEROXIN4 (PEX4;* AT5G25760*)* by calculating the ΔCt value according to the following formula:

$$\Delta C_t = \frac{2^{Ct(PEX4)}}{2^{Ct(GOI)}}$$

The expression of the GOI in each sample was then normalised to the expression level in Col-0 by calculating the ΔΔCt:

$$\Delta\Delta C_t = \frac{\Delta C_t}{mean(\Delta C_t(Col-0))}$$

6.5.5 Sequencing

Poly(A) RNA enrichment, library preparation, and sequencing were carried out at the MPIPZ Genome Center, Cologne, Germany using the following conditions: The RNAs were processed by poly-A enrichment followed by application of basic components of “NEBNext Ultra II Directional RNA Library Prep Kit for Illumina” with a homebrew barcoding regime. Sequencing was performed on a HiSeq3000 sequencer by sequencing-by-synthesis with 1 × 150-bp single-read length.

6.5.6 Read count and differential gene expression analysis

Sequence reads were preprocessed with CutAdapt to remove any residual adaptors, and the low-quality bases (Q<15) were trimmed from the ends with Trimmomatic (Bolger et al., 2014; Martin, 2011). Only reads with a minimum length of 50 nucleotides were kept. Salmon was used to quantify the abundance of transcripts from the *Arabidopsis* reference genome Reference Transcript Dataset for *Arabidopsis* (including guanine/cytosine bias, unstranded samples; Patro et al., 2017; R. Zhang et al., 2017). Fragments Per Kilobase of transcript per Million (FPKM) values and corrected *p*-values were obtained using DESeq2 by performing two comparisons: (1) intra-genotype and inter-time point; and (2) inter-genotype and intra-time point. The DEGs were defined via DESeq2 (i.e. adjusted *p*-value < 0.05 and absolute Log_2(Fold Change) > 1).

6.5.7 Co-expression and GO-enrichment analysis

To perform the co-expression analysis in Col-0 and *ap2-12* during the LD time course, the DEGs between Col-0 and *ap2-12* at each time point were identified and a list of genes that were DEGs at least at one time point of the analysis was obtained. The Pearson correlation between the expression of different genes [in terms of log_2(FPKM + 1)] was calculated. This dataset was processed via the “DiffCorr” package (Fukushima, 2013; Fukushima & Nishida, 2016) in R to generate a plot in which each gene (represented by a node) was linked to another gene when the correlation was greater than 0.85. The aforementioned plot was ultimately represented via the “igraph” package and the modules or clusters of co-expression were determined via the “fastgreedy.community” algorithm. The correspondence between the defined clusters in Col-0 and *ap2-12* was established via a hypogeometric test. The genes from a selected cluster from *ap2-12* were used to perform a GO analysis via the BiNGO tool from the Cytoscape platform for visualisation. The output from the GO analysis was visualised via Revigo (Supek et al., 2011).

6.6 Characterisation of plant material

6.6.1 Flowering time

For flowering-time experiments, one single plant was grown per pot. Flowering time was scored by counting the number of rosette leaves, and the number of cauline leaves on the primary inflorescence. Plant age was used to score the bolting time and days until the first open flower. Plant age was calculated from the first day on which the plants were exposed to light. Bolting time was scored as the time point at which the inflorescence had elongated 0.5 cm from the rosette. The time until the first flower open was considered to be when the petals of any of the flowers of the plant were visible. This parameter was not scored for *ap2-12* mutant plants, due to the effect of the mutation on floral development. The flowering time of the *mir172a-2 b-3 d-3* mutant under SDs was not scored after 30 days. Therefore, for the plants that did not bolt within this time, the number of rosette leaves at this time point was considered in the analysis.

6.6.2 GUS staining

For GUS staining, plants were grown on soil and were harvested directly into 90% ice-cold acetone. Samples were fixed by incubating for 1 h on ice. After rinsing with 50 mM phosphate buffer, GUS staining solution was added (Table 6-14). Following 20 min of vacuum infiltration, the samples were incubated at 37°C for 2 h. The staining reaction was stopped by rinsing three times with 50 mM phosphate buffer for 5 min. To remove chlorophyll from the samples, they were dehydrated in a series of ethanol solutions of increasing concentration [10% (v/v), 30% (v/v), 60% (v/v) and 70% (v/v)] for 30 min in each solution. Samples were stored in 70% (v/v) ethanol at 4°C until they were imaged.

6.6.3 Plant photographs

Whole plants were photographed together with their pots in front of a dark background using a Canon Eos 800 camera. Close-up images of flowers and other plant tissues were taken using a Zeiss Stemi 508 stereomicroscope equipped with a camera, or using a Keyence VHX7000 digital microscope.

Table 6-14. Components of the GUS staining solution.

Reagent	Stock solution	Volume for 25 mL
K ferrocyanide $K_4[Fe(CN)_6]\cdot 3H_2O$	200 mM	625 µL
K ferricyanide $K_3[Fe(CN)_6]$	200 mM	625 µL
X-Gluc ($C_{20}H_{26}N_2O_7ClBr \bullet H_2O$)	50 mg mL^{-1} in dimethylformamide	500 µL
Trtion X-100	10% (v/v)	250 µL
EDTA	0.5 M	500 µL
KPO_4 buffer, pH 7.0	50 mM KH_2PO_4 50 mM K_2HPO_4	to 25 mL

6.7 Microscopy and image analysis

6.7.1 Confocal imaging

Shoot apices at different developmental stages were dissected under a stereomicroscope and fixed with 4% (v/v) paraformaldehyde (PFA). The fixed samples were washed twice for 1 min in phosphate-buffered saline (PBS) and cleared with ClearSee (Kurihara et al., 2015) for 3–4 days at room temperature. Before imaging lines containing a fluorescent reporter, samples were kept in PFA for 2 h at room temperature after fixation and were then transferred to PBS for 2 days and then to ClearSee for 3–4 days. The cell wall was stained with Renaissance 2200 [0.1% (v/v) in ClearSee] (Musielak et al., 2015) for at least 1 day.

Confocal microscopy was performed with a TSC SP8 confocal microscope (Leica) for cell segmentation and SAM morphology quantification, with a LSM780 confocal laser scanning miscroscope (Zeiss) for describing protein accumulation patterns from reporters, and with a Stellaris 5 confocal microscope (Leica) for fluorescence quantification. The microscopy parameters used are listed in Table 6-15.

Table 6-15. Parameters used for confocal microscopy image acquisitions.

[a]Smart offset set between -7 and -8%. [b]Digital offset set at -9988.

Chapter	Experiment	Microscope	Channel	Excitation wavelength (nm)	Laser power (%)	Detection wavelength (nm)	Detector	Gain (V)
2	*MIR172A* expression Col-0 vs. *ft-10 tsf-1*	Leica SP8	VENUS	514	12	520–560	HyD	430
			Renaissance	405	1	435–505	PMT	Variable
	MIR172D expression Col-0 vs. *ft-10 tsf-1*	Leica SP8	VENUS	514	10	520–560	HyD	430
			Renaissance	405	1	435–505	PMT	Variable
3	MorphoGraphX and morphology analysis	Leica SP8	Renaissance[a]	405	1	435–470	PMT	Variable
	AP2-VENUS vs. rAP2-VENUS shift	Zeiss LSM 780	VENUS[b]	514	10	517–570	GaAsP	900–1000
			Renaissance	405	2	410–503	GaAsP	Variable
	AP2-VENUS / *ap2* vs. AP2-VENUS / *ap2-12 soc1-2*	Leica Stellaris 5	VENUS	515	5	520–600	SiPM	2.5
			Renaissance	405	0.1	455–463	SiPM	Variable
	SOC1-GFP/*soc1-2* vs. SOC1-GFP/*soc1-2 ap2-12*	Leica Stellaris 5	GFP	488	2	500–557	SiPM	2.5
			Renaissance	405	0.1	450–470	SiPM	Variable
4	TOE2-mScarlet-2HA time course	Leica Stellaris 5	mScarlet	569	7	584–624	SiPM	2.5
			Renaissance	405	0.1	442–454	SiPM	Variable
	Validation of TOE2-mScarlet-2HA lines and time course under LD	Zeiss LSM 780	mScarlet	568	5	584–624	GaAsP	800
			Renaissance	405	0.2	442–454	GaAsP	Variable
	SPL4-VENUS SD time course	Leica SP8	VENUS	514	4	519–535	HyD	50
			Renaissance	405	3	435–472	PMT	Variable
	SPL4-VENUS LD time course	Zeiss LSM 780	VENUS	514	3	517–570	GaAsP	786
			Renaissance	405	2	441–455	GaAsP	Variable

6.7.2 Cell segmentation and SAM morphology quantification

The Z stacks of SAMs were acquired with a step size of 0.4 µm and were converted to .tif files with Fiji. MorphoGraphX (MGX) software (https://morphographx.org/; Barbier de Reuille et al., 2015; Kierzkowski et al., 2012) was used to extract the surface of the meristem and to project the Renaissance signal of the cell wall from the outer cell layers (L1), which was used to segment the images. Cells were auto-segmented and corrected manually. The geometry of the surface was displayed as Gaussian curvatures with a neighbouring radius of 10 µm. The boundary between the meristem and the developing primordia was defined by a negative Gaussian curvature. The area of each of the cells in the SAM was extracted. The meristem area was calculated as the sum of the areas of the cells that comprised the meristem.

To quantify the morphology of the meristem, its height and width was estimated (Supplemental Figure 3-2A). For this, the orthogonal views from the Z stack were generated and were used to estimate the meristem height and the width according to the following criteria: (1) the height aligned with the apical-basal axis, (2) the width was perpendicular to the height and (3) the width was measured from the most apical forming primordium. The measurements performed on each orthogonal view were considered as technical replicates; thus, he plotted values corresponded to the means of the two estimations of each of the measured parameters. The parabolas to represent meristem morphology were plotted in an XY-coordinate system (Supplemental Figure 3-2B) using the formula in Supplemental Figure 3-2C. For representation purposes, the parabolas were coloured according to the identity of primordia that were formed at the SAM periphery (Supplemental Figure 3-2E–G).

To confirm the accuracy of the calculated parabolas against the original shape of the meristem, several points were defined using Fiji in the orthogonal views (i.e. the limits of each cell in the L1 were marked). The XY coordinates were exported for further processing using R. The points were rotated several times at a constant angle (0.01 rad) using the origin of coordinates as the rotation axis. Curvature fitting was performed for each of the rotated coordinates and the curvature with the highest R^2 was selected. The parabola was cut at the most apical

primordium. From each curve, height and width were inferred (i.e. height was y of the maximum of the parabola, width was the distance between the two points in which x = 0). Then, the mean of measurements from different orthogonal views but corresponding to the same sample was obtained for each of these parameters. The final parabola was obtained using the formula in the previous paragraph and the estimated height and width (Supplemental Figure 3-3B–C).

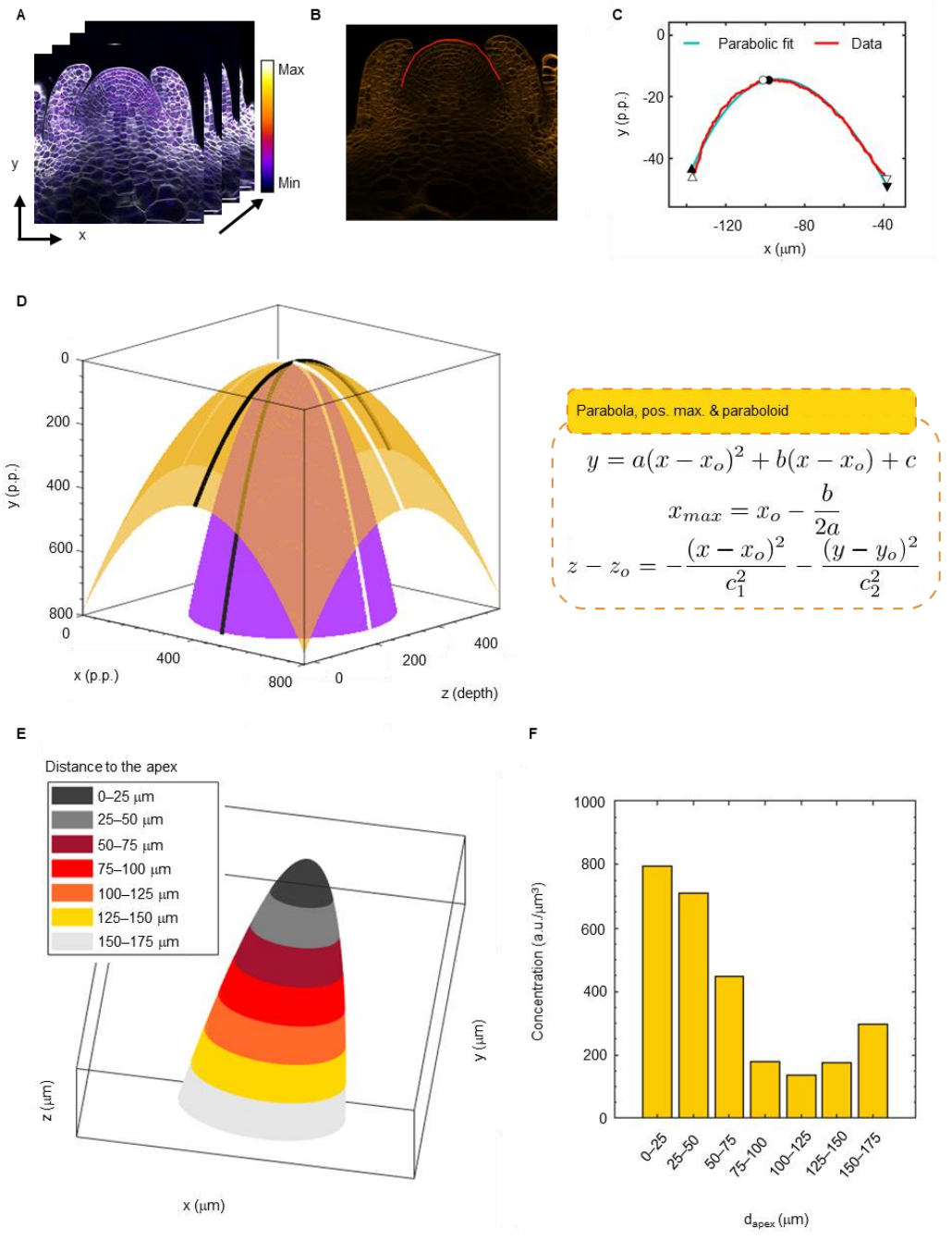

Figure 6-2. Fluorescence quantification explanation pipeline.

(See description in the next page)

(A) SAM fluorescence confocal microscopy images were obtained from the lateral side. In the image: slices from z-stack meristem from a 12-days-old plant grown under LDs containing the *AP2::AP2:VENUS* reporter. In white membrane marker channel and in in fire-color look up table (Fiji) AP2-VENUS fluorescence signal. Scale bar = 20 μm. The acquisition parameters are described in Materials and Methods. (B) A curved line (in red) is marked out above meristem outline until the beginning of the primordia on the sum of slice projection of certain z-stack slice interval. (C) Parabolic fitting of the previous parabola. Triangles mark the beginning and end points of the drawn curve line (black) and fitted parabola (white). Circles represent the apex position for drawn curve line (black) and fitted parabola (white). (D) 3D paraboloid masks built from the previously extracted orthogonal parabolas. In orange, paraboloid using original curvature values. In purple, paraboloid with higher curvature to exclude from the quantification the fluorescence signal in new emerging primordia boundaries. On the right, main set of equations describing the 2D parabola in the xy-plane, its maximum position and the 3D paraboloid. The 2D equation of the parabola in the zy plane is omitted for simplicity. When applied to the corresponding z-stack slice, pixels whose positions lie outside the paraboloid will have their intensity values are set to zero. (E) 3D paraboloid sections of 25 μm length, with the SAM apex coordinates as the origin, in which the 3D paraboloid is subdivided for intensity quantification. (F) Signal concentration (a.u./μm^3) by 3D paraboloid subsection as a function of the distance to the apex (in μm). The concentration is defined as the quotient between the total intensity in a given region and the total volume of voxels included in the subsection. Figure generated by Gabriel Rodríguez Maroto.

6.7.3 Fluorescence quantification

Confocal fluorescence z-stacks were processed and analysed using a Matlab custom made code (https://gitlab.com/slcu/teamHJ/pau/RegionsAnalysis). Due to the difference in the resolution between the xy plane and the *z*-direction (depth), the z-stack was resized by increasing the number of slices in the z-direction through bicubic interpolation to obtain a homogeneous volumetric resolution. Fluorescence signal was also detected in SAM biological boundaries. To exclude fluorescence signals outside the region of interest and quantify only the fluorescence intensity within the meristematic region, a pre-processing step was performed: a 3D paraboloid mask was constructed using the curvature of the meristem (Figure 6-2).

First, a stack-slice interval that contained the apex of the meristem was selected and the cell wall signal present within this interval was projected in each orthogonal plane (xy and yz) (Figure 6-2A). Then, two curved lines following the parabolic outline of the SAM were drawn in the xy and yz planes, in the sum of slice projection of each plane (Figure 6-2B). Later, a parabolic fitting of the two drawn lines was performed (Figure 6-2C). For this fitting, tilting of the drawn curve lines was considered. From the two orthogonal parabolas fitted per each z-stack, the apex was computed to derive the equation for the 3D paraboloid. The z_o coordinate of the paraboloid was determined from averaging the apices of the orthogonal parabolas (Figure 6-2D). Finally, the parameter *a* in the parabola equation, i.e the curvature, was used to substitute the denominator terms in the paraboloid equation (c_1^2 and c_2^2; Figure 6-2D) so

the paraboloid equation matched the linear and quadratic terms of each of the equations at $y=y_o$ and $x=x_o$ respectively (Figure 6-2D). Since the z-stack did not always include the beginning and end of the meristem in the yz plane (lateral view), only xy curvature was used ($c_2^2 = c_1^2$). To discretize the 3D paraboloid, a 2D parabolic mask was created for each of the z-stack slices. In each slice of the z-stack, all intensity values of the pixels outside the paraboloid were set to 0 (Figure 6-2D–E). To quantify the signal, the 3D paraboloid was divided into consecutive paraboloid sections of 25 μm width (Figure 6-2E). Signal concentration in each of the 3D paraboloid subsections was extracted computing the quotient between the total intensity and the total volume of the voxels in that subsection. For representation purposes, the calculated concentration was divided by 1000.

The signal that appeared at boundary regions of new primordia was not considered in the quantification, as this led to biases in the quantification. To exclude the fluorescence signal at the boundaries, the paraboloid curvature was increased respect to the original (Figure 6-2D) by not undoing the conversion back from μm to pixel values of this parameter (i.e $a_{pix} = a_{mic}$ in the increased-curvature paraboloid and $a_{pix} = \alpha \cdot a_{mic}$ in the original paraboloid; a_{pix} and a_{mic} are the curvatures in μm and pixels, respectively; $\alpha<1$ is the image resolution; Figure 6-2D).

Table 6-16. Primers used for genotyping.

Short name	Sequence (5′–3′)	Origin
EB01	AATCATCCACGACGAAATTGATGTCTG	Mathieu et al., 2009
EB02	TTTGATTTGTAGATCTTCTCTGACAAC	Mathieu et al., 2009
EB03	CTGCGTAAGCAGTATCAAACCCGCCTG	Mathieu et al., 2009
EB04	TGGTCCGGTTTCAATAGTGTC	Yant et al., 2010
EB05	TTTGTCAAATTTCCCATCTGC	Yant et al., 2010
EB06	GGTGCAGCAAAACCCACACTTTTACTTC	Mathieu et al., 2009
EB07	CCTGAGCCGCATATCTTGAC	Mathieu et al., 2009
EB08	CCAAGGAAGAGTTCGTACACG	Mathieu et al., 2009
EB09	GGTTTTGGTTGTGGTGGTTT	Maida Romera-Branchat
EB10	TCCAGAAATGACCGGCTAAAGTC	Seonghoe Jang
EB11	CCCATTTGACGTGAATGTAGACAC	Ryosuke Hayama
EB12	TAAGCTCAATGATATTCCCGTACA	Fernando Andrés Lalaguna
EB13	CAGGTTCAAAACAAGCCAAGA	Fernando Andrés Lalaguna

EB14	CTGGCAGTTGAAGTAAGAG	Seonghoe Jang
EB15	CACGAGGTTGGTCTCTCTTAAG	Seonghoe Jang
EB18	AAGTCTTACCTTGTGGAAGAA	Youbong Hyun
EB19	AAAGAAGTCTTACCTTGTGAT	Youbong Hyun
EB20	GCAACTTCTCTTAGCTTCATC	Youbong Hyun
EB40	TCTAAGTGATGATTAGGAAGTTGTTTC	Vítor da Silveira Falavigna
EB41	ATATCACAAACCGTTTAGAAGCTTC	Immink et al., 2012
EB42	GTTCACGTAGTGGGCCATC	Immink et al., 2012
EB120	TGACTGAGAGAGAGAGAGTGAGAG	Vítor da Silveira Falavigna
EB140	AGTGGGGGCATATAGGTACGA	This study
EB141	TGTAACCGATGGAGGGAAAAAGA	This study
B161	TCCCCTCCACATACAAAAGTG	Annabel van Driel
B162	AAATATGAGATTCCCAACGGC	Annabel van Driel
B164	GAAGAGTTTGTGCATATACTGCG	Annabel van Driel
B165	GAAGGGAAGTGAAAGAGCCTC	Annabel van Driel
B166	TCCCAGCAGAAATCAGTTCAC	Annabel van Driel
B167	AGTTGTGCTCTACACGAACGG	Annabel van Driel
B163	ATTTTGCCGATTTCGGAAC	Annabel van Driel
oDM277	TCGACTATTCCGCCATGTTTG	Ó'Maoiléidigh et al., 2021
oDM278	ACCTACCTGAAGAAGATCTGGATG	Ó'Maoiléidigh et al., 2021
oDM199	TCAGCCCTTGGATTCGTGAGG	Ó'Maoiléidigh et al., 2021
oDM200	TAACGCCCTAATCCGTCATTGACC	Ó'Maoiléidigh et al., 2021
oDM194	TGACCTGAGTATCTGAGATCTCAG	Ó'Maoiléidigh et al., 2021
oDM195	CCTCCGATCTGTGAATTCCTAC	Ó'Maoiléidigh et al., 2021
oDM247	CTTCACCCTAAATCTCTTCCTCTCCTTCAG	Ó'Maoiléidigh et al., 2021
oDM248	CACCTCAAGTTATCATATCGGAGG	Ó'Maoiléidigh et al., 2021
oDM251	GTCTGAATCCTCTTGCTTTCCTCTTTGC	Ó'Maoiléidigh et al., 2021
oDM252	TCACAGCATGTGCATGATCAAG	Ó'Maoiléidigh et al., 2021

Table 6-17. Primers used for colony PCR.

Short name	Sequence (5′–3′)	Vector/Sequence to detect	Origin
EB76	TCGCGTTAACGCTAGCATGGATCTC	pDONR201	Serena della Pina
EB77	TGTAACATCAGAGATTTTGAGACAC	pDONR201	Serena della Pina
EB102	GTGTCTAAGGGTGAAGCCGT	mScarlet	This study
EB103	CTTGTAGAGTTCGTCCATAC	mScarlet	This study
EB117	TGCGATCTTGTACTTGAGTCTGT	pFAST-R1	This study
EB118	GGGTCATAACGTGACTCCCT	pFAST-R1	This study

Table 6-18. Primers used for primer walking.

All the listed oligonucleotides are forward primers, except for EB112, which is expected to bind to the region downstream of the stop codon.

Short name	Sequence (5′–3′)	Gene/sequence	Origing
EB80	GCAAGTGACAAGATCAAATCCA	*TOE2*	This study
EB81	TCCGAAGACAAAACAAACCAAA	*TOE2*	This study
EB82	TGCAAGGATAGGACAGCAGG	*TOE2*	This study
EB83	TTTTCGCCCGTAACCTGTGT	*TOE2*	This study
EB84	TGTAGGAACTAGGAAACACATGCT	*TOE2*	This study
EB85	AGCTAGCTTCTACACCTTTTTCT	*TOE2*	This study
EB86	AGAAATCACAGAAAAGCTTAACACA	*TOE2*	This study
EB87	GCTGGATCTCAATCTCGACG	*TOE2*	This study
EB88	GCAGGGATTGCGGTAAACAA	*TOE2*	This study
EB89	TCCTGGGATCTAAGTATGGGCT	*TOE2*	This study
EB90	CGGCTTCACCATGTCCCTAA	*TOE2*	This study
EB91	ACAGGTCTATGTTGTTGCTTGT	*TOE2*	This study
EB92	AGGAAGAGTTCCAAGTTGTGT	*TOE2*	This study
EB104	GAGAGATCTGAGGGTCGTCA	*mScarlet*	Yohanna Miotto
EB105	GATCACGGCTTCACCCTTAG	*mScarlet*	Yohanna Miotto
EB112	GTTGTTTCCAAGAAAGTCTT	*TOE2*	This study

Table 6-19. Primers used for qRT-PCR.

Short name	Sequence (5′–3′)	Gene	Origin
EB60	TTACGAAGGCGGTGTTTTTC	*PEX4*	Annabel van Driel
EB61	GGCGAGGCGTGTATACATTT	*PEX4*	Annabel van Driel
EB155	CATCATCCTTCTCAGCCCTTC	*TOE2*	B. Zhang et al., 2015
EB156	GCCTTCCAACTTATTCCAACC	*TOE2*	B. Zhang et al., 2015
B251	CCTCGCTCACGTAGCTCTCAGTATC	*TOE3*	Annabel van Driel
B252	CGAGCAGCAGCATGTGCAGT	*TOE3*	Annabel van Driel

Table 6-20. Primers used for molecular cloning.

Short name	Sequence (5′–3′)	Use	Origin
EB43	ATGCCAAGTTTGTACAAAAAAGCAGGCT TCTCGCACCTTGCTCAGTTAAGGA	Linearisation of *TOE2g* to be inserted in pDONR201 via PIPE cloning.	This study
EB44	GCCCACTTTGTACAAGAAAGCTGGGTC CTTGGTGTATTGAATTAATGTAAGAGTTT TTAATTTCTAAAACTTAT	Linearisation of *TOE2g* to be inserted in pDONR201 via PIPE cloning.	This study
EB47	TAGGACCCAGCTTTCTTGTACAAAGTGG	Linearisation of PDONR201 (PIPE cloning)	Fernando Andrés Lalaguna
EB48	GAAGCCTGCTTTTTTGTACAAACTTGGC	Linearisation of PDONR201 (PIPE cloning)	Fernando Andrés Lalaguna
EB67	AGATAAAATCGCACCTTGCTCAGT	Amplification of *TOE2g*	This study
EB68	CGGTTTTGCCTGTTTCCGGTTT	Amplification of *TOE2g*	This study
EB69	AAACCGGAAACAGGCAAAACCG	Amplification of *TOE2g*	This study
EB70	TGAGAATCCTGATGATGCTGCATTTG	Amplification of *TOE2g*	This study
EB71	CAAATGCAGCATCATCAGGATTCTCA	Amplification of *TOE2g*	This study
EB72	GGAGTTAAATCAAGATTATTGTGGTGT	Amplification of *TOE2g*	This study
EB98	CCTCCAGAACCACCTCCACCTGGTGGT GGTTGTGGGCGGT	Linearisation of *mScarlet*	This study
EB99	ATGTTCCTGATTATGCTTGATAGCTTCC TCCTTCCTCCGC	Linearisation of *mScarlet*	This study
EB100	ACCGCCCACAACCACCACCAGGTGGAG GTGGTTCTGGAGG	Linearisation of pDONR with *TOE2*	This study
EB101	GCGGAGGAAGGAGGAAGCTATCAAGCA TAATCAGGAACAT	Linearisation of pDONR with *TOE2*	This study
EB115	AACGCGGCGTCGTCGGGCTTGTCACTC TCAGCTACACGCCC	Generation of *rTOE2*	This study
EB143	CAAGCCCGACGACGCCGCGTTTGAAAA CAGTGGCGGTGCT	Generation of *rTOE2*	This study

7 List of abbreviations

Abbreviation	Definition
5' RACE	5' Rapid Amplification of cDNA Ends
9A	9 Alanin
AG	*AGAMOUS*
AGO	*ARGONAUTE*
AN3	*ANGUSTIFOLIA3*
ANOVA	Analysis of the variance
ANT	*AINTEGUMENTA*
AP1	*APETALA1*
AP2	*APETALA2*
AP2-LIKE	*APETALA2-LIKE*
ARF3	*AUXIN RESPONE TRANSCRIPTION FACTOR 3*
bZIP	basic leucine zipper
Cas9	CRISPR associated protein 9
CDF1	*CYCLING DOF FACTOR 1*
CKX3	*CYTOKININ OXIDASE 3*
CKX5	*CYTOKININ OXIDASE 5*
CLV1	*CLAVATA1*
CLV3	*CLAVATA3*
Cly1	*Cleistogamy 1*
CO	*CONSTANS*
CRISPR	Clustered regularly interspaced short palindromic repeats
CRY1	*CRYPTOCHROME1*
CRY2	*CRYPTOCHROME2*
CYP735A	Cytochrome P450 monooxygenase
CYP735A1	*CYTOCHROME P450 FAMILY 735 SUBUNIT A1*
CYP735A2	*CYTOCHROME P450 FAMILY 735 SUBUNIT A2*
CZ	Central zone

DCL	*DICER-LIKE*
DEG	Differentially expressed gene
dSpm	defective Suppressor-Mutator
EAT	*EARLY ACTIVATION TAGGED*
eat-D	*early activation tagged - Dominant*
FD	Transcription factor FD
FKF1	*FLAVIN-BINDING, KELCH REPEAT, F-BOX 1*
FLC	*FLOWERING LOCUS C*
FPKM	Fragments per Kilobase of transcript per Million
FT	*FLOWERING LOCUS T*
FUL	*FRUTIFULL*
GFP	Green Fluorescent Protein
GI	*GIGANTEA*
gl15	*Glossy15*
GO	Gene ontology
GUS	β-Glucuronidase
HB29 / ZHDF11	*HOMEOBOX29 / ZINC FINGER HOMEODOMAIN 11*
HEN1	*HUA ENHANCER 1*
ids1	*indeterminate spikelet 1*
LB	Lysogeny Broth
LD	Long Days
LFY	*LEAFY*
miR156	microRNA156
MIR172	*MICRORNA172*
miR172	microRNA172
miRNA	microRNA
NVG	Nuclear localisation signal - VENUS - GUS
PBS	Phospate-buffered saline
PCR	Polymerase Chain Reaction
PEBP	Phosphatidylethanolamine-binding protein

PEX4	*PEROXIN4*
PFA	Paraformaldehyde
PhyA	PhytocromeA
PhyB	PhytocromeB
PIPE	Polymerase Incomplete Primer Extension
piRNA	PIWI-interacting RNA
PPT	Phosphinotricin
PZ	peripheral zone
qRT-PCR	quantative Real time PCR
RAM	Root Apical Meristem
rAP2	miR172-resistant APETALA2
RFP	Red fluorescent protein
RNA-Seq	RNA-Sequencing
rTOE2	miR172-resistant TARGET OF EAT 2
SAM	Shoot Apical Meristem
SD	Short Days
sid1	*sister of ids1*
siRNA	small interference RNA
SMZ	*SCHLAFMÜTZE*
SNZ	*SCHNARCHZAPFEN*
SOC1	*SUPPRESSOR OF OVEREXPRESSION OF CONSTANS 1*
SPL	*SQUAMOSA PROMOTER-BINDING PROTEIN-LIKE*
STM	*SHOOTMERISTEMLESS*
SUC2	*SUCROSE-PROTON SYMPORTER 2*
SVP	*SHORT VEGETATIVE PHASE*
TCP1	*TB1, CYC, PCF (TCP) DOMAIN PROTEIN 1*
TFL1	*TERMINAL FLOWER 1*
TOE1	*TARGET OF EAT 1*
toe1-D	*target of eat 1 - Dominant*
TOE2	*TARGET OF EAT 2*

TOE3	*TARGET OF EAT 3*
ts4	*tasselseed4*
TSF	*TWIN SISTER OF FT*
UTR	Untranslated region
wSD	weeks under Short Days
WUS	*WUSCHEL*

8 List of materials

8.1 List of figures

8.2 List of tables

8.3 List of supplemental figures

8.4 List of supplemental tables

8.5 List of appendix figures

9 References

Abe, M., Kobayashi, Y., Yamamoto, S., Daimon, Y., Yamaguchi, A., Ikeda, Y., Ichinoki, H., Notaguchi, M., Goto, K., & Araki, T. (2005). FD, a bZIP protein mediating signals from the floral pathway integrator FT at the shoot apex. *Science*. https://doi.org/10.1126/science.1115983

Abe, M., Kosaka, S., Shibuta, M., Nagata, K., Uemura, T., Nakano, A., & Kaya, H. (2019). Transient activity of the florigen complex during the floral transition in arabidopsis thaliana. *Development (Cambridge)*. https://doi.org/10.1242/dev.171504

An, H., Roussot, C., Suárez-López, P., Corbesier, L., Vincent, C., Piñeiro, M., Hepworth, S., Mouradov, A., Justin, S., Turnbull, C., & Coupland, G. (2004). CONSTANS acts in the phloem to regulate a systemic signal that induces photoperiodic flowering of Arabidopsis. *Development*. https://doi.org/10.1242/dev.01231

Andrés, F., & Coupland, G. (2012). The genetic basis of flowering responses to seasonal cues. *Nature Reviews Genetics*, *13*(9), 627–639. https://doi.org/10.1038/nrg3291

Aukerman, M. J., & Sakai, H. (2003). Regulation of Flowering Time and Floral Organ Identity by a MicroRNA and Its APETALA2-Like Target Genes. *Plant Cell*. https://doi.org/10.1105/tpc.016238

Axtell, M. J., & Bartel, D. P. (2005). Antiquity of microRNAs and their targets in land plants. *Plant Cell*. https://doi.org/10.1105/tpc.105.032185

Azpeitia, E., Tichtinsky, G., Le Masson, M., Serrano-Mislata, A., Lucas, J., Gregis, V., Gimenez, C., Prunet, N., Farcot, E., Kater, M. M., Bradley, D., Madueño, F., Godin, C., & Parcy, F. (2021). Cauliflower fractal forms arise from perturbations of floral gene networks. *Science*. https://doi.org/10.1126/science.abg5999

Balanzà, V., Martínez-Fernández, I., Sato, S., Yanofsky, M. F., Kaufmann, K., Angenent, G. C., Bemer, M., & Ferrándiz, C. (2018). Genetic control of meristem arrest and life span in Arabidopsis by a FRUITFULL-APETALA2 pathway. *Nature Communications*, *9*(1). https://doi.org/10.1038/s41467-018-03067-5

Barbier de Reuille, P., Routier-Kierzkowska, A. L., Kierzkowski, D., Bassel, G. W., Schüpbach, T., Tauriello, G., Bajpai, N., Strauss, S., Weber, A., Kiss, A., Burian, A., Hofhuis, H., Sapala, A., Lipowczan, M., Heimlicher, M. B., Robinson, S., Bayer, E. M., Basler, K., Koumoutsakos, P., … Smith, R. S. (2015). MorphoGraphX: A platform for quantifying morphogenesis in 4D. *ELife*, *4*(MAY), 1–20. https://doi.org/10.7554/eLife.05864

Barton, M. K., & Poethig, R. S. (1993). Formation of the shoot apical meristem in Arabidopsis thaliana: An analysis of development in the wild type and in the shoot meristemless mutant. *Development*. https://doi.org/10.1242/dev.119.3.823

Bartrina, I., Otto, E., Strnad, M., Werner, T., & Schmülling, T. (2011). Cytokinin regulates the activity of reproductive meristems, flower organ size, ovule formation, and thus seed yield in Arabidopsis thaliana. *Plant Cell*. https://doi.org/10.1105/tpc.110.079079

Bernier, G. (1988). The Control of Floral Evocation and Morphogenesis. *Annual Review of Plant Physiology and Plant Molecular Biology*. https://doi.org/10.1146/annurev.pp.39.060188.001135

Blázquez, M. A., & Weigel, D. (1999). Independent regulation of flowering by phytochrome B and gibberellins in Arabidopsis. *Plant Physiology*. https://doi.org/10.1104/pp.120.4.1025

Bolger, A. M., Lohse, M., & Usadel, B. (2014). Trimmomatic: A flexible trimmer for Illumina sequence data. *Bioinformatics*. https://doi.org/10.1093/bioinformatics/btu170

Bommert, P., Nagasawa, N. S., & Jackson, D. (2013). Quantitative variation in maize kernel row number is controlled by the FASCIATED EAR2 locus. *Nature Genetics*, *45*(3), 334–337. https://doi.org/10.1038/ng.2534

Borner, R., Kampmann, G., Chandler, J., Gleißner, R., Wisman, E., Apel, K., & Melzer, S. (2000). A MADS domain gene involved in the transition to flowering in Arabidopsis. *Plant Journal*, *24*(5), 591–599. https://doi.org/10.1046/j.1365-313X.2000.00906.x

Bowman, J. L., Smyth, D. R., & Meyerowitz, E. M. (1989). Genes directing flower development in Arabidopsis. *The Plant Cell*. https://doi.org/10.1105/tpc.1.1.37

Brand, U., Fletcher, J. C., Hobe, M., Meyerowitz, E. M., & Simon, R. (2000). Dependence of stem cell fate in Arabidopsis on a feedback loop regulated by CLV3 activity. *Science*. https://doi.org/10.1126/science.289.5479.617

Briscoe, J., Pierani, A., Jessell, T. M., & Ericson, J. (2000). A homeodomain protein code specifies progenitor cell identity and neuronal fate in the ventral neural tube. *Cell*. https://doi.org/10.1016/S0092-8674(00)80853-3

Briscoe, J., & Small, S. (2015). Morphogen rules: Design principles of gradient-mediated embryo patterning. In *Development (Cambridge)*. https://doi.org/10.1242/dev.129452

Chen, X. (2004). A MicroRNA as a Translational Repressor of APETALA2 in Arabidopsis Flower Development. *Science*. https://doi.org/10.1126/science.1088060

Chickarmane, V. S., Gordon, S. P., Tarr, P. T., Heisler, M. G., & Meyerowitz, E. M. (2012). Cytokinin signaling as a positional cue for patterning the apical-basal axis of the growing Arabidopsis shoot meristem. *Proceedings of the National Academy of Sciences of the United States of America*. https://doi.org/10.1073/pnas.1200636109

Chuck, G., Meeley, R., & Hake, S. (2008). Floral meristem initiation and meristem cell fate are regulated by the maize AP2 genes ids1 and sid1. *Development*. https://doi.org/10.1242/dev.024273

Chuck, G., Meeley, R., Irish, E., Sakai, H., & Hake, S. (2007). The maize tasselseed4 microRNA controls sex determination and meristem cell fate by targeting Tasselseed6/indeterminate spikelet1. *Nature Genetics*. https://doi.org/10.1038/ng.2007.20

Clark, S. E., Running, M. P., & Meyerowitz, E. M. (1993). CLAVATA1, a regulator of meristem and flower development in Arabidopsis. *Development*. https://doi.org/10.1242/dev.119.2.397

Clark, S. E., Running, M. P., & Meyerowitz, E. M. (1995). CLAVATA3 is a specific regulator of shoot and floral meristem development affecting the same processes as CLAVATA1. *Development*. https://doi.org/10.1242/dev.121.7.2057

Clark, Steven E., Williams, R. W., & Meyerowitz, E. M. (1997). The CLAVATA1 gene encodes a putative receptor kinase that controls shoot and floral meristem size in arabidopsis. *Cell*. https://doi.org/10.1016/S0092-8674(00)80239-1

Clyde, D. E., Corado, M. S. G., Wu, X., Paré, A., Papatsenko, D., & Small, S. (2003). A self-organizing system of repressor gradients establishes segmental oomplexity in Drosophila. *Nature*. https://doi.org/10.1038/nature02189

Corbesier, L., Vincent, C., Jang, S., Fornara, F., Fan, Q., Searle, I., Giakountis, A., Farrona, S., Gissot, L., Turnbull, C., & Coupland, G. (2007). FT protein movement contributes to long-distance signaling in floral induction of Arabidopsis. *Science*. https://doi.org/10.1126/science.1141752

D'Ario, M., & Sablowski, R. (2019). Cell Size Control in Plants. In *Annual Review of Genetics*.

https://doi.org/10.1146/annurev-genet-112618-043602

Díaz-Manzano, F. E., Cabrera, J., Ripoll, J. J., del Olmo, I., Andrés, M. F., Silva, A. C., Barcala, M., Sánchez, M., Ruíz-Ferrer, V., de Almeida-Engler, J., Yanofsky, M. F., Piñeiro, M., Jarillo, J. A., Fenoll, C., & Escobar, C. (2018). A role for the gene regulatory module microRNA172/TARGET OF EARLY ACTIVATION TAGGED 1/FLOWERING LOCUS T (miRNA172/TOE1/FT) in the feeding sites induced by Meloidogyne javanica in Arabidopsis thaliana. *New Phytologist*. https://doi.org/10.1111/nph.14839

Du, S. S., Li, L., Li, L., Wei, X., Xu, F., Xu, P., Wang, W., Xu, P., Cao, X., Miao, L., Guo, T., Wang, S., Mao, Z., & Yang, H. Q. (2020). Photoexcited cryptochrome2 interacts directly with toe1 and toe2 in flowering regulation. *Plant Physiology*. https://doi.org/10.1104/PP.20.00486

Edwards, K., Johnstone, C., & Thompson, C. (1991). A simple and rapid method for the preparation of plant genomic DNA for PCR analysis. In *Nucleic Acids Research*. https://doi.org/10.1093/nar/19.6.1349

Elfving, N., Davoine, C., Benlloch, R., Blomberg, J., Brännström, K., Müller, D., Nilsson, A., Ulfstedt, M., Ronne, H., Wingsle, G., Nilsson, O., & Björklund, S. (2011). The Arabidopsis thaliana Med25 mediator subunit integrates environmental cues to control plant development. *Proceedings of the National Academy of Sciences of the United States of America*. https://doi.org/10.1073/pnas.1002981108

Erickson, R. O., & Meicenheimer, R. D. (1977). Photoperiod Induced Change in Phyllotaxis in Xanthium. *American Journal of Botany*. https://doi.org/10.2307/2442253

Fletcher, J. C. (1999). Signaling of cell fate decisions by CLAVATA3 in Arabidopsis shoot meristems. *Science*. https://doi.org/10.1126/science.283.5409.1911

Fornara, F., de Montaigu, A., & Coupland, G. (2010). SnapShot: Control of flowering in arabidopsis. In *Cell*. https://doi.org/10.1016/j.cell.2010.04.024

Fowler, S., Lee, K., Onouchi, H., Samach, A., Richardson, K., Morris, B., Coupland, G., & Putterill, J. (1999). GIGANTEA: A circadian clock-controlled gene that regulates photoperiodic flowering in Arabidopsis and encodes a protein with several possible membrane-spanning domains. *EMBO Journal*. https://doi.org/10.1093/emboj/18.17.4679

Fuchs, M., & Lohmann, J. U. (2020). Aiming for the top: non-cell autonomous control of shoot stem cells in Arabidopsis. *Journal of Plant Research*. https://doi.org/10.1007/s10265-020-01174-3

Fujiwara, M., Goh, T., Tsugawa, S., Nakajima, K., Fukaki, H., & Fujimoto, K. (2021). Tissue growth constrains root organ outlines into an isometrically scalable shape. *Development (Cambridge)*. https://doi.org/10.1242/dev.196253

Fukushima, A. (2013). DiffCorr: An R package to analyze and visualize differential correlations in biological networks. *Gene*. https://doi.org/10.1016/j.gene.2012.11.028

Fukushima, A., & Nishida, K. (2016). Using the DiffCorr Package to Analyze and Visualize Differential Correlations in Biological Networks. In *Computational Network Analysis with R: Applications in Biology, Medicine and Chemistry*. https://doi.org/10.1002/9783527694365.ch1

Gao, J., Zhang, K., Cheng, Y. J., Yu, S., Shang, G. D., Wang, F. X., Wu, L. Y., Xu, Z. G., Mai, Y. X., Zhao, X. Y., Zhai, D., Lian, H., & Wang, J. W. (2022). A robust mechanism for resetting juvenility during each generation in Arabidopsis. *Nature Plants*. https://doi.org/10.1038/s41477-022-01110-4

Gao, Y., Zhang, D., & Li, J. (2015). TCP1 Modulates DWF4 Expression via Directly Interacting with the GGNCCC Motifs in the Promoter Region of DWF4 in Arabidopsis thaliana.

Journal of Genetics and Genomics. https://doi.org/10.1016/j.jgg.2015.04.009

Greb, T., & Lohmann, J. U. (2016). Plant Stem Cells. In *Current Biology*. https://doi.org/10.1016/j.cub.2016.07.070

Gruel, J., Landrein, B., Tarr, P., Schuster, C., Refahi, Y., Sampathkumar, A., Hamant, O., Meyerowitz, E. M., & Jönsson, H. (2016). An epidermis-driven mechanism positions and scales stem cell niches in plants. *Science Advances*. https://doi.org/10.1126/sciadv.1500989

Hake, S. (1996). Shootmeristemless ties the knot. *Trends in Plant Science*. https://doi.org/10.1016/s1360-1385(96)80036-7

Hempel, F. D., & Feldman, L. J. (1994). Bi-directional inflorescence development in Arabidopsis thaliana: Acropetal initiation of flowers and basipetal initiation of paraclades. *Planta*. https://doi.org/10.1007/BF01089045

Heo, J. B., & Sung, S. (2011). Vernalization-mediated epigenetic silencing by a long intronic noncoding RNA. *Science*. https://doi.org/10.1126/science.1197349

Horiguchi, G., Kim, G. T., & Tsukaya, H. (2005). The transcription factor AtGRF5 and the transcription coactivator AN3 regulate cell proliferation in leaf primordia of Arabidopsis thaliana. *Plant Journal*. https://doi.org/10.1111/j.1365-313X.2005.02429.x

Huang, Z., Shi, T., Zheng, B., Yumul, R. E., Liu, X., You, C., Gao, Z., Xiao, L., & Chen, X. (2017). APETALA2 antagonizes the transcriptional activity of AGAMOUS in regulating floral stem cells in Arabidopsis thaliana. *New Phytologist*. https://doi.org/10.1111/nph.14151

Hyun, Y., Richter, R., Vincent, C., Martinez-Gallegos, R., Porri, A., & Coupland, G. (2016). Multi-layered Regulation of SPL15 and Cooperation with SOC1 Integrate Endogenous Flowering Pathways at the Arabidopsis Shoot Meristem. *Developmental Cell*, *37*(3), 254–266. https://doi.org/10.1016/j.devcel.2016.04.001

Immink, R. G. H., Posé, D., Ferrario, S., Ott, F., Kaufmann, K., Valentim, F. L., de Folter, S., van der Wal, F., van Dijk, A. D. J., Schmid, M., & Angenent, G. C. (2012). Characterization of SOC1's central role in flowering by the identification of its upstream and downstream regulators. *Plant Physiology*. https://doi.org/10.1104/pp.112.202614

Iwasaki, Y. W., Siomi, M. C., & Siomi, H. (2015). PIWI-interacting RNA: Its biogenesis and functions. *Annual Review of Biochemistry*. https://doi.org/10.1146/annurev-biochem-060614-034258

J. L. Bowman, J. Alvarez, D. Weigel, E. M. Meyerowitz, & D. R. Smyth. (1993). Control of flower development in Arabidopsis thaliana by APETALA1 and interacting genes. *Development*, *119*, 721–743.

Jacqmard, A., Gadisseur, I., & Bernier, G. (2003). Cell division and morphological changes in the shoot apex of Arabidopsis thaliana during floral transition. *Annals of Botany*, *91*(5), 571–576. https://doi.org/10.1093/aob/mcg053

Jang, S., Torti, S., & Coupland, G. (2009). Genetic and spatial interactions between FT, TSF and SVP during the early stages of floral induction in Arabidopsis. *Plant Journal*. https://doi.org/10.1111/j.1365-313X.2009.03986.x

Jeong, H. L., Seong, J. Y., Soo, H. P., Hwang, I., Jong, S. L., & Ji, H. A. (2007). Role of SVP in the control of flowering time by ambient temperature in Arabidopsis. *Genes and Development*. https://doi.org/10.1101/gad.1518407

Jofuku, K. D., Den Boer, B. G. W., Van Montagu, M., & Okamuro, J. K. (1994). Control of arabidopsis flower and seed development by the homeotic gene APETALA2. *Plant Cell*.

https://doi.org/10.2307/3869820

Jones-Rhoades, M. W., Bartel, D. P., & Bartel, B. (2006). MicroRNAs and their regulatory roles in plants. In *Annual Review of Plant Biology*. https://doi.org/10.1146/annurev.arplant.57.032905.105218

Jones, A. R., Forero-Vargas, M., Withers, S. P., Smith, R. S., Traas, J., Dewitte, W., & Murray, J. A. H. (2017). Cell-size dependent progression of the cell cycle creates homeostasis and flexibility of plant cell size. *Nature Communications*. https://doi.org/10.1038/ncomms15060

Jung, J. H., Ju, Y., Seo, P. J., Lee, J. H., & Park, C. M. (2012). The SOC1-SPL module integrates photoperiod and gibberellic acid signals to control flowering time in Arabidopsis. *Plant Journal*. https://doi.org/10.1111/j.1365-313X.2011.04813.x

Jung, J. H., Lee, H. J., Ryu, J. Y., & Park, C. M. (2016). SPL3/4/5 Integrate Developmental Aging and Photoperiodic Signals into the FT-FD Module in Arabidopsis Flowering. *Molecular Plant*. https://doi.org/10.1016/j.molp.2016.10.014

Jung, J. H., Lee, S., Yun, J., Lee, M., & Park, C. M. (2014). The miR172 target TOE3 represses AGAMOUS expression during Arabidopsis floral patterning. *Plant Science*. https://doi.org/10.1016/j.plantsci.2013.10.010

Jung, J. H., Seo, P. J., Kang, S. K., & Park, C. M. (2011). miR172 signals are incorporated into the miR156 signaling pathway at the SPL3/4/5 genes in Arabidopsis developmental transitions. *Plant Molecular Biology*. https://doi.org/10.1007/s11103-011-9759-z

Jung, J. H., Seo, Y. H., Pil, J. S., Reyes, J. L., Yun, J., Chua, N. H., & Park, C. M. (2007). The GIGANTEA-regulated microRNA172 mediates photoperiodic flowering independent of CONSTANS in Arabidopsis. *Plant Cell*. https://doi.org/10.1105/tpc.107.054528

Kamthan, A., Chaudhuri, A., Kamthan, M., & Datta, A. (2015). Small RNAs in plants: Recent development and application for crop improvement. *Frontiers in Plant Science*. https://doi.org/10.3389/fpls.2015.00208

Kardailsky, I., Shukla, V. K., Ahn, J. H., Dagenais, N., Christensen, S. K., Nguyen, J. T., Chory, J., Harrison, M. J., & Weigel, D. (1999). Activation tagging of the floral inducer FT. *Science*. https://doi.org/10.1126/science.286.5446.1962

Kiba, T., Takei, K., Kojima, M., & Sakakibara, H. (2013). Side-Chain Modification of Cytokinins Controls Shoot Growth in Arabidopsis. *Developmental Cell*. https://doi.org/10.1016/j.devcel.2013.10.004

Kierzkowski, D., Nakayama, N., Routier-Kierzkowska, A. L., Weber, A., Bayer, E., Schorderet, M., Reinhardt, D., Kuhlemeier, C., & Smith, R. S. (2012). Elastic domains regulate growth and organogenesis in the plant shoot apical meristem. *Science*. https://doi.org/10.1126/science.1213100

Kinoshita, A., & Richter, R. (2020). Genetic and molecular basis of floral induction in Arabidopsis thaliana. *Journal of Experimental Botany*. https://doi.org/10.1093/jxb/eraa057

Kinoshita, A., Vayssières, A., Richter, R., Sang, Q., Roggen, A., Van Driel, A. D., Smith, R. S., & Coupland, G. (2020). Regulation of shoot meristem shape by photoperiodic signaling and phytohormones during floral induction of arabidopsis. *ELife*. https://doi.org/10.7554/ELIFE.60661

Klepikova, A. V., Logacheva, M. D., Dmitriev, S. E., & Penin, A. A. (2015). RNA-seq analysis of an apical meristem time series reveals a critical point in Arabidopsis thaliana flower initiation. *BMC Genomics*. https://doi.org/10.1186/s12864-015-1688-9

Klock, H. E., & Lesley, S. A. (2009). The polymerase incomplete primer extension (PIPE)

method applied to high-throughput cloning and site-directed mutagenesis. *Methods in Molecular Biology*. https://doi.org/10.1007/978-1-59745-196-3_6

Kobayashi, Y., Kaya, H., Goto, K., Iwabuchi, M., & Araki, T. (1999). A pair of related genes with antagonistic roles in mediating flowering signals. *Science*. https://doi.org/10.1126/science.286.5446.1960

Koornneef, M., Hanhart, C. J., & van der Veen, J. H. (1991). A genetic and physiological analysis of late flowering mutants in Arabidopsis thaliana. *MGG Molecular & General Genetics*. https://doi.org/10.1007/BF00264213

Kosentka, P. Z., Overholt, A., Maradiaga, R., Mitoubsi, O., & Shpak, E. D. (2019). EPFL signals in the boundary region of the SAM restrict its size and promote leaf initiation. *Plant Physiology*. https://doi.org/10.1104/pp.18.00714

Kurihara, D., Mizuta, Y., Sato, Y., & Higashiyama, T. (2015). ClearSee: A rapid optical clearing reagent for whole-plant fluorescence imaging. *Development (Cambridge)*. https://doi.org/10.1242/dev.127613

Kwiatkowska, D. (2004). Structural integration at the shoot apical meristem: Models, measurements, and experiments. *American Journal of Botany*. https://doi.org/10.3732/ajb.91.9.1277

Kwiatkowska, D. (2008). Flowering and apical meristem growth dynamics. In *Journal of Experimental Botany*. https://doi.org/10.1093/jxb/erm290

Lam, J. K. W., Chow, M. Y. T., Zhang, Y., & Leung, S. W. S. (2015). siRNA versus miRNA as therapeutics for gene silencing. In *Molecular Therapy - Nucleic Acids*. https://doi.org/10.1038/mtna.2015.23

Landrein, B., Refahi, Y., Besnard, F., Hervieux, N., Mirabet, V., Boudaoud, A., Vernoux, T., & Hamant, O. (2015). Meristem size contributes to the robustness of phyllotaxis in Arabidopsis. *Journal of Experimental Botany*. https://doi.org/10.1093/jxb/eru482

Laufs, P., Grandjean, O., Jonak, C., Kiêu, K., & Traas, J. (1998). Cellular parameters of the shoot apical meristem in Arabidopsis. *Plant Cell*. https://doi.org/10.1105/tpc.10.8.1375

Lauter, N., Kampani, A., Carlson, S., Goebel, M., & Moose, S. P. (2005). microRNA172 down-regulates glossy15 to promote vegetative phase change in maize. *Proceedings of the National Academy of Sciences of the United States of America*. https://doi.org/10.1073/pnas.0503927102

Laux, T., Mayer, K. F. X., Berger, J., & Jürgens, G. (1996). The WUSCHEL gene is required for shoot and floral meristem integrity in Arabidopsis. *Development*. https://doi.org/10.1242/dev.122.1.87

Lee, D. Y., Lee, J., Moon, S., Park, S. Y., & An, G. (2007). The rice heterochronic gene SUPERNUMERARY BRACT regulates the transition from spikelet meristem to floral meristem. *Plant Journal*. https://doi.org/10.1111/j.1365-313X.2006.02941.x

Lee, H., Suh, S. S., Park, E., Cho, E., Ahn, J. H., Kim, S. G., Lee, J. S., Kwon, Y. M., & Lee, I. (2000). The AGAMOUS-IIKE 20 MADS domain protein integrates floral inductive pathways in Arabidopsis. *Genes and Development*. https://doi.org/10.1101/gad.813600

Lee, J. H., Ryu, H. S., Chung, K. S., Posé, D., Kim, S., Schmid, M., & Ahn, J. H. (2013). Regulation of temperature-responsive flowering by MADS-box transcription factor repressors. *Science*. https://doi.org/10.1126/science.1241097

Lee, R. C., Feinbaum, R. L., & Ambros, V. (1993). The C. elegans heterochronic gene lin-4 encodes small RNAs with antisense complementarity to lin-14. *Cell*. https://doi.org/10.1016/0092-8674(93)90529-Y

Leibfried, A., To, J. P. C., Busch, W., Stehling, S., Kehle, A., Demar, M., Kieber, J. J., & Lohmann, J. U. (2005). WUSCHEL controls meristem function by direct regulation of cytokinin-inducible response regulators. *Nature*. https://doi.org/10.1038/nature04270

Lenhard, M., Bohnert, A., Jürgens, G., & Laux, T. (2001). Termination of stem cell maintenance in Arabidopsis floral meristems by interactions between Wuschel and Agamous. *Cell*. https://doi.org/10.1016/S0092-8674(01)00390-7

Li, D., Liu, C., Shen, L., Wu, Y., Chen, H., Robertson, M., Helliwell, C. A., Ito, T., Meyerowitz, E., & Yu, H. (2008). A Repressor Complex Governs the Integration of Flowering Signals in Arabidopsis. *Developmental Cell*. https://doi.org/10.1016/j.devcel.2008.05.002

Lian, H., Wang, L., Ma, N., Zhou, C. M., Han, L., Zhang, T. Q., & Wang, J. W. (2021). Redundant and specific roles of individual MIR172 genes in plant development. *PLoS Biology*. https://doi.org/10.1371/journal.pbio.3001044

Lohmann, J. U., Hong, R. L., Hobe, M., Busch, M. A., Parcy, F., Simon, R., & Weigel, D. (2001). A molecular link between stem cell regulation and floral patterning in Arabidopsis. *Cell*. https://doi.org/10.1016/S0092-8674(01)00384-1

Long, J. A., Moan, E. I., Medford, J. I., & Barton, M. K. (1996). A member of the KNOTTED class of homeodomain proteins encoded by the STM gene of Arabidopsis. *Nature*. https://doi.org/10.1038/379066a0

Lyndon, R. F. (1978). Phyllotaxis and the initiation of primordia during flower development in silene. *Annals of Botany*. https://doi.org/10.1093/oxfordjournals.aob.a085581

Lyndon, R. F., & Battey, N. H. (1985). The growth of the shoot apical meristem during flower initiation. *Biologia Plantarum*. https://doi.org/10.1007/BF02879875

Mahla, R. S. (2016). Stem cells applications in regenerative medicine and disease therapeutics. In *International Journal of Cell Biology*. https://doi.org/10.1155/2016/6940283

Mandel, T., Candela, H., Landau, U., Asis, L., Zelinger, E., Carles, C. C., & Williams, L. E. (2016). Differential regulation of meristem size, morphology and organization by the ERECTA, CLAVATA and class III HD-ZIP pathways. *Development (Cambridge)*. https://doi.org/10.1242/dev.129973

Martin, M. (2011). Cutadapt removes adapter sequences from high-throughput sequencing reads. *EMBnet.Journal*. https://doi.org/10.14806/ej.17.1.200

Martínez-Fernández, I., de Moura, S. M., Alves-Ferreira, M., Ferrándiz, C., & Balanzà, V. (2020). Identification of players controlling meristem arrest downstream of the FRUITFULL-APETALA2 pathway. *Plant Physiology*, *184*(2), 945–959. https://doi.org/10.1104/pp.20.00800

Mathieu, J., Warthmann, N., Küttner, F., & Schmid, M. (2007). Export of FT Protein from Phloem Companion Cells Is Sufficient for Floral Induction in Arabidopsis. *Current Biology*. https://doi.org/10.1016/j.cub.2007.05.009

Mathieu, J., Yant, L. J., Mürdter, F., Küttner, F., & Schmid, M. (2009). Repression of flowering by the miR172 target SMZ. *PLoS Biology*. https://doi.org/10.1371/journal.pbio.1000148

Mayer, K. F. X., Schoof, H., Haecker, A., Lenhard, M., Jürgens, G., & Laux, T. (1998). Role of WUSCHEL in regulating stem cell fate in the Arabidopsis shoot meristem. *Cell*. https://doi.org/10.1016/S0092-8674(00)81703-1

Meicenheimer, R. D. (1979). Relationships between Shoot Growth and Changing Phyllotaxy of Ranunculus. *American Journal of Botany*. https://doi.org/10.2307/2442505

Merelo, P., González-Cuadra, I., & Ferrándiz, C. (2022). A cellular analysis of meristem activity

at the end of flowering points to cytokinin as a major regulator of proliferative arrest in Arabidopsis. *Current Biology*. https://doi.org/10.1016/j.cub.2021.11.069

Miksche, J. P., & Brown, J. A. M. (1965). Development of Vegetative and Floral Meristems of Arabidopsis thaliana. *American Journal of Botany*. https://doi.org/10.2307/2440112

Mirabet, V., Besnard, F., Vernoux, T., & Boudaoud, A. (2012). Noise and robustness in phyllotaxis. *PLoS Computational Biology*. https://doi.org/10.1371/journal.pcbi.1002389

Mizukami, Y., & Fischer, R. L. (2000). Plant organ size control: AINTEGUMENTA regulates growth and cell numbers during organogenesis. *Proceedings of the National Academy of Sciences of the United States of America*. https://doi.org/10.1073/pnas.97.2.942

MK., C. (1936). New facts in support of the hormonal theory of plant development. *Dokl. Akad. Nauk.*

Montgomery, T. A., Howell, M. D., Cuperus, J. T., Li, D., Hansen, J. E., Alexander, A. L., Chapman, E. J., Fahlgren, N., Allen, E., & Carrington, J. C. (2008). Specificity of ARGONAUTE7-miR390 Interaction and Dual Functionality in TAS3 Trans-Acting siRNA Formation. *Cell*. https://doi.org/10.1016/j.cell.2008.02.033

Moose, S. P., & Sisco, P. H. (1994). Glossy15 controls the epidermal juvenile-to-adult phase transition in maize. *Plant Cell*. https://doi.org/10.2307/3869973

Moose, S. P., & Sisco, P. H. (1996). Glossy15, an APETALA2-like gene from maize that regulates leaf epidermal cell identity. *Genes and Development*. https://doi.org/10.1101/gad.10.23.3018

Musielak, T. J., Schenkel, L., Kolb, M., Henschen, A., & Bayer, M. (2015). A simple and versatile cell wall staining protocol to study plant reproduction. *Plant Reproduction*. https://doi.org/10.1007/s00497-015-0267-1

Nair, S. K., Wang, N., Turuspekov, Y., Pourkheirandish, M., Sinsuwongwat, S., Chen, G., Sameri, M., Tagiri, A., Honda, I., Watanabe, Y., Kanamori, H., Wicker, T., Stein, N., Nagamura, Y., Matsumoto, T., & Komatsuda, T. (2010). Cleistogamous flowering in barley arises from the suppression of microRNA-guided HvAP2 mRNA cleavage. *Proceedings of the National Academy of Sciences of the United States of America*. https://doi.org/10.1073/pnas.0909097107

Ó'Maoiléidigh, D. S., van Driel, A. D., Singh, A., Sang, Q., Le Bec, N., Vincent, C., de Olalla, E. B. G., Vayssières, A., Romera Branchat, M., Severing, E., Martinez Gallegos, R., & Coupland, G. (2021). Systematic analyses of the MIR172 family members of Arabidopsis define their distinct roles in regulation of APETALA2 during floral transition. *PLOS Biology*. https://doi.org/10.1371/journal.pbio.3001043

Ogawa, M., Shinohara, H., Sakagami, Y., & Matsubayash, Y. (2008). Arabidopsis CLV3 peptide directly binds CLV1 ectodomain. *Science*. https://doi.org/10.1126/science.1150083

Ohto, M. A., Fischer, R. L., Goldberg, R. B., Nakamura, K., & Harada, J. J. (2005). Control of seed mass by APETALA2. *Proceedings of the National Academy of Sciences of the United States of America*. https://doi.org/10.1073/pnas.0409858102

Onouchi, H., Igeño, M. I., Périlleux, C., Graves, K., & Coupland, G. (2000). Mutagenesis of plants overexpressing CONSTANS demonstrates novel interactions among Arabidopsis flowering-time genes. *Plant Cell*. https://doi.org/10.1105/tpc.12.6.885

Ottoline Leyser, H. M., & Furner, I. J. (1992). Characterisation of three shoot apical meristem mutants of Arabidopsis thaliana. *Development*. https://doi.org/10.1242/dev.116.2.397

Park, W., Li, J., Song, R., Messing, J., & Chen, X. (2002). CARPEL FACTORY, a Dicer

homolog, and HEN1, a novel protein, act in microRNA metabolism in Arabidopsis thaliana. *Current Biology*. https://doi.org/10.1016/S0960-9822(02)01017-5

Pasquinelli, A. E., Reinhart, B. J., Slack, F., Martindale, M. Q., Kuroda, M. I., Maller, B., Hayward, D. C., Ball, E. E., Degnan, B., Müller, P., Spring, J., Srinivasan, A., Fishman, M., Finnerty, J., Corbo, J., Levine, M., Leahy, P., Davidson, E., & Ruvkun, G. (2000). Conservation of the sequence and temporal expression of let-7 heterochronic regulatory RNA. *Nature*. https://doi.org/10.1038/35040556

Patro, R., Duggal, G., Love, M. I., Irizarry, R. A., & Kingsford, C. (2017). Salmon provides fast and bias-aware quantification of transcript expression. *Nature Methods*. https://doi.org/10.1038/nmeth.4197

Putterill, J., Robson, F., Lee, K., Simon, R., & Coupland, G. (1995). The CONSTANS gene of arabidopsis promotes flowering and encodes a protein showing similarities to zinc finger transcription factors. *Cell*. https://doi.org/10.1016/0092-8674(95)90288-0

Ramachandran, V., & Chen, X. (2008). Small RNA metabolism in Arabidopsis. In *Trends in Plant Science*. https://doi.org/10.1016/j.tplants.2008.03.008

Rédei, G. P. (1962). SUPERVITAL MUTANTS OF ARABIDOPSIS. *Genetics*. https://doi.org/10.1093/genetics/47.4.443

Reinhart, B. J., Slack, F. J., Basson, M., Pasquienelll, A. E., Bettlnger, J. C., Rougvle, A. E., Horvitz, H. R., & Ruvkun, G. (2000). The 21-nucleotide let-7 RNA regulates developmental timing in Caenorhabditis elegans. *Nature*. https://doi.org/10.1038/35002607

Ripoll, J. J., Roeder, A. H. K., Ditta, G. S., & Yanofsky, M. F. (2011). A novel role for the floral homeotic gene APETALA2 during arabidopsis fruit development. *Development*. https://doi.org/10.1242/dev.073031

Rojo, E., Sharma, V. K., Kovaleva, V., Raikhel, N. V., & Fletcher, J. C. (2002). CLV3 is localized to the extracellular space, where it activates the Arabidopsis CLAVATA stem cell signaling pathway. *Plant Cell*. https://doi.org/10.1105/tpc.002196

Romberger, J. A., & Gregory, R. A. (1977). The Shoot Apical Ontogeny of the Picea Abies Seedling. III. Some Age-Related Aspects of Morphogenesis. *American Journal of Botany*. https://doi.org/10.2307/2441712

Sablowski, R., & Carnier Dornelas, M. (2014). Interplay between cell growth and cell cycle in plants. In *Journal of Experimental Botany*. https://doi.org/10.1093/jxb/ert354

Salvi, S., Sponza, G., Morgante, M., Tomes, D., Niu, X., Fengler, K. A., Meeley, R., Ananiev, E. V., Svitashev, S., Bruggemann, E., Li, B., Hainey, C. F., Radovic, S., Zaina, G., Rafalski, J. A., Tingey, S. V., Miao, G. H., Phillips, R. L., & Tuberosa, R. (2007). Conserved noncoding genomic sequences associated with a flowering-time quantitative trait locus in maize. *Proceedings of the National Academy of Sciences of the United States of America*. https://doi.org/10.1073/pnas.0704145104

Samach, A., Onouchi, H., Gold, S. E., Ditta, G. S., Schwarz-Sommer, Z., Yanofsky, M. F., & Coupland, G. (2000). Distinct roles of constans target genes in reproductive development of Arabidopsis. *Science*. https://doi.org/10.1126/science.288.5471.1613

Sang, Q., Vayssières, A., Ó'Maoiléidigh, D. S., Yang, X., Vincent, C., Bertran Garcia de Olalla, E., Cerise, M., Franzen, R., & Coupland, G. (2022). MicroRNA172 controls inflorescence meristem size through regulation of APETALA2 in Arabidopsis. *New Phytologist*, *235*(1), 356–371. https://doi.org/10.1111/nph.18111

Sawa, M., Nusinow, D. A., Kay, S. A., & Imaizumi, T. (2007). FKF1 and GIGANTEA complex formation is required for day-length measurement in Arabidopsis. *Science*.

https://doi.org/10.1126/science.1146994

Scheres, B. (2007). Stem-cell niches: Nursery rhymes across kingdoms. In *Nature Reviews Molecular Cell Biology*. https://doi.org/10.1038/nrm2164

Schlegel, J., Denay, G., Wink, R., Pinto, K. G., Stahl, Y., Schmid, J., Blümke, P., & Simon, R. (2021). Control of arabidopsis shoot stem cell homeostasis by two antagonistic cle peptide signalling pathways. *ELife*. https://doi.org/10.7554/eLife.70934

Schmid, M., Uhlenhaut, N. H., Godard, F., Demar, M., Bressan, R., Weigel, D., & Lohman, J. U. (2003). Dissection of floral induction pathways using global expression analysis. *Development*. https://doi.org/10.1242/dev.00842

Schoof, H., Lenhard, M., Haecker, A., Mayer, K. F. X., Jürgens, G., & Laux, T. (2000). The stem cell population of Arabidopsis shoot meristems is maintained by a regulatory loop between the CLAVATA and WUSCHEL genes. *Cell*. https://doi.org/10.1016/S0092-8674(00)80700-X

Schwab, R., Palatnik, J. F., Riester, M., Schommer, C., Schmid, M., & Weigel, D. (2005). Specific effects of microRNAs on the plant transcriptome. *Developmental Cell*, *8*(4), 517–527. https://doi.org/10.1016/j.devcel.2005.01.018

Shannon, S., & Meeks-Wagner, D. R. (1991). A Mutation in the Arabidopsis TFL1 Gene Affects Inflorescence Meristem Development. *The Plant Cell*. https://doi.org/10.1105/tpc.3.9.877

Shindo, C., Aranzana, M. J., Lister, C., Baxter, C., Nicholls, C., Nordborg, M., & Dean, C. (2005). Role of FRIGIDA and FLOWERING LOCUS C in determining variation in flowering time of Arabidopsis. *Plant Physiology*. https://doi.org/10.1104/pp.105.061309

Simpson, G. G. (2004). The autonomous pathway: Epigenetic and post-transcriptional gene regulation in the control of Arabidopsis flowering time. In *Current Opinion in Plant Biology*. https://doi.org/10.1016/j.pbi.2004.07.002

Sokolowski, T. R., Erdmann, T., & ten Wolde, P. R. (2012). Mutual Repression Enhances the Steepness and Precision of Gene Expression Boundaries. *PLoS Computational Biology*. https://doi.org/10.1371/journal.pcbi.1002654

Su, Y. H., Zhou, C., Li, Y. J., Yu, Y., Tang, L. P., Zhang, W. J., Yao, W. J., Huang, R., Laux, T., & Zhang, X. S. (2020). Integration of pluripotency pathways regulates stem cell maintenance in the arabidopsis shoot meristem. *Proceedings of the National Academy of Sciences of the United States of America*. https://doi.org/10.1073/pnas.2015248117

Suárez-López, P., Wheatley, K., Robson, F., Onouchi, H., Valverde, F., & Coupland, G. (2001). CONSTANS mediates between the circadian clock and the control of flowering in Arabidopsis. *Nature*. https://doi.org/10.1038/35074138

Supek, F., Bošnjak, M., Škunca, N., & Šmuc, T. (2011). Revigo summarizes and visualizes long lists of gene ontology terms. *PLoS ONE*, *6*(7). https://doi.org/10.1371/journal.pone.0021800

Takei, K., Yamaya, T., & Sakakibara, H. (2004). Arabidopsis CYP735A1 and CYP735A2 encode cytokinin hydroxylases that catalyse the biosynthesis of trans-Zeatin. *Journal of Biological Chemistry*. https://doi.org/10.1074/jbc.M406337200

Tal, L., Friedlander, G., Gilboa, N. S., Unger, T., Gilad, S., & Eshed, Y. (2017). Coordination of meristem doming and the floral transition by late termination, a kelch repeat protein. *Plant Cell*. https://doi.org/10.1105/tpc.17.00030

Tao, Z., Shen, L., Liu, C., Liu, L., Yan, Y., & Yu, H. (2012). Genome-wide identification of SOC1 and SVP targets during the floral transition in Arabidopsis. *Plant Journal*. https://doi.org/10.1111/j.1365-313X.2012.04919.x

Todesco, M., Rubio-Somoza, I., Paz-Ares, J., & Weigel, D. (2010). A collection of target mimics for comprehensive analysis of MicroRNA function in Arabidopsis thaliana. *PLoS Genetics*. https://doi.org/10.1371/journal.pgen.1001031

Torti, S., Fornara, F., Vincent, C., Andrés, F., Nordström, K., Göbel, U., Knoll, D., Schoof, H., & Coupland, G. (2012). Analysis of the Arabidopsis shoot meristem transcriptome during floral transition identifies distinct regulatory patterns and a leucine-rich repeat protein that promotes flowering. *Plant Cell*. https://doi.org/10.1105/tpc.111.092791

Turck, F., Fornara, F., & Coupland, G. (2008). Regulation and identity of florigen: Flowering Locus T moves center stage. In *Annual Review of Plant Biology*. https://doi.org/10.1146/annurev.arplant.59.032607.092755

Uchida, N., & Torii, K. U. (2019). Stem cells within the shoot apical meristem: identity, arrangement and communication. In *Cellular and Molecular Life Sciences*. https://doi.org/10.1007/s00018-018-2980-z

Valverde, F., Mouradov, A., Soppe, W., Ravenscroft, D., Samach, A., & Coupland, G. (2004). Photoreceptor Regulation of CONSTANS Protein in Photoperiodic Flowering. *Science*. https://doi.org/10.1126/science.1091761

Vaucheret, H. (2008). Plant ARGONAUTES. In *Trends in Plant Science*. https://doi.org/10.1016/j.tplants.2008.04.007

Vaughan, J. G. (1951). The morphology and growth of the vegetative and reproductive apices of Arabidopsis thaliana (L.) Heynh., Capsella bursa-pastoris (L.) Medic. and Anagallis arvensis L. *Botanical Journal of the Linnean Society*, *55*(359), 279–301.

Wang, J. W., Czech, B., & Weigel, D. (2009). miR156-Regulated SPL Transcription Factors Define an Endogenous Flowering Pathway in Arabidopsis thaliana. *Cell*, *138*(4), 738–749. https://doi.org/10.1016/j.cell.2009.06.014

Weigel, D. (1995). The APETALA2 domain is related to a novel type of DNA binding domain. In *The Plant cell*. https://doi.org/10.1105/tpc.7.4.388

Werner, J. D., Borevitz, J. O., Henriette Uhlenhaut, N., Ecker, J. R., Chory, J., & Weigel, D. (2005). FRIGIDA-independent variation in flowering time of natural Arabidopsis thaliana accessions. *Genetics*. https://doi.org/10.1534/genetics.104.036533

Wigge, P. A., Kim, M. C., Jaeger, K. E., Busch, W., Schmid, M., Lohmann, J. U., & Weigel, D. (2005). Integration of spatial and temporal information during floral induction in Arabidopsis. *Science*. https://doi.org/10.1126/science.1114358

Wilson, R. N., Heckman, J. W., & Somerville, C. R. (1992). Gibberellin is required for flowering in Arabidopsis thaliana under short days. *Plant Physiology*. https://doi.org/10.1104/pp.100.1.403

Wollmann, H., Mica, E., Todesco, M., Long, J. A., & Weigel, D. (2010). On reconciling the interactions between APETALA2, miR172 and AGAMOUS with the ABC model of flower development. *Development*. https://doi.org/10.1242/dev.036673

Würschum, T., Groß-Hardt, R., & Laux, T. (2006). APETALA2 regulates the stem cell niche in the Arabidopsis shoot meristem. *Plant Cell*, *18*(2), 295–307. https://doi.org/10.1105/tpc.105.038398

Xie, Y., Zhou, Q., Zhao, Y., Li, Q., Liu, Y., Ma, M., Wang, B., Shen, R., Zheng, Z., & Wang, H. (2020). FHY3 and FAR1 Integrate Light Signals with the miR156-SPL Module-Mediated Aging Pathway to Regulate Arabidopsis Flowering. *Molecular Plant*. https://doi.org/10.1016/j.molp.2020.01.013

Xu, C., Liberatore, K. L., Macalister, C. A., Huang, Z., Chu, Y. H., Jiang, K., Brooks, C., Ogawa-

Ohnishi, M., Xiong, G., Pauly, M., Van Eck, J., Matsubayashi, Y., Van Der Knaap, E., & Lippman, Z. B. (2015). A cascade of arabinosyltransferases controls shoot meristem size in tomato. *Nature Genetics*. https://doi.org/10.1038/ng.3309

Xu, M., Hu, T., Zhao, J., Park, M. Y., Earley, K. W., Wu, G., Yang, L., & Poethig, R. S. (2016). Developmental Functions of miR156-Regulated SQUAMOSA PROMOTER BINDING PROTEIN-LIKE (SPL) Genes in Arabidopsis thaliana. *PLoS Genetics*. https://doi.org/10.1371/journal.pgen.1006263

Yamaguchi, A., Kobayashi, Y., Goto, K., Abe, M., & Araki, T. (2005). TWIN SISTER of FT (TSF) acts as a floral pathway integrator redundantly with FT. *Plant and Cell Physiology*. https://doi.org/10.1093/pcp/pci151

Yamaguchi, A., Wu, M. F., Yang, L., Wu, G., Poethig, R. S., & Wagner, D. (2009). The MicroRNA-Regulated SBP-Box Transcription Factor SPL3 Is a Direct Upstream Activator of LEAFY, FRUITFULL, and APETALA1. *Developmental Cell*. https://doi.org/10.1016/j.devcel.2009.06.007

Yanai, O., Shani, E., Dolezal, K., Tarkowski, P., Sablowski, R., Sandberg, G., Samach, A., & Ori, N. (2005). Arabidopsis KNOXI proteins activate cytokinin biosynthesis. *Current Biology*, *15*(17), 1566–1571. https://doi.org/10.1016/j.cub.2005.07.060

Yanovsky, M. J., & Kay, S. A. (2003). Living by the calendar: How plants know when to flower. In *Nature Reviews Molecular Cell Biology*. https://doi.org/10.1038/nrm1077

Yant, L., Mathieu, J., Dinh, T. T., Ott, F., Lanz, C., Wollmann, H., Chen, X., & Schmid, M. (2010). Orchestration of the floral transition and floral development in arabidopsis by the bifunctional transcription factor APETALA2. *Plant Cell*, *22*(7), 2156–2170. https://doi.org/10.1105/tpc.110.075606

Yao, Y., Guo, G., Ni, Z., Sunkar, R., Du, J., Zhu, J. K., & Sun, Q. (2007). Cloning and characterization of microRNAs from wheat (Triticum aestivum L.). *Genome Biology*. https://doi.org/10.1186/gb-2007-8-6-r96

Yoo, S. K., Chung, K. S., Kim, J., Lee, J. H., Hong, S. M., Yoo, S. J., Yoo, S. Y., Lee, J. S., & Ahn, J. H. (2005). CONSTANS activates SUPPRESSOR OF OVEREXPRESSION OF CONSTANS 1 through FLOWERING LOCUS T to promote flowering in Arabidopsis. *Plant Physiology*. https://doi.org/10.1104/pp.105.066928

Yu, B., Yang, Z., Li, J., Minakhina, S., Yang, M., Padgett, R. W., Steward, R., & Chen, X. (2005). Methylation as a crucial step in plant microRNA biogenesis. *Science*. https://doi.org/10.1126/science.1107130

Zeevaart, J. A. D. (2006). Florigen coming of age after 70 years. In *Plant Cell*. https://doi.org/10.1105/tpc.106.043513

Zhai, Q., Zhang, X., Wu, F., Feng, H., Deng, L., Xu, L., Zhang, M., Wang, Q., & Li, C. (2015). Transcriptional mechanism of jasmonate receptor COI1-mediated delay of flowering time in arabidopsis. *Plant Cell*. https://doi.org/10.1105/tpc.15.00619

Zhang, B., Wang, L., Zeng, L., Zhang, C., & Ma, H. (2015). Arabidopsis TOE proteins convey a photoperiodic signal to antagonize CONSTANS and regulate flowering time. *Genes and Development*, *29*(9), 975–987. https://doi.org/10.1101/gad.251520.114

Zhang, L., Gennaro, D. De, Lin, G., Chai, J., & Shpak, E. D. (2021). ERECTA family signaling constrains CLAVATA3 and WUSCHEL to the center of the shoot apical meristem. *Development (Cambridge)*. https://doi.org/10.1242/dev.189753

Zhang, R., Calixto, C. P. G., Marquez, Y., Venhuizen, P., Tzioutziou, N. A., Guo, W., Spensley, M., Entizne, J. C., Lewandowska, D., Have, S. Ten, Frey, N. F., Hirt, H., James, A. B., Nimmo, H. G., Barta, A., Kalyna, M., & Brown, J. W. S. (2017). A high quality Arabidopsis

transcriptome for accurate transcript-level analysis of alternative splicing. *Nucleic Acids Research*. https://doi.org/10.1093/nar/gkx267

Zhou, Y., Gan, X., Viñegra de la Torre, N., Neumann, U., & Albani, M. C. (2021). Beyond flowering time: diverse roles of an APETALA2-like transcription factor in shoot architecture and perennial traits. *New Phytologist*. https://doi.org/10.1111/nph.16839

Zhu, Q. H., & Helliwell, C. A. (2011). Regulation of flowering time and floral patterning by miR172. *Journal of Experimental Botany*. https://doi.org/10.1093/jxb/erq295

Zhu, Q. H., Upadhyaya, N. M., Gubler, F., & Helliwell, C. A. (2009). Over-expression of miR172 causes loss of spikelet determinacy and floral organ abnormalities in rice (Oryza sativa). *BMC Plant Biology*. https://doi.org/10.1186/1471-2229-9-149

10 Acknowledgements

If you are reading this, it means that you have successfully gone through my doctoral thesis. However, it is honest to say that you might have skipped most of it (I hope not all of it) in order to reach this section. Regardless of the reason why you are reading the acknowledgements, it is clear that this is one of the most personal and special sections of this text. Whereas my name is the only one appearing at the cover page of this document, many of the experiments shown here are the output of many discussions and team effort. Therefore, it would be absolutely unfair to finish this text without saying thanks to all the ones who showed support during this stage of my scientific career.

First of all, I am deeply grateful to George. Thanks for giving me the chance to join your team and for your supervision. It has been an amazing time facing the complexity of the regulation of flowering. I have really enjoyed all the scientific discussions, especially the ones in reduced groups or the 1-on-1 meetings. It has been really meaningful that you have always shared your ideas and thoughts about my project. This is to say that I generally ended our scientific discussions feeling that I had learned a lot. Moreover, thanks for staying supportive during the annoying organisation of my doctoral examination.

The next one to thank is Alice. It has been a blast to work together with you and to have your guidance to learn new techniques and to get to know better my project. I really appreciate how you listened to my thoughts about the project from the very beginning. I feel so lucky to have inherited all the great work that you did in starting the generation of plant material and in the harvesting and preparation of material for the RNA-Seq. At the beginning, I admit that I was scared of the day, in which you would leave the lab. However, finding myself moving forward with my project after you left made me feel confident of myself and, from my point of view, it is a clear sign that your supervision has been amazing. You really deserve the best for your future, and I hope that this includes lots of chances to eat *polvorones*.

Thanks again to George and Alice for being part of my thesis advisory committee, together with Cristina. Muchísimas gracias por aceptar la invitación para formar parte del TAC, y además por hacerlo con tanta rapidez y ganas, a pesar de no saber del cierto en qué clase de comité te estabas involucrando. Ha sido estupendo tener tu punto de vista y espero que puedas notar en este texto que tus sugerencias se han tenido en cuenta, a pesar de una infrarrepresentación de tu querido *FUL* en este texto. Y que no quede en el olvido que has sido la persona que me descubrió los *negronis*.

I am really grateful to John for correcting this text, which has improved incredibly from its early versions. In the middle of the stress caused by the writing of this thesis, having your point of view has helped me to make this phase really rewarding. Of course, it is really kind that you are joining my examination committee as a minute taker. This includes as well George, Bart and Stan. Thank you so much for your interest in my project.

Previous work from other colleagues in the lab has incredibly facilitated my job here, especially due to the availability of an enormous number of tools. For this reason, thanks to Diarmuid for leading the generation of material to study *MIR172* genes. Thanks to Atsuko for establishing a strategy to perform segmentation analyses of the meristem during floral transition. As well, thanks to Qing and Xia for generating such great materials to study the *AP2-LIKE* genes.

One of the first places that I saw first when I came for the first time to work to the lab was my office. For sure, at the beginning, I could not expect how lucky I was to end up in office F-O-03. Thanks to Annabel for becoming a reference person for the first days, and being always up to answer my multiple questions, as well as your enthusiasm when playing “Nein Mann”. Muchas gracias Eva por tu proximidad des del principio. Es increíble como tus “hombre” y “ostia” hacían que me sintiera como en casa. And, of course, infinite thanks to Adrian. It was priceless when you said to me that you admired my organisation in my experiments, when I was exactly feeling that I was not doing so. I have learned from you during our scientific discussions and I am certain that I have a more refined sense of humour after dealing with your jokes (I honestly only remember the *Wanderine*). And here comes the acknowledgements

to our last incorporation in the office. Moltíssimes gràcies per tot Alba. Esto incluye todas las risas, ya sea riéndonos de cualquier tontería o de las desgracias que rodeaban nuestro trabajo experimental. Tus consejos me han servido mucho para afrontar estos últimos meses.

It is always funny to look back to judge how those who were once strangers become really good friends. Thanks Martina for all the funny moments that we have shared together, including your wedding. Not many people here can brag of having experienced something that is undeniably typical from Aosta. Thanks to Vítor for your useful tips in the lab and such many funny moments together with you and Jana, in the *Weihnachtsmärkte*, at the TATA Bar and… yes! At a Japanese Karoke! Thanks to Yohanna for answering my questions in the lab and as well for your infinite kindness. I am certain that we give more hugs now in the group and this is thanks to you.

Muchas gracias a Edouard por tu ayuda con el análisis del RNA-Seq. Tus consejos siempre han hecho que los problemas que tenía con este conjunto de datos fueran mucho más livianos. También, en este sentido, infinitas gracias a Gabriel. Es genial ver como un matemático ha sido capaz de tomar las riendas de un confocal, y como has conseguido poner números a algo que hasta ahora simplemente podíamos juzgar mirando imágenes. I això no hauria estat possible sense els consells d'en Pau. Moltíssimes gràcies per compartir sempre les teves idees i curiositats amb nosaltres, i per ajudar a establir una col·laboració entre el teu laboratori i el grup del George. This has been absolutely helpful for the last stages of this project, together with the material that Kang shared with me. Thanks a lot Kang for being such a nice colleague and sharing interest for *AP2.*

This is already getting longer and longer, and I cannot help feeling that I could not thank everyone who has helped me. I would like to thank all the members of the Coupland group and please apologise me if you do not see directly your names here. This includes as well all the student helpers, that have allowed to generate quite ambitious material in this project. For sure, this includes the technicians from our group, and especially Sabine. It has been amazing to work together with you. I am glad that now you have more time to go body boarding! Many

thanks to all the students that I have supervised. Thanks Rohit for all your incredible work with *TOE2* and the confocal with the *MIR172* reporter lines. Thanks Dustin for your support in the flowering-time analysis of the F2 of the *soc1-2* × *ap2-12* cross. Y muchísimas gracias Yaiza por toda tu ayuda durante este último año. Anque te vayas a estudiar neurociencias, sé que te vas emocionar cada vez que veas una Arabidopsis. And lastly, thanks to all the members of our incredibly fructiferous garden: thanks to all the Fellows of the Royal Salad!

I have enjoyed a lot my time in the group and as well at the institute. This for sure includes all the good times at the TATA Bar! It has been amazing to share my time there with all of you, to get to know such many colleagues from different departments that become good friends, and to develop further our passion for karaoke. I am glad that now the TATA Bar is in good hands with Josep and Marco!

Estoy muy agradecido pot todos los buenos momentos que he vivido con la gente que he conocido fuera del instituto, en un intento de dominar la lengua de este lugar. Muchísimas gracias por todos los buenos momentos y las risas a Carla, Cris y Marta. Durant tot aquest procés, he tingut el suport de molts amics. Moltíssimes gràcies a la Cristina i a la Fàtima, per mantenir el contacte durant aquests anys i poder compartir les vivències durant els nostres doctorats en tònica de Rauw Rauw. He gaudit molt també compartint aquesta experiència alemanya amb la Judit, el Pablo i l'Aixa, ja sigui intentant entendre com sobreviure un cap de setmana d'Oktoberfest, o admirant a l'Emma (ara que ja sabem que té nom). Moltes gràcies a la meva estimada secta de la Judit, l'Anna i la Berta, per ser de les primeres visites en aquesta nova aventura regada amb aigua de Colònia. Moltíssimes gràcies a la Bet per la teva amistat incondicional, i també moltes gràcies a la Júlia, per totes les discussions sobre 100sia i gustos musicals. Com no, moltíssimes gràcies a totes les de "La vida adulta". Recordo amb molta estima el primer carnaval amb vosaltres i, per descomptat, l'experiència Motomami amb l'Anna!

I finalment, moltíssimes gràcies a tot el suport que he rebut de tota la meva família, del grup de les "cervecitas" del cap de setmana, i, per suposat, dels meus pares. Gràcies per creure

en mi i per recordar-me que el que estic fent val la pena. Tinc moltíssimes ganes de celebrar això amb vosaltres, aquí a Colònia, o al Frankfurt Pai. Us estimo molt!

Erklärung zur Dissertation
gemäß der Promotionsordnung vom 12. März 2020

Diese Erklärung muss in der Dissertation enthalten sein.
(*This version must be included in the doctoral thesis*)

„Hiermit versichere ich an Eides statt, dass ich die vorliegende Dissertation selbstständig und ohne die Benutzung anderer als der angegebenen Hilfsmittel und Literatur angefertigt habe. Alle Stellen, die wörtlich oder sinngemäß aus veröffentlichten und nicht veröffentlichten Werken dem Wortlaut oder dem Sinn nach entnommen wurden, sind als solche kenntlich gemacht. Ich versichere an Eides statt, dass diese Dissertation noch keiner anderen Fakultät oder Universität zur Prüfung vorgelegen hat; dass sie - abgesehen von unten angegebenen Teilpublikationen und eingebundenen Artikeln und Manuskripten - noch nicht veröffentlicht worden ist sowie, dass ich eine Veröffentlichung der Dissertation vor Abschluss der Promotion nicht ohne Genehmigung des Promotionsausschusses vornehmen werde. Die Bestimmungen dieser Ordnung sind mir bekannt. Darüber hinaus erkläre ich hiermit, dass ich die Ordnung zur Sicherung guter wissenschaftlicher Praxis und zum Umgang mit wissenschaftlichem Fehlverhalten der Universität zu Köln gelesen und sie bei der Durchführung der Dissertation zugrundeliegenden Arbeiten und der schriftlich verfassten Dissertation beachtet habe und verpflichte mich hiermit, die dort genannten Vorgaben bei allen wissenschaftlichen Tätigkeiten zu beachten und umzusetzen. Ich versichere, dass die eingereichte elektronische Fassung der eingereichten Druckfassung vollständig entspricht."

Teilpublikationen:

13.06.2023 ENRIC BERTRAN GARCIA DE OLALLA
Datum, Name und Unterschrift

Erklärung zum Gesuch um Zulassung zur Promotion
gemäß der Promotionsordnung vom 12. März 2020

1. Zugänglichkeit von Daten und Materialien

Die Dissertation beinhaltet die Gewinnung von Primärdaten oder die Analyse solcher Daten oder die Reproduzierbarkeit der in der Dissertation dargestellten Ergebnisse setzt die Verfügbarkeit von Datenanalysen, Versuchsprotokollen oder Probenmaterial voraus.

☐ Trifft nicht zu
☒ Trifft zu.
In der Dissertation ist dargelegt wie diese Daten und Materialien gesichert und zugänglich sind (entsprechend den Vorgaben des Fachgebiets beziehungsweise der Betreuerin oder des Betreuers).

2. Frühere Promotionsverfahren

Ich habe bereits einen Doktortitel erworben oder ehrenhalber verliehen bekommen.
Oder: Für mich ist an einer anderen Fakultät oder Universität ein Promotionsverfahren eröffnet worden, aber noch nicht abgeschlossen.
Oder: Ich bin in einem Promotionsverfahren gescheitert.
☒ Trifft nicht zu
☐ Zutreffend
wenn zutreffend, Erläuterung:

3. Straftat

Ich bin nicht zu einer vorsätzlichen Straftat verurteilt worden ist, bei deren Vorbereitung oder Begehung der Status einer Doktorandin oder eines Doktoranden missbraucht wurde.

Ich versichere, alle Angaben wahrheitsgemäß gemacht zu haben.

13.06.2023	ENRIC BERTRAN GARCIA DE OLALLA	
Datum	Name	Unterschrift